Structural assessment of inner-city quay walls' capacity to resist multifunctional loads

FEM analysis of a traditional quay wall and a sheet pile wall to assess their capacity for current and future multifunctional loads

Author: N.A. van Vliet

Date: March 28th, 2025

TU Delft

Structural assessment of inner-city quay walls' capacity to resist multifunctional loads

FEM analysis of a traditional quay wall and a sheet pile wall to assess their capacity for current and future multifunctional loads

By

N.A. van Vliet

In partial fulfilment of the requirements for the degree of:

Master of Science
in Civil Engineering

at the Delft University of Technology,
to be defended publicly on Friday March 28th, 2025, at 04:00 PM.

Supervisor:	Prof. dr. M. Veljkovic	TU Delft
Thesis committee:	Dr. F. Kavoura	TU Delft
	Dr. F. Messali	TU Delft
	MSc M. Longo	TU Delft

An electronic version of this thesis is available at http://repository.tudelft.nl/

Preface

This thesis marks the culmination of my Master of Science (MSc) in Civil Engineering, with a specialization in Structural Engineering, at the esteemed Technical University of Delft (TU Delft). My research focuses on the structural assessment of inner-city quay walls, specifically their capacity to bear multifunctional loads. As urban areas evolve, understanding the strength and stability of quay walls under current and future load conditions has become critical to ensuring sustainable infrastructure. In this context I applied Finite Element Method (FEM) analysis to evaluate the structural response of a quay wall selected as case study. Two configurations are considered, the as-built condition (which in this thesis is referred to as the traditional geometry and a strengthened condition via the application of sheet piles. The ability of both configurations to withstand the multifunctional loads expected in modern urban environments is assessed.

This thesis represents a deeper exploration into the field of applied mechanics of structures, a direction I pursued throughout my MSc. The knowledge and skills developed during both my Bachelor's and Master's studies at TU Delft played a pivotal role in shaping this research. Courses in soil mechanics, finite element modelling with DIANA software, and constitutive modelling of soils provided the foundation for the work presented here. Additionally, the principles of structural design, particularly in the context of steel structures, were instrumental in assessing the structural integrity of quay walls.

Throughout this journey, I not only honed my technical expertise but also cultivated the essential skills needed to conduct independent research. I gained invaluable experience in writing a comprehensive thesis report, keeping my supervisors informed and engaged, and managing my time effectively to balance research, analysis, and reporting. This thesis marks a milestone in my academic career.

Contents

Preface **4**

Abstract **8**

Acknowledgments **9**

1 Introduction **10**
1.1 History of quay walls in Amsterdam 10
1.2 Research scope and aim 11
1.3 Research questions 13
1.4 Research methodology 13
1.5 Structure of this thesis 14

2 Literature Review **15**
2.1 Quay wall geometries 15
2.1.1 Traditional 15
2.1.2 Sheet pile 18
2.2 Material properties 22
2.2.1 Timber 22
2.2.2 Masonry 23
2.2.3 Steel 24
2.3 Constitutive models within FEM 27
2.3.1 Constitutive models for soils 27
2.3.2 Constitutive models for masonry 30
2.3.3 Constitutive models for timber 32
2.3.4 Constitutive models for steel 32
2.4 Failure mechanisms 33
2.4.1 Traditional failure mechanisms 33
2.4.2 Sheet pile failure mechanisms 38

3 Case Study **41**
3.1 Soil investigation 41
3.1.1 DINOloket 42
3.1.2 CPT data 46
3.1.3 Assumed simplification soil layers 50
3.1.4 Soil properties 50
3.2 Structural configurations 54
3.2.1 Traditional geometry 54
3.2.2 Sheet pile geometry 57
3.3 Loads on quay walls 62
3.3.1 Current loads 62
3.3.2 Multifunctional loads 65
3.3.3 Loading history 70

4 Development and Implementation of the Finite Element Models 71
4.1 Traditional model DIANA 71
4.1.1 Geometry and materials 71
4.1.2 Boundary conditions and loads 80
4.1.3 Mesh and analysis 82
4.2 Traditional model Plaxis 85
4.2.1 Geometry and materials 85
4.2.2 Boundary conditions and loads 94
4.2.3 Mesh and analysis 94
4.3 Sheet pile model DIANA 97
4.3.1 Geometry and materials 97
4.3.2 Boundary conditions and loads 99
4.3.3 Mesh and analysis 99
4.4 Sheet pile model Plaxis 102
4.4.1 Geometry and materials 102
4.4.2 Boundary conditions and loads 103
4.4.3 Mesh and analysis 103

5 Numerical Results 106
5.1 Traditional model 106
5.1.1 Failure mechanism: excessive displacements 106
5.1.2 Failure mechanism: timber piles 110
5.1.3 Verification of the results 114
5.2 Sheet pile model 123
5.2.1 Failure mechanism: excessive displacements 123
5.2.2 Failure mechanism: structural failure 127
5.2.3 Verification of the results 130

6 Discussion 137
6.1 Interpretation of key findings 137
6.2 Comparison with reality 139
6.3 Comparison with literature 141
6.4 Limitations and sources of uncertainty 143
6.4.1 Differences between software DIANA and Plaxis 143
6.4.2 Hinged connection pile-kesp 149
6.4.3 Soil layer simplifications 150
6.4.4 Consolidation not considered 151
6.4.5 Deterioration materials not considered 151
6.4.6 Safety factors not considered 156
6.4.7 Combining multifunctional loads with TAK-load 157
6.4.8 Energy load 157
6.4.9 Tree load 157
6.4.10 Limited consideration of failure mechanisms 157
6.4.11 Plane strain limitations 158

7 Final remarks and recommendations 159
7.1 Research problem and objectives 159

7.2 Key findings 160
7.2.1 Sub-questions 160
7.2.2 Main research question 161
7.2.3 Software comparison: DIANA and Plaxis 161
7.3 Implications 163
7.4 Recommendations for future research 164
7.4.1 Increase soil layer complexity 164
7.4.2 Location of loading 165
7.4.3 Deterioration of the structure 165
7.4.4 Environmental effects 165
7.5 Closing statement 166

8 Bibliography 167

Appendix A: Maple worksheet sheet pile design 171

Appendix B: Geometries other quay wall construction types 187

Appendix C: Failure mechanisms not considered in thesis 192

Appendix D: Comparison of phase displacements traditional model from DIANA and Plaxis 200

Abstract

The renewal of quay walls in Amsterdam presents an opportunity to integrate multifunctional features that introduce additional loads to the existing structures. These loads are caused by the self-weight of trees offering climate adaptable cities, energy storage powering the energy transition or steel panels, which allow additional protection against sea level rise by increasing the retaining height of the quay walls. This research investigates the structural performance of two quay wall configurations at the Marnixkade, which is a street along a quay wall that is in the west of Amsterdam, where renewal is to take place. Out of multiple structural quay-wall configurations, a traditional timber-masonry quay wall and a modern steel sheet pile wall are chosen. The traditional quay wall is currently the most occurring quay wall type, whereas the steel sheet pile wall has been selected as it enables rapid design for high strength and is therefore often seen as emergency structure in Amsterdam for deteriorated quays. Although other methods are in development by different companies, little information is known, and they are therefore not considered.

Using Finite Element Analysis (FEA) in Plaxis and DIANA, both models are analysed with different load cases and validated against analytical checks. The base case follows from the TAK (Dutch document, abbreviated as Toetsing Amsterdamse Kademuren (Ingenieursbureau Gemeente Amsterdam, 2023), which is a guide that provides information on how to structurally assess quay walls in FE software), standard, which applies a distributed downward load of 10 kN/m^2 from 0.5 m up to 8 m from the waterside of the quay. Additional functionalities are then introduced to assess their impact on structural behaviour compared to the base case. This is done through imposing additional distributed loads of a tree, energy storage and steel panels to increase water retaining height or a combination of them on the structure. A simplified two-layered soil model, consisting of a clay layer over sand, is used to simulate ground conditions. Structural forces in terms of cross-sectional normal forces, shear forces and bending moments, as well as horizontal displacements are considered for the failure mechanisms.

Results indicate that the traditional timber-masonry quay wall exhibits higher stress concentrations in the timber piles, while the steel sheet pile wall is more susceptible to excessive horizontal displacements. It should be noted that the results are based on undeteriorated material properties; in reality, timber pile degradation and steel corrosion are common and can significantly reduce the structural performance of quay walls. Without proper in-situ measurements, the uncertainty in model predictions remains high. Adapting quay walls to additional loads from multifunctionalities requires careful reconsideration of material behaviour and structural limits, as strengthening might be required. While the steel sheet pile wall can be modified through stronger sections or higher-grade steel, reinforcement options for the traditional timber-masonry structure are more limited, involving adjustments in pile count, diameter, or masonry thickness.

Acknowledgments

First and foremost, I would like to express my deepest gratitude to Michele Longo and Francesco Messali for their invaluable reflections and constructive criticism on my numerical modelling, particularly in DIANA. Their insights and feedback greatly enhanced the accuracy and reliability of my work. I am also immensely grateful to Florentia Kavoura and Milan Veljkovic for their guidance and support throughout this thesis. Their advice helped me maintain a structured timeline and stay on track, while their thought-provoking questions allowed me to refine both the general overview and the details of my research.

A special thanks to Matthijs Griffioen, sustainability advisor, and Aziz Cherkaoui, geotechnical advisor, from the Ingenieursbureau of Amsterdam for their constructive feedback and willingness to answer my questions. Their expertise and availability were invaluable throughout this process. I am appreciative of Na Hao, PhD candidate in Geotechnical Engineering, for her assistance in modelling with Plaxis. Her feedback and answers to my questions about soil modelling provided me guidance to improve my numerical analyses. Additionally, I would like to thank Mandy Korff for being available to answer some of my questions, further supporting my research.

Beyond academic and professional guidance, I am incredibly grateful to my parents, sisters, and girlfriend for their unwavering support throughout this journey. They stood by me through the difficult stages—whether it was defining my research focus, troubleshooting inaccurate numerical models, or reconciling significant discrepancies between different software results. Their encouragement pushed me forward, especially when I struggled with progress and perfectionism. When I finally reduced the differences in my models to approximately 30%, they reminded me that clarity in writing and completing my thesis was more important than striving for absolute precision. Without their support, I would not have reached the finish line.

1 Introduction

1.1 History of quay walls in Amsterdam

Amsterdam, the capital of the Netherlands, has maintained a profound and enduring relationship with water throughout its history. The city's origins trace back to settlements near the mouth of the Amstel River, where early inhabitants constructed a dam to manage water flow. This infrastructure lent the city its name. During the 17th century, Amsterdam witnessed significant economic expansion because of the Dutch Golden Age, driven by maritime trade facilitated by the Dutch East India Company. Between 1860 and 1900, Amsterdam's population surged from approximately 240,000 to 500,000, prompting extensive urban development. This period also saw the formation of the iconic city centre characterized by its concentric canal network (Hemel, 2023).

The construction of the canals necessitated the development of quay walls to stabilize the soil and prevent collapse into the waterways. Due to the region's soft and unstable soil conditions, timber piles were employed as foundational supports to minimize soil settlements. Initially, these quay walls primarily served as cargo-handling zones managed by private entities. Over time, their functions evolved, and they now serve as public roads with significant cultural and historical value, under the purview of municipal maintenance. Currently, Amsterdam boasts over 200 kilometres of quay walls, integral to its urban infrastructure. The growth of Amsterdam is visualised in Figure 1.

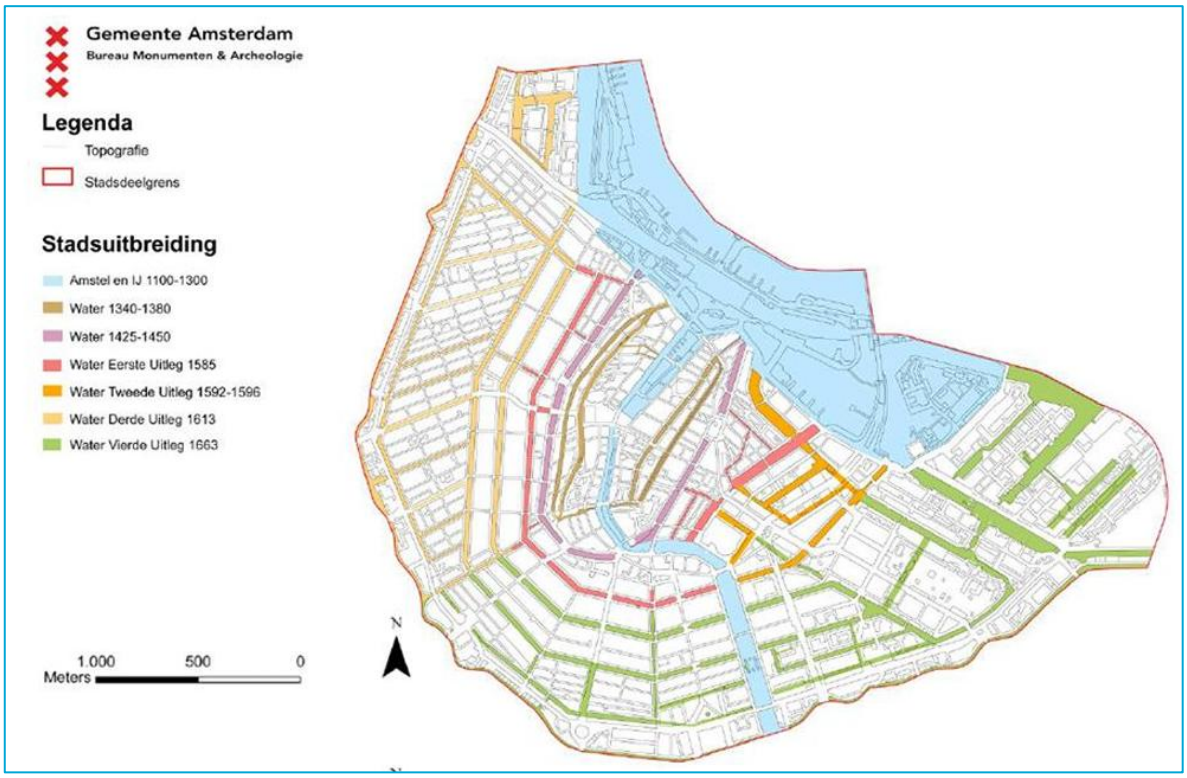

Figure 1 - Geographical expansion of historic centre of Amsterdam (Gemeente Amsterdam: Bureau Monumenten & Archeologie, 2023)

In recent decades, many quay walls have shown signs of deterioration due to the timber foundation piles deteriorating (Pagella, Ravenshorst, Grad, & Van der Kuilen, 2022) and the increased mechanical loads associated with modern vehicular traffic that were not anticipated before 1900. On September 1, 2020, the Grimburgwal quay wall suffered a collapse, prompting heightened scrutiny from municipal authorities (Korff, Hemel, & Peters, 2022). This incident underscored the urgency of evaluating the structural integrity of quay walls citywide. The dual mandate of preserving Amsterdam's cultural heritage while ensuring the structural resilience of its quay walls poses a substantial engineering and logistical challenge. Addressing these issues requires a multidisciplinary approach encompassing historical preservation, urban planning, and civil engineering innovations to adapt these vital structures to contemporary demands and future uncertainties.

1.2 Research scope and aim

The municipality must maintain 200km of quay walls and 850 road bridges. To do this, the Program of Bridges and Quay walls was set up. In the coming years attention will be given to assessing the structural condition of the quay walls and bridges.

Many numerical models have been made of the currently existing quay walls (Spannenburg, 2020) (Voortman, 2021) (Sharma, Longo, & Messali, 2024), also analytical quay wall models exist (Hemel, 2023). Unfortunately, many input variables are currently unknown, and research has been performed to obtain insight into the material properties and layouts of the quays. An example is that of micro-drilling (Pagella G, 2024) to obtain the timber properties of the piles. An analytical quay wall model (Hemel, 2023) has been constructed for the quay wall in Figure 2. Bending properties have been obtained by four-point bending tests from the Overamstel experiments (Hemel, 2023). Another model focused on foundation defects and tried to estimate residual structural capacity under a partly failing foundation (Voortman, 2021). Also, the dynamic effects of traffic loading have been researched (Sharma, Longo, & Messali, 2024).

The Toetskader Amsterdamse Kademuren (TAK), translated from Dutch as Test framework of Amsterdam Quay walls, has been designed to structurally test quay walls on timber foundation piles that are being maintained by the municipality of Amsterdam (Ingenieursbureau Gemeente Amsterdam, 2023) in a uniform manner. Currently, version 3.2 is the most up to date version and version 4 is being developed. The TAK has been designed for the Programma Bruggen en Kademuren (PBK), translated as Program of Bridges and Quay walls, and for the Verkeer & Openbare Ruimte (V&OR), translated as Traffic and Public Space.

When assessing quay walls, an initial archival investigation takes place. Both digital and physical sources are consulted to estimate the geometry of the quays. Furthermore, divers perform an inspection and timber samples are taken to obtain the soft shell. The observations regarding the geometry, material properties and loads form the basis for modelling the quay in Plaxis finite element software and to perform structural verification according to the TAK. These results are the starting point for checking the multiple failure mechanisms.

Figure 2 - Cutaway drawing of historical quay wall structure at Reguliersgracht (Hemel, 2023)

Currently, many life-extension and renewal projects are taking place. The municipality of Amsterdam is not only interested in renewing the quay walls, but also in integrating innovative aspects which could lead to their multifunctionality. Therefore, funding has been awarded to a group of researchers to develop multifunctional quay walls. Studies into extracting geothermal energy (Haasnoot, 2020) from the sheet piles and introducing green vegetation (Mulder, Lubelli, & Dijkhuis, 2023) have already been performed. Although not all additional functionalities have an effect in the structural performance of the quay wall, some have a large one. An example is the thermal energy extraction, for which only a limited number of small pipes is required, thereby limiting the loads. However, if battery packs are to be integrated into the quay wall, this would cause severe gravity loads. Tree loads could have a large impact as well, as they add a large point load due to gravity and even greater horizontal wind loads on the quay wall.

This research therefore aims at to fill the gap of the structural performance of quay walls affected by the loads imposed to the quay wall structure by the additional functionalities. Therefore, initially a traditional quay wall model is created, which is the as built geometry, consisting of a masonry wall on

a timber foundation. The behaviour of the traditional model under standard loading (which reflects the base case load from the TAK of 10 kN/m^2) is modelled with the aid of finite element software and the behaviour verified using different models and analytical checks. The additional loads caused by the multifunctionalities are estimated and used as input for the model. Correspondingly, a sheet pile geometry is implemented under base loading conditions and verified, as well as its reaction to the additional loads. The location of the Marnixkade is selected as the location for the case study. Therefore, this limits the scope to the specific soil conditions at this location.

1.3 Research questions

The main research question is the following:
Multifunctional quay walls: How do a structural configuration of timber-masonry and a steel sheet pile quay wall at the Marnixkade in Amsterdam respond to loads caused by added functionalities when compared to the original behaviour of the structure in a Finite Element Analysis (FEA)?

To answer this question, various preliminary questions are formulated that will guide the way. Those are:

- *What quay wall typologies do currently exist for inner-city quay walls?*
- *What material models and corresponding properties provide an accurate basis for a structural Finite Element model (FE model) of the quay walls?*
- *What are the loads that currently need to be considered when designing a quay wall?*
- *What are the failure mechanisms of quay walls?*

After the preliminary questions are answered, a case study for the Marnixkade is introduced. There, the soil conditions for this specific location are analysed. Furthermore, the specific geometry of the quay wall as built in the Marnixkade, which is referred to in this thesis as the traditional geometry, is explained. Also, a sheet pile geometry is designed. Both geometries are different structural configurations compared in this thesis. Lastly, the additional loads arising from multifunctionalities are explained for the models. With the created FE models, the following questions are answered:

- *What are the structural responses of the traditional timber-masonry quay wall configuration at the Marnixkade under standard loading conditions and when additional functionalities and their corresponding loads are added to the quay wall in a FE model?*
- *What are the structural responses of the sheet pile wall configuration at the Marnixkade under standard loading conditions and when additional functionalities and their corresponding loads are added to the quay wall in a FE model?*

1.4 Research methodology

In the Literature Review, all preliminary questions are answered. Various quay wall geometries as well as their occurrence are explained. Also, the material models for the quay wall structure and its corresponding properties are extensively reviewed, including those of sheet piles. Multiple constitutive models are also elaborated upon. The last part of the Literature Review considers the failure mechanisms of the traditional quay wall and those of sheet pile walls, which is how the structural performance is assessed. After general knowledge of quay walls has been obtained in the Literature Review, the case study of the Marnixkade is introduced in Chapter 3. In this chapter the specific soil conditions are analysed and then simplified to obtain input for the FE models. Thereafter, the specific geometry of the Marnixkade of the traditional (as built) geometry is illustrated. Also, a sheet pile

geometry is designed for this specific location. The last part of this chapter investigates the current and additional loads that could arise from the multifunctionalities.

Using the previously obtained information regarding the soil, geometry, material properties, constitutive models and loads, the FE models are created. Both DIANA and Plaxis FE software are used to model the structural configurations (traditional quay wall and sheet pile) and obtain the structural responses of the quay. The input for the FE models is described in Chapter 4. The Chapter starts with the implementation of the traditional configuration, followed by the model of the sheet pile configuration. For both configurations, first the implementation in DIANA is given followed by Plaxis. The models are explained for the different software in the same manner. Initially, the geometry and materials are described. Secondly, the loads and boundary conditions are listed. Thirdly, the mesh and analysis are explained.

In Chapter 5 the numerical results and verification of the analysis are given, in which the following two sub-questions are answered:

- *What are the structural responses of the traditional timber-masonry quay wall configuration at the Marnixkade under standard loading conditions and when additional functionalities and their corresponding loads are added to the quay wall in a FE model?*
- *What are the structural responses of the sheet pile wall configuration at the Marnixkade under standard loading conditions and when additional functionalities and their corresponding loads are added to the quay wall in a FE model?*

For each of the different load cases arising from the multifunctionalities, the structural responses are measured in terms of cross-sectional shear forces, normal forces and bending moments. Furthermore, the horizontal and total displacements during loading are used. The different loading combinations result in unity checks for the relevant failure mechanisms. The results are then verified using Literature and the comparison between the different software.

The results are discussed in Chapter 6. Since almost no data is available at this location, the output of the FE model of both structural configurations in the different software is compared against each other to verify the results. Furthermore, Literature is used to see if the responses are within the range of reasonable values. Limitations and sources of uncertainty are given. Lastly, in Chapter 7 the final remarks and recommendations for future research are given.

1.5 Structure of this thesis

Initially a Literature Review is performed in Chapter 2. Section 2.1, contains information regarding traditional (as built) quay wall geometries and sheet pile geometries. Thereafter, in section 2.2, the material properties are introduced. In section 2.3, the constitutive models for the FEM are reviewed. Lastly, in section 2.3.3, the failure mechanisms for both traditional and sheet pile structural configurations are given.

In Chapter 3 the Case Study of the Marnixkade is introduced. It demonstrates the soil conditions, modelled structural configurations and multifunctional loads. Chapter 4 illustrates the input in the FE software DIANA and Plaxis for both structural configurations. In Chapter 5 the Numerical Results are given. Chapter 6 contains the Discussion on the results. The final remarks and recommendations for this thesis can be found in Chapter 7.

2 Literature Review

2.1 Quay wall geometries

Multiple quay wall geometries exist in Amsterdam. The traditional quay wall is the type 1 quay wall, which consists of a masonry wall on a timber foundation. Also type 2 quay walls, existing out of a concrete L-wall are often seen. A steel cantilever wall is also used. Other less often used geometries are a constructed slope and a weight wall with a steel foundation. The distribution of these quay walls can be seen in Table 1.

Table 1 - Main quay wall types of Amsterdam (Ingenieursbureau Gemeente Amsterdam, 2023)

Main structural type	Presence (%)
Weight wall based on wooden substructure and piles masonry wall (type 1)	75
Concrete L-wall founded on (wooden, steel, concrete) piles (type 2)	
Sheet pile (steel, plastic, wood, concrete and other)	20
Slope construction	5
Weight wall on steel foundation	<1

Type 1 and sheet pile construction types are discussed. Other geometries are not directly relevant to answer the research questions. Therefore, the type 2 quay wall geometry and three innovative designs of the Innovatiepartnerschap Kademuren (IPK), translated as Innovation partnership Quay Walls) are discussed in Appendix B. This IPK program has been set up to be able to accurately increase the innovative designs of quay walls. The discussed designs are:

- G-force
- Kade 2.020
- Koningsgracht

Since slope constructions and weight walls on a steel foundation have a very low presence, they are not further discussed in this thesis.

2.1.1 Traditional

In Figure 3 a principal cross section of type 1 is shown, which occurs most out of all quay wall types in Amsterdam. It consists of a masonry wall with a capstone, supported by a timber floor on a beam (often named kesp), with timber foundation piles to support the beam. The wall is resisting the soil from sliding into the water and the floor and beams are there to transfer the active soil pressure to the piles. The water level is often at NAP-0.4m and the timber floor at NAP-1.0m (Ingenieursbureau Gemeente Amsterdam, 2023). The most important elements of this quay are discussed.

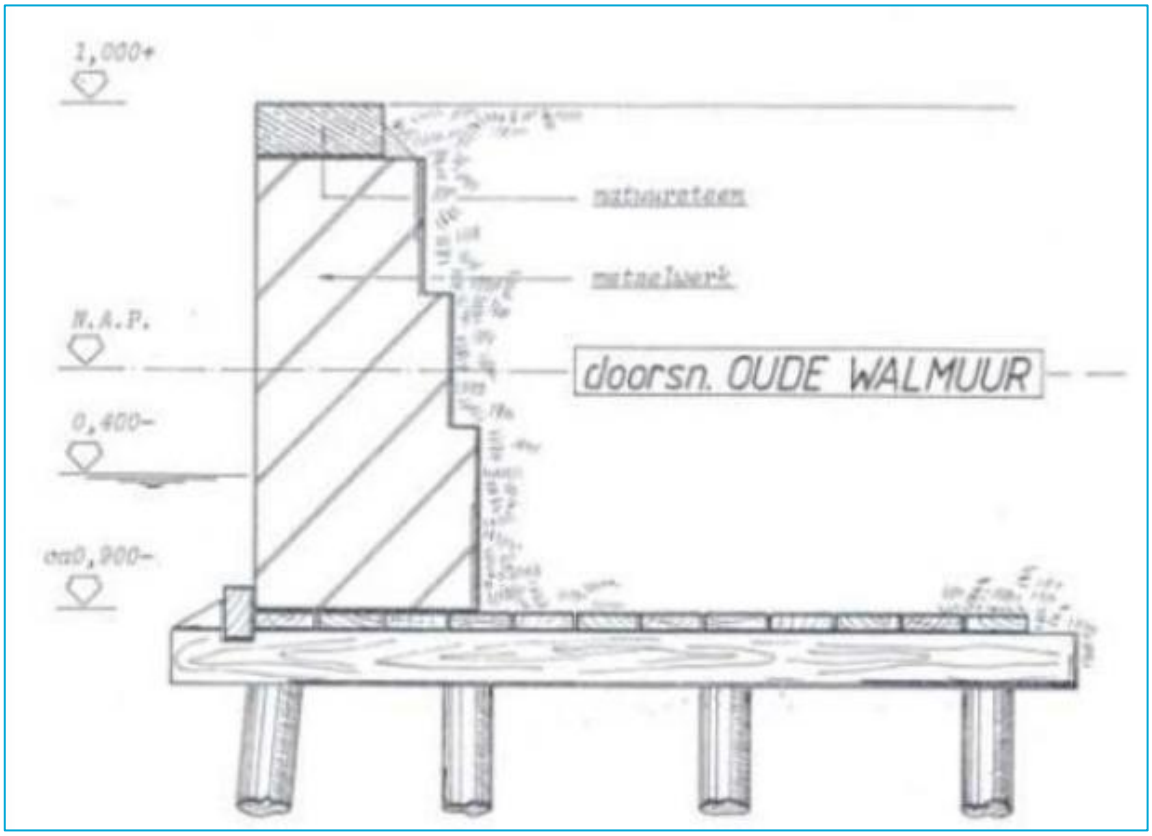

Figure 3 – Cross-section type 1 quay walls (Gemeente Amsterdam, 2023)

<u>Foundation piles</u>

The foundation piles of the type 1 quay walls are made from timber and have a pile tip that reaches till the first sand layer, which is often at approximately NAP-13.0m. When the pile tip is at an unknown depth, it can be assumed that the pile tip is at 0.5m into the first sand layer (Ingenieursbureau Gemeente Amsterdam, 2023). This means that the piles are approximately 12m long.

The timber piles have a circular cross section and are generally tapered from the head of the piles to the pile tip. Often the tapering is unknown, therefore the following guidelines have been constructed. If the head diameter of the timber piles is greater than 250mm, the average taper can be defined from Table 2. If the diameter is smaller than 240mm, a taper of 7.5 mm/m can be assumed (Ingenieursbureau Gemeente Amsterdam, 2023).

Table 2 - Taper of timber piles (Augustzoon, 2022)

Head diameter [mm]	**280**	**270**	**260**	**250**	**240**
Avg taper (11m piles) [mm/m]	11.8	11.4	11	10.6	10.2
Avg taper (16m piles) [mm/m]	10.5	10.1	9.8	9.4	9.1

The diameter (*D*) is of great importance for the capacity of the timber foundation piles. It determines the section modulus, thereby strongly influencing the bending capacity. If the bending capacity of the timber piles is insufficient, this causes lateral failure of the pile foundation, which is the most common and severe failure mechanism observed in Amsterdam's city centre is (Hemel, 2023). Unfortunately, the full diameter often cannot be used as bacterial decay of the piles can cause a soft shell, which provides little strength. More information on the timber material properties can be found in section 2.2.1.

The number of piles is also of great importance to determine the resistance of the quay wall. The piles are always located in rows perpendicular to the canals of 3 or 4 depending on the height of the wall. This relation is given in Table 3. The distance between the piles parallel to the canal should be taken as 1 m when it cannot be derived from diving inspections or archives with drawings (Ingenieursbureau Gemeente Amsterdam, 2023).

Table 3 - Relation number of piles and height of the quay wall (Ingenieursbureau Gemeente Amsterdam, 2023)

Period	**Wall height [m]**	**Piles per kesp**
1880 - 1890	+1.25 à +1.75	3
	+1.75 à +2.5	4
	+2.5 à +3.0	5
	>+3.0	5 à 6
1900 - 1910	+1.5 à +2.25	3
	+2.25 à +3.0	4
	+>3.0	5 à 6

<u>Wall</u>

The wall needs to resist the active soil pressures to prevent the soil from collapsing into the canal. A higher ground level means a higher wall and thus more soil pressures. This causes the walls to be thicker. This relation is visualised in Table 4, which should be used as estimate if diving inspections or archival document don't bring up any results. The wall is fully constructed from masonry (Ingenieursbureau Gemeente Amsterdam, 2023).

Table 4 - Relationship height and thickness of the quay wall (Ingenieursbureau Gemeente Amsterdam, 2023)

Top wall [NAP +/- m]	**Bottom wall [NAP +/- m]**	**Height wall [m]**	**Thickness wall bottom [m]**
+0.40	-0.90	1.30	0.55
+0.70	-0.90	1.60	0.66
+1.00	-0.90	1.90	0.77
+1.30	-0.90	2.20	0.88
+1.70	-0.90	2.60	0.99
+2.00	-0.90	2.90	1.10
+2.30	-0.90	3.20	1.21
+2.60	-0.90	3.50	1.45

2.1.2 Sheet pile

Steel sheet piles have become increasingly popular for constructing inner-city quay walls, thanks to their strength, versatility, and ease of installation. These interlocking vertical steel sections form a continuous wall, ideal for retaining soil and supporting waterfront infrastructure in urban environments. In areas where space is limited, steel sheet piles offer a minimal footprint, making them well-suited for dense, inner-city projects.

In recent years, steel sheet piles have also proven invaluable as emergency structures for stabilizing failing quay walls (Figure 4). Many older quay walls in Amsterdam are deteriorating due to age, increased loading demands, and exposure to harsh environmental conditions. However, a disadvantage of steel sheet piles is that corrosion can also deteriorate the thickness and thus resistance of the section. Steel sheet piles offer a rapid, cost-effective solution for emergency stabilization, preventing further soil erosion and structural collapse. Their fast installation reduces disruption in busy urban areas, ensuring safety and maintaining access to critical waterfronts.

Figure 4 - Temporary sheet pile quay wall (SkyGeo, 2024)

Additionally, their resilience to various soil and water conditions, combined with high resistance to lateral and vertical forces, makes them ideal for long-term and temporary applications. Modern steel sheet piles are often made from recycled materials and can be reused, enhancing their sustainability profile. Their durability and low maintenance further ensure a long service life, making them a reliable choice for both emergency and permanent quay wall solutions.

<u>Design</u>

For sheet piles, two major design choices are to be made, the sheet pile length and the section modulus, which is determined by the steel profile, steel grade and soil conditions. Furthermore, an anchor is often used as this strengthens the wall and therefore can decrease the required embedment depth and section modulus. However, in the case of Amsterdam, anchors are not allowed as they conflict with the foundations of nearby buildings. Therefore, a cantilevered sheet pile is chosen for the design.

The behaviour of the soil is a very important manner for sheet pile design. To determine the lateral (horizontal) stressed on the sheet pile, the vertical effective stresses are required. The effective

vertical stresses (σ') can be calculated by subtracting the pore pressures (p) from the total stresses (σ) (Verruijt, 2001):

$$\sigma' = \sigma - p$$

The total stress can be calculated for a homogeneous soil by multiplying the depth (d) of the layer with the dry density (γ_{dry}) or the saturated density of the soil (γ_{sat}), when the soil is below the water table. The pore pressure can be calculated by multiplying the depth with de density of the water (γ_{wat} = 10 kN/m^2). This calculated in graphically illustrated in Figure 5.

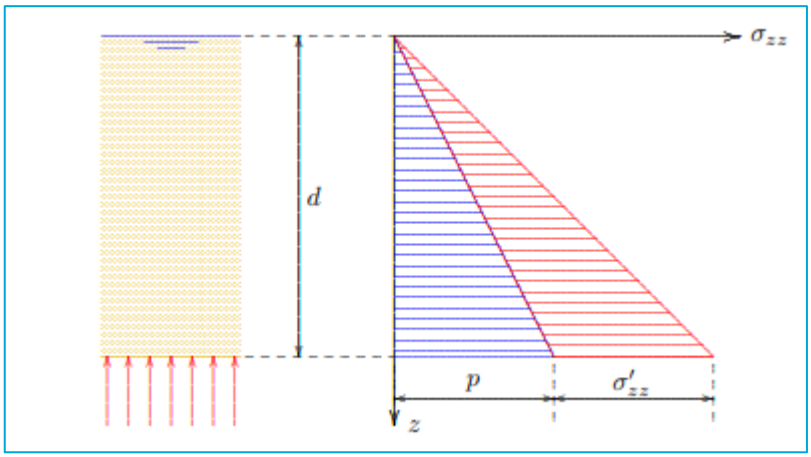

Figure 5 - Stresses in a homogeneous layer (Verruijt, 2001)

By using the coefficients of active (K_a) and passive earth pressure (K_p), the lateral pressures on both side of the sheet pile can be calculated from the effective stresses (Verruijt, 2001). To do this, the friction angle (φ) is used (Kitch W. , 2015):

$$K_a = \frac{1 - \sin\varphi}{1 + \sin\varphi}$$

$$K_p = \frac{1 + \sin\varphi}{1 + \sin\varphi}$$

The sheet pile is assumed to rotate around point O (Figure 6) and thereby creating active and passive zones in the sheet pile. Using the derived active and passive pressures from the effective stresses on both sides and the lateral earth pressure coefficients, the pressures on the sheet pile can be calculated and are illustrated for a general case in Figure 7. There are 2 unknowns that need to be derived, the embedded depth (D) of the sheet pile and the location of point O with respect to the bottom of the sheet pile (L_5), the point where the active zone becomes passive at the right bottom. Fortunately, the sum of horizontal forces and sum of moments give 2 equations, which means the unknowns can be solved for.

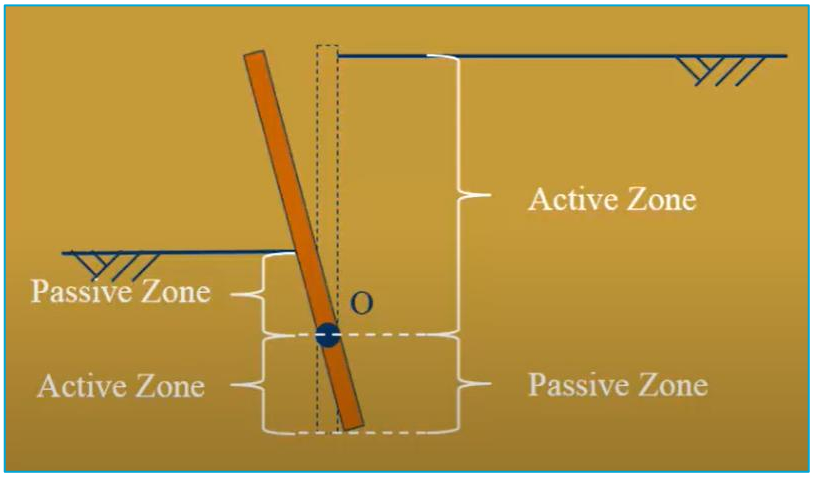

Figure 6 - Cantilever sheet pile: active and passive soil zones (Kitch W. , 2015)

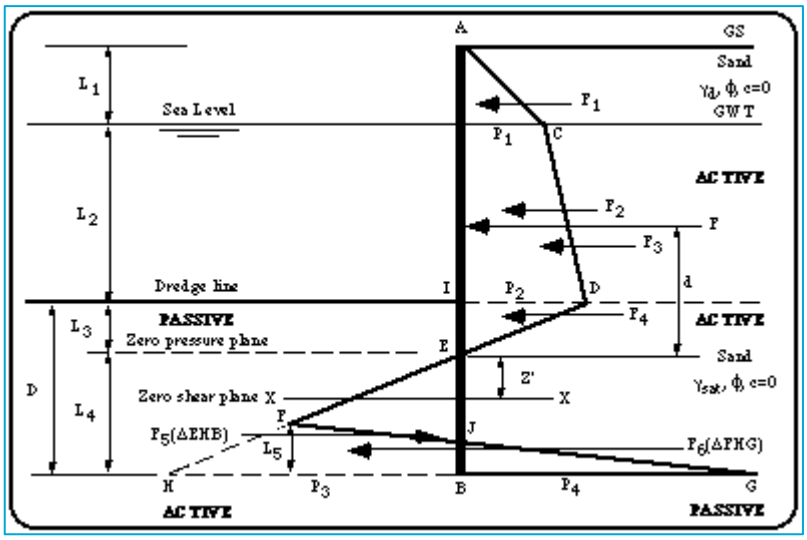

Figure 7 - Equilibrium forces and moments (Ghally, 2025)

With the embedded depth (*D*) known, a Factor of Safety (*FoS*) is often applied to sheet piles ranging from 1.5 to 2. Furthermore, the L_1 and L_2 need to be added to the sheet pile length *L*. This means the total length can be estimated using:

$$L = L_1 + L_2 + FoS * D$$

As the unknowns, L_5 and *D*, are solved, the force distribution in the sheet pile in Figure 7 is fully known. From this force distribution the point of zero shear is calculated from the bottom, which is the location of the maximum bending moment. This moment is calculated from the pressure distribution. The maximum moment enables the selection of a sheet pile profile with a section modulus that can resist the bending moment occurring in the sheet pile. A small section is expected because of the limited retaining height of the sheet pile wall. Limitations of this method is that the horizontal displacements are not considered and those can be severe, especially in clay soils in Amsterdam. Therefore, these should be checked when the section profile is implemented in finite element software.

Another limitation is the fact that this method is normally used for sand soils. Since lateral pressures in the clay over a long period of time approach those for a granular soil (United States Steel, 1984),

such as sand, the long-term condition is thus applied and verified. Initially, clay will require a smaller embedment depth as it offers additional cohesive strength over sand.

2.2 Material properties

2.2.1 Timber

Although many wood species exist, this thesis will focus on spruce wood, since it is the most commons species in quay walls in Amsterdam (van Tussenbroek, 2012). Spruce wood, sourced from various species within the *Picea* genus, is commonly used in foundation piles for quay walls due to its durability and mechanical properties. Quay walls require materials that can withstand heavy loads and constant exposure to moisture. Spruce wood, characterized by its straight grain and high strength-to-weight ratio, is well-suited for this purpose. Its ability to resist compressive forces makes it an ideal material for foundation piles. Additionally, spruce wood's natural resistance to decay in waterlogged environments enhances its longevity these constructions, where durability is crucial. As such, spruce wood's structural integrity and resilience to moisture contribute to its frequent use in quay wall foundations, playing a pivotal role in stabilizing these essential infrastructures.

For reference, the most important properties from softwoods, among which spruce wood have been included in Table 5. "*In the current assessment of quay walls, C24 timber class is used according to the 'CROW / CUR – Recommendation 124 Structural safety of existing bridges and viaducts for local authorities'"* (Hemel, 2023). However, differences in literature exist, as C14 was assumed for pine wood and C30 for the un-sawned round spruce piles to research hidden structural capacity (Voortman, 2021). Other input for Diana was defined as E = 12000 N/mm^2, v = 0.3 and ρ = 350 kg/m^3 (Voortman, 2021). Another study used the strength class C27 (Spannenburg, 2020), based upon an average age of 142.5 years of the Herengracht quay wall piles, which should correspond to a mean Young's Modulus of bending of 11.86 GPa (Kránitz, 2014).

Table 5 - Most important strength classes for softwood based on edgewise bending tests - strength stiffness and density values (EN 338, 2016)

	Class	C16	C18	C24	C27	C30
Strength properties in N/mm^2						
Bending	$f_{m,k}$	**16**	**18**	**24**	**27**	**30**
Tension parallel	$f_{t,0,k}$	**8.5**	**10**	**14.5**	**16.5**	**19**
Tension perpendicular	$f_{t,90,k}$	**0.4**	**0.4**	**0.4**	**0.4**	**0.4**
Compression parallel	$f_{c,0,k}$	**17**	**18**	**21**	**22**	**24**
Compression perpendicular	$f_{c,90,k}$	**2.2**	**2.2**	**2.5**	**2.5**	**2.7**
Shear	$f_{v,k}$	**3.2**	**3.4**	**4.0**	**4.0**	**4.0**
Stiffness properties in kN/mm^2						
Mean modulus of elasticity in parallel bending	$E_{m,0,mean}$	**8.0**	**9.0**	**11.0**	**11.5**	**12.0**
5 percentile modulus of elasticity parallel bending	$E_{m,0,k}$	**5.4**	**6.0**	**7.4**	**7.7**	**8.0**
Mean modulus of elasticity perpendicular	$E_{m,90,mean}$	**0.27**	**0.30**	**0.37**	**0.38**	**0.40**
Mean shear modulus	G_{mean}	**0.50**	**0.56**	**0.69**	**0.72**	**0.75**
Density in kg/m^3						
5 percentile density	ρ_k	**310**	**320**	**350**	**360**	**380**
Mean density	ρ_{mean}	**370**	**380**	**420**	**430**	**460**

Although spruce wood is praised for its longevity, it is not meant to last forever. Therefore, timber piles have decayed, and foundations are thus partly failing, but still, they remain standing due to

redistribution over other piles (Voortman, 2021). The decay of timber piles has been monitored using micro-drilling (Pagella G, 2024) to get insight into the remaining mechanical properties. In this research an algorithm was developed to determine the soft shell, which is assigned to give zero compression strength. Other research investigated the mechanical properties of spruce foundation piles (Pagella, Ravenshorst, Grad, & Van der Kuilen, 2022). Initially the piles were subdivided into categories, old sound for piles with a decay of less than 15% and old decayed for a soft shell between 15% and 65%. The saturated wet compression strength for old sound piles was found to be 13.0 MPa (95% avg.sound cross section)., whereas the old decayed piles had 8.5 MPa remaining (62% avg.sound cross section). It should be noted that the tip showed more decay than the head of the pile. Since, the piles are often tapered, it is found reasonable that the smaller cross-sections of the tips show a larger decay. The modulus elasticity of the wet region ($MOE_{stat,wet}$) was found to be 9340 MPa for old sound piles and 6050 MPa for old decayed piles.

Lateral failure of the timber foundation piles, which is the most severe problem for quay walls, occurs due to the bending properties of timber failing to meet its demands. Two common indicators are the bending modulus of elasticity (E_b) and the modulus of rupture (*MOR*). The *MOR* is often referred to as bending strength f_m [N/mm^2]. The bending modulus of elasticity quantifies a material's resistance to bending deformation. It combines Young's modulus with the object's geometry, reflecting stiffness under bending forces. A higher bending modulus indicates greater rigidity, essential for structural elements to maintain shape and effectively support loads. The *MOR* measures a material's strength at the point of failure under bending stress. *MOR* is commonly used in evaluating brittle materials like ceramics, concrete, and wood to assess their structural capacity under load. Four-point bending tests on Overamstel timber foundation piles were performed from which the mean value of E_b was found to be 16.5 GPa while the *MOR* had a mean value of 23.2 N/mm^2. Also, on average a soft shell of 21 mm was found, with maximum values reaching up to 45 mm (Hemel, 2023).

2.2.2 Masonry

Masonry plays a significant role in the construction of quay walls in Amsterdam, particularly in historic areas. Quay walls, which line the city's numerous canals, traditionally relied on brick or stone masonry to provide stability and durability against water pressure and soil movement. Masonry's high compressive strength made it well-suited for both the horizontal and vertical loads imposed by the weight of the water and soil behind the walls. In Amsterdam, these walls are often constructed with tightly packed brick, laid in patterns that distribute pressure evenly. The masonry has often been laid on top of a mortar layer to solve problems related to an uneven floor. This mortar layer is called 'vlijlaag' in Dutch and can be seen in Figure 8 (Ingenieursbureau Gemeente Amsterdam, 2023).

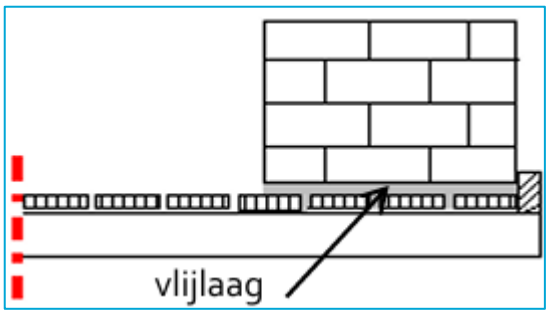

Figure 8 - Masonry wall connected by vlijlaag (Ingenieursbureau Gemeente Amsterdam, 2023)

For new masonry the stones and mortar can be tested according to the Eurocode (EN-1996-1-1, 2019). For existing quay wall structures in Amsterdam, it is often unknown what the properties are of the masonry. Therefore, research is ongoing into the material properties of the masonry, and it is expected that results of the material properties will be published in the TAK 4.0, which is an update of the TAK 3.2 (Ingenieursbureau Gemeente Amsterdam, 2023). For assessing current masonry, the following assumptions should be made (Ingenieursbureau Gemeente Amsterdam, 2023):

- Category II stones should be assumed (EN-1996-1-1, 2019). Partial factors are high according due to great uncertainties of the compression strength not being known as well as the production control system not being verified. Therefore, CC1 gives $\gamma_M = 2.0$ and CC2 gives $\gamma_M = 2.2$ (Ingenieursbureau Gemeente Amsterdam, 2023).
- Brick stones are assumed, which have a perforation volume <25% and a brick compression strength of $f_k = 15.0$ N/mm^2 (Ingenieursbureau Gemeente Amsterdam, 2023).
- Mortar M5 is assumed for new masonry structures, which gives the following properties (NPR 9096-1-1, 2023):
    - Compressive strength: $f_k = 5.0$ N/mm^2
    - Shear strength: $f_{vk0} = 0.20$ N/mm^2
    - Bending strength: $f_{fl,b,k} = 2.0$ N/mm^2
- For the masonry the volumetric weight that needs to be considered is (Ingenieursbureau Gemeente Amsterdam, 2023):
    - $\gamma_{dry} = 20$ kN/m^3
    - $\gamma_{wet} = 23$ kN/m^3
- Poisson's ratio: $\nu = 0.2$ (Ingenieursbureau Gemeente Amsterdam, 2023)

According to the Dutch guidelines, for masonry structures build before 1945, the following should be used (NPR 9998, 2020):

- Youngs modulus: $E_m = 5000$ N/mm^2
- Compressive strength: $f_m = 8.5$ N/mm^2
- Tensile strength: $f_t = \min(f_{t,per};\ f_{t,par}) = \min(0.1; 0.35) = 0.1\ N/mm^2$; as a conservative approach the minimum out of the tensile strength parallel and perpendicular to the ribbon joint is chosen.
- Mode-I tensile fracture energy $G_{f,t} = \min(G_{f,t,per};\ G_{f,t,par}) = \min(10; 35) = 10\ J/m^2$
- Compressive fracture energy $G_{f,c} = 20\ 000\ J/m^2$

2.2.3 Steel

Steel is one of the most versatile and widely used materials in construction and engineering. Among its various applications, steel sheet piles play a crucial role in providing structural support in marine environments, retaining walls, and deep foundation systems. Sheet piling is an effective solution for earth retention and excavation support, offering strength, durability, and ease of installation. Multiple types of sheet pile exist, those are listed below (ArcelorMittal, 2025).

AZ Sections

AZ sections (Figure 9) are widely recognized for their high bending resistance and efficient load distribution. Their Z-shaped profile allows for excellent structural performance, making them ideal for deep foundation systems, marine structures, and cofferdams. The continuous form of AZ piles ensures better integrity and minimizes deflections under heavy loads.

Figure 9 - AZ section (ArcelorMittal, 2025)

U-Type Sections

U-type sheet piles (Figure 10) have a U-shaped profile and are commonly used in retaining walls, trenches, and flood protection structures. They offer superior interlock strength and stiffness, making them effective in applications where stability is critical. U-type sections are often chosen for projects requiring both temporary and permanent structural solutions.

Figure 10 - U-Type section (ArcelorMittal, 2025)

Combined Walls

Combined wall (Figure 11) systems utilize a combination of sheet piles and structural elements such as H-beams or box piles to create high-load-bearing walls. These systems are used in projects requiring enhanced resistance to lateral forces, such as quay walls, breakwaters, and deep excavation projects. Combined walls offer flexibility in design and can be customized to meet specific engineering demands.

Figure 11 - Combined wall (ArcelorMittal, 2025)

Steel Tubes

Steel tubes (Figure 12) are used in conjunction with sheet piles for additional reinforcement in foundation systems. These tubes provide increased rigidity and strength, making them suitable for offshore structures, bridge foundations, and heavy-duty retaining walls. The integration of steel tubes with sheet piles enhances overall load-bearing capacity and stability.

Figure 12 - Steel tube (ArcelorMittal, 2025)

With various profiles available, selecting the right type of sheet pile is essential to meet structural and environmental demands. In many cases, combined walls and steel tubes provide excessive strength for standard applications, making them less suitable for typical retaining structures and excavation supports. Instead, an AZ section or AU section should be chosen based on the requirements of the Marnixkade, which offers a small retaining height. AU-14 offers an elastic section modulus of 1405 cm^3/m, whereas AU-25 offers 2500 cm^3/m (ArcelorMittal, 2025). AZ 14-700 offers an elastic section modulus of 1405 cm^3/m, whereas AZ 52-700 offers 5155 cm^3/m

(ArcelorMittal, 2025). Although the AZ-section offers superior bending resistance, the required section modulus of a small AU-profile is sufficient according to the assumptions made in the design.

Steel grades

S235 is a type of structural steel commonly used in the construction industry. It's part of the European standard EN 10025-2, where the "S" stands for "structural" and the number 235 refers to the minimum yield strength of 235 megapascals (MPa). This makes S235 a relatively low-carbon steel, which gives it good weldability and ease of fabrication. It's typically used in general construction applications, like beams, columns, and frames, as well as in manufacturing structures for bridges and machinery. Because of its relatively low strength compared to higher-grade steels, it's usually chosen for applications where the load demands aren't extreme.

Steel grades that are often used in sheet piles and specified in the Eurocode (NEN-EN 10248-1, 2023) are the following: S240, S270, S320, S355, S390, S430, S460 and S500.

Corrosion

Corrosion is a significant factor affecting the durability and lifespan of steel sheet piles. Exposure to water, oxygen, and chemical contaminants can lead to material degradation, reducing structural integrity over time.

Common types of corrosion in steel sheet piles include (Gibson Stainless & Specialty Inc, 2017):

- Uniform Corrosion: A gradual and even material loss across the steel surface, typically occurring in atmospheric or submerged environments.
- Pitting Corrosion: Localized corrosion that results in small pits or holes in the steel, often caused by chloride exposure in marine conditions.
- Crevice Corrosion: Occurs in confined spaces, such as interlocks, where stagnant water and oxygen deprivation accelerate deterioration.
- Galvanic Corrosion: Happens when two dissimilar metals are in contact in a conductive environment, leading to accelerated corrosion of one metal.

To enhance the longevity of steel sheet piles, various protective measures can be implemented (Cocoon Holland, 2025):

- Design for Durability: Construct the structure to eliminate any risk of corrosion by avoiding narrow gaps or openings where moisture can accumulate. Ensure a maintenance-friendly design for easy inspection and upkeep.
- Use Corrosion-Resistant Materials: Select materials that have high resistance to corrosion or can endure humid conditions without degradation.
- Apply Protective Coatings: When storing steel components for extended periods, use a rust-preventive coating that acts as a barrier against air and moisture, effectively stopping corrosion before it begins.

2.3 Constitutive models within FEM

A constitutive model is necessary in the Finite Element Method (FEM) because it defines the material's behaviour by relating stresses to strains, allowing the simulation to predict how a material deforms under applied loads. While FEM provides a framework for solving equilibrium equations and tracking displacements, it cannot determine internal forces or deformations without knowing how the material responds to stress. The constitutive model fills this gap by characterising material properties such as elasticity and plasticity, ensuring accurate and realistic results based on the physical behaviour of the material being modelled.

In this section, the various constitutive models that can be used for specific materials are expanded upon for the different materials. Thereafter, the final choice for each model is explained.

2.3.1 Constitutive models for soils

Constitutive models are the mathematical representations of soil behaviour under various stress and strain conditions. They are critical in the FEM for simulating realistic soil responses. Many research using different soil models has been performed for different applications (Mouazen & Neményi, 1999) (Genes & Kocak, 2004) (Vakili, Barciaga, Lavasan, & Schanz, 2013).

Various models that exist are:

- Linear Elastic: this is the simplest model and only applicable to small deformations where plastic deformation does not occur.
- Mohr-Coulomb: this method combines elastic deformation with a yield point, after which plastic deformation occurs. It is widely accepted, mathematically simple and its parameters have a clear physical meaning (Labuz & Zang, 2012).
- Drucker-Prager: this is a smooth approximation of the Mohr-Coulomb yield criterion. It excludes the corners in the π-plane (Labuz & Zang, 2012).
- Hardening Soil: The hardening soil model account for gradually increasing deformation with increasing stress (Schanz, Vermeer, & Bonnier, 1999), which makes it very useful for advanced geotechnical designs involving progressive failure. An alternative to this model is the Hardening Soil small strain (HSss) model (Benz, 2007), that has different behaviour at small strains.

Nonlinear models are superior to linear models for modelling soils in quay walls because soil behaviour is inherently nonlinear due to its stress-dependent stiffness, plasticity, and complex failure mechanisms. Linear models assume a constant relationship between stress and strain, which does not capture key soil responses such as strain softening, hardening, and the dependency of stiffness on confinement. Additionally, nonlinear approaches allow for more accurate simulation of soil-structure interaction, crucial in predicting wall displacements, bearing capacity, and potential failure zones. The TAK has selected the Hardening Soil model with small strain (HSss) as the constitutive model that should be used to model a quay wall in Plaxis FE software. Since in this thesis the assumptions of the TAK have been followed to model the quay wall, also the HSss model is selected. The HSss model is particularly effective as it accounts for strain-dependent stiffness degradation, improving the accuracy of deformation predictions in quay walls. In contrast, linear models oversimplify soil behaviour, leading to inaccurate estimations of deformations and stability, which can result in unsafe designs or overly conservative construction.

Hardening Soil with small strain model (HSss)

The original Hardening Soil model assumes elastic unloading and reloading, but soil stiffness decreases nonlinearly with strain. Standard lab tests show stiffness can drop to less than half its initial value at measurable strains. For geotechnical analysis, very small-strain stiffness and its non-linear behaviour must be considered (Figure 13), which is addressed by the Hardening Soil model with small-strain stiffness (Plaxis Material Models Manual, 2025).

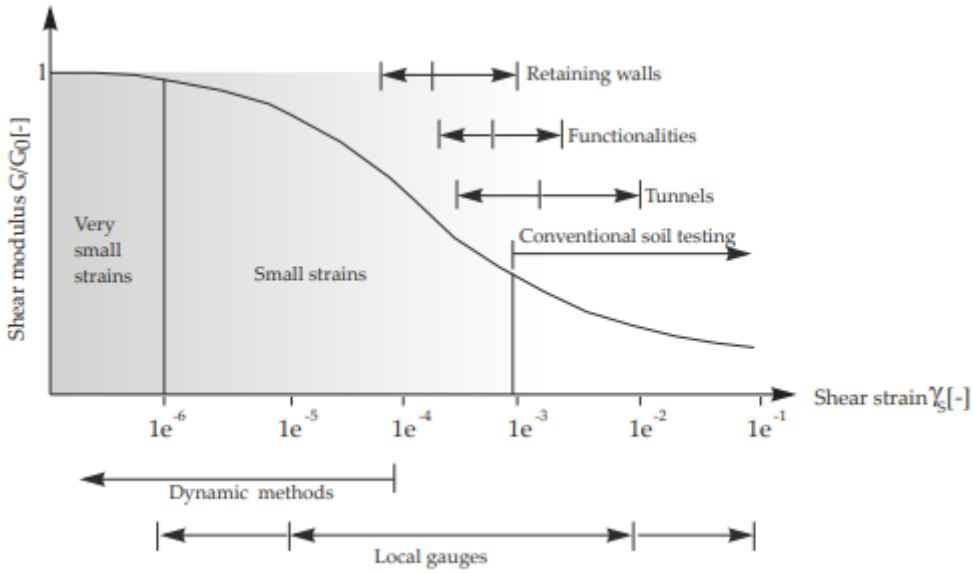

Figure 13 - Characteristic stiffness-strain behaviour of soil with typical strain ranges for laboratory tests and structures (Atkinson & Sallfors, 1991)

The density of the soil can be specified in two different ways, either by specifying the dry (γ_{dry}) and saturated weight (γ_{sat}) or by specifying the dry unit weight and porosity (n). In the latter, the saturated unit weight is obtained from the following equation, where also the density of the water (γ_{water}) should be specified:

$$\gamma_{sat} = \gamma_{dry} + n * \gamma_{water}$$

The specific meaning of these variables is explained below.

- γ_{dry} [kN/m³]: Dry Unit Weight - The weight of soil per unit volume when it is completely dry. which should be used as the soil density for the soil above the waterline.
- γ_{sat} [kN/m³]: Saturated Unit Weight - The weight of soil per unit volume when it is saturated with water, which should be used as the soil density for the soil below the waterline.
- n [-]: Porosity - Porosity is the measure of the void spaces in a material, expressed as a percentage of the total volume, which affects its ability to absorb fluids or allow passage of gases.

Soil parameters that are especially important for the HSss model are the stiffnesses. With increasing strain, the stiffness is increasing, as visualised in Figure 14:

- E_{50}^{ref} [kN/m²]: Secant stiffness in standard drained triaxial test
- E_{oed}^{ref} [kN/m²]: Tangent stiffness for primary oedometer loading
- E_{UR}^{ref} [kN/m²]: Unloading / reloading stiffness from drained triaxial test

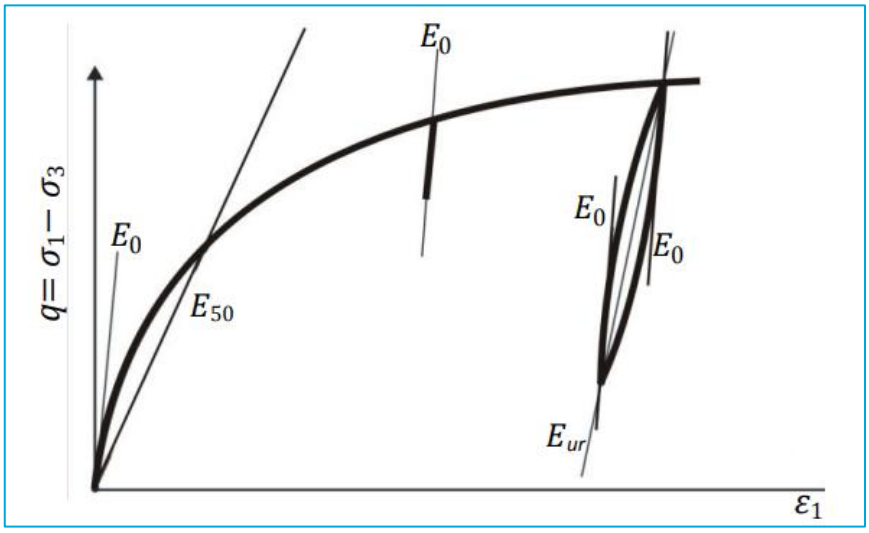

Figure 14 - Stiffness parameters E_{50}, E_{UR}, and $E_0 = 2\ G_0\ (1 + \nu_{UR})$ of the Hardening Soil model with small-strain stiffness in a triaxial test (Plaxis Material Models Manual, 2025)

Other soil parameters are the following:

- *c'* [kPa]: Effective Cohesion - This is the soil's resistance to shearing when external forces are applied. It represents the internal "glue" that helps soil particles stick together. This is visualized in the left image of Figure 15.
- *ϕ'* [°]: Effective Angle of Internal Friction - The measure of soil's ability to resist shearing forces due to internal friction between particles. This is visualized in the left image of Figure 15.
- *ψ'* [°]: Dilatancy Angle - This describes the rate at which the volume of a soil sample changes when it is sheared. Positive dilatancy means the volume increases, and negative means it decreases. This is visualized in the right image of Figure 15.

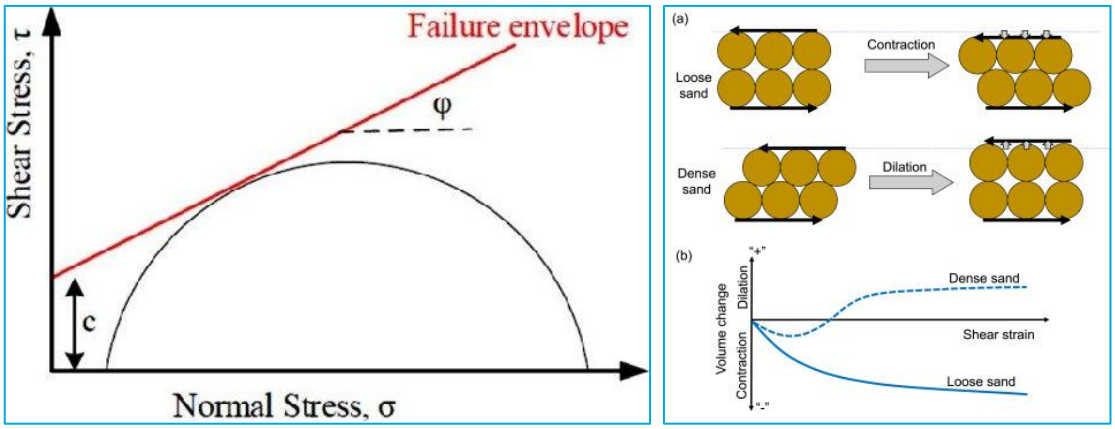

Figure 15 – Left: Friction angle and cohesion (Giwangkara, Mohamed, Nor, Khalid, & Mudiyone, 2020); Right: Dilatancy angle (Tsai, Huang, & Chen, 2023)

- *OCR* [-]: Overconsolidation Ratio - This is the ratio of the maximum effective vertical stress that a soil has experienced in the past to its current effective vertical stress. The OCR indicates soil consolidation history, with values below 1 for normally consolidated soils and above 1 for over-consolidated soils. Factors like past loads, load duration, and soil composition influence OCR. Over-consolidated soils, with higher OCR values, exhibit lower

compressibility, greater shear strength, and reduced susceptibility to settlement (VJ Tech, 2023).

- $R_f = q_f/q_a$ [-]: Failure ratio - Ratio of ultimate load (q_f) to allowable load (q_a). It indicates the factor of safety in geotechnical design. A higher ratio suggests a more conservative design, ensuring stability, while a lower ratio may indicate a design closer to failure conditions. The default of both DIANA and Plaxis is 0.9 (Plaxis Material Models Manual, 2025).
- p_{ref} [kPa]: Reference pressure – For soil stiffness and hardening characteristics to be accurately compared, a reference pressure must be established. Often the value of 100 kPa (equal to 0.1 N/mm^2) is used.
- K_0^{nc} [-]: Coefficient of earth pressure at rest for normally consolidated soil - Refers to the ratio of horizontal stress to vertical stress in a soil at rest. Can be calculated from the friction angle with: $K_0 = 1 - \sin(\varphi)$ (DIANA User Manual, 2025).
- γ_7^{ref} [10^{-4}]: Threshold shear strain at which: $G_s = 0.722 * G_0$. This value is significant in soil mechanics because it marks the strain level beyond which nonlinearity in soil behaviour becomes more pronounced, meaning the stiffness of the soil starts to decrease more rapidly with increasing strain.
- G_0^{ref} [kN/m²]: Reference shear modulus at very small strains ($\varepsilon < 10^{-6}$)
- m [-]: Stress Dependency Parameter - A dimensionless parameter that defines the stress dependency of the soil's stiffness.

The parameter m ensures that the shear modulus G_0 is stress dependent by means of the following equation (Plaxis Material Models Manual, 2025):

$$G_0 = G_0^{ref}\left(\frac{c\cos(\varphi) - \sin(\varphi)}{c\cos(\varphi) + p^{ref}\sin(\varphi)}\right)^m$$

2.3.2 Constitutive models for masonry

Modelling masonry structures with the FEM involves choosing between several strategies that vary in complexity and computational demand. Broadly, these can be categorized into micro-modelling, where individual units and mortar joints are explicitly represented; macro-modelling, where masonry is treated as a homogeneous continuum; and meso-modelling, which blends aspects of both. While micro-models offer high fidelity by capturing discrete behaviour such as joint sliding and block-mortar interaction, they are computationally expensive and often impractical for large-scale structures. Macro or continuum-based approaches, on the other hand, trade detail for efficiency and are widely used in structural analysis of masonry buildings, especially at the global scale.

Although masonry is inherently a heterogeneous and discontinuous material, it is often idealized as a homogeneous continuum to simplify numerical modelling. This simplification is justified when the scale of interest is significantly larger than the size of individual bricks or blocks, and when the objective is to capture the overall structural response rather than localized failure mechanisms. This is the case for the quay wall. In such cases, the discrete components of masonry are "smeared" into a continuous medium with averaged mechanical properties. Nonlinear behaviour, including cracking and crushing, are then represented through constitutive models embedded in the continuum formulation.

The simplest models that can be used assume *Linear Isotropic Elasticity* or *Orthotropic Elasticity* (DIANA User Manual, 2025). An isotropic model assumes material properties are the same in all directions, while an orthotropic model accounts for different properties along three mutually

perpendicular directions. Among the various constitutive models available for this type of continuum representation, this thesis focuses exclusively on the Total Strain Crack Model (TSCM) in DIANA. The TSCM is a smeared crack model used in finite element analysis to simulate the nonlinear behaviour of brittle materials like masonry under different loading conditions. In this model, masonry is treated as a single homogeneous material with averaged properties, meaning that the individual characteristics of bricks and mortar are not explicitly modelled but represented collectively. This approach is adopted in this thesis using the DIANA FEA software (DIANA User Manual, 2025).

The TSCM assumes isotropic material behaviour, meaning mechanical properties are identical in all directions. It is based on the concept of total strain, where stresses are evaluated as a direct function of strain, following a hypo-elastic formulation. The model calculates stress-strain responses in the principal strain directions, a method referred to as the rotating crack model, where the crack orientation evolves with changes in the strain field. This makes the model particularly effective for simulating tensile crack initiation and propagation in masonry structures.

In terms of failure mechanisms, the TSCM primarily captures mode-I tensile failure, which involves crack opening due to normal tensile stresses. However, it does not inherently account for mode-II shear failure, associated with sliding along cracks under shear stresses. As such, while the TSCM is well-suited for modelling cracking due to tensile loads, it may have limitations in scenarios where shear-dominated behaviour is significant. This trade-off is considered acceptable in this work, given the focus on tensile cracking as the dominant mode in the masonry structures under investigation.

In this thesis for tension a linear crack energy curve is used and is implemented according to the models used in earlier research intro traffic loads on quays (Longo, Sharma, & Messali, 2024) in DIANA. For compression these properties (NPR 9998, 2020) have been implemented, which follow a parabolic compression curve visualized in Figure 16. The crack bandwidth is specified to Govindjee. “In Govindjee's projection method, the crack bandwidth *h* is considered as the projected length of the element containing the crack on to the crack plane. Therefore, in addition to element size this method also considers of the element aspect ratio and crack orientation” (DIANA User Manual, 2025). In Plaxis this model is not possible, and therefore a linear elastic model is assumed. Cracking is verified not to occur in DIANA in section 5.1.3, which allows for the implementation of the linear elastic model.

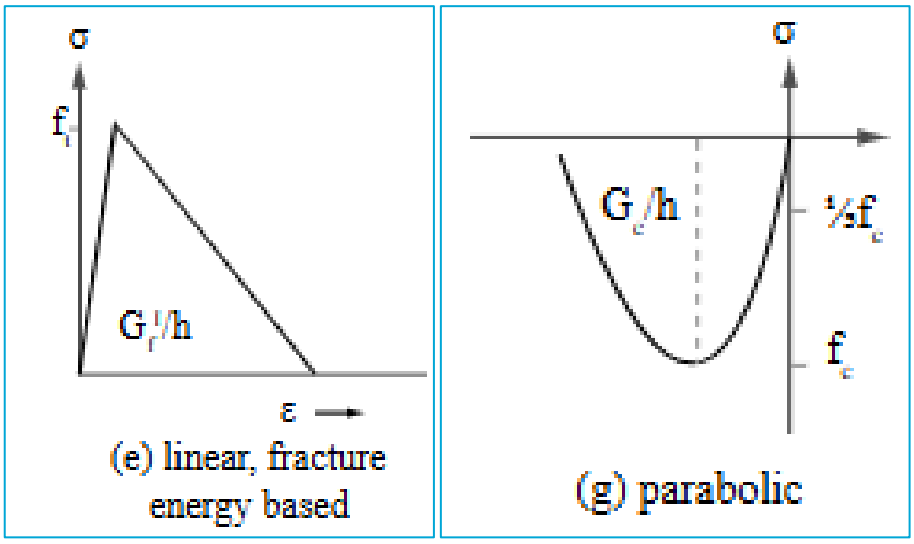

Figure 16 - TSCRM model tensile curve (left) and compressive curve (right) (DIANA User Manual, 2025)

2.3.3 Constitutive models for timber

Timber is an anisotropic material, meaning its mechanical properties vary depending on the direction of the applied load. This anisotropy arises from the fibrous, layered structure of wood, where the fibres run primarily in the longitudinal direction (along the grain), while the radial and tangential directions reflect the growth patterns of the tree. The resulting differences in stiffness, strength, and deformation behaviour across these directions are significant and must be considered when modelling timber for structural applications. For instance, timber is much stronger and stiffer along the grain (longitudinal direction) compared to perpendicular to the grain (radial and tangential directions), leading to distinctly different responses under load depending on the orientation of the grain relative to the applied forces.

The *Linear Elastic Isotropic* model assumes uniform material properties in all directions, meaning the material behaves the same regardless of loading direction. While this simplification can be useful for rough estimates or when directional effects are negligible, it does not fully capture timber's inherent anisotropy. However, for many structural applications, the isotropic model is often sufficient, especially when the behaviour of the overall structure is the focus and finer directional variations are less critical.

In contrast, when a more detailed representation of timber's directional properties is needed, a *Linear Orthotropic* model can be used. This model accounts for the different mechanical properties in the longitudinal, radial, and tangential directions and reflects the distinct elastic moduli and Poisson's ratios in each direction. While more complex, it provides a more accurate response under load, especially for cases where the loading direction aligns with the grain.

In this thesis for both DIANA and Plaxis a *Linear Elastic Isotropic* model is used, where the stiffness (and for the unity check strength) parallel to the grain is employed, which is much stiffer than perpendicular to the grain as mentioned above. Therefore, the stiffness perpendicular to the piles is overestimated, but since the stresses parallel to the piles (and grain) are governing this simplification is justified.

2.3.4 Constitutive models for steel

The FE modelling of steel sheet piles can utilize various constitutive models in DIANA depending on the complexity of the analysis. The *Linear Elastic Isotropic* model assumes uniform material properties in all directions and is widely used for elastic behaviour within service loads. The *Orthotropic Elasticity* model accounts for directional stiffness, but is typically unnecessary for steel sheet piles, which are generally isotropic; it is mainly relevant in research contexts for orthotropic steel decks (Kallitsas, 2016). The *Fraction Model*, potentially representing time-dependent or viscoelastic behaviour (Besseling, 1958), is not useful for the scope of this thesis. The *Direct Stiffness Matrix for Shells* is a numerical formulation essential when modelling sheet piles as shell elements; however, it cannot be used in plane strain. The *Von Mises and Tresca Plasticity* models enable plastic deformation analysis under yield conditions, but are not necessary in this case, as the sheet pile remains in the elastic phase. The *Modified Two-Surface Model* is a plasticity model capable of capturing complex material behaviour under cyclic loading, but it is considered too complex for the current scope. The *Simple Stress Model* is not used as there is not a no tension or no compression condition. For the current application focusing on service-level behaviour, the *Linear Elastic Isotropic* model is chosen due to its simplicity and sufficient accuracy and is employed in both Plaxis and DIANA.

2.4 Failure mechanisms

In this section initially the failure mechanisms of the traditional quay wall are considered. Secondly, the failure mechanisms of the sheet pile are considered.

2.4.1 Traditional failure mechanisms

The different failure mechanisms for the traditional geometry will be described below and follow the recommendations provided by the TAK (Ingenieursbureau Gemeente Amsterdam, 2023). The following failure mechanisms are considered in this thesis:

- Failure of the piles
- Horizontal movement of the structure

Other failure mechanisms that are not considered and are described in Appendix C. Those are:

- Geotechnical bearing capacity
- Sliding of the wall
- Tilting of the masonry wall
- Failure of the structural wall
- Failure of the general stability
- Structural failure of the floor
- Absence or failure of the underwater screen

<u>Failure of the piles</u>

Timber foundation piles should be tested according to the Eurocode (NEN 8707, 2018) for the normal force and a combination of bending and shear. Both verifications are shown.

Normal force

Timber has very different properties the direction parallel and perpendicular to the grain. The normal force acts in the direction of the piles, which is parallel to the grain, therefore the compressive stresses should be checked according to the following formula:

$$UC_c = \frac{\sigma_{c,0,d}}{f_{c,0,d}} \leq 1.0$$

For these combinations $f_{c,0,d}$ can be determined using:

$$f_{c,0,d} = k_{mod} * \frac{f_{c,0,k}}{\gamma_M}$$

Where:

- $f_{c,0,k} = 21\ N/mm^2$ for C24 timber (EN 338, 2016)
- γ_M = 1.3 for sawn timber sections (EN 1995-1-1, 2011)
- $k_{mod} = 0.7$ (EN 1995-1-1, 2011)

$$f_{c,0,d} = k_{mod} * \frac{f_{c,0,k}}{\gamma_M} = 0.7 * \frac{21}{1.3} = 12.6$$

The compressive stress can be calculated by dividing the normal force acting on the pile by the area of the pile.

$$A_{pile} = \frac{1}{4}\pi D_{pile}^2$$

$$\sigma_{c,o,d} = \frac{N_d}{A_{pile}}$$

Tension is not verified, as it is not observed in the piles.

Shear

Shear should be checked according to:

$$UC_s = \frac{\tau_d}{f_{v,d}} \leq 1.0$$

The resisting stress against shear can be calculated using (EN 1995-1-1, 2011):

$$f_{v,d} = k_{mod} * \frac{f_{v,k}}{\gamma_M}$$

By using:

$f_{v,k} = 4\ N/mm^2$ for C24 timber (EN 338, 2016)

$$f_{v,d} = k_{mod} * \frac{f_{v,k}}{\gamma_M} = 0.7 * \frac{4}{1.3} = 2.15\ N/mm^2$$

The shear stress in the circular piles can be calculated using:

$$\tau_d = \frac{4 * V}{3 * A_{pile}}$$

Bending in x- or y-direction

The unity check for bending can be performed using:

$$UC_{m,y} = \frac{\sigma_{m,y,,d}}{f_{m,y,d}} \leq 1.0$$

$$UC_{m,z} = \frac{\sigma_{m,z,,d}}{f_{m,z,d}} \leq 1.0$$

The bending stresses can be obtained by using the section modulus in the following formula:

$$W_y = W_z = \frac{\pi D_{pile}^3}{32}$$

$$\sigma_{m,y,d} = \frac{M_y}{W_y}$$

$$\sigma_{m,z,d} = \frac{M_z}{W_z}$$

The resisting stress against bending can be calculated using:

$$f_{m,y,d} = k_{mod} * k_{h,y} * \frac{f_{m,k}}{\gamma_M}$$

$$f_{m,z,d} = k_{mod} * k_{h,z} * \frac{f_{m,k}}{\gamma_M}$$

By using:

- $k_{h,y} = k_{h,z} = k_m = 1.0$ in the case of timber piles (EN 1995-1-1, 2011)
- $f_{m,k} = 24\ N/mm^2$ (EN 338, 2016)

$$f_{m,y,d} = f_{m,z,d} = 0.7 * 1.0 * \frac{24}{1.3} = 12.92\ N/mm^2$$

The following combinations should be checked for bending and axial forces (Ingenieursbureau Gemeente Amsterdam, 2023):

- Bending combined (EN 1995-1-1, 2011):

$$UC_{m,y,m} = \frac{\sigma_{m,y,d}}{f_{m,y,d}} + k_m \frac{\sigma_{m,z,d}}{f_{m,z,c}} \leq 1.0$$

$$UC_{m,m,z} = k_m \frac{\sigma_{m,y,d}}{f_{m,y,d}} + \frac{\sigma_{m,z,d}}{f_{m,z,c}} \leq 1.0$$

$k_m = 1.0$ in the case of timber piles (EN 1995-1-1, 2011)

This mechanism can be disregarded as in the plane strain model no bending in the y-direction occurs.

- Bending and tension combined (EN 1995-1-1, 2011):

$$UC_{t,m,y,m} = \frac{\sigma_{t,0,d}}{f_{t,0,d}} + \frac{\sigma_{m,y,d}}{f_{m,y,d}} + k_m \frac{\sigma_{m,z,d}}{f_{m,z,d}} \leq 1.0$$
$$UC_{t,m,m,z} = \frac{\sigma_{t,0,d}}{f_{t,0,d}} + k_m \frac{\sigma_{m,y,d}}{f_{m,y,d}} + \frac{\sigma_{m,z,d}}{f_{m,z,d}} \leq 1.0$$

This mechanism can be disregarded as tension is not observed.

- Bending and compression combined (EN 1995-1-1, 2011):

$$UC_{c,m,y,m} = \frac{\sigma_{c,0,d}}{f_{c,0,d}} + \frac{\sigma_{m,y,d}}{f_{m,y,d}} + k_m \frac{\sigma_{m,z,d}}{f_{m,z,d}} \leq 1.0$$
$$UC_{c,m,,m,z} = \frac{\sigma_{c,0,d}}{f_{c,0,d}} + k_m \frac{\sigma_{m,y,d}}{f_{m,y,d}} + \frac{\sigma_{m,z,d}}{f_{m,z,d}} \leq 1.0$$

The unity checks for these combinations will result in the same result, as k_m = 1.0. Since bending in the y-direction cannot occur, this combination can be simplified to the following combination:

$$UC_{c,m} = \frac{\sigma_{c,0,d}}{f_{c,0,d}} + \frac{\sigma_{m,z,d}}{f_{m,z,d}} \leq 1.0$$

Failure of the piles is shown in Figure 17.

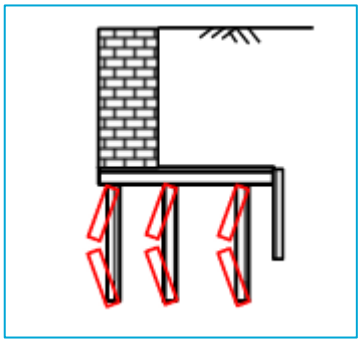

Figure 17 - Failure of the piles (Ingenieursbureau Gemeente Amsterdam, 2023)

<u>Horizontal movement of the structure</u>

Horizontal movement in the serviceability limit state should be checked (Figure 18 - Horizontal movement of the structure). For existing quay walls, only the additional displacements should be checked from the current point in time to the end of life. Three criteria should be verified (Ingenieursbureau Gemeente Amsterdam, 2023):

- Functionality: it is expected that the quay wall will fail before the functionality is lost, therefore a limit of 50 mm of horizontal displacement of the capstone is set.
- Aesthetics: this is not considered since the quay walls are already deformed
- Unacceptable displacement surrounding structures: since in Amsterdam most walls are at more than 7m from the quay wall and founded on their own piles, this may be neglected. Additionally, brittle pipes and cables should be checked, they have a limited displacement of 10mm. Ductile pipes and cables have a limited displacement of 50mm.

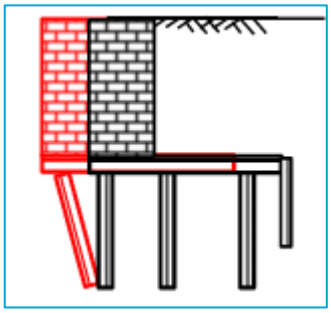

Figure 18 - Horizontal movement of the structure (Ingenieursbureau Gemeente Amsterdam, 2023)

Comparison checks with dissertation Hemel (Hemel, 2023)
It is important to compare various sources. Figure 19 shows possible failure modes of a conventional quay wall model on timber piles. These failure modes are compared to those of the TAK3.2, to check similarities.

The first failure mode; global stability is also described in TAK as failure of the general stability. The second failure mode is overturning or sliding of the masonry wall which is separated in the TAK. The axial bearing capacity is like the general bearing capacity of the TAK. The headstock or floor failure is separated in the TAK. In his research, Hemel focused on lateral failure of the pile foundation, which is related to the failure of the piles. The pile kesp connection is still being developed and therefore not described in the TAK as a failure mechanism. The fact that the failure modes overlap is expected, since Hemel, M. also collaborated with the Ingenieursbureau of Amsterdam to develop the TAK.

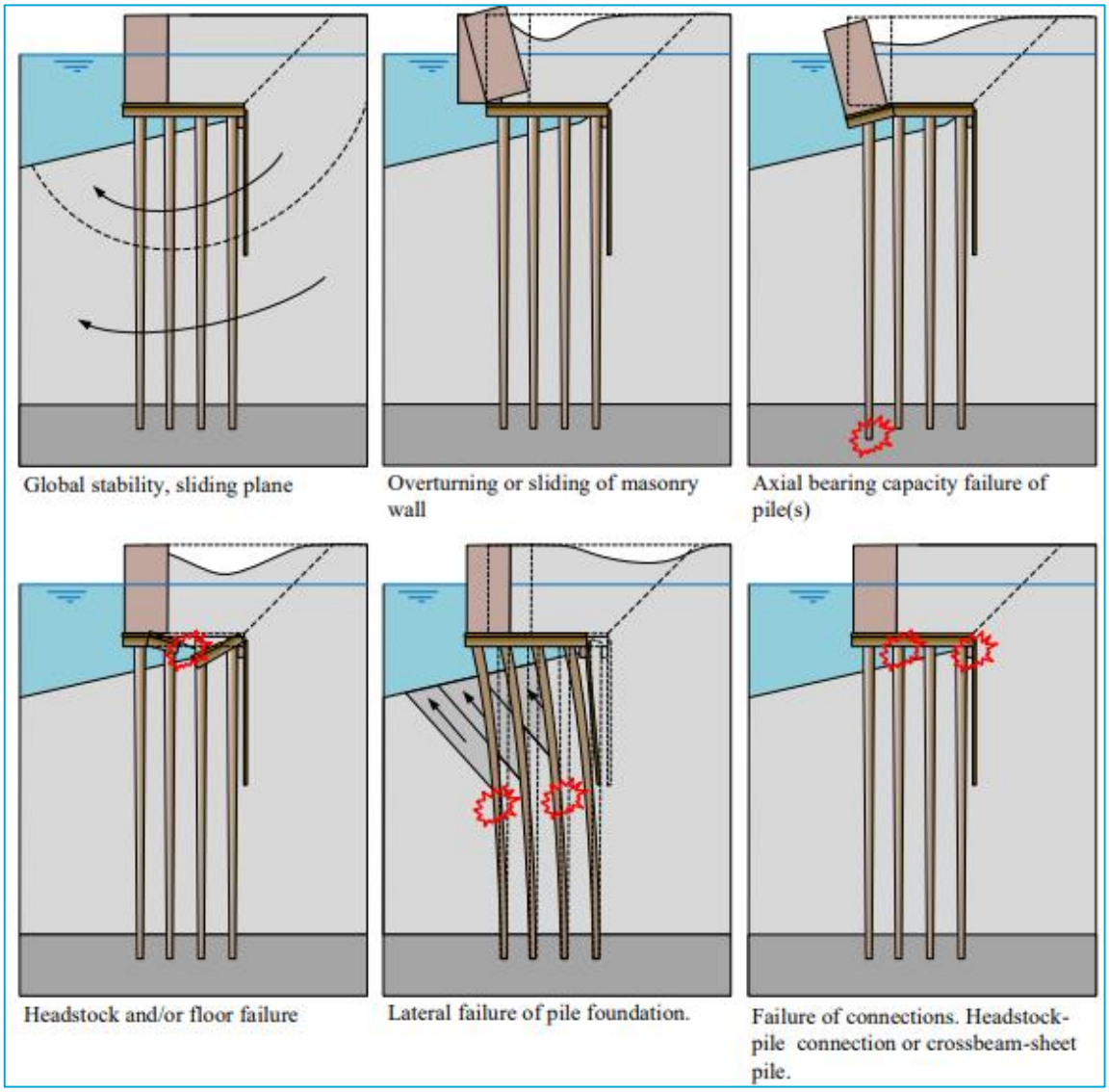

Figure 19 - Failure modes foundation (Hemel, 2023)

2.4.2 Sheet pile failure mechanisms

According to the Eurocode (EN 1993-5, 2008) several ultimate and serviceability limit states should be verified when a sheet pile, which acts as a retaining wall, is designed.

Ultimate limit state criteria

The following ultimate limit state criteria shall be considered (EN 1993-5, 2008):

- Failure of the construction by failure in the soil (the soil resistance is exceeded)
- Structural failure
- Combination of failure in the soil and structural failure.

For retaining walls (EN 1993-5, 2008):

- Failure due to bending and/or axial force
- Failure due to overall flexural buckling, taking account of the restraint provided by the soil
- Local buckling due to overall bending
- Local failure at points of load application (e.g. web crippling)
- Fatigue

Serviceability limit state criteria

For retaining walls (EN 1993-5, 2008):

- Deformation limits necessary to suit the serviceability of the retaining wall itself
- Limits to horizontal displacements, vertical settlements or vibrations, necessary to suit structures directly connected to, or adjacent to, the retaining wall itself.

The scope of this thesis is structural engineering and therefore, the structural effects in the ultimate limit state are considered and other failure mechanisms are left out of scope. The steps for the cross-section checks will now be explained. Initially, the cross-section is classified. Then, the individual contributions of bending, shear and normal forces can be checked. It is important to also check for the interaction of bending and shear as well as bending and a normal force. The final check is bending, shear and axial force combined. It is important to note that corrosion is not considered.

Furthermore, in the serviceability limit state the deformations are reflected upon. According to the Eurocode (EN 1997-1, 2005) for the deformation it should hold that: “A limiting value for a particular deformation is the value at which a serviceability limit state, such as unacceptable cracking or jamming of doors, is deemed to occur in the supported structure. This limiting value shall be agreed during the design of the supported structure.”

Classification

The classification can be made upon Table 5-1: Classification of cross-sections from the Eurocode (EN 1993-5, 2008). If the height of the cross section, the thickness of the flanges and the steel grade are known, then the cross section can be classified. The dimensions pf Z-piles and U-piles are given in Figure 20.

With the steel grade, ε can be determined using the equation below:

$$\varepsilon = \sqrt{\frac{235}{f_y}}$$

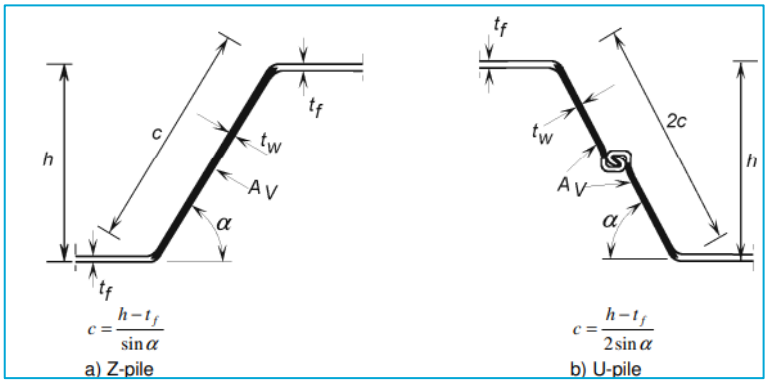

Figure 20 - Cross-section dimensions sheet piles (EN 1993-5, 2008)

This can now be used to check whether it should belong to class 1, 2 or 3. For class 1 (additional rotational check should be carried out) and 2 the following should hold for U-profiles:

$$\frac{b/t_f}{\varepsilon} \leq 37$$

For class 3 the following should hold (again for U-profiles):

$$\frac{b/t_f}{\varepsilon} \leq 49$$

<u>Bending</u>

The design moment resistance of the cross-section $M_{c,Rd}$ does depend on the classification (EN 1993-5, 2008).

$$\text{Class 1 or 2: } M_{c,Rd} = \frac{\beta_B * W_{Pl} * f_y}{\gamma_{M0}}$$

$$\text{Class 3: } M_{c,Rd} = \frac{\beta_B * W_{El} * f_y}{\gamma_{M0}}$$

Here β_B is a factor that takes account of a possible lack of shear force transmission in the interlocks and is smaller or equal to 1. The unity check can be calculated to check the cross-section.

$$UC_{bending} = \frac{M_{Ed}}{M_{c,Rd}}$$

<u>Shear</u>

The plastic shear resistance of each web is given by (EN 1993-5, 2008):

$$V_{Pl,Rd} = \frac{A_v f_y}{\sqrt{3}\gamma_{M0}}$$

A_v is the projected shear area for each web, which is:

$$A_v = t_w(h - t_f)$$

The unity check can be calculated to check the cross-section:

$$UC_{shear,force} = \frac{V_{Ed}}{V_{Pl,Rd}}$$

<u>Normal force</u>

The plastic design resistance of the cross-section is given by (EN 1993-5, 2008):

$$N_{Pl,Rd} = \frac{A * f_y}{\gamma_{M0}}$$

The unity check can be calculated to check the cross-section:

$$UC_{normal,force} = \frac{N_{Ed}}{N_{Pl,Rd}}$$

Bending and shear

When bending and shear coincide, initially the relative shear force needs to be considered. If the acting shear force (V_{Ed}) is not exceeding 50% of the resistance ($V_{Pl,Rd}$), the design bending moment resistance ($M_{c,Rd}$) does not have to be reduced. If V_{Ed} does exceed 50% of $V_{Pl,Rd}$, the shear force should be reduced to $M_{V,Rd}$ (EN 1993-5, 2008).

$$M_{v,Rd} = [\beta_B W_{Pl} - \frac{\rho A_v^2}{4t_w \sin(\alpha)}] \frac{f_y}{\gamma_{M0}}$$

Where:

$$\rho = (2\ V_{Ed}/V_{Pl,Rd} - 1)^2$$

Bending and normal force

The effects of the normal force on the bending moment resistance does not have to be considered for U-profiles if the relative normal force is small enough, depending on the cross-section class (EN 1993-5, 2008).

Class 1 and 2: $\frac{N_{Ed}}{N_{Pl,Rd}} \leq 0.25$

Class 3: $\frac{N_{Ed}}{N_{Pl,Rd}} \leq 0.1$

If the threshold defined above is not met, the design bending moment resistance should be reduced to $M_{N,Rd}$ to allow the axial force to be taken by the cross-section.

Class 1 and 2: $M_{N,Rd} = 1.33\, M_{c,Rd}(1 - N_{Ed}/N_{Pl,Rd})$ but $M_{N,Rd} \leq M_{c,Rd}$

Class 3: $M_{N,Rd} = M_{c,Rd}(1 - N_{Ed}/N_{Pl,Rd})$ but $M_{N,Rd} \leq M_{c,Rd}$

3 Case Study

The Marnixkade has been chosen as the case study for this thesis, since it is the location where the test beds of the redesigned multifunctional quay walls are going to take place. Sections A, B and D (see Figure 21) from the Marnixkade should be completely renewed according to the municipality documents (Gemeente Amsterdam, 2023). To narrow down the location even further, a choice must be made between A, B and D. Since location A is in a corner, the plane strain assumption for modelling is not valid for this location, therefore this location is eliminated. Also, location D is not preferred as it is also closer to a corner, thereby prone to collapse due to ships using additional throttle to make a turn, which caused the Grimburgwal to collapse (Korff, Hemel, & Peters, 2022). Therefore, location B is selected for the case study.

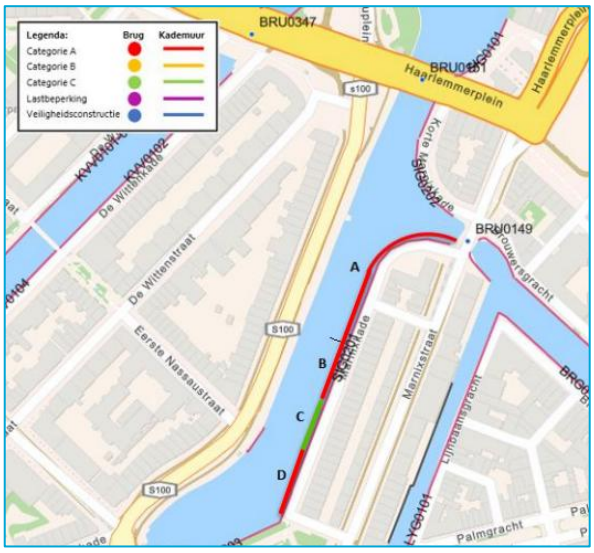

Figure 21 - SIG0201 (Gemeente Amsterdam, 2023)

In this Chapter the soil conditions are first investigated. Thereafter, the layout of the traditional (as built) geometry is demonstrated in more detail. Correspondingly, a design for the sheet pile is made. The last section contains information on the current and future multifunctional loads and load cases.

3.1 Soil investigation

Since the soil layers and corresponding properties are of the utmost importance for the design of quay walls, the soil conditions are extensively researched in this section. DINOloket has a lot of data on the soils in the Netherlands, therefore this is the first source that is considered. Secondly, Lankelma Geotechnisch Adviesbureau has performed cone penetration tests, which results are also investigated. In the third subsection, a new layering technique is introduced based on the available CPT data. Fourthly, available data on soil properties from the Overamstel experiments and TAK is introduced, and it is explained how the simplified soil layer system properties are obtained, for which a trade-off between accuracy and simplicity is made.

3.1.1 DINOloket

At the Marnixkade, soil investigation has been conducted (Figure 22). Two types of site investigations have been conducted, those are geotechnical drilling investigations and geotechnical cone penetration testing. Those types are explained below

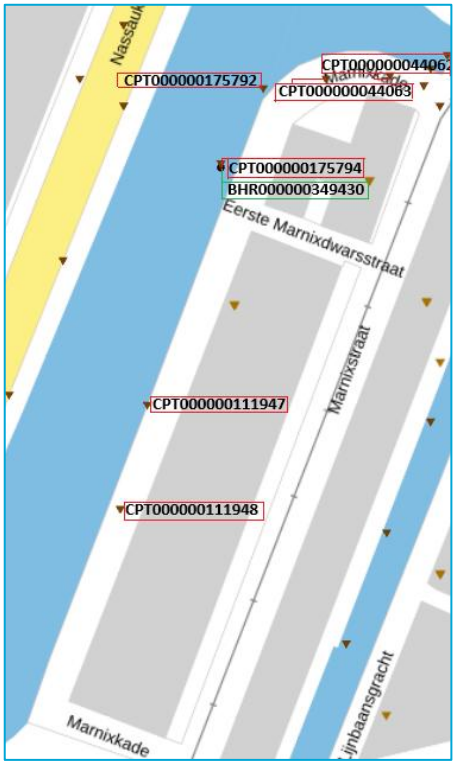

Figure 22 - DINOloket soil investigations (DINOloket, 2024)

Geotechnical Drilling Investigation

In a geotechnical borehole sample description (BHR-GT-BMB), the composition of the soil is described. In geotechnical borehole sample analyses (BHR-GT-BMA), a geological borehole sample is analysed. Together, they form the geotechnical drilling investigation. Agreements have been made within the BRO (Basisregistratie Ondergrond - Dutch Subsurface Registry) regarding the conditions (standards and protocols) that geotechnical drilling investigations must comply with (DINOloket, 2024).

Geotechnical Borehole Sample Analysis

This analysis involves the following determinations:

- Water content
- Organic matter content
- Lime content
- Bulk density
- Bulk density of solid particles
- Grain size distribution

- Undrained shear strength
- Settlement properties
- Consistency limits
- Shear stress development under load
- Shear strength at horizontal deformation
- Saturated permeability

Geotechnical cone penetration testing

During geotechnical cone penetration testing, the resistance encountered by the cone (a cone-shaped point on a penetration rod) as it moves downward is measured. The data from this process is recorded in a chart, known as the cone penetration test report, which shows the force required to push through the various soil layers. Generally, the probe will need less force to push through clay or peat (low cone resistance) than through sand (high cone resistance). From this, the mechanical properties of the subsurface can be inferred, including its load-bearing capacity.

In Figure 22 the relevant analysis codes for location B are:

- CPT000000175794: shown in Figure 23. It displays a very small cone resistance, an indication for a clay layer until approximately NAP-12m, where the first sand layer is observed until approximately NAP-14m, matching observations in literature regarding Amsterdam (Hemel, 2023). Then there is some clay or peat again followed by the second sand layer at NAP-18m according to the cone resistance.
- BHR000000349430: the CPT-data results in the build-up of the different soil layers shown in Figure 24. The main distinctions are a top sand layer, a little bit of peat, a large clay layer from approximately NAP-4.6m until NAP-12.6m and then again, a small peat layer, followed by the first sand layer at NAP-13.2m.

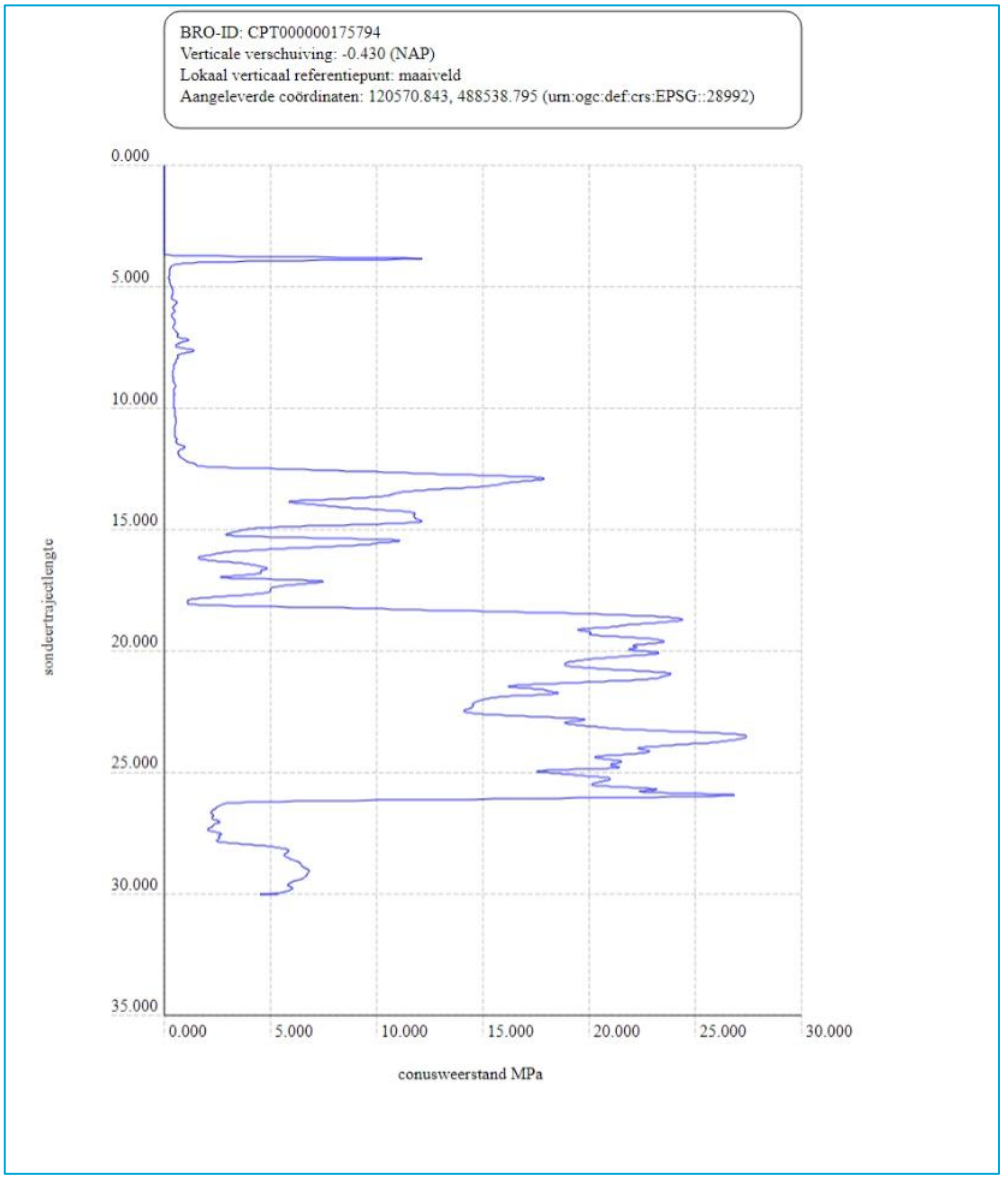

Figure 23 – Cone resistance CPT000000175794 (DINOloket, 2024)

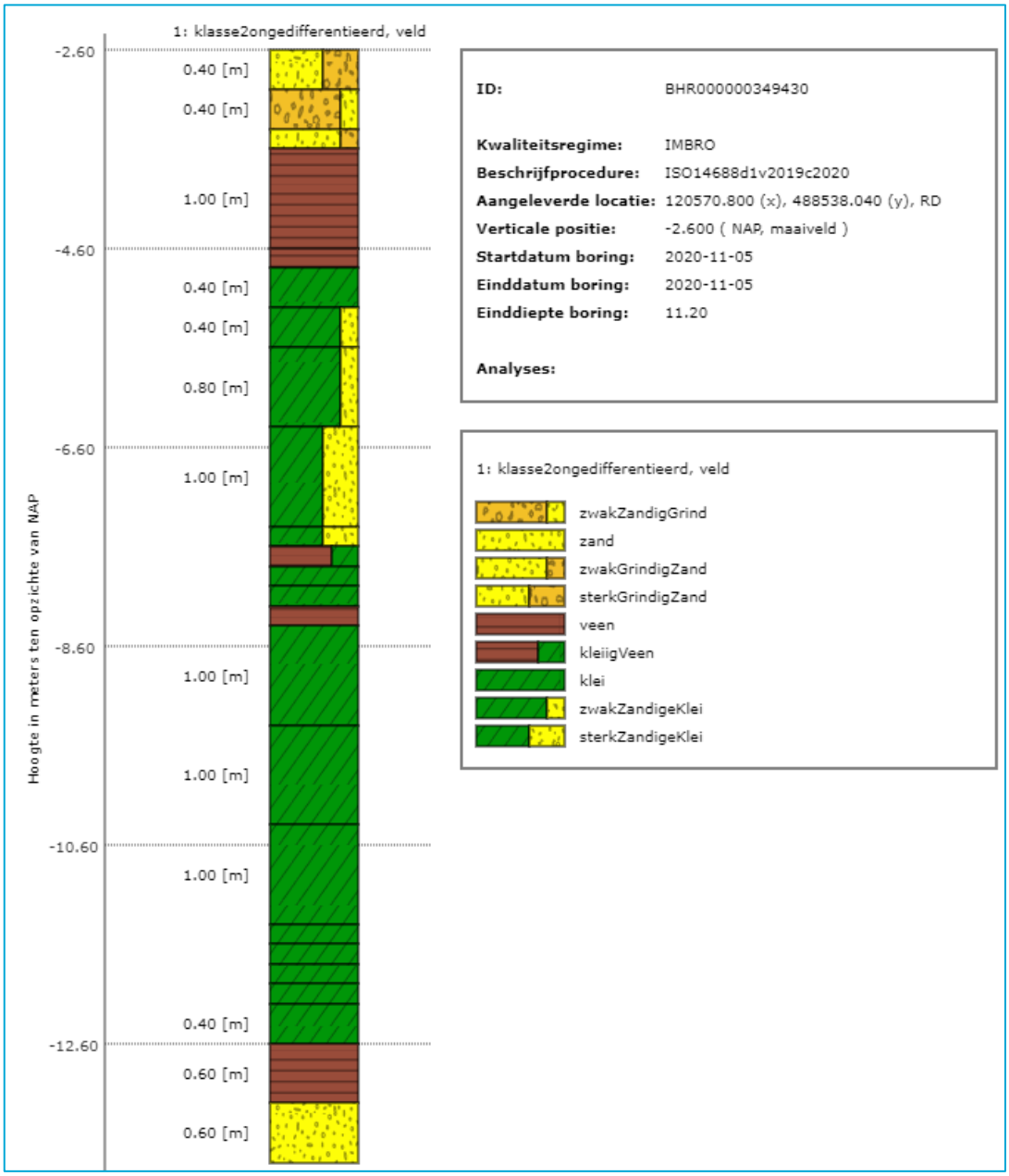

Figure 24 - Soil layers BHR000000349430 (DINOloket, 2024)

Another method would be to use the subsurface layer of the GeoTop v1.6 model of DINOloket, which is able to identify the specific soil layers at a location using an apple corer. The results in Figure 25 are obtained. The different layers are explained in Table 6.

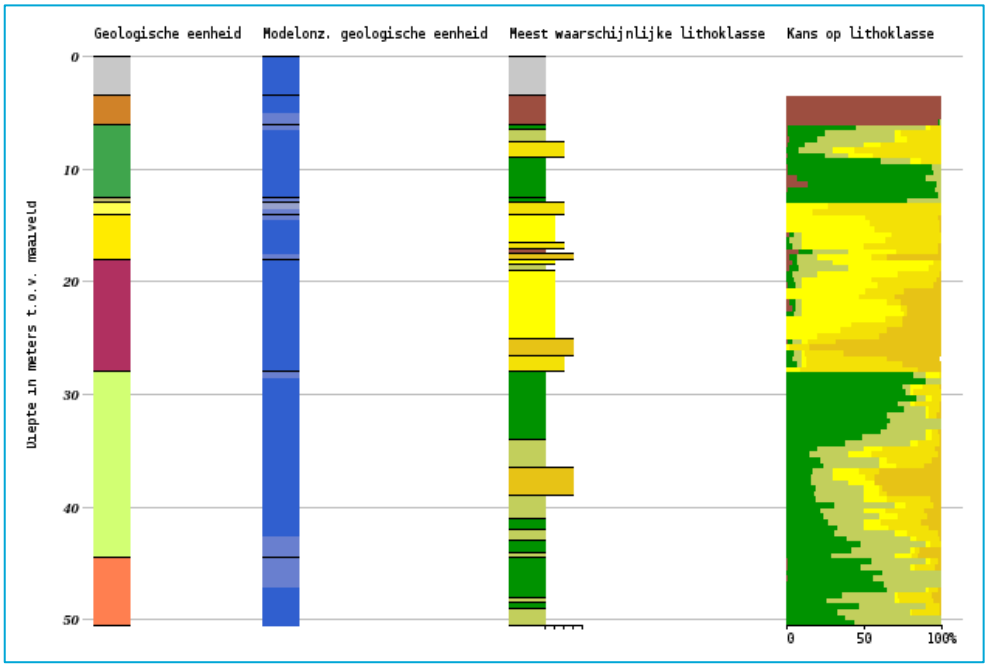

Figure 25 - GeoTop v1.16 soil layers Marnixkade (DINOloket, 2024)

Table 6 - Explanation legend GeoTop v1.6 soil layers (DINOloket, 2024)

Color	Dutch name	Soil Type
AAOP	Anthropogene afzettingen, opgebrachte grond	Sand
NIHO	Formatie van Nieuwkoop, Hollandveen laagpakket	Peat
NAWO	Formatie van Naaldwijk, Laagpakket van Wormer	Clay
NAWOVE	Formatie van Naaldwijk, Laagpakket van Wormer, Laag van Velsen	Clay
BXWISIKO	Formatie van Boxtel, laagpaketten van Wierden, Singraven en Kootwijk	Sand
BX	Formatie van Boxtel	Silty Clay/Sand
KRBXDE	Formatie van Kreftenheyde/Boxtel	Sand
EE	Eem formatie	Silty Clay/Sand
DR	Formatie van Drente	Clay

3.1.2 CPT data

The firm Lankelma Geotechnisch Adviesbureau has performed cone penetration tests at the Marnixkade according to the NEN-EN ISO 22476-1 standard. They conducted these tests at 16-10-2018 and put their findings in a report (Lankelma Geotechnisch Adviesbureau, 2018), of which the results are displayed in this chapter. The locations where the CPT's have been performed are displayed in Figure 26. When comparing the locations with Figure 21, it can be observed that location DKM4 gives the best results for section B.

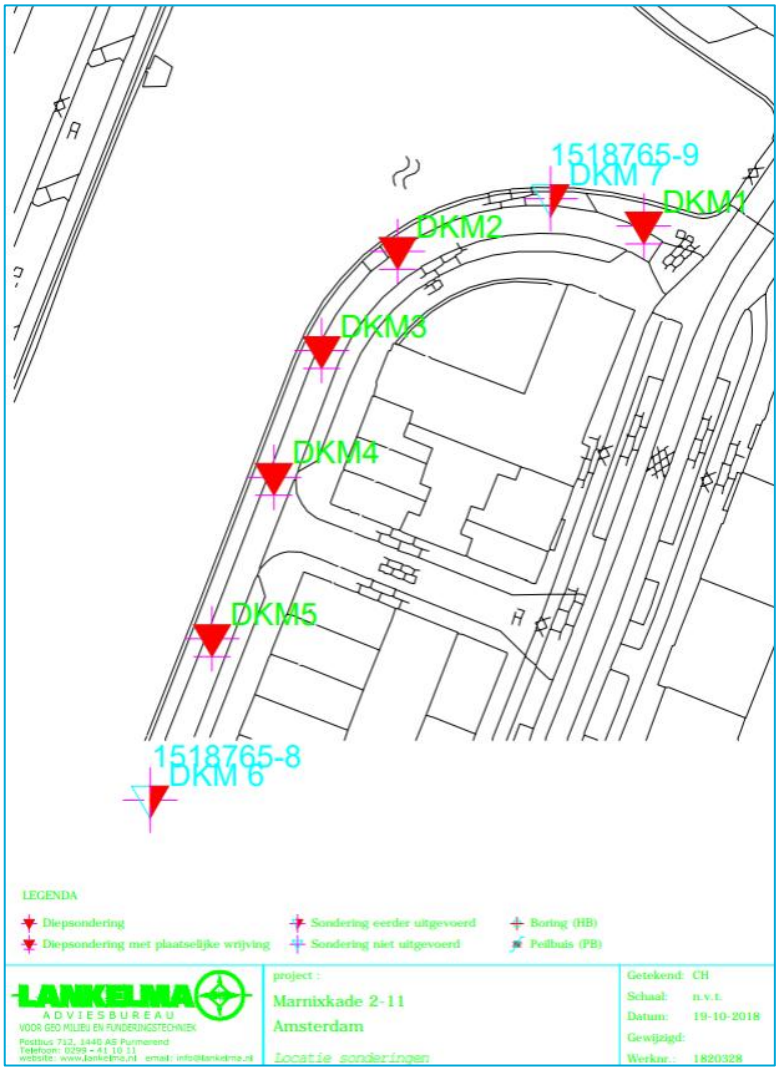

Figure 26 - Locations CPT's (Lankelma Geotechnisch Adviesbureau, 2018)

Using the CPT data from location DKM4 (Lankelma Geotechnisch Adviesbureau, 2018), the plots in Figure 27 can be obtained. In the report soil layers are derived according to the cone resistance and friction ratio. To perform this step, a mesh size (or layer thickness) is put into code over which these properties are averaged. Then a soil layer is assigned to this layer based upon the minimum Euclidian distance, for which the properties from Table 7 are chosen, which are based on the report (Lankelma Geotechnisch Adviesbureau, 2018).

Example of Euclidian distance soil type assignment

At each depth CPT results are obtained. The data consists of the cone resistance (q_c) and the friction ratio (R_f). The following data can be found:

$q_{c,data} = 7.8 \frac{N}{mm^2}$

$R_{f,data} = 1.2\ \%$

Additionally, from Table 7 the following properties are used, which are repeated here:

$q_{c,finesand} = 7.5 \frac{N}{mm^2}$

$R_{f,finesand} = 1.0\ \%$

Now, the Euclidian distance ($x_{finesand}$) between the data point and the soil type 'Fine sand' can be found using:

$x_{finesand} = \sqrt{(q_{c,data} - q_{c,finesand})^2 + (R_{f,data} - R_{f,finesand})^2} = \sqrt{(7.8 - 7.5)^2 + (1.2 - 1.0)^2} =$ 0.361

This process is repeated for all soil types for the data point. The data point and thus soil layer is assigned its soil type based on the minimum Euclidian distance of the soil types.

When using different mesh sizes, the soil layers in Figure 28 are obtained. Again, a large clay/peat layer is found until approximately a depth of 13 m, where the first sand layer is found. Below this layer, there is mixture of clay and sand, which is only observed when refining the mesh to 0.1 m. At a depth of 19m the second sand layer is found. Note that 0 m depth is at NAP+0.47m.

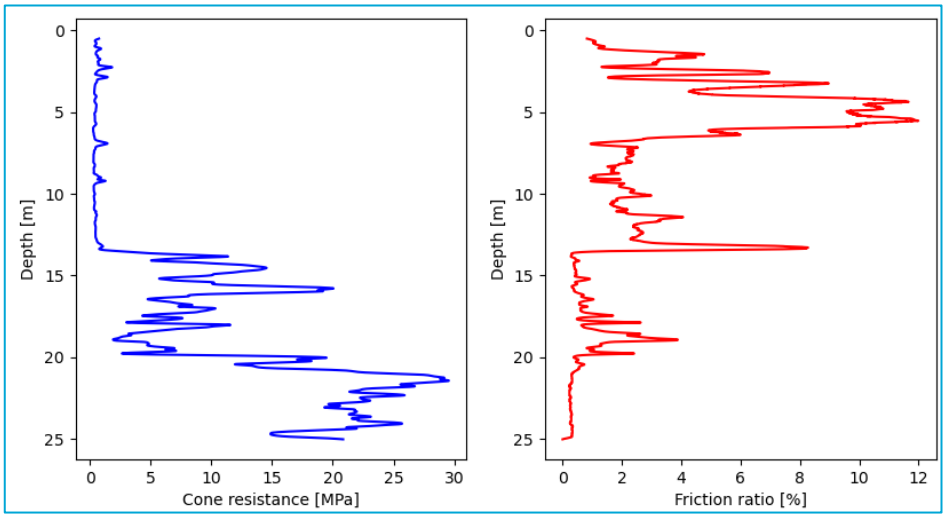

Figure 27 - CPT results at DKM4

Table 7 - Soil type mean properties

Soil type	Cone resistance [Mpa]	Friction ratio [%]
Fine sand	7.5	1.0
Silty/Clayey sand	3.5	1.4
Clay	2.5	4.5
Peat	2.5	8.5

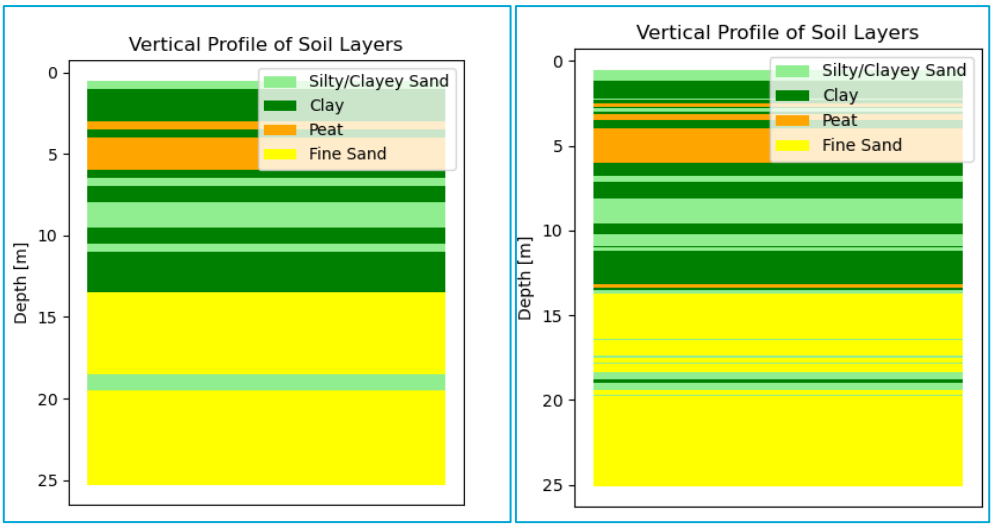

Figure 28 - Soil layers (left: mesh = 0.5m, right: mesh = 0.1m)

A method often used in literature is the Robertson classification, where based on the cone resistance and friction ratio a soil layer is assigned, corresponding to the number of that area in the plot. The plot is found in Figure 29. In this plot the soil layers assigned according to Table 7 with different colours shown in the legend. The Robertson method uses a larger number of soil types shown in Table 8.

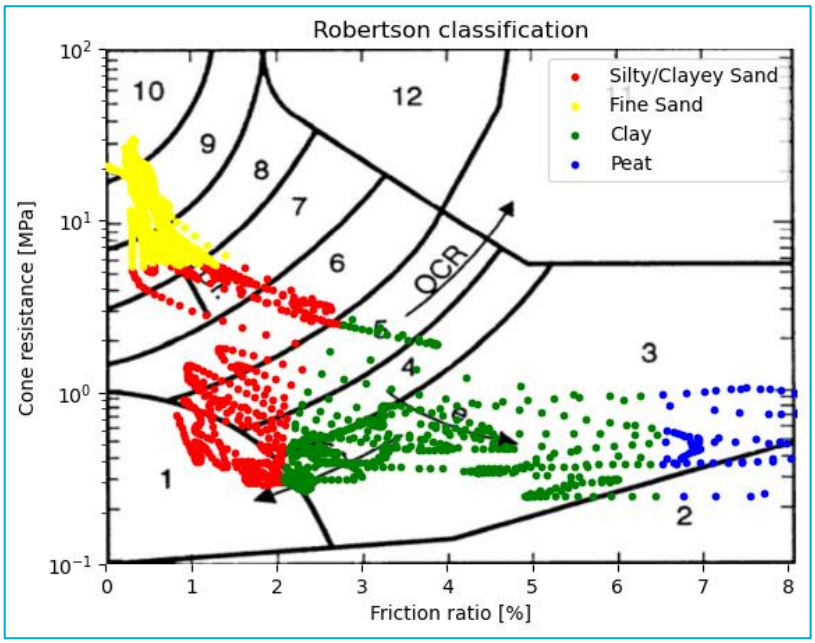

Figure 29 - Robertson method verification of results (Robertson, 2010)

Table 8 - Robertson soil types (Robertson, 2010)

Zone	Soil Behaviour Type
1	Sensitive fine grained
2	Organic material
3	Clay
4	Silty Clay to clay
5	Clayey silt to silty clay
6	Sandy silt to clayey silt
7	Silty sand to sandy silt
8	Sand to silty sand
9	Sand
10	Gravelly sand to sand
11	Very stiff fine grained
12	Sand to clayey sand

3.1.3 Assumed simplification soil layers

Figure 29 gives a clear distinction between the different soil types selected. When looking into Figure 28, it can be observed where these soil layers are present. A model often requires a trade-off between accuracy and simplicity. Therefore, a choice is made of a system existing out of 4 layers, that have a thickness of 13m, 3m, 4m and 5m (until the bottom of the CPT test). These layers can be seen in Figure 30. When plotting the layers in Figure 31, different clusters appear, which is a good sign.

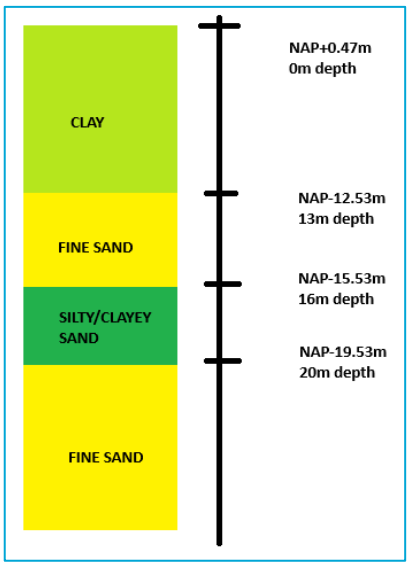

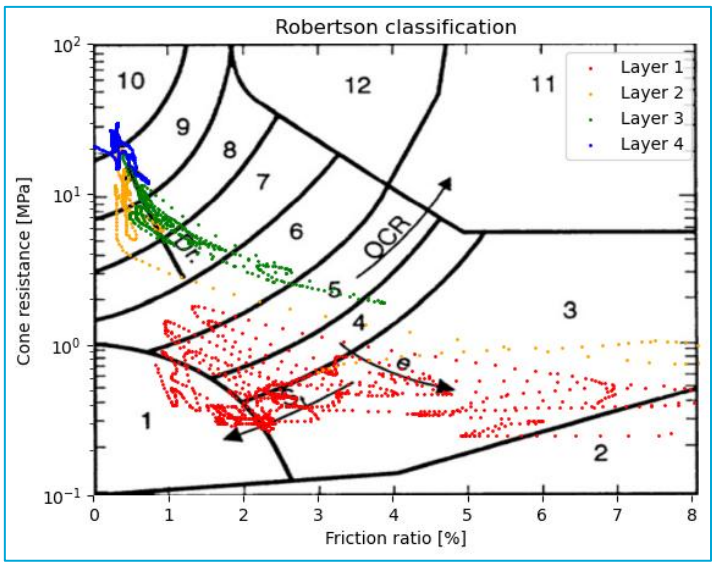

Figure 30 - Assumed soil layers Figure 31 - Robertson classification plot layers

3.1.4 Soil properties

In his doctoral thesis, Hemel, M.J. performed multiple experiments at the Overamstel site (Hemel, 2023). The geotechnical parameters are listed in Table 9 were used as input for the analytical pile group model at the Overamstel for undrained conditions. Assuming zero friction for clay layers is generally considered conservative in geotechnical engineering. This is because it simplifies the analysis by focusing only on the cohesive strength of the clay, which can provide a safer estimate of stability under undrained conditions. Although these values are not further used in this thesis, they provide additional reference.

Table 9 - Geotechnical modelling parameters for full scale lateral pile group experiment Overamstel (Hemel, 2023)

Depth (-NAP) [m]	γ_{sat} [kN/m³]	γ' [kN/m³]	Sort	Dutch name	q_c [kPa]	s_u [kN/m²]	ϕ [°]
2.6 - 4.0	16.9	6.9	clay	Geulopvulling	200	30	0
4.0 - 6.0	10.1	0.1	peat	Holland veen	400	30	0
6.0 - 7.0	19.1	9.1	clay	Oude zeeklei	400	45	0
7.0 - 8.2	18	8	sand	Wadzand	1500	0	34
8.2 - 11.6	17	7	clay	Hydrobiaklei	500	50	0
11.6 - 12.2	11.7	1.7	peat	Basisveen	1500	0	0
12.2 - 14.0	19	9	sand	Eerste zandlaag	10000	0	33

Although the location of the Overamstel is different than that of the Marnixkade, a similar buildup in soil layers is observed. Again, clay and peat are found until the sand layer at NAP-12.2m. This buildup of the soil is typical for soils in Amsterdam, which is displayed in Figure 32.

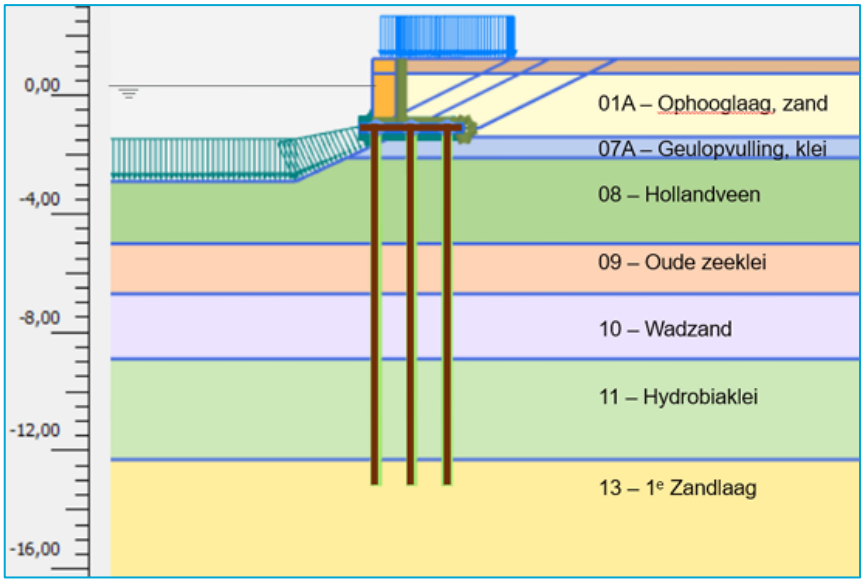

Figure 32 - Typical soil profile Amsterdam (Ingenieursbureau Gemeente Amsterdam, 2023)

The numbers in are used for the soil layers in Figure 32 - Typical soil profile Amsterdam correspond to the parameter set of the Noord-Zuid Lijn (Grondonderzoek Noord/Zuidlijn; Parameterset definitief ontwerp en D4 en D5 kenmerk 01270L, 2001), for which extensive research into the soil has been performed.

Table 10 - Ground parameters used for Plaxis 2D (Ingenieursbureau Gemeente Amsterdam, 2023)

Layer	Dutch name	γ_{dry} [kN/m³]	γ_{sat} [kN/m³]	c' [kPa]	ϕ' [°]	ψ' [°]	E_{50}^{ref} [kN/m²]	E_{oed}^{ref} [kN/m²]	E_{UR}^{ref} [kN/m²]	γ_7^{ref} [10⁻⁴]	G_0^{ref} [kN/m²]	m [-]
-	Verharding	18	20	0.5	32.5	2.5	20000	20000	60000	1	89.5	0.5
o1A	Ophooglaag	17	19	1	30	0	17134	15000	50000	1	81	0.5
o7A	Geulopv. Klei	13.9	13.9	7.1	20	0	4284	2200	15000	2	15	0.8
o8	Hollandveen	10.5	10.5	3.6	18	0	2000	1085	7000	2	7	0.8
o9	Oude Zeeklei	16.5	16.5	5	26	0	7500	3780	20000	2	47	0.8
10	Wadzand	17.9	17.9	1.4	27	0	10000	5890	25000	1	53.5	0.5
11	Hydrobiaklei	15.2	15.2	5.7	27	0	5000	2850	10000	2	33	0.8
12	Basisveen	11.7	11.7	4.3	18	0	2000	1065	7000	2	7	0.8
13	1e zandlaag	16.6	19.7	0.1	33	3	35000	20000	100000	1	121.5	0.5
14	Allerod	18.5	18.5	0.1	28	0	15000	7000	30000	1	59.5	0.5
15	Geulopvulling	18.6	18.6	0.1	27	0	8400	4000	25000	1	53.5	0.8
17	2e zandlaag	18	20	0.1	33	3	32000	25000	80000	1	105.5	0.5

A short physical interpretation of the properties in Table 10 is listed briefly below. A full description is given in the Literature Review on the constitutive models of the soils in section 2.3.1.

- γ_{dry} [kN/m³]: Dry Unit Weight - The weight of soil per unit volume when it is completely dry. which should be used as the soil density for the soil above the waterline at NAP-0.4m for the Marnixkade.
- γ_{sat} [kN/m³]: Saturated Unit Weight - The weight of soil per unit volume when it is saturated with water, which should be used as the soil density for the soil below the waterline at NAP-0.4m for the Marnixkade.
- *c'* [kPa]: Effective Cohesion - This is the soil's resistance to shearing when external forces are applied. It represents the internal "glue" that helps soil particles stick together.
- *ϕ'* [°]: Effective Angle of Internal Friction - The measure of soil's ability to resist shearing forces due to internal friction between particles.
- *ψ'* [°]: Dilatancy Angle - This describes the rate at which the volume of a soil sample changes when it is sheared. Positive dilatancy means the volume increases, and negative means it decreases.
- E_{50}^{ref} [kN/m²]: Secant stiffness in standard drained triaxial test.
- E_{oed}^{ref} [kN/m²]: Tangent stiffness for primary oedometer loading.
- E_{UR}^{ref} [kN/m²]: Unloading / reloading stiffness from drained triaxial test.
- γ_7^{ref} [10⁻⁴]: Threshold shear strain at which: $G_s = 0.722 * G_0$.
- G_0^{ref} [kN/m²]: Reference shear modulus at very small strains ($\varepsilon < 10^{-6}$).
- *m* [-]: Stress Dependency Parameter - A dimensionless parameter that defines the stress dependency of the soil's stiffness.

To get an accurate soil response, soil properties need to be chosen for the soil layers clay and sand in Figure 30. Since the layers below the first layers are not modelled in this thesis, they are considered out of scope. For the clay layer, the soil layers 07A, 08, 09, 11 and 12 (all layers that have clay or peat in their name) in Table 10 are averaged. For the first sand layer, layer 13 is used, which is the first sand layer. This results in the soil properties in Table 11. These soil properties are used as input for the top 2 layers assumed in Figure 30, which will be implemented in the FE models in this thesis. Note, that DIANA uses the porosity and dry density to calculate the saturated density, which is therefore higher than in Table 11.

Table 11 - Soil properties assumed soil layers

Layer	Name	γ_{droog} [kN/m³]	γ_{nat} [kN/m³]	c' [kPa]	ϕ' [°]	ψ' [°]	E_{50}^{ref} [kN/m²]	E_{oed}^{ref} [kN/m²]	E_{UR}^{ref} [kN/m²]	γ_7^{ref} [10^{-4}]	G_0^{ref} [kN/m²]	m [-]
1	Clay	14.02	14.02	5.16	23.8	0	3726.8	2396	11800	2	21800	0.8
2	Sand	16.6	16.6	2.9	30	0	35000	20000	100000	1	122500	0.5

3.2 Structural configurations

The structural configurations compared in this thesis, the traditional and sheet pile geometry, will be described in this section.

3.2.1 Traditional geometry

In this subsection the traditional structure used in this thesis is described. It follows the geometry from other researchers (Sharma, Longo, & Messali, 2024). There are a few simplifications made that are adjustments to that of Figure 33. The masonry wall and capstone are merged as one continuous masonry wall with a thickness of 0.65 m and a height of 1.6 m, with the top level at NAP+0.58m. Additionally, the piles are not modelled as tapered, but with diameter of 200 mm. Two other simplifications are made to the soil. The first is the fact that no stiff pavement and sand layer are modelled. Secondly, erosion of the soil below the timber piles and around mainly the first pile row is not considered. The soil starts at the end of the timber beam (which is also referred to as kesp), and has a downwards slope of 1V:3H to the left bottom of the picture in Figure 33b. This follows the TAK recommendation of the initial stages of modelling in Plaxis (Ingenieursbureau Gemeente Amsterdam, 2023). It is recommended to model in the last step the actual soil profile including erosion. However, since no data is obtained, the initial soil profile is kept.

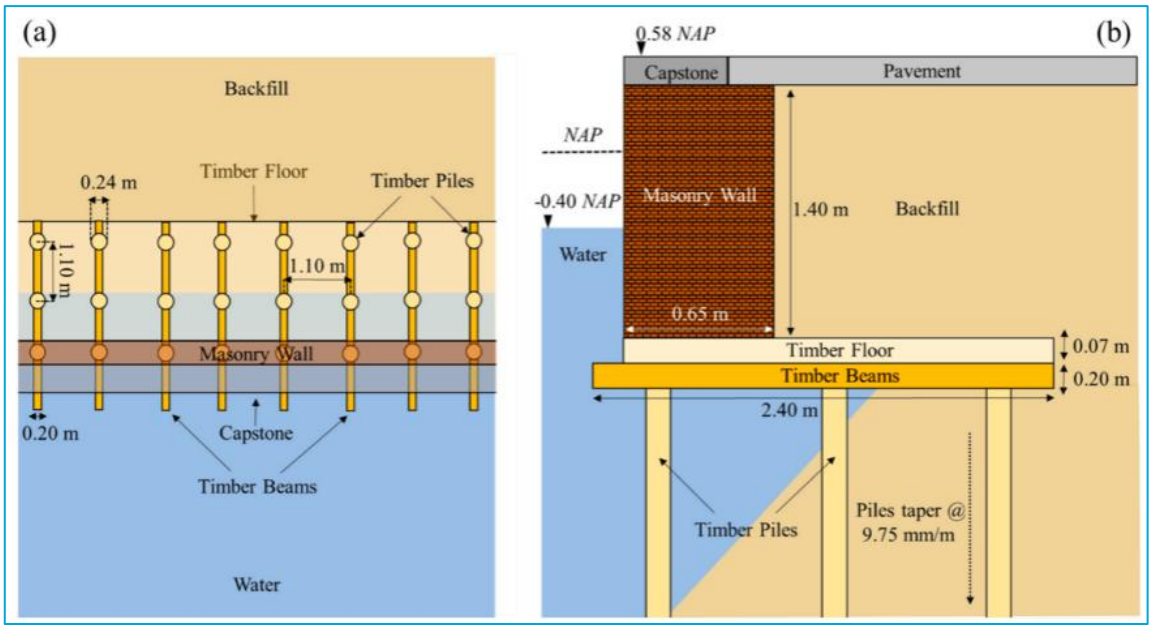

Figure 33 - Geometry of case-study Marnixkade (a) plan view and (b) transversal cross-section (Sharma, Longo, & Messali, 2024)

The internal loads, which are related to the structure itself, and the resulting forces of the soil pressure will be described. The self-weight of the structure can be determined using its volumetric density and geometry. In finite element programs the volumetric weight of the elements can be inputted, and the program will automatically consider the self-weight for the given geometry. The vertical and horizontal stresses of the soil on the quay can be estimated using soil mechanics theory. Both loads will now be explained further individually.

Self-weight of the structure

The self-weight of the structure can be based on the geometry as defined in Figure 33, which is based on inspections (NEBEST B.V., 2016). Note that the estimates weights in this section are specific to the Marnixkade, as the piles per kesp (Table 3) and thickness of the wall (Table 4) are different for the various quay walls.

When the Marnixkade is modelled in plane strain, the distance between the piles, which is 1.1m can be assumed as 1m to simplify the transversal cross-section parameters to unit width of 1m. Note that this section can also be justified as this is the approach for uninspected quay walls as discussed previously. As indicated earlier, it is assumed that the capstone is modelled as a continuation of the masonry wall. This makes that the masonry wall is 1.6 m high, rather than 1.4m. The thickness remains 0.65 m. Using the dry and wet volumetric weight of the masonry and assuming that the top 1 m is above NAP-0.40m and therefore dry, the load of the masonry wall on the floor can be defined per meter per meter unit width as:

$$q_{wall,actual} = h_{dry} * \gamma_{dry} + (h - h_{dry}) * \gamma_{wet} = 1.0 * 20 + (1.6 - 1) * 23 = 33.8 \frac{kN}{m^2}$$

Note that in Plaxis it is recommended to model the masonry as non-porous (Ingenieursbureau Gemeente Amsterdam, 2023), thereby the division in dry and saturated unit weight holds no value, as one value should be specified. In the case of the masonry the dry unit weight is chosen for the non-porous material with a density of 19.5 kN/m^3. Therefore, in DIANA the same value is used. Thus, the model does assume the following value:

$$q_{wall} = h_{wall} * \gamma_{masonry} = 1.6 * 19.5 = 31.2 \frac{kN}{m^2}$$

From the inspections (NEBEST B.V., 2016) the diameter of the cap size was found as between 200 mm and 260 mm with an average of 235 mm. Furthermore, the tapering assumed was 9.75 mm/m (Sharma, Longo, & Messali, 2024). Reflecting on Table 2, this appears to be a correct assumption as for piles with a cap size of 240mm, 10.2 mm/m or 9.1 mm/m taper is chosen for piles of respectively 11 m and 16 m long. Since the piles modelled are 12 m long, the assumption is correct. In a simplified model the piles are assumed to have a diameter of 200mm according and are not modelled as tapered. Using the mean volumetric weight of timber C24 from Table 5, the load of the piles per meter can be calculated:

$$A_{pile} = \frac{1}{4}\pi d^2 = \frac{1}{4}\pi (0.2)^2 = 0.031416\, m^2$$

$$q_{pile} = A_{pile} * \rho_{mean} * g = 0.031416 * 420 * 9.81 = 129.4 \frac{N}{m} = 0.1294 \frac{kN}{m}$$

The floor can also be modelled like the masonry as a load per unit width. Since the thickness of 0.07m was assumed, this gives the following load per meter per meter unit width:

$$q_{floor} = t_{floor} * \rho_{mean} * g = 0.07 * 420 * 9.81 = 288.4 \frac{N}{m} = 0.2884 \frac{kN}{m}$$

The kesp does not have a unit width, but a square cross section of 0.2 m x 0.2 m. Since the kesps are assumed one meter apart, this gives the following load per meter per meter unit width:

$$q_{kesp} = A_{kesp} * \rho_{mean} * g = (0.2 * 0.2) * 420 * 9.81 = 164.8 \frac{N}{m} = 0.1648 \frac{kN}{m}$$

Note that the density of the timbe of 420 kg/m^3 is tested according to a moisture content (*MC*) of 12%. The *MC* can be determined using the following equation:

$$MC = \frac{(m_{wet} - m_{dry})}{m_{dry}} * 100$$

After rewriting the equation above, the dry density (m_{dry}) of the timber can be determined as 375 kg/m^3. When the *MC* is thus increased up to or above 100%, this means that the density increases by a factor 2 which is significant. However, compared to the soil weight this increase is small. Since the actual *MC* in the timber is considered unknown, it is therefore neglected.

The mechanics scheme of the internal loads in the model including dimensions is visualised in Figure 34. Note that the kesp and floor element are schematised as a line element.

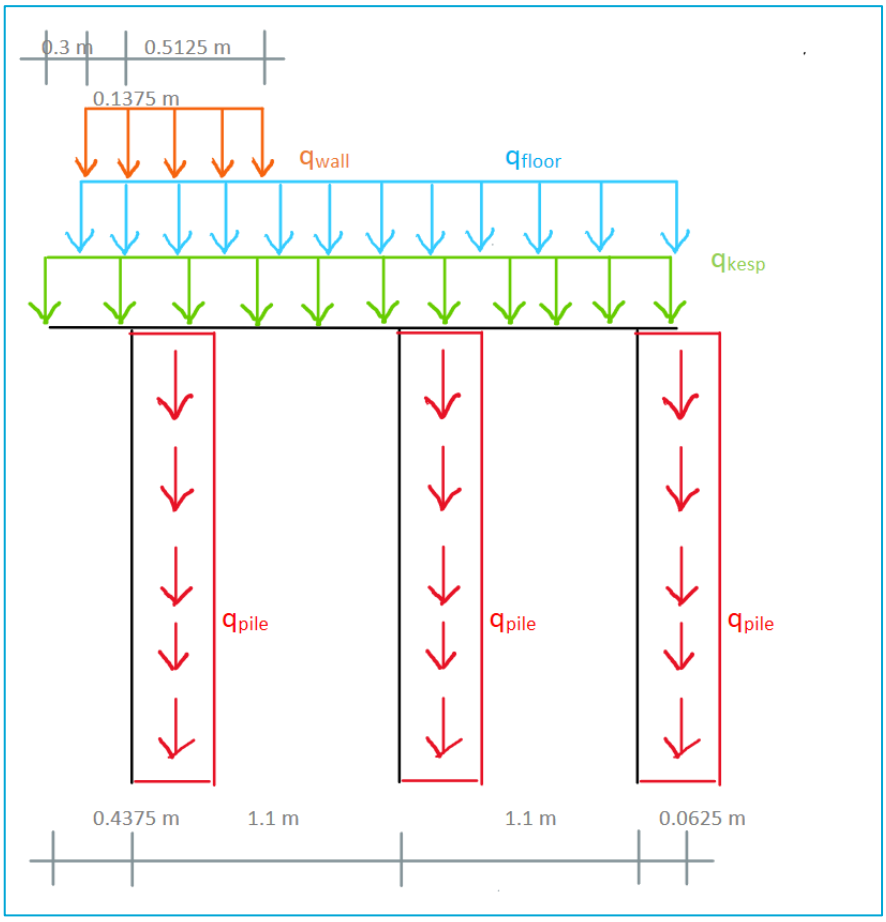

Figure 34 - Mechanics scheme self-weight quay wall: q_{floor} = self-weight of the floor, q_{kesp} = self-weight of the kesp, q_{wall} = self-weight of the wall, q_{pile} = selft-weight of the pile

3.2.2 Sheet pile geometry

When the left and the right side the sheet pile wall are considered, the effective pressures can be calculated from the soil conditions, under the following assumptions of the Marnixkade:

$$\gamma_{sat} = \gamma_{dry} = 14.02\ kN/m^3$$

$$p = 10\ kN/m^3$$

The right side has a water level of 0.98 m (L_1) below the ground level, whereas the left side of the quay has the ground level at 0.89m (L_2) below the water level as indicated in Figure 35. Note that negative pore pressures are not considered. This makes the height difference between the two ground levels 1.87m. For the specific situation at the Marnixkade, according to the TAK (Ingenieursbureau Gemeente Amsterdam, 2023) a base load of 10 kN/m should be considered at the top right of the quay, which increases the effective stresses at this side. This is accounted for in the soil stress plots of Figure 35 which shows the numerical output of the soil stress calculated in Maple, of which the entire workbook is given in Appendix A.

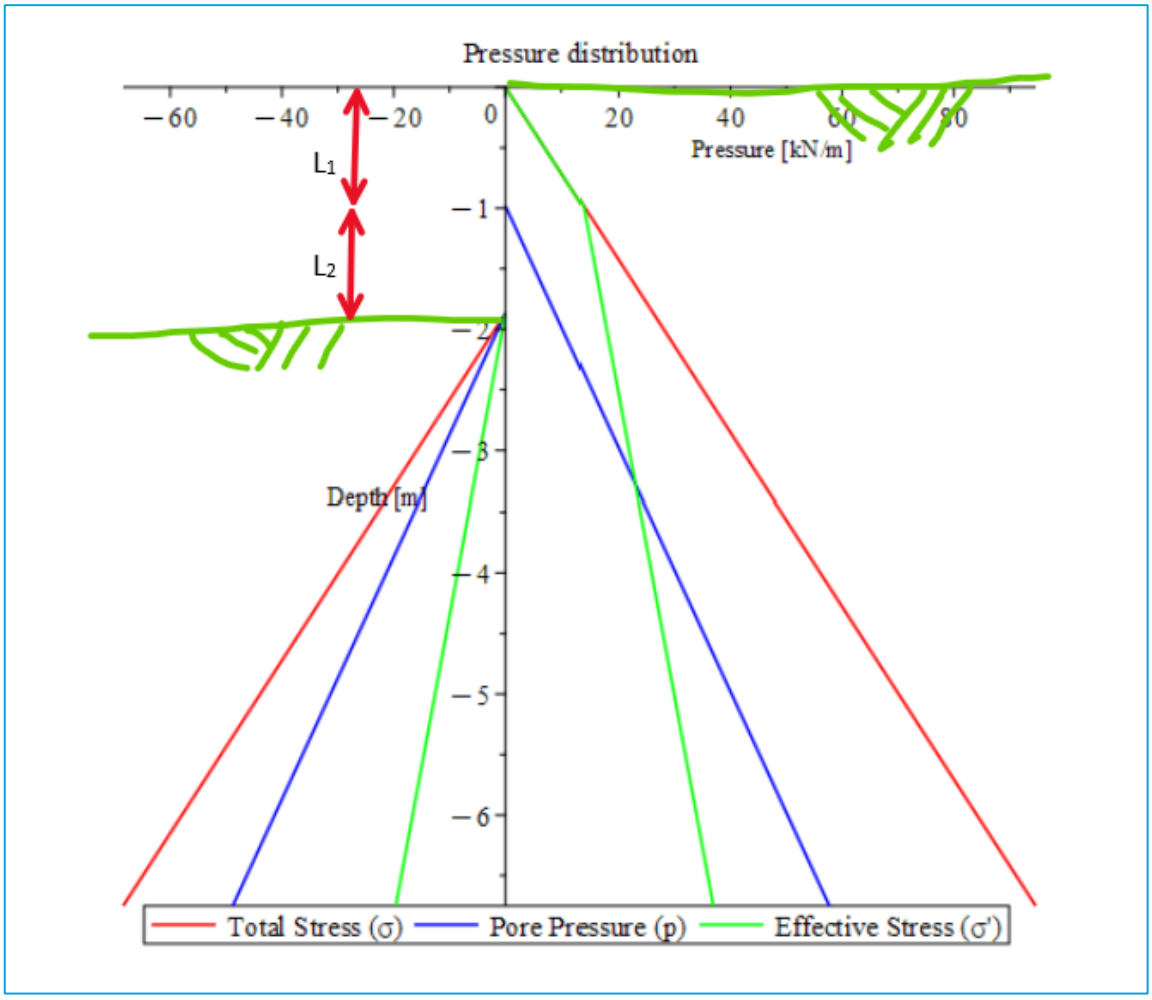

Figure 35 - Marnixkade pressure distribution with surcharge load

The conversion from soil stresses to active and passive pressure is given in Figure 36, which is obtained by multiplying the effective stresses with K_a for the active pressure and K_p for the passive pressure (Verruijt, 2001). To do this, the friction angle 0f 23.8 degrees is used (Kitch W. , 2015):

$$K_a = \frac{1 - \sin\varphi}{1 + \sin\varphi} = \frac{1 - \sin(23.8)}{1 + \sin(23.8)} = 0.425$$

$$K_p = \frac{1 + \sin\varphi}{1 + \sin\varphi} = \frac{1 + \sin(23.8)}{1 - \sin(23.8)} = 2.353$$

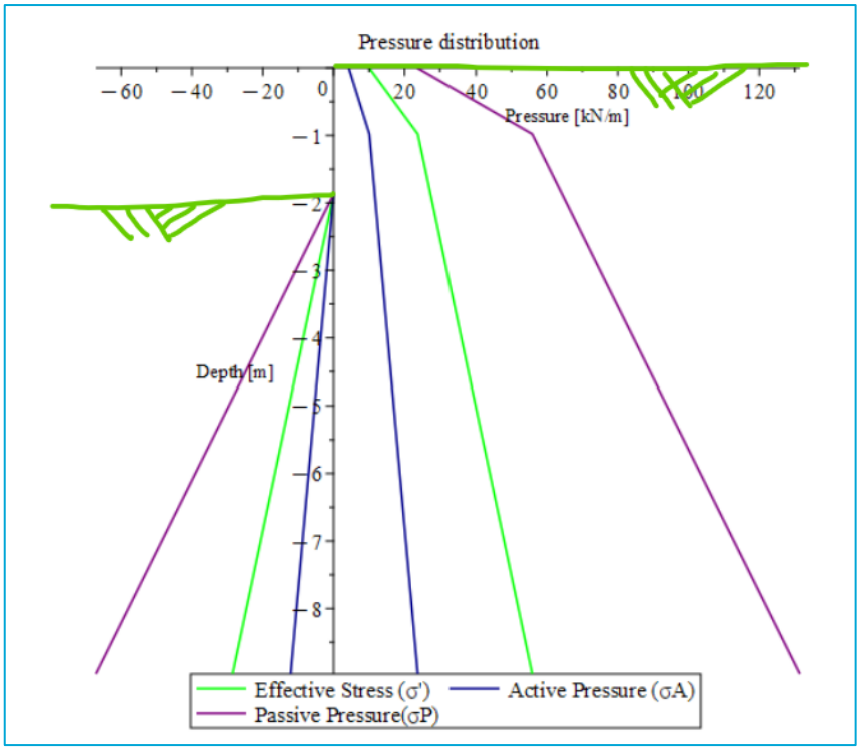

Figure 36 - Marnixkade active and passive soil pressures with surcharge load

The sheet pile is assumed to rotate around point O (Figure 37) and thereby creating active and passive zones in the sheet pile. There are 2 unknowns that need to be derived, the embedded depth *D* of the sheet pile and the location of point O with respect to the bottom of the sheet pile (*z*), the point where the active zone becomes passive at the right bottom. Fortunately, the sum of horizontal forces and sum of moments give 2 equations, which means the unknowns can be solved for. The resulting pressure on the sheet pile is calculated and illustrated in Figure 37.

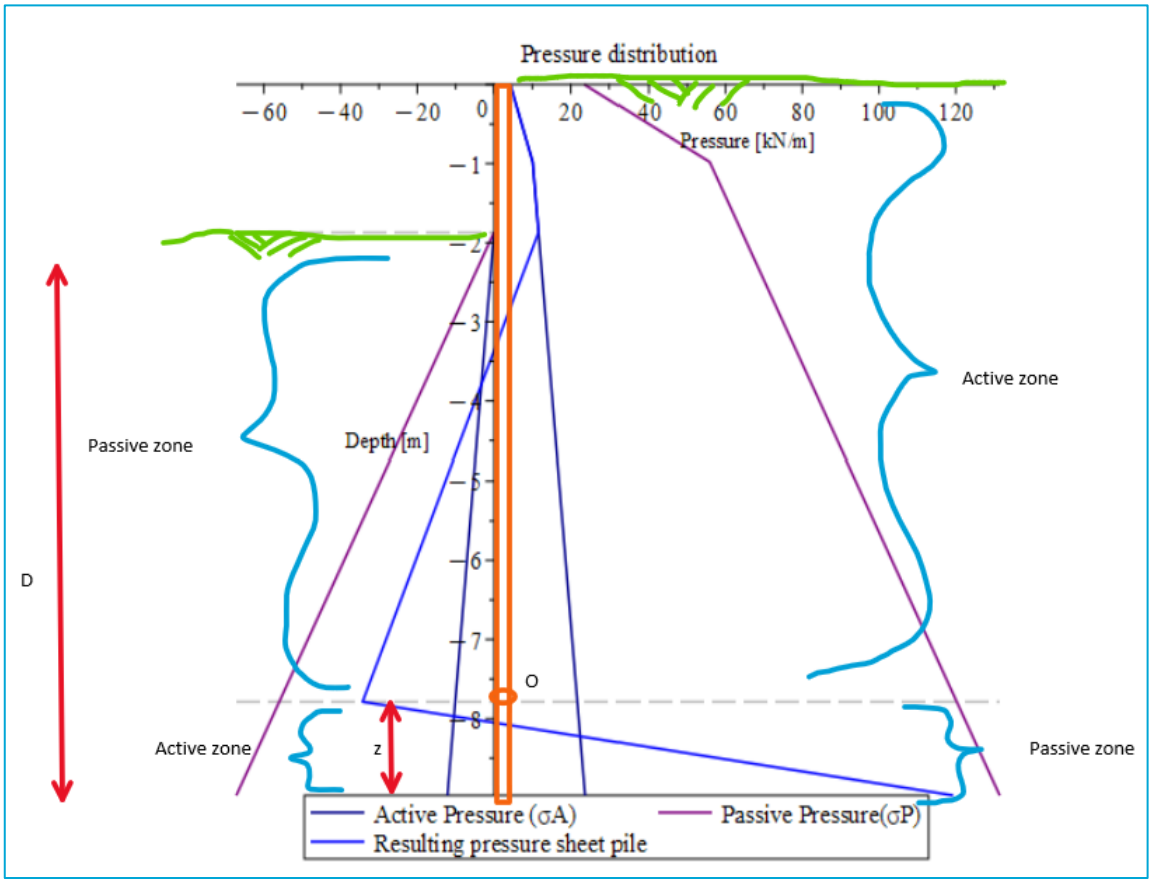

Figure 37 - Sheet pile active and passive zones and resulting pressure diagram. The sheet pile is orange coloured, and the centre of rotation (O) is included

The two equations used to solve for the unknowns, are briefly expanded upon. Therefore, the resulting pressure diagram from the sheet pile is illustrated in Figure 38, which follows the points A', Q, F', M, G, N and J. To simplify the calculation of the horizontal force equilibrium, the red, blue and green polygon can be used. Therefore, to calculate force equilibrium, the following equation can be used:

$$\sum F_{hor} = Area_{AA'QF'CB} - Area_{F'CE'} + Area_{GJE'} = 0$$

The moment equilibrium is calculated from taking equilibrium around point B. The full workout of the calculations in Maple is given in Appendix A.

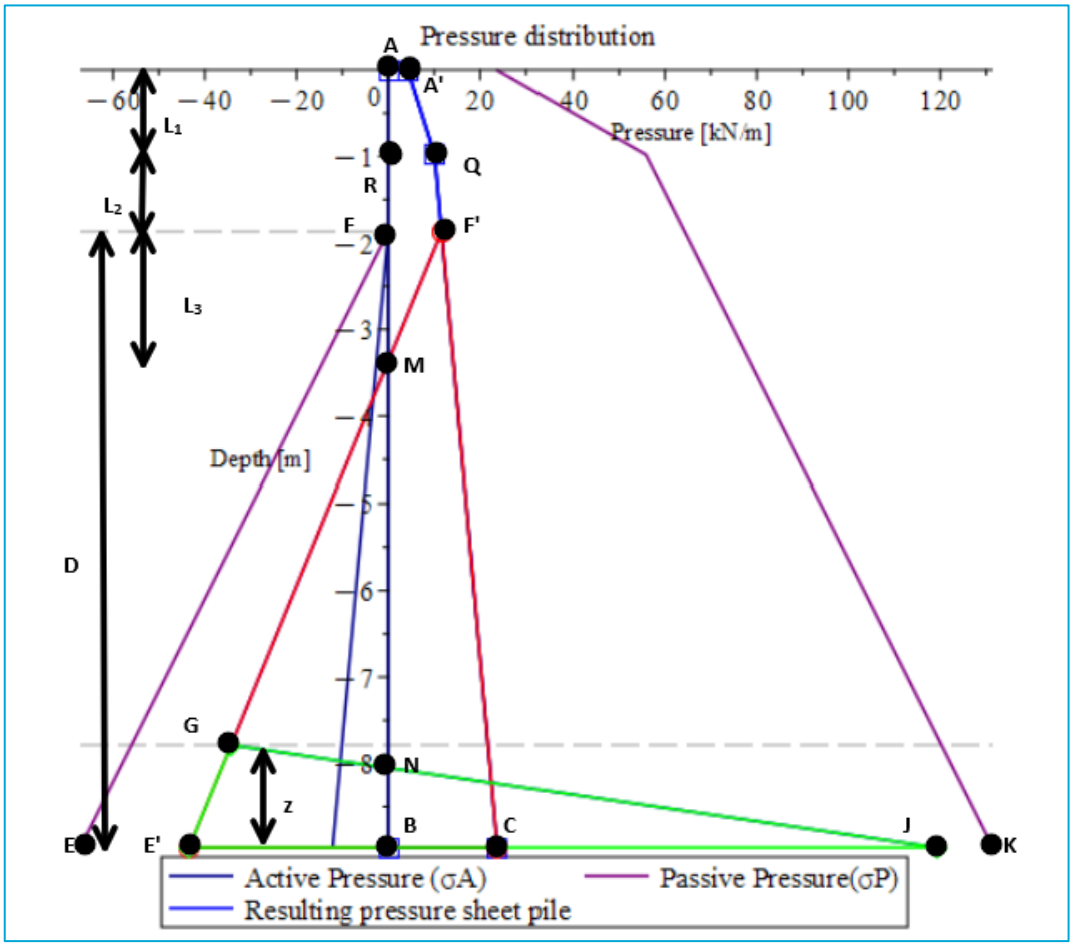

Figure 38 - Adopted notation system to calculate horizontal force and moment equilibrium to determine unknowns D and z. The red, blue and green polygon are shapes that are used to simplify the horizontal force equilibrium calculation.

The embedded depth *D* was given as output and equal to 7.1m. A Factor of Safety (*FoS*) is often applied to sheet piles ranging from 1.5 to 2. Furthermore, the L1 and L2 need to be added to the sheet pile length *L*. This means the total length can be estimated using:

$$L = L_1 + L_2 + FoS * D$$

The Length *L* was rounded to make it easy to fabricate to 15 m.

The section modulus was estimated from the maximum moment. The point of the maximum moment is where the shear force equals zero from the pressure distribution above. This turned out to give a moment of 91.94 kNm at 2.56 m from the bottom of the sheet pile. An initial section of AU14 was chosen, which is a small profile from ArcelorMittal and has a section modulus of 1410 cm^3/m. The steel strength is chosen to be 240 N/mm^2. The resulting bending stresses and unity check can be calculated from:

$$\sigma = \frac{M}{W} = \frac{91.94 * 10^6}{1410 * 10^3} = 65.2\ N/mm^2$$

$$UC = \frac{\sigma}{f_{yd}} = \frac{65.2}{240} = 0.27$$

Therefore, this section is sufficient to resist the stresses that occur. A section with a low section modulus is expected because of the limited retaining height of the sheet pile wall. Limitations of this method is that the displacements are not considered and those can be severe, especially in clay soils

in Amsterdam. Therefore, these should be checked when the section profile is implemented in finite element software.

Another limitation is the fact that this method is normally used for sand soils. Since lateral pressures in the clay over a long period of time approach those for a granular soil (United States Steel, 1984), such as sand, the long-term condition is thus applied and verified. Initially, clay will require a smaller embedment depth as it offers additional cohesive strength over sand.

3.3 Loads on quay walls

Initially, in this section all current loads acting on the quay walls will be discussed. The loads are present from traffic, parked cars, humans and trees. Also, one could think of bollard forces due to houseboats (Ingenieursbureau Gemeente Amsterdam, 2023). After the current loads are described, multifunctionalities and its corresponding loads are described. Since the aim of this research is the applicability of additional functionalities, the structural effects of these additions will be estimated. The last part of this section is related to the loading steps, which is of vital importance for an accurate representation of particularly soil stresses.

3.3.1 Current loads

Various current loads need to be accounted for when designing quay walls. Those include permanent and variable loads. These loads are:

- Ground level: parking and traffic
- Trees: self-weight and horizontal loads due to wind
- Bollard and mooring ring loads
- Accidental loads

<u>Ground level: parking and traffic</u>

Depending on the location in Amsterdam different loads should be distinguished. Four situations can be described, those are (Neijzing & Altman, 2023):

1. Along a primary traffic or public transport route
2. Within the city ring S100
3. Between the city ring S100 and the ring A10
4. Outside the ring A10

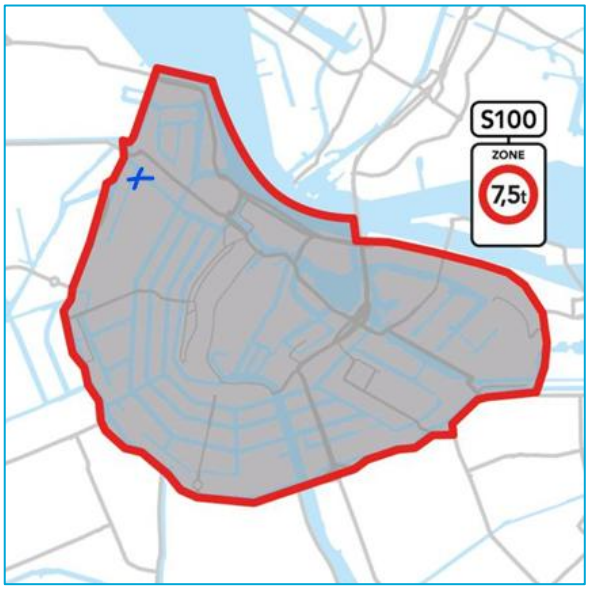

Figure 39 - Ring S100 (blue cross indicates location Marnixkade) (Ingenieursbureau Gemeente Amsterdam, 2023)

Since the scope of this thesis is the Marnixkade, situation 2: within the city ring S100 is taken (Figure 39). Heavy vehicles are banned, and the acceptable weight of a vehicle is 7.5 tonnes. Vehicles between 7.5 and 30 tonnes must have a permit and heavier transport is only allowed on a predefined

driving route after request. For this situation a load of 10 kN/m^2 should be applied for the ground level from the quay wall construction to the façade of the adjacent buildings with a maximum distance of 10m calculated from the quay wall (Neijzing & Altman, 2023).

<u>Trees: self-weight and horizontal loads due to wind</u>
Considering trees as variable loads in Amsterdam is often too conservative. The horizontal loads caused by the winds on trees is the most important load and trees are shielded by buildings. This was concluded after three large storms hit Amsterdam in February 2022 and did not cause any quay walls to collapse. Therefore, when the following two point are satisfied, tree loads do not need to be considered:

1. The distance between the façade and the trees is not more than 10m.
2. The height of the buildings behind the tree is approximately equal or greater to that of the top of the trees.

When the tree does not satisfy these two points, the additional loads of the tree must be calculated and used when verifying the structure (Ingenieursbureau Gemeente Amsterdam, 2023).

For the Marnixkade, which is the location of interest in this thesis the two check have been performed. In Figure 41 it can be observed that the height of the trees is less than the height of the building behind the trees. In Figure 40, it can be confirmed that de distance between the façade and the tree is 7.85 m, thus less than 10 m. These checks have been performed multiple times along the Marnixkade and every time both criteria were met. Therefore, both criteria are satisfied, and tree loads do not have to be considered as additional load for the current TAK load case at the Marnixkade. Note that this recommendation from the TAK is violated in the section on multifunctionalities caused by green infrastructure. In the case of exceptionally large trees in good soil conditions, the TAK load might underestimate the tree load.

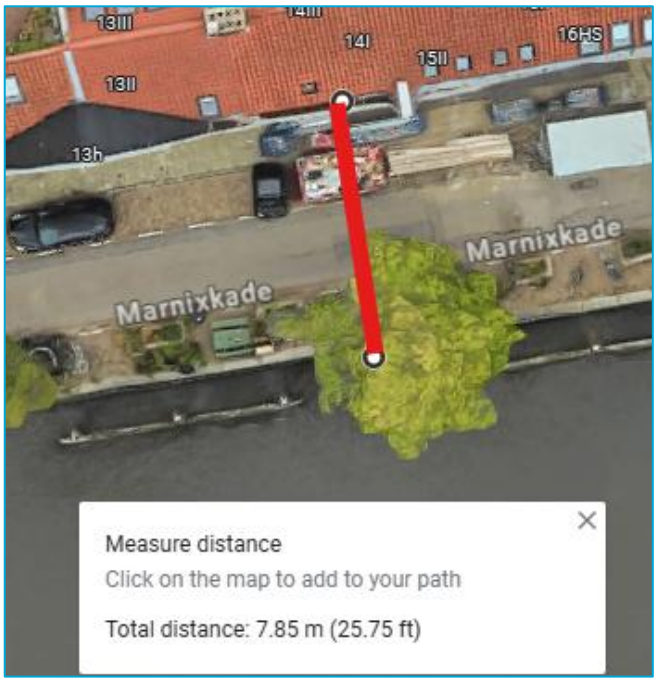

Figure 40 - Distance trees to facade Marnixkade (Google Maps, 2024)

Figure 41 - Height trees compared to height buildings Marnixkade (Google Maps, 2024)

<u>Bollard and mooring ring loads</u>

According to the map in Figure 42 it can be observed that the Marnixkade is a busy shipping route, it connects Het IJ to the Nieuwe Meer. Therefore, ships of class IV should be able to go this route.

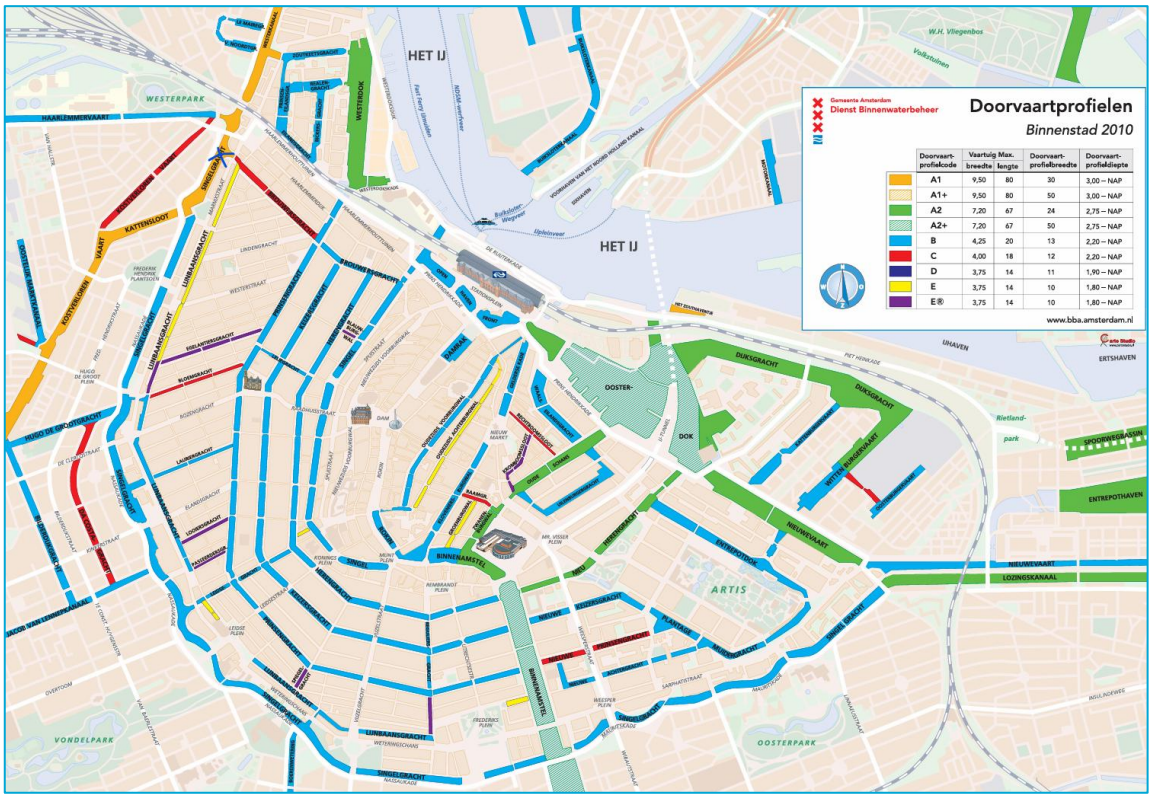

Figure 42 - Shipping routes inner-city Amsterdam (Dienst Binnenwaterbeheer, 2024)

<u>Accidental loads</u>

During canal-side construction, cranes frequently lift heavy loads, with stabilizers positioned near or on quay structures. Each request requires individual evaluation based on the exemption application and therefore should not be considered as a design load (Ingenieursbureau Gemeente Amsterdam, 2023).

3.3.2 Multifunctional loads

Various multifunctionalities can be incorporated into the quay walls in Amsterdam. Examples are:

- Energy storage methods
- Integrated additional height
- Green infrastructure
- Smart technology for monitoring
- Waste management

The functionalities will be briefly described followed by an estimate of their structural effects on the quay walls. In the numerical implementation in Chapter 4, they are repeated and summarized in Table 21.

<u>Energy storage methods</u>

Quay walls in the inner cities of the Netherlands have a large potential in providing geothermal energy storage (Haasnoot, 2020). Both a design based around sheet piles and a design based around concrete piles with a 'L' wall on top show large potential and are economically feasible. Geotechnical risks due to thermal expansion are limited. However, the structural effects of small tubes able to extract thermal energy are limited.

However, storing the energy extracted by the quay wall in a battery pack can lead to serious loads, which will now be illustrated. Two types of batteries are studied: lead-acid and lithium-ion batteries. Lead-acid have a better reliability, score better regarding sustainability and safety and have less costs than lithium-ion batteries (May, Davidson, & Monahov, 2018). Therefore, lead-acid batteries were chosen. The weight of these batteries was derived from the energy density, which was given in both Wh/L and Wh/kg, as being 22.7*10^3 kg/m^3. The density of clay, which the battery is assumed to replace has a density of 14.02*10^3 kg/m^3. This enables it to calculate the added load ($q_{energy,battery}$) to the quay wall when a cubic meter of clay soil is replaced by a lead-acid battery.

$$q_{energy,battery} = (\rho_{lead-acid,battery} - \rho_{clay,soil}) * g = (22.7 * 10^3 - 22.7 * 10^3) * 9.81 = 8.48\ kN/m^3$$

An estimate based on assumptions of the writher of this thesis is now made on how much energy storage is required in the quay. The energy stored should be enough to provide a household of 4 person including an electric car with a month of energy. The energy required for a household of 4 is equal to 382 kWh (EnergieDirect, 2024). Furthermore, a Tesla model S with a usable battery of 95 kWh and a range of 575 km (Database, 2023) is assumed as the car of the household, which should be charged 4 times monthly. This means that a total of 782 kWh is required for storage. The energy density of the selected lead-acid battery is 85 kWh/m^3 (Database, 2023). The last assumption is that energy usage is expected to go up in the future, and as the quay wall is to be designed for 100 years, an additional factor of 1.5 is used to account for this. This is a guess of the writer of this thesis. Now the required volume of energy storage can be calculated.

$$V_{storage} = E_{month} * C_{growth,factor} * E_{density} = 782 * 1.5 * 85 = 13.45\ m^3$$

The final assumptions are that the batteries are placed in a line along the quay. The house is assumed to have a width of 10m. This means that per m width of quay wall for a plane strain model a total volume of 1.345 m^3/m is required. When a height of a battery of 1m is assumed, the total length of this battery in the cross-section of the plane strain models is 1.345m, which is rounded up to 1.4 for

simplicity. Along this line, the 8.48 kN/m should then be applied. The load is applied starting 650 mm from the water until 2050 mm from the water at the ground level.

Integrated additional height

Given Amsterdam's vulnerability to a high-water level, defence systems which give additional height to the quay wall such as deployable barriers of high-durability materials capable of withstanding water pressure and tide variations can be integrated in the design of quay walls. A possible design for such a structure can be seen in Figure 43.

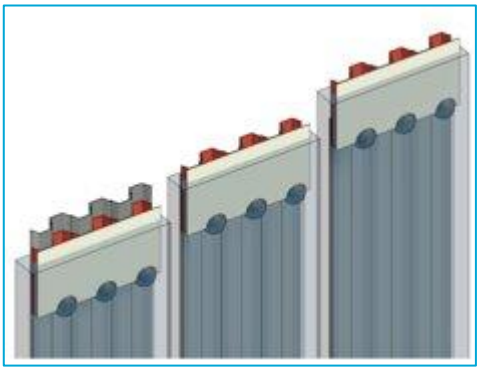

Figure 43 – Additional height panels

It is assumed that these panels are made from steel S355, which has a density of ρ = 7850 kg/m^3. The thickness is assumed to be 20mm. The additional resisting height would be 1 m. Therefore, the plates are considered as 1.2m long, as they also need to be connected to the quay wall. The resulting normal force (N_{Ed}) from the self-weight of the structure is calculated:

$$N_{Ed} = F_{self,weight} = \frac{1}{2} * \rho_{plate} * g * h_{panel} = 1.2 * 7850 * 9.81 = 1848.2\ N = 1.848\ kN$$

For a 20mm thick plate this results in a 1.85kN force (per unit width) due to gravity. It is observed that this is a small force compared to the 10 kN/m^2, which should be applied at ground level for situation 2. However, since the effects are at the edge of the structure, it should be accounted for when verifying the structure.

Another load that needs to be considered is the horizontal pressure from the water. When a unit-width cross-section is assumed, the load applied is given in Figure 44. The quay wall should normally prevent the soil from collapsing into the water. Therefore, the additional hydrostatic pressures in case of a high-water level work favourable and should not be included, whereas the self-weight of the panel does put additional load on the quay wall structure when it is pushed into the water and should thus be considered.

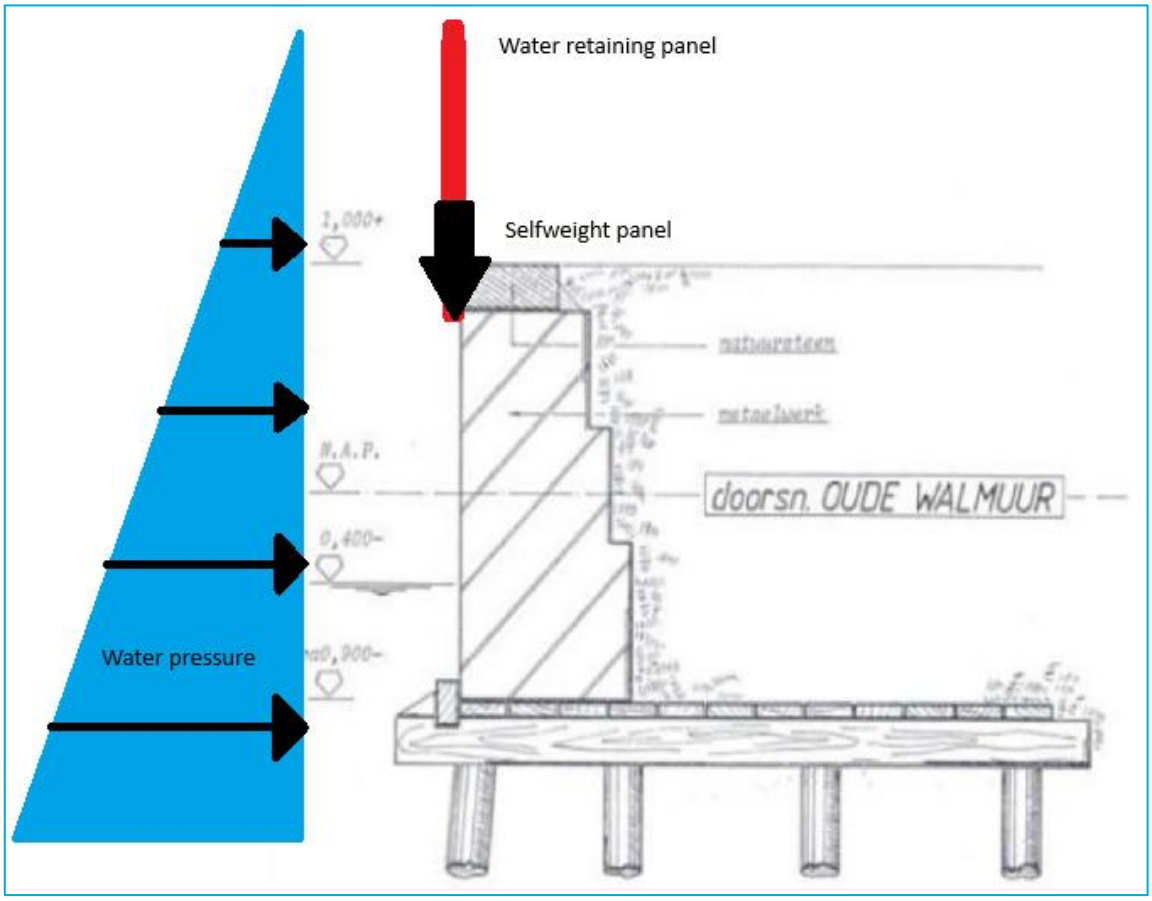

Figure 44 - Loads because of retaining panels (blue: additional water pressure; red: water retaining panel)

It should be checked if the plate is able to resist the loads from the self-weight and the hydrostatic pressure, resulting in normal forces, bending and shear. For the hydrostatic pressure, given the height of 1.2m the following hydrostatic force per unit width m is assumed:

$$V_{Ed} = F_{hydrostatic} = \frac{1}{2} * \rho_{water} * g * h_{panel} = 1.2 * 1000 * 9.81 = 7063.3\ N = 7.06\ kN$$

This is the shear force (V_{Ed}) acting on the panel. The moment acting on the structure can be bound by multiplying the resulting force of the hyrdrostatic pressure with the arm, which is a third of the height for the triangle shaped hydrostatic pressure.

$$M_{y,Ed} = F_{hydrostatic} * e = 7.06 * \frac{1}{3} * 1.2 = 2.83\ kNm$$

The plastic resistances of the cross-section for the normal force, bending and shear can be calculated using the following equations (EN 1993-1-1, 2016):

$$N_{pl,Rd} = \frac{A * f_y}{\gamma_{M0}} = \frac{20 * 1000 * 355}{1.0} = 71 * 10^5 N = 7.1 * 10^3 kN$$

$$V_{pl,Rd} = \frac{A_v * f_v}{\gamma_{M0}} = \frac{20 * 1000 * \frac{355}{\sqrt{3}}}{1.0} = 71 * 10^5 N = 7.1 * 10^3 kN$$

$$M_{pl,Rd} = \frac{I * f_y}{\frac{t}{2} * \gamma_{M0}} = \frac{\frac{1}{12} * 1000 * 20^3 * 355}{\frac{20}{2} * 1.0} = 23.67 * 10^6\ Nmm = 23.67\ kNm$$

The resulting unity checks from the individual contribution of the normal force, shear and bending are given below.

$$UC_{normal,force} = \frac{N_{Ed}}{N_{Pl,Rd}} = \frac{1.85}{7100} = 0.00026$$
$$UC_{shear,force} = \frac{V_{Ed}}{V_{Pl,Rd}} = \frac{7.06}{4100} = 0.0017$$
$$UC_{bending} = \frac{M_{y,Ed}}{M_{Pl,Rd}} = \frac{2.83}{23.67} = 0.119$$

Since the shear force is less than half of the plastic resistance, reduction due to bending and shear interaction is not necessary (EN 1993-1-1, 2016). The reduced moment resistance due to the interaction of bending and normal force for a solid rectangular section is given (EN 1993-1-1, 2016):

$$M_{N,y,Rd} = M_{Pl,Rd} * (1 - \left(\frac{N_{Ed}}{N_{Pl,Rd}}\right)^2) = 23.67(1 - \left(\frac{1.85}{7100}\right)^2) = 23.67$$
$$UC_{bending} = \frac{M_{y,Ed}}{M_{N,y,Rd}} = \frac{2.83}{23.67} = 0.119$$

It is observed that the effect of the normal force on the bending resistance is limited. This can be attributed to the low relative normal force. All unity checks are very small, as 0.119 is currently the governing unity check, which is not economical. Limitations of the current calculations are that it excludes the effects of corrosion and the impulse forces of moving water on the structure. Therefore, 20 mm can be used as a safe estimate for the panel, which results in a force of 1.85 kN at the waterside of the quay wall.

<u>Green infrastructure</u>

Incorporate green roofs or vertical gardens to improve urban biodiversity, manage stormwater, and enhance air quality. Green spaces can also provide aesthetic value and help mitigate the urban heat island effect. Unfortunately, strict regulations apply for UNESCO World Heritage sites and the quay walls must consist of masonry at the water side. The structural effects due to green vegetation is less compared to that of trees and parked cars, for which at the Marnixkade a load of 10 kN/m^2 should be applied at the ground level.

The structural effects of a tree are estimated to check this assumption using the largest trees. Therefore, data analysis on Elm tree, the tree species for Amsterdam quays, has been performed (Kremer, 2024). This showed that the largest fully grown tree has a diameter of approximately 0.8 m and a height of 15 m. Furthermore, an Elm tree density of 560 kg/m^3 can be applied. Since trees are tapered, a cone shape was used to calculate the volume of the tree trunk. Lastly, the weight of the wet leaves is 100% of the trunk weight in the summer. The resulting forces of the tree can now be calculated using the sum of the two:

$$V_{trunk} = \frac{\pi * \left(\frac{d_{trunk}}{2}\right)^2 * h_{tree}}{3} = \frac{\pi * \left(\frac{0.8}{2}\right)^2 * 15}{3} = 2.513\ m^3$$
$$F_{trunk} = V_{trunk} * \gamma_{trunk} = V_{trunk} * \ \rho_{elm,trunk} * g = 2.513 * 560 * 9.81 = 13606.92\ N = 13.607\ kN$$
$$F_{leaves} = F_{trunk} = 13.607\ kN$$
$$F_{tree} = F_{trunk} + F_{leaves} = 13.607 + 13.607 = 27.61\ kN$$

This point load is significant because with a diameter of 0.8m only an area of 0.502m^2 is used. However, close to the tree, there is expected to be reserved space for the tree to grow. Therefore, parked cars or other significant loads do not have to be considered at this location. In the plane strain model with unit thickness, it would is assumed to spread this out over 1 m with 27.61 kN/m as load, rather than 10 kN/m, which is considered in the TAK. Note that this will probably slightly overestimate the load as it will be distributed over a larger area using the root system.

Smart technology for monitoring

Implement smart sensors for monitoring water levels, structural health, and environmental conditions. This data can aid in real-time management and maintenance. The structural effects of the applied sensors are very limited, since the weight and volume of these devices is small.

Waste management

Another option is to design waste collection and recycling facilities into the quay wall to keep the area clean and promote sustainability. Underground containers look like Figure 45 - Trash collection system. In a quay wall, you would put those containers directly next to the masonry wall. Note that since these containers should be accessed by people, cars cannot park here. The weight of these containers is 1200 kg over an area of 2.03 m by 1.78 m (EarthBin, 2024). This means that the distributed load per unit area is equal to:

$$q_{container} = \frac{G_{container} * g}{A_{container}} = \frac{G_{container} * g}{b_{container} * h_{container}} = \frac{1200 * 9.81}{2.03 * 1.78} = 3257.9 \frac{N}{m^2} = 3.26 \frac{kN}{m^2}$$

Therefore, the load on top of the quay wall is considered less than 10 kN/m^2, which is the situation for which the quay wall should be tested. Thus, this situation is not governing and can be neglected. The weight of the waste is 3 kN/m^3 for uncompacted or poorly compacted waste to 17 kN/m^3 for compacted waste (Zekkos, et al., 2006). Since the waste is not well compacted, a density in the middle of 10 kN/m^3 is assumed. This means that the weight of the waste is also less than the soil it replaces and therefore does not have to be considered.

Figure 45 - Trash collection system (Lapper, 2024)

3.3.3 Loading history

To accurately determine the current stresses in the subsoil, a Finite Element Model must consider the loading history of the site and the construction of the quay structure. For the initial phases, a standard phasing has been developed based on historical data regarding the development of the canals and quay walls. The standard phasing steps can also be changed if there is clear reason to do so (Ingenieursbureau Gemeente Amsterdam, 2023). The steps are:

- *Initial phase (K_0 procedure)*: stresses in the soil are initialised
- *Lower water table*: the water table is lowered
- *Excavate*: the soil is excavated where the floor, kesp, and masonry wall will come. Also, the backfill soil is removed with a slope 1V:3H.
- *Add piles*: the piles are embedded in the ground
- *Add wall*: the kesp, floor, and masonry wall are built
- *Backfill soil*: the soil is backfilled
- *Heighten water table*: water table is returned to its normal level
- *Add traffic/parking loads*: loads are added

4 Development and Implementation of the Finite Element Models

In this Chapter all FE models are explained. Initially, the traditional models are explained. Secondly, the sheet pile models are expanded upon. In both structural configurations, first the implementation in the software DIANA is explained, followed by the implementation in Plaxis.

4.1 Traditional model DIANA

For the model in DIANA FEA a structural analysis is carried out in a plane strain model using plane strain elements (Figure 46). The model thickness is set to 1000mm. The default mesh type setting is set to Hexa/Quad elements. This means that by default quadrilateral elements are used. To prevent distorted elements, triangular elements have also been used. In Figure 53 the mesh can be seen. Furthermore, the default mesh order is set to quadratic and the mid-side node location on shape. The units used in DIANA are listed in Table 12.

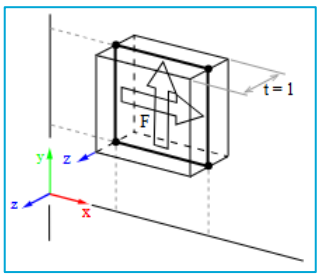

Figure 46 - Plane strain elements, characteristics (DIANA User Manual, 2025)

Table 12 - DIANA traditional model: user defined units

Quantity	Unit	Symbol
Length	millimetre	mm
Mass	ton	T
Force	newton	N
Time	second	s
Temperature	kelvin	K
Angle	degree	°

4.1.1 Geometry and materials

The general overview of the geometry at the end of the construction sequence can be found in Figure 47. It implements the structural configuration of the traditional quay wall, which is described earlier in section 3.2.1. This sequence is very important for the analysis, which enables non-linear soil to have the correct stress-strain state before applying external loads. Therefore, a Geomechanical staged construction analysis is used. The geometry does change over the different analysis steps, which also explains why the soil polygons are split up into different parts.

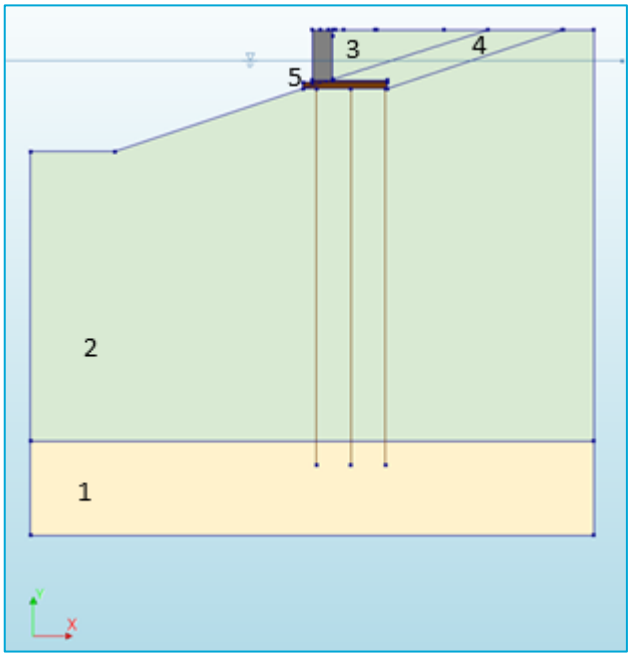

Figure 47 - Overview geometry traditional model DIANA: 1 Soil_Bottom; 2 Soil_Top; 3: Soil_Backfill; 4: Soil_Excavation; 5: Soil_Timber

The water level is also shown as a horizontal blue line at the top of the model going through the masonry wall and the clay layer. This water level is referred to as the *Normal water level* and is assumed to be at NAP-400mm. NAP coincides with the x-axis of the model, which is located 580 mm below the soil surface at the right side of the quay, or 1290 mm from the bottom of the kesp upwards. The y-axis coincides with the left side of the masonry wall. Note that during the construction another water level is used, which is referred to as *Excavation water level*. This water level is located at NAP-1400mm.

In Figure 48 the geometry of the construction during different stages is shown coloured by their respective materials. The different shapes are divided into different subgroups. Understanding the different shapes present in the model is important to later properly understand the construction stages. Those are Piles, Quay and Soil. The subgroup Piles consists of Pile 1, Pile 2 and Pile 3, numbered from left to right. The subgroup Quay consists of the polygons Wall, Floor and Kesp. The Kesp is connected to the Piles using a rigid connection, as translations in both x and y direction are restrained. In the Plane Strain model in DIANA the rotational DOF is prevented, thereby effectively making this a hinged connection. This is an unconservative approach, as will be discussed in the Discussion in section 6.4.2, which shows the results of both hinged and rigid connections between the Piles and Kesp in Plaxis. DIANA does not offer this setting; therefore, the hinged connection is modelled in DIANA and Plaxis. The former comparison in the Discussion serves as reference to show the implications of this approach. The connections between the different elements are described at the end of this section, after the elements. The described connections are between the Floor and Wall, the Soil and Floor, and the Wall and Soil. The Soil polygons are the following:

- Soil_Bottom (1): the bottom sand layer in Figure 47.
- Soil_Top (2): largest soil polygon (see Figure 47) and connected the sand layer. It is clay.
- Soil_Backfill (3): triangular shape only present after backfilling the soil, it is shown on the right in Figure 48. It is clay.

- Soil_Excavation (4): present before and after construction but removed in stages in between to install the quay wall. It connects Soil_Backfill and Soil_Top.
- Soil_Timber (5): present initially, but in a later stage removed and replaced by the quay elements. It is clay.

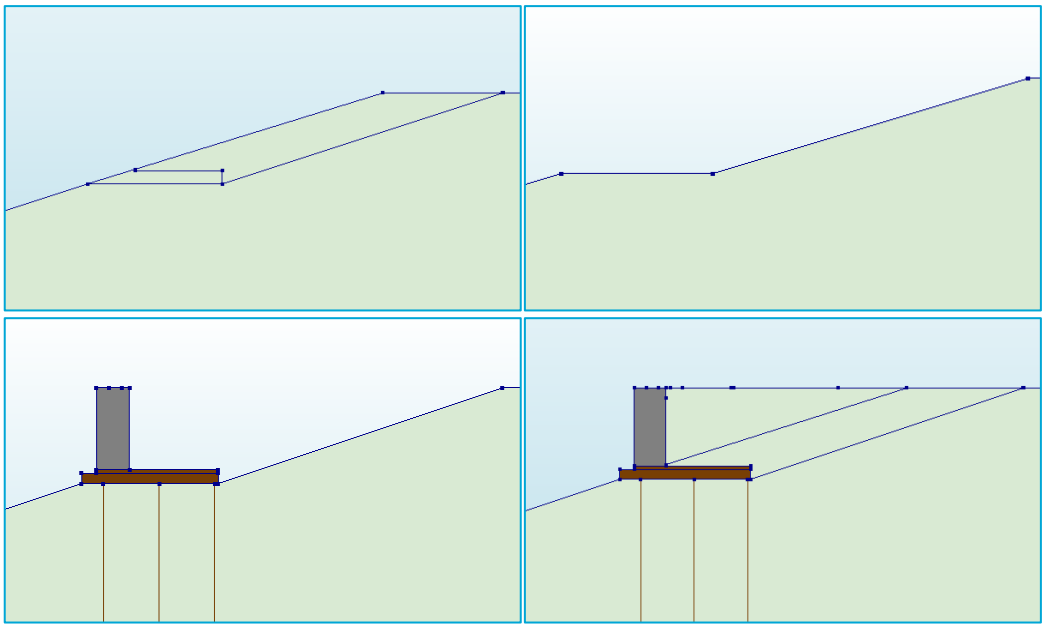

Figure 48 - Geometry during different stages: initial phase (top left), after excavation (top right); after construction quay (bottom left); after backfilling soil (bottom right)

Piles

The piles are modelled as *Numerically Integrated Bending Piles*. These are modelled with Class-III beam elements using Mindler-Reissner theory, i.e. with axial deformation, shear deformation, curvature and torsion. A circular pile shape is chosen with a diameter of 200 mm. The total length of the piles is 12 m. Tapering is not considered. The spacing between the piles is set to 1100 mm. Embedding was set to *All clashing shapes*. This means that the software automatically embeds the piles in the overlapping soil elements. The exact location of the piles, which are modelled using lines are given in and the unit is different.

Table 13.

DIANA uses 4 parameters to determine the Soil-Structure Interaction (SSI). The first two determine the pile shaft to soil interface (DIANA User Manual, 2025). Note that those should be different for the clay and sand layer, as both soils have different material properties. In this thesis the piles were modelled as one element, thereby requiring averaging of those properties. The properties are listed below:

- *Stiffness normal to pile (R_N)*: Value of the linear stiffness modulus that sets the relation between the normal traction and the normal relative displacement of the pile shaft to soil interface in the pile element y direction.
- *Shear stiffness along pile (R_S)*: Value of the linear stiffness modulus that sets the relation between the shear traction and the shear relative displacement of the pile shaft to soil interface in the pile element x direction.

The last 2 parameters of the SSI determine the pile tip to soil interface (DIANA User Manual, 2025), for this only the bottom sand layer is relevant:

- *Spring stiffness in pile direction* K_n: Value of the linear stiffness modulus that sets the relation between the force and the relative displacement at the pile tip in the pile x direction, which is in the direction of the pile.
- *Spring stiffness normal to pile* K_s: Value of the linear stiffness modulus that sets the relation between the force and the relative displacement at the pile tip in the normal direction to the pile.

The linear properties for the piles are given in

Table 14. The *Young's Modulus* and *Mass density* are obtained in the Literature Review in section 2.2.1 for C24 Timber. The SSI parameter for the stiffness normal to the pile is set manually to 75 N/mm^3. This normal stiffness is a slightly lower than the unloading-reloading stiffness of sand of 100 N/mm^3 and higher than that of clay of 11.8 N/mm^3 mentioned in Table 18. It is assumed to be conservative for the bending moments and normal forces in the piles to have a greater stiffness, thereby attracting more forces. Therefore, the value of 75 is higher than what would be expected upon specifying a linear interface stiffness based on the weighted average of the sand and clay layer. The shear stiffness (*G*) is approximated by taking the normal stiffness (*E*) and dividing this by a factor 2.5 as can be derived by filling in the average Poisson's ratio ($\nu = 0.25$) for clay and sand.

$$G = \frac{E}{2(1+\nu)}$$

Using this method, the shear stiffness of the pile is derived to be 30 N/mm^3. In section 4.2.1 it is explained how Plaxis obtains the pile shaft to soil properties and these values are listed in Table 27 for both the clay and sand layer. After averaging the stiffnesses weighted to lengths embedded the soil layers, the following values are obtained: $R_S = 0.00434\ N/mm^3$ and $R_N = 0.00434\ N/mm^3$. Upon reflection therefore the manually set values seem very high. The reader is referred to section 6.4.1 in the Discussion for the comparison between the two software.

Additionally, the pile tip to soil interface in pile direction (K_n) was set to $60 * 10^3\ N/mm$. Again, the shear stiffness (K_s) follows as $24 * 10^3\ N/mm$ by dividing by a factor of 2.5. In Plaxis the stiffness normal to the pile (K_F) for the sand layer is found to be 2.28 N/mm^2 in section 4.2.1. The area (*A*) of the piles is $3.14 * 10^4\ mm^2$. Upon multiplication a value for the base stiffness following Plaxis can be derived:

$$K_{n,Plaxis} = K_F * A = 2.28 * 3.14 * 10^4 = 7.17 * 10^4\ N$$

It is found that the value set in DIANA initially is a bit higher than Plaxis and the unit is different.

Table 13 - Coordinates piles DIANA (values in millimetres)

	Top coordinate (X, Y)	**Bottom coordinate (X, Y)**
Pile 1	(137.5, -1290)	(137.5, -13290)
Pile 2	(1237.5, -1290)	(1237.5, -13290)
Pile 3	(2337.5, -1290)	(2337.5, -13290)

Table 14 - Material properties piles

Property	Value	Unit
Young's Modulus	11000	N/mm^2
Mass density	4.2E-10	T/mm^3
Stiffness normal to pile	75	N/mm^3
Shear stiffness along pile	30	N/mm^3
Derive interface stiffness	FALSE	-
Shaft interface failure model	No failure	-
Shaft interface normal stiffness	Linear	-
Spring stiffness in pile direction K_n	6.00E+04	N/mm
Spring stiffness normal to pile K_s	2.40E+04	N/mm
Pile tip failure model	No failure	-

Quay

The wall is constructed out of masonry, the properties have been described in the Literature Review in 2.2.2 and follow pre 1945 masonry (NPR 9998, 2020). As material model, the Total Strain Based Crack Model (DIANA User Manual, 2025) using a rotating crack model is employed, which has been explained in section 2.3.2. The properties are listed in Table 15 and match models of modelled quays under traffic loading (Sharma, Longo, & Messali, 2024). The coordinates of this polygon for the exact geometry are given in Table 17.

Table 15 – Material properties masonry wall

Symbol	Property	Value	Unit
E	Young's Modulus	5000	N/mm^2
v	Poisson's ratio	0.25	-
γ	Mass density	1.95E-09	T/mm^3
	Crack orientation	Rotating	-
	Tensile curve*	Linear-crack energy	-
f_t	Tensile strength*	0.1	N/mm^2
$G_{f,t}$	Mode-I tensile fracture energy*	0.01	N/mm
	Crack bandwidth specification	Govindjee	-
	Reduction model	No reduction	-
	Compression Curve	No failure	-
f_c	Compressive strength	8.5	N/mm^2
$G_{f,c}$	Compressive fracture energy	20	N/mm
	Reduction model	Vecchio and Collins 1993	-
	Lower bound reduction curve	0.4	-
	Confinement model	No increase	-

The floor and kesp are constructed out of C24 timber. A linear elastic model has been chosen for both structural elements. The kesp has a thickness of 200 mm and the floor has a thickness of 70mm. However, where the floor has the plane strain model width of 1000 mm, the kesp only has a width of 200 mm, which cannot be put into the plane strain model. In the plane strain model, the kesp stiffness should be adjusted to account for this difference, as the following equation should hold:

$$E_{model} I_{model} = E_{reality} * I_{reality}$$

After rewriting, to free E_{model}, the following equation is obtained, which can be rewritten and simplified (where the property $h_{model} = h_{reality}$ is used):

$$E_{model} = \frac{E_{reality} * I_{reality}}{I_{model}} = \frac{E_{reality} * \frac{1}{12} * b_{reality} * h_{reality}^3}{\frac{1}{12} * b_{model} * h_{model}^3} = \frac{E_{reality} * b_{reality}}{b_{model}}$$

This correction should also be applied to account for the difference in density:

$$\rho_{model} = \frac{\rho_{reality} * b_{reality}}{b_{model}}$$

The material properties of the floor and the kesp, for which stiffness and density have been corrected, are listed in Table 16. The coordinates of both polygons are listed in Table 17.

Table 16 - Material properties floor and kesp

Property	Unit	Floor	$Kesp_{model}$
Young's Modulus	N/mm^2	11000	2200
Poisson's ratio	-	0.35	0.35
Mass density	T/mm^3	4.20E-10	8.40E-11

Table 17 – Coordinates quay polygons in traditional model DIANA (values in millimetres)

Wall		Kesp		Floor	
X	Y	X	Y	X	Y
0	-1020	-300	-1290	0	-1090
650	-1020	2400	-1290	2400	-1090
650	580	2400	-1090	2400	-1020
0	580	-300	-1090	0	-1020
0	-1020	-300	-1290	0	-1090

<u>Soil</u>

The soil consists of multiple polygons, which have already been briefly described. All soil polygons consist of clay, except Soil_Bottom, which consists of sand. The division of the soil into various polygons is necessary for the Geomechanical staged construction analysis to allow parts to be switched on and off. For both clay and sand a Hardening Soil with small strain has been adopted of which the properties that are similar in DIANA and Plaxis are listed in Table 18. The properties are extensively described in the Literature Review in section 2.3.1, which explains the adopted constitutive model, a Hardening Soil small stiffness model with Mohr-Coulomb yield criterion, in detail. The values are obtained from the Case Study in section 3.1.4. The failure ratio (R_f [-]) was set 0.8 for clay and 0.7 for sand in DIANA. The soil polygon coordinates are listed in Table 19.

Table 18 - Material properties Hardening Soil with small strain model DIANA and Plaxis

Symbol	Description	Unit	Clay	Sand
E_{50}^{ref}	Reference triaxial secant stiffness	N/mm^2	3.7268	35
E_{UR}^{ref}	Unloading-reloading stiffness	N/mm^2	11.8	100
E_{oed}^{ref}	Reference oedometer tangent stiffness	N/mm^2	2.396	20
ν_{UR}	Poisson's ratio	-	0.3	0.2
c'_{ref}	Cohesion	N/mm^2	0.00516	0.0029
ϕ'	Friction angle at shear failure	°	23.8	30
ψ	Dilatancy angle at shear failure	°	0	0
p_{ref}	Reference pressure	N/mm^2	0.1	0.1
m	Stress-dependency exponent	-	0.8	0.5
OCR	Overconsolidation ratio	-	1	1
$\sigma_{tension}$	Tension cut-off value	N/mm^2	0	0
K_0^{nc}	Earth pressure coefficient at rest	-	0.596	0.5
γ_{dry}	Dry density	N/mm^3	1.402E-05	1.666E-05
n	Porosity	-	0.3333	0.3333

Table 19 – Coordinates soil polygons in traditional model DIANA (values in millimetres)

Soil_Bottom		Soil_Top		Soil_Backfill		Soil_Excavation		Soil_Timber	
X	Y	X	Y	X	Y	X	Y	X	Y
-9000	-15530	-9000	-12530	650	0	650	-1020	-300	-1290
9000	-15530	9000	-12530	650	580	650	-989.41	650	650
9000	-12530	9000	580	5610	580	5610	580	650	-1020
-9000	-12530	8010	580	650	0	8010	580	2400	-1020
-9000	-15530	2400	-1290			2400	-1290	2400	-1290
		-300	-1290			2400	-1020	-300	-1290
		-6300	-3290			650	-1020		
		-9000	-3290						
		-9000	-12530						

Connection Floor-Wall

Between the Floor and Wall a linear elastic interface is specified. In the manual DIANA (DIANA User Manual, 2025) prescribes the interfaces to be modelled with the following normal stiffness (K_n) and tangential stiffness (K_t):

$$K_n = 1000 * \frac{E_{adj}}{l_{el}}$$

$$K_t = \frac{K_n}{100}$$

Where E_{adj} is the is the elasticity modulus of the adjacent mesh set which is the lowest elasticity modulus of the two sides and l_{el} is the characteristic length of an element. Figure 49 is provided for reference. The Young's Modulus of the masonry and timber are 5000 N/mm^2 and 11000 N/mm^2 respectively, therefore E_{adj} is set to 5000 N/mm^2. The characteristic element length is set to 50 mm as explained in section 4.1.3. Filling in all obtained values results in:

$$K_n = 1000 * \frac{5000}{50} = 1 * 10^5\ N/mm^3$$

$$K_t = \frac{1 * 10^5}{100} = 1000\ N/mm^3$$

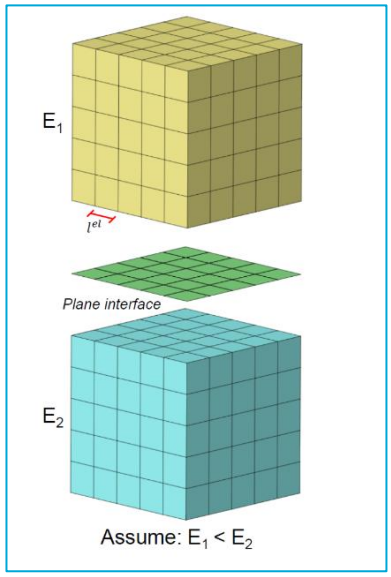

Figure 49 - Interface between two different materials (DIANA User Manual, 2025)

It is stated in the manual that these formulas are only used as the initial guess and should be calibrated. However, calibration is not performed. The interface is visualised in Figure 51. Additionally, it should be stated that the Wall could come loose from the Floor if the friction is not able to resist the lateral soil pressures exerted on the Wall. However, often the *Schuifhout* (a wooden part) is preventing sliding as illustrated in Figure 50.

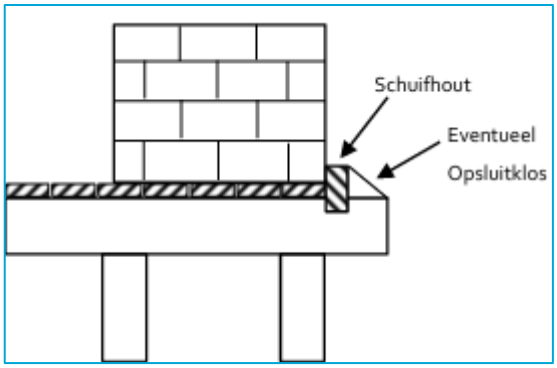

Figure 50 - Floor-Wall connection in detail. The 'Schuifhout' and possible ´Oplsluitklos´ are also shown. These are not modelled in the models in the thesis but are often present in quay walls and prevent sliding of the Wall (Ingenieursbureau Gemeente Amsterdam, 2023)

Connection Wall-Soil

The connection between the Wall and the Soil is made using Structural Line Interfaces in which Coulomb Friction is applied. The linear stiffnesses are derived in the same manner as for the elastic Floor-Wall interface. The Young's Modulus of the masonry and clay soil are 5000 N/mm^2 and 11.8 N/mm^2 respectively, therefore E_{adj} is set to 8 N/mm^2. The characteristic element length is set to 50 mm. This results in the following values:

$$K_n = 1000 * \frac{E_{adj}}{l_{el}} = 1000 * \frac{11.8}{50} = 236\ N/mm^3$$

$$K_t = \frac{K_n}{100} = \frac{236}{100} = 2.36\ N/mm^3$$

Additionally, a tension cut-off criterion is specified, for which the following settings are used according to Table 20, which reflect the properties of the soil in Table 18. The tension-cutoff is required to correctly model the soil, which cannot take tension.

Table 20 - Coulomb Friction interface settings

Symbol	Description	Unit	Value
c	Cohesion	N/mm^2	0.00516
ϕ	Friction angle	°	23.8
ψ	Dilatancy angle	°	0
f_{tco}	Tensile cutoff value	N/mm^2	0

<u>Connection Floor-Soil</u>

The Floor-Soil interface is the same as the Wall-Soil interface, the calculation is repeated. The Young's Modulus of the timber and clay soil are 11000 N/mm^2 and 11.8 N/mm^2 respectively, therefore E_{adj} is set to 11.8 N/mm^2. The characteristic element length is set to 50 mm. This results in the following values:

$$K_n = 1000 * \frac{E_{adj}}{l_{el}} = 1000 * \frac{11.8}{50} = 236\ N/mm^3$$

$$K_t = \frac{K_n}{100} = \frac{236}{100} = 2.36\ N/mm^3$$

Again, a tension cut-off criterion is specified, for which the following settings are used according to Table 20, which reflect the properties of the soil in Table 18. The tension-cutoff is required to correctly model the soil, which cannot take tension.

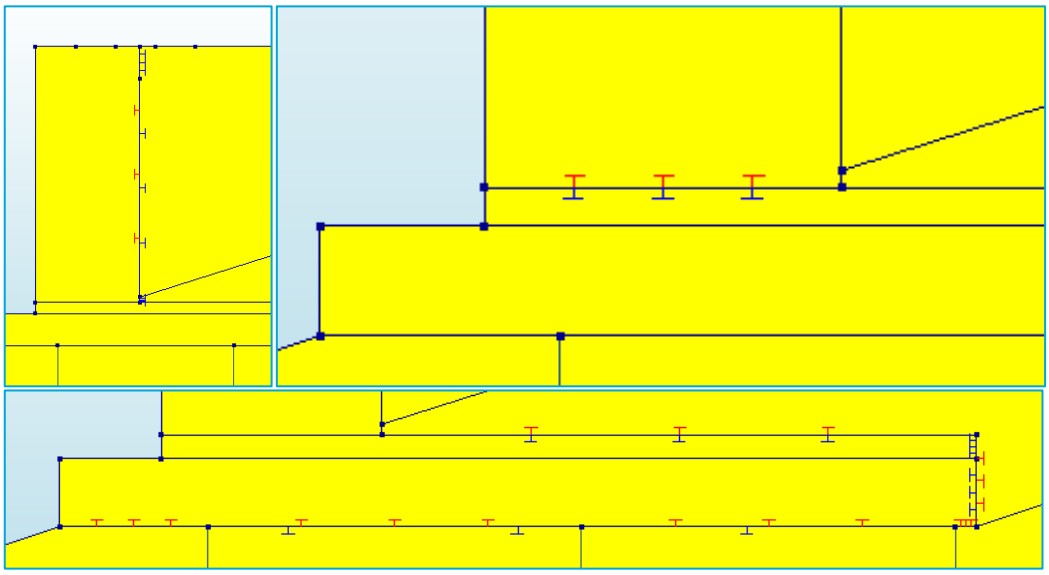

Figure 51 - Interfaces visualised. Top left: Floor-Soil; Top right: Floor-Wall; Bottom: Floor-Soil

4.1.2 Boundary conditions and loads

The boundary conditions for this FE model are visualised in Figure 52. The supports at the bottom restrain translations in both the X- and Y-direction (horizontal and vertical). The supports at the left and right side of the model restrain movement in the X-direction (horizontal).

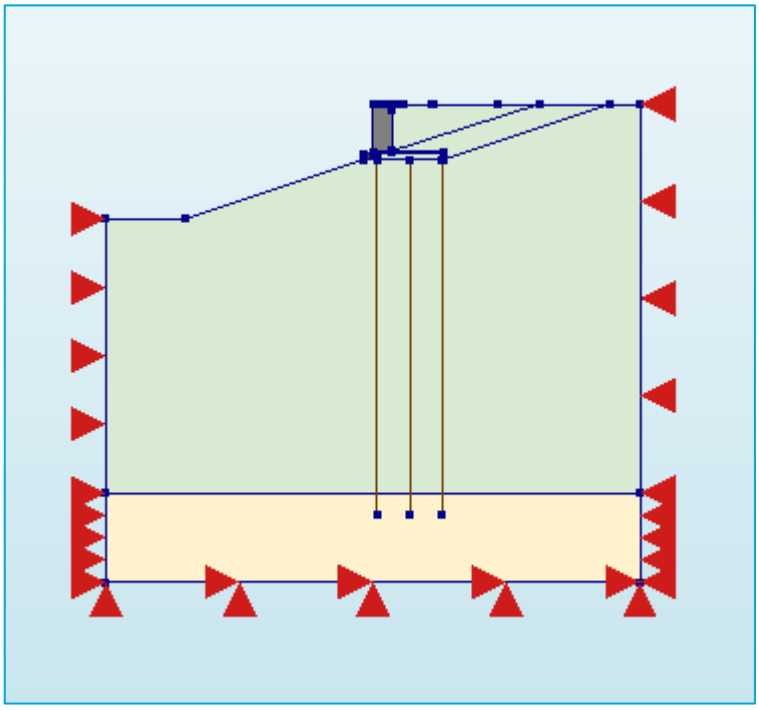

Figure 52 - Boundary conditions traditional model DIANA

The loads acting on the quay walls have extensively been explained in section 3.3. Therefore, a further explanation is not given in this section. The loads, their magnitude, and where they act on the quay are briefly repeated in Table 21.

Table 21 - Overview loads DIANA

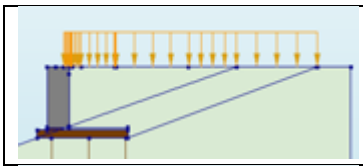	**TAK**		
	Magnitude (Y)	-10	N/mm
	X_{start}	500	mm
	X_{end}	8000	mm
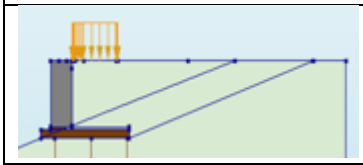	**Energy storage**		
	Magnitude (Y)	-8.48	N/mm
	X_{start}	650	mm
	X_{end}	2050	mm
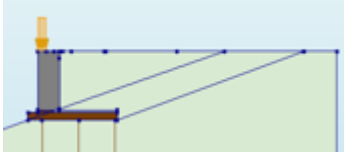	**Panel**		
	Magnitude (Y)	-7.392	N/mm
	X_{start}	0	mm
	X_{end}	250	mm
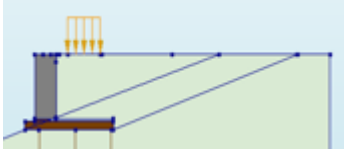	**Tree**		
	Magnitude (Y)	-27.61	N/mm
	X_{start}	1000	mm
	X_{end}	2000	mm

Using the obtained loads, various combinations are tested for their structural performance. Initially, a reference case is tested to see the structural performance under standard loading conditions, this is the TAK combination. Secondly, multiple combinations of the TAK with one additional

multifunctionality are tested. Lastly, the load from the TAK and all multifunctionalities combined are tested. The load combinations are summarised in Table 22.

Table 22 - Load combinations DIANA

Combination	TAK	Tree	Energy storage	Panel
TAK	1			
TAK+Tree	1	1		
TAK+Energy	1		1	
TAK+Panel	1			1
TAK+AllMF	1	1	1	1

4.1.3 Mesh and analysis

The mesh that is used for the analysis is different for the various shapes and is given in Figure 53. For the bottom sand layer (Soil_Bottom) and the largest clay block (Soil_Top), quad elements have been chosen with a mesh size of 250 mm. For the other shapes a triangular mesh size has been chosen to prevent distorted elements. For the floor an element size of 50 mm is chosen. Respectively for the wall and kesp a mesh size of 200 mm and 100 mm have been chosen. The shapes of the backfill (Soil_Backfill) and excavation (Soil_Excavation) have a mesh size of 200 mm.

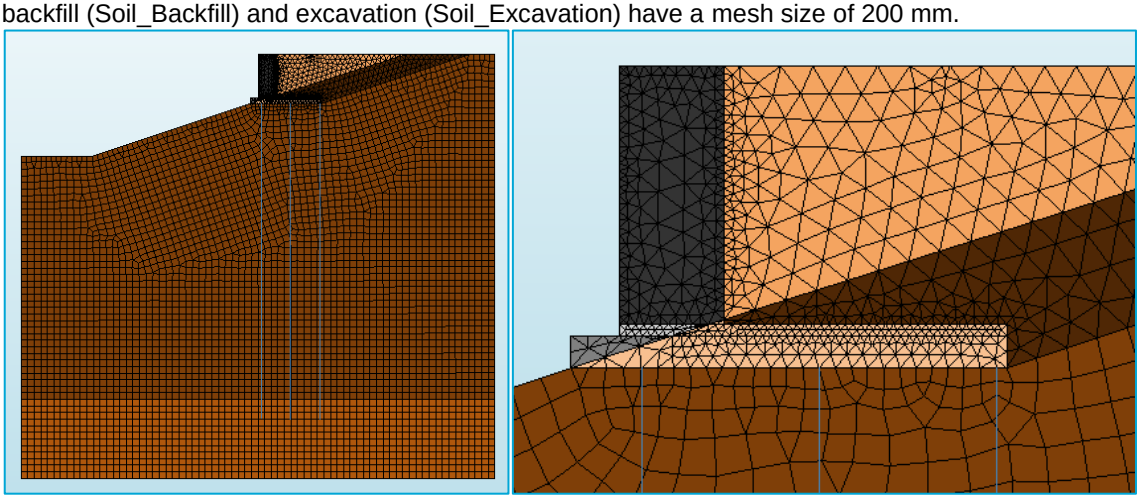

Figure 53 - Mesh traditional model DIANA overview (left) and zoomed in on quay structure (right)

For the analysis a Geomechanical staged construction analysis was selected. The construction sequence is illustrated in Table 23. In the latest stage the load combination TAK is added. For the other combinations, only the last phase changes, as another load is applied there. Two specific settings used in the analysis, *Clear displacements* and *Init stresses* are also shown in Table 23. *Clear displacements* refers to the displacements calculated at each stage after removing previous displacements, isolating the effect of the current load step. *Init stresses* represent the pre-existing stress state in the model before any load is applied, accounting for factors like soil weight and initial conditions. These terms ensure the model captures the evolving system response, with clear displacements tracking new deformations and initial stresses providing a baseline for accurate load predictions, especially in complex geotechnical scenarios such as for a quay wall.

The solution was set to Parellel Direct Sparse. This solver shows both a high performance and memory efficient usage for solving large sparse symmetric and unsymmetric linear systems of equations by shared multiprocessors (DIANA User Manual, 2025).

The iteration method selected for the phases when the phreatic level is varied is Newton regular with a maximum number of iterations of 1000 and a convergence tolerance of 0.001. A Secant (Quasi-Newton) approach is used as iteration method for the remaining structural phases, where the maximum number of iterations is also set to 1000. The type of the method is set to BFGS, which is the Broyden-Fletcher-Goldfarb-Shanno Algorithm (Nayak, 2020). First tangent is set to previous iteration. The convergence norm is set to satisfy both a displacement and a force norm, with a convergence tolerance of 0.01. If convergence is not found, the analysis is set to continue.

Table 23 - Stages of the construction of the traditional model in DIANA

	Initial Phase (K0_procedure) Clear displacements Init stresses TRUE
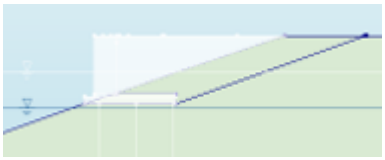	**Lower water table** Clear displacements Init stresses
	Excavate Clear displacements Init stresses
	Add piles Clear displacements TRUE Init stresses
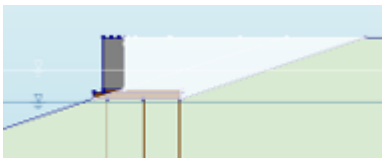	**Add wall** Clear displacements Init stresses
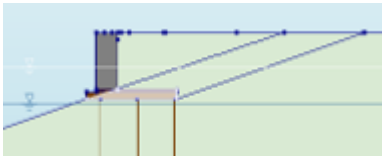	**Backfill soil** Clear displacements Init stresses
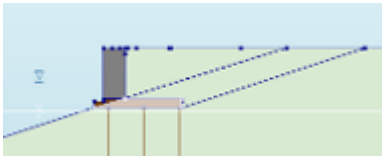	**Heighten water table** Clear displacements Init stresses
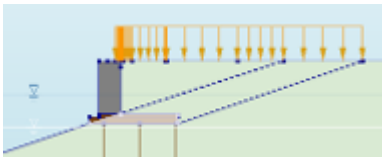	**Add loads** Clear displacements Init stresses

4.2 Traditional model Plaxis

A plane strain model is used to model the traditional quay wall in Plaxis 2D. 15-Noded elements are selected. The model units are defined as in Table 24.

Table 24 - Plaxis 2D traditional model units

Quantity	Unit
Length	mm
Force	N
Time	day
Mass	kg
Temperature	K
Energy	kJ
Power	kW
Stress	N/mm^2
Weight	N/mm^3

4.2.1 Geometry and materials

The general overview of the geometry at the end of the construction sequence can be found in Figure 54 and mimics the structure modelled in DIANA. A difference is that the kesp and floor are modelled in a single plate element rather than two different elements. In Plaxis 2D the Staged construction analysis is used. The geometry does change over the different phases, which again explains why the soil polygons are split up into different parts.

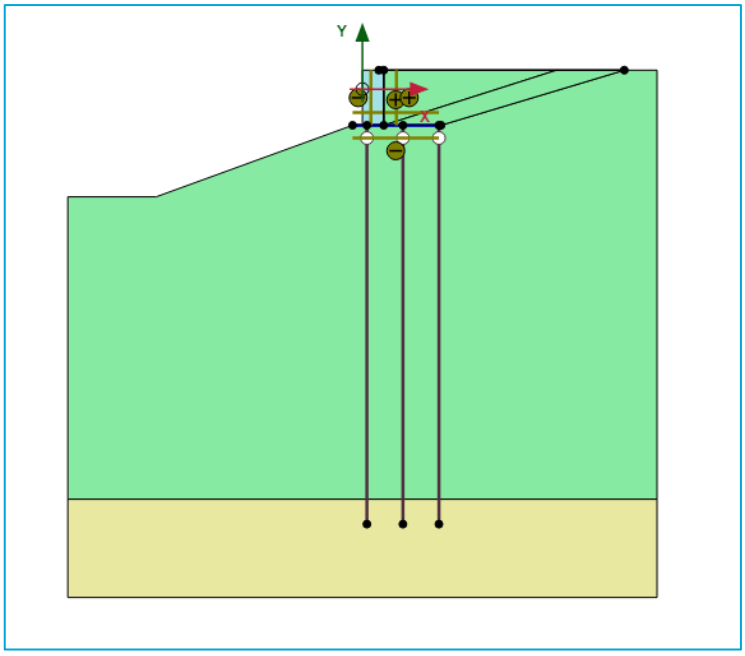

Figure 54 – Overview geometry traditional model Plaxis 2D

The *Normal water level* is not shown in the model but is assumed to be at NAP-400mm. NAP coincides with the x-axis of the model, which is 580 mm below the top right side of the model. The y-axis coincides with the left side of the masonry wall. Note that during the construction another water level is used, which is referred to as *Excavation water level*. This water level is located at NAP-1400mm.

In Figure 55 the geometry of the construction during different phases is shown coloured by their respective materials. The shapes present in the model change throughout the phases. Those are subdivided into Piles, Quay and Soil. The subgroup Piles consists of Pile 1, Pile 2 and Pile 3, numbered from left to right. The subgroup Quay consists of the polygon Wall and the plate Kesp_Floor. The Soil consists of the following polygons:

- Bottom: the bottom sand layer in Figure 54.
- Top: largest soil polygon (see Figure 54) and connected the sand layer. It is clay.
- Backfill: triangular shape only present after backfilling the soil, it is shown on the right in Figure 55. It is clay.
- Excavation: present before and after construction but removed in stages in between to install the quay wall. It connects Backfill and Top.

Compared to DIANA the major differences are that the kesp and the floor are modelled as a single plate element instead of two different plane strain elements. Also, the place where in the later stages the quay wall geometry is present is not modelled in Plaxis 2D, as there cannot be overlapping elements. This effectively means that there is more excavated soil at the initialisation of the soil, which can be seen when the left image of Figure 48 is compared with the left image of Figure 55. Furthermore, the interfaces are described at the bottom of this section.

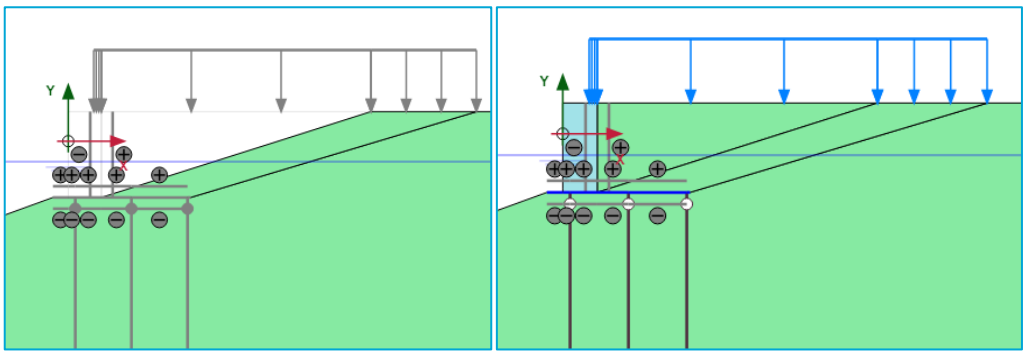

Figure 55 - Geometry during different stages: before construction (left) and after construction (right)

<u>Piles</u>

The piles have been modelled as embedded beam rows. The coordinates of the piles are given in Table 25. Note that the y-coordinate of the top is different than in DIANA in and the unit is different.

Table 13. This has to do with the fact that the plate is modelled as a line element in Plaxis in 2D, instead of a polygon in DIANA. Timber C24 is the material used for the piles. An elastic material type is selected with properties as in Table 26. Since it is important to understand how the pile behave under loading and interact with the surrounding soil, this is expanded upon. With the diameter (*D*) and Young's Modulus (*E*) of the pile, the area (*A*), moment of inertia (*I*), equivalent diameter (D_{eq}) and equivalent radius (R_{eq}) are calculated in the following manner (Plaxis Reference Manual, 2025):

$$A = \frac{1}{4}\pi D^2 = \frac{1}{4}\pi 200^2 = 3.14 * 10^4\ mm^2$$

$$I = \frac{\pi D^4}{64} = \frac{\pi 200^4}{64} = 7.85 * 10^7\ mm^4$$

$$D_{eq} = \sqrt{\frac{12EI}{EA}} = \sqrt{\frac{12 * 11000 * 7.85 * 10^7}{11000 * \ 3.14 * 10^4}} = 173.21\ mm$$

$$R_{eq} = \frac{D_{eq}}{2} = \frac{173.2}{2} = 86.60\ mm$$

These parameters are necessary to model the interface stiffnesses, which will be described below Table 25 and Table 26.

Table 25 - Pile coordinates Plaxis 2D (values in millimetres)

	Top coordinate (X, Y)	Bottom coordinate (X, Y)
Pile 1	(137.5, -1104)	(137.5, -13290)
Pile 2	(1237.5, -1104)	(1237.5, -13290)
Pile 3	(2337.5, -1104)	(2337.5, -13290)

Table 26 - Material properties timber piles in Plaxis 2D

Property	Value	Unit
γ	4.20E-06	N/mm^3
$L_{spacing}$	1100	mm
Coss section type	Predefined	-
Predefined cross section type	Solid circular beam	-
Diameter	200	mm
E	11000	N/mm^2
Axial skin resistance	Layer dependent	-
Lateral resistance	Unlimited	-
F_{max}	1.00E+05	N
Default values	FALSE	-

In Plaxis multiple stifnesses are being determined in two steps. Initially the interface stiffness factors (*ISF*) are determined, whereafter the interface stiffnesses are calculated. The abbreviations used and physical meaning are all visualised in Figure 56. The interface stiffness factors (*ISF*) are calculated using the information provided by the software (Plaxis Reference Manual, 2025):

$$ISF_{RS} = 2.5\left(\frac{L_{spacing}}{D}\right)^{-0.75} = 2.5\left(\frac{1100}{200}\right)^{-0.75} = 0.696$$

$$ISF_{RN} = 2.5\left(\frac{L_{spacing}}{D}\right)^{-0.75} = 2.5\left(\frac{1100}{200}\right)^{-0.75} = 0.696$$

$$ISF_{KF} = 25\left(\frac{L_{spacing}}{D}\right)^{-0.75} = 25\left(\frac{1100}{200}\right)^{-0.75} = 6.96$$

From the interface stiffness factors, the interface stiffnesses are determined using the following equations:

$$R_S = ISF_{RS}\frac{G_{soil}}{L_{spacing}}$$

$$R_N = ISF_{RN}\frac{G_{soil}}{L_{spacing}}$$

$$K_F = ISF_{KF}\frac{G_{soil}R_{eq}}{L_{spacing}}$$

Note that these are dependent on the shear modulus of the soil (G_{soil}). As explained in the Literature Review in section 2.3.1, for a hardening soil model the shear modulus depends on the stress. Therefore, as the stress level varies throughout the length of the pile, only an initial assumption is made, to get an idea of what the value approximately should be.

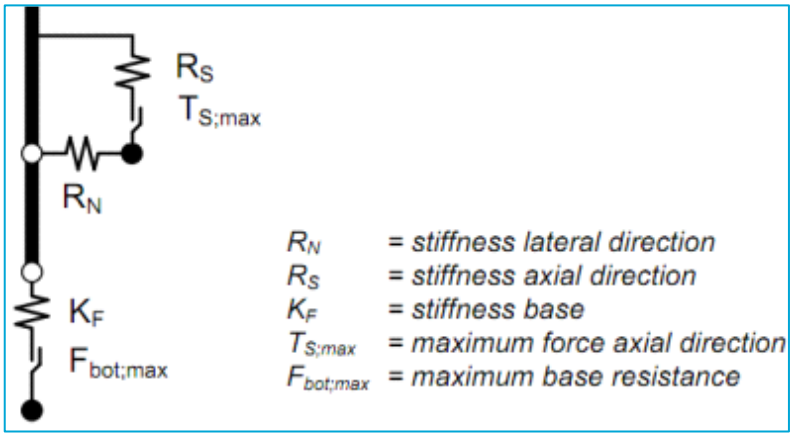

Figure 56 - Modelling of soil-pile interaction (Plaxis Reference Manual, 2025)

For the initial assumption a linear elastic soil is assumed, in which the shear modulus (G_{soil}) does depend on Poisson's ratio (v) and the Young's Modulus (E) of its respective soil (either clay or sand), according to the equations below:

$$G_{clay} = \frac{E_{clay}}{2(1+v_{clay})} = \frac{11.8}{2(1+0.3)} = 4.54\ N/mm^2$$

$$G_{sand} = \frac{E_{sand}}{2(1+v_{sand})} = \frac{100}{2(1+0.2)} = 41.7\ N/mm^2$$

Note that these properties have been listed Table 18 and for the stiffness the unloading-reloading stiffness has been used. All interface stiffnesses are now calculated using the given equations. Note that for the stiffness of the base (K_F), the equivalent radius (R_{eq}) is required. This parameter is visualised in Figure 57 and determines the size of the elastic zone in the soil under the embedded beam in which plastic soil behaviour is excluded (Plaxis Reference Manual, 2025). The approximated values of the interface stiffnesses are given in Table 27.

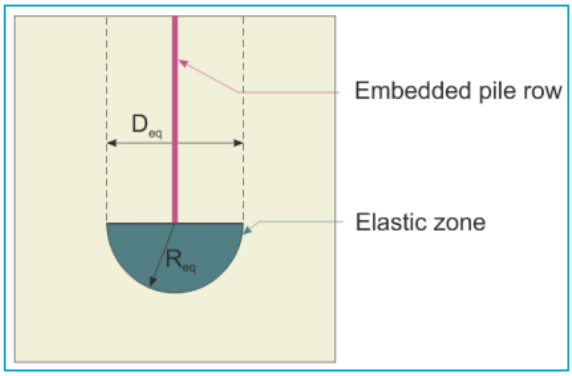

Figure 57 - Plastic zone surrounding the bottom of the pile (Plaxis Reference Manual, 2025)

Table 27 - Approximated interface stiffnesses

Symbol	Description	Unit	Clay	Sand
R_S	Stiffness lateral direction	[N/mm^3]	0.0029	0.0264
R_N	Stiffness axial direction	[N/mm^3]	0.0029	0.0264
K_F	Stiffness base	[N/mm^2]	2.4872	22.8347

The finalise this section and reflect on the implementation of the piles in Plaxis, three statements with highlighted sections from Plaxis (Plaxis Reference Manual, 2025) below should be considered. The

1st and 2nd statement are contradictory. Whereas the first statement states that Embedded Beams are not able to accurately model laterally loaded piles (which is the case for the modelled timber quay wall piles), the second states that the Embedded Beams can deal with this application. Therefore, it is questionable whether Plaxis can accurately model the piles for this specific application. Additionally, the 3rd statement advises to calibrate the bearing capacity with test results, which cannot be performed for this thesis.

Statement 1

"In addition to displacement differences and shear forces in axial direction along the pile, the pile can undergo transverse forces, t⊥, due to lateral displacements. These transverse forces are not limited in the special interface element that connects the pile with the soil, but, in general, they are limited due to failure conditions in the surrounding soil itself. However, embedded beams are not meant to be used as laterally loaded piles and will therefore not show accurate failure loads when subjected to transverse forces." – Section 6.6.4 on page 294 (Plaxis Reference Manual, 2025)

Statement 2

"A quay wall is an earth retaining structure used to moor ships. It bears vertical loads caused by storage and handling equipment and horizontal loads from the wind, soil pressure and ship impacts. Quay walls might differ in type and magnitude of the terminal. The key requirement for ships is the retaining height; when handling the freight, it is necessary to provide sufficient area and bearing capacity. For larger quay walls, using relieve platforms frees the quay walls from the high soil pressure brought by the high retaining height and the vertical loads induced by massive storage. The presence of the relieving platform, generally coupled with bearing piles, reduces the horizontal loads on the quay wall and, consequently, the bending moments. The structure could comprise an anchorage at the connection point of the quay wall and the relieving platform.

The bearing piles of the relieving platform take a part of the horizontal load that is typically taken by the retaining wall. For this reason, these piles are subjected to transverse forces induced by the lateral displacement field of the soil. The embedded beam row elements of PLAXIS 2D can realistically deal with this application. Furthermore, if the quay has a bulk-storage load, there are horizontal components difficult to model with other approaches (e.g. sub-grade reaction models). PLAXIS 2D can easily deal with this complex loading conditions." – Section 12.2.2 on page 579 (Plaxis Reference Manual, 2025)

Statement 3

> "In contrast to what is common in the Finite Element Method, the bearing capacity of an embedded beam is considered to be an input parameter rather than the result of the finite element calculation. The user should realise the importance of this input parameter. Preferably, the input value of this parameter should be based on representative pile load test or pull out test data. Moreover, it is advised to perform a calibration in which the behaviour of the embedded beam is compared with the behaviour as measured from the test. When embedded beams are used in a row, the group action must be taken into account when defining their bearing capacity." - Section 6.6 on page 284 (Plaxis Reference Manual, 2025)

Quay

The Wall is modelled as a soil polygon. The Kesp_Floor shape is modelled as a plate. Their respective coordinates can be found in Table 28. The masonry material was set to be Linear Elastic (which is later verified in the verifications section of the results) and Non-Porous, which is in accordance with the TAK (Ingenieursbureau Gemeente Amsterdam, 2023), its properties are in Table 29 and have been mentioned in the Literature Review. The Young's Modulus has been adapted to follow the implementation of the masonry in DIANA from before 1945 (NPR 9998, 2020).

Table 28 - Quay coordinates Plaxis 2D

Wall		Kesp_Floor	
X	Y	X	Y
0	-1104	-300	-1104
650	-1104	2400	-1104
650	580		
0	580		
0	-1104		

Table 29 - Masonry material properties Plaxis 2D

Symbol	Description	Unit	Value
E	Young's Modulus	N/mm^2	5000
v	Poisson's ratio	-	0.2
γ	Mass density	N/mm^3	1.95E-05

For Kesp_Floor element, an elastic material type is chosen. The material properties of the timber plate can be found in Table 30. Those have been derived by combining the geometry of the kesp and floor illustrated in Figure 58. The area of the combined shape is calculated using:

$$A_{combined} = A_{kesp} + A_{floor} = b_{kesp} * h_{kesp} + b_{floor} * h_{floor} = 200 * 200 + 1000 * 70 = 11 * 10^4\ mm^2$$

By using the density of the timber C24: γ = 4.20E-06 N/mm^3 and the stiffness: E = 11000 N/mm^2, the shape unit weight and stiffness can be derived using the following equations:

$$w = A_{combined} * \rho = 11 * 10^4 * 4.2 * 10^{-6} = 4.62 * 10^{-1}\ {}^{N}/_{mm/m} = 4.62 * 10^{-4}\ {}^{N}/_{mm/mm}$$

$$EA_{combined} = E * A_{combined} = 11000 * 11 * 10^4 = 1.21 * 10^9\ N/mm^2$$

Note in the unit weight an additional division over the length arises. This is related to the area of the shape, which is assumed per meter of the plane strain model. To derive the bending stiffness of this combined cross section, initially the centre of gravity with respect to the bottom of the kesp is derived.

$$y_{center} = \frac{A_{kesp} * \frac{h_{kesp}}{2} + A_{floor} * (h_{kesp} + \frac{h_{floor}}{2})}{A_{tot}} = \frac{40000 * \frac{200}{2} + 70000 * (200 + \frac{70}{2})}{1100000} = 185.91\ mm$$

With the derived centre of gravity, Steiner's rule can be employed to calculate the section's moment of inertia.

$$I_{combined} = I_{kesp} + a_{kesp}^2 * A_{kesp} + I_{floor} + a_{floor}^2 * A_{floor}$$
$$I_{kesp} = \frac{1}{12} * b_{kesp} * h_{kesp}^3 = \frac{1}{12} * 200 * 200^3 = 1.33 * 10^8\ mm^4$$
$$a_{kesp} = y_{center} - \frac{h_{kesp}}{2} = 185.91 - \frac{200}{2} = 85.91\ mm$$
$$I_{floor} = \frac{1}{12} * b_{floor} * h_{floor}^3 = \frac{1}{12} * 1000 * 70^3 = 2.86 * 10^6\ mm^4$$
$$a_{floor} = h_{kesp} + \frac{h_{floor}}{2} - y_{center} = 200 + \frac{70}{2} - 185.91 = 49.09\ mm$$

Filling in all obtained values results in:

$$I_{combined} = 1.33 * 10^8 + 85.91^2 * 40000 + 2.86 * 10^6 + 49.09^2 * 70000 = 6.26 * 10^8\ mm^4$$

The final step is calculating the EI of the combined cross section. Note that again the final step an additional division over the length arises, again accounting for the plane strain model width.

$$EI_{combined} = E * I = 11000 * 6.26 * 10^8 = 6.88 * 10^{12}\ {}^{N/mm^2}/_{m} = 6.88 * 10^9\ {}^{N/mm^2}/_{mm}$$

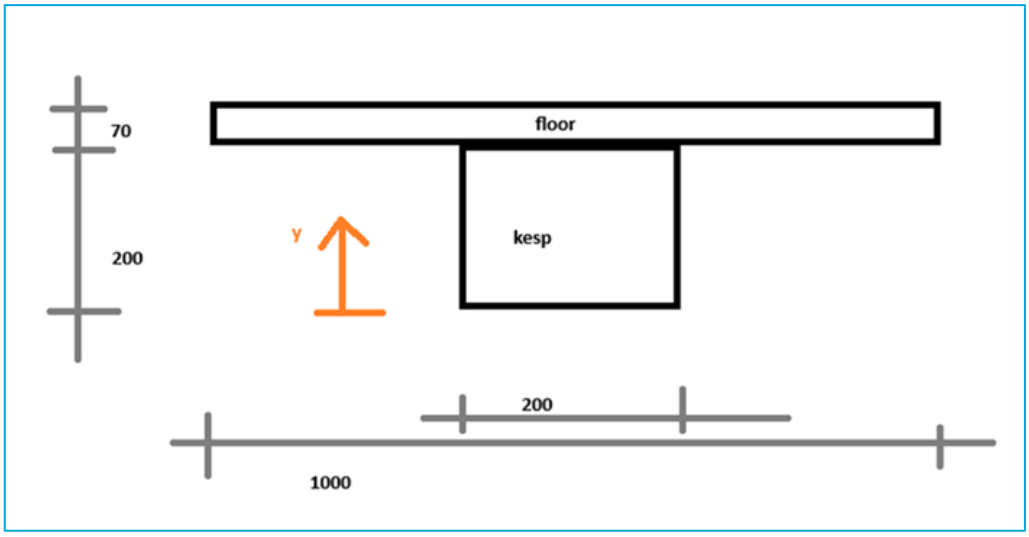

Figure 58 - Geometry of kesp and floor with local y-axis to derive properties of plate Kesp_Floor in Plaxis 2D

Table 30 - Derived Kesp_Floor material properties Plaxis 2D

Property	Value	Unit
w	4.62E-04	N/mm/mm
EA_1	1.21E+09	N/mm/mm
EI	6.884E+09	Nmm^2/mm
v	0.35	-

Soil

The soil consists of multiple polygons, which have already been briefly described. All soil polygons consist of clay, except for Bottom, which consists of sand. The division of the soil into various polygons is necessary for the Staged construction analysis to allow parts to be switched on and off, like DIANA. For both clay and sand a Hardening Soil with small strain has been adopted of which the properties are in Table 18. Additional properties that only apply to Plaxis are in Table 31. All properties have been explained in the Literature Review in section 2.3.1 and the values are obtained in section 3.1.4. The soil polygon coordinates are listed in Table 32.

Table 31 – Additional material properties HSss model Plaxis 2D

Symbol	Description	Unit	Clay	Sand
$R_f = q_a/q_f$	Failure ratio	-	0.9	0.9
γ_{sat}	Saturated density	N/mm^3	1.402E-05	1.666E-05
G_0^{ref}	Reference shear modulus at very small strains ($\varepsilon < 10^{-6}$)	N/mm^2	21.8	122.5
$\gamma_{0.7}$	Threshold shear strain at which $G_s = 0.722G_0$	-	0.0002	0.0001

Table 32 - Soil polygon coordinates Plaxis 2D

Bottom		Top		Backfill		Excavation	
X	Y	X	Y	X	Y	X	Y
-9000	-15530	-9000	-12530	650	0	650	-1104
9000	-15530	-9000	-3290	650	580	5935	580
9000	-12530	-6300	-3290	5610	580	8010	580
-9000	-12530	-300	-1104	650	0	2400	-1104
-9000	-15530	2400	-1104			650	-1104
		8010	580				
		9000	580				
		9000	-12530				
		-9000	-12530				

Connection Floor-Wall

The connection between the floor and wall is defined through an interface, which is set to be derived from the adjacent soil. The interface stiffnesses are computed in multiple steps. The stiffness G_{soil} is automatically determined depending on the soil model (Plaxis Reference Manual, 2025).

$$G_{soil} = \frac{E}{2(1+\nu)} = \frac{5000}{2(1+0.2)} = 2083\ N/mm^2$$

The shear and compression moduli are related by the expressions (Plaxis Reference Manual, 2025):

$$G_i = R_{inter}^2 G_{soil} \leq G_{soil}$$

$$E_{oed,i} = 2G_i \frac{1-\nu_i}{1-2\nu_i}$$

In these expressions ν_i is Poisson's ratio for the interface, which is equal to 0.45. R_{inter} is the interface stiffness, which in this case is set so *Rigid*, thus $R_{inter} = 1$. This option is used when the interface should not have a reduced strength with respect to the strength in the surrounding soil (Plaxis Reference Manual, 2025). This gives the following values:

$$G_i = 1^2 2083 \leq 2083$$

$$G_i = 2083\ N/mm^2$$

$$E_{oed,i} = 2 * 2083 \frac{1-0.45}{1-2*0.45} = 22.9 * 10^3\ N/mm^2$$

With those values the elastic interface shear stiffness (K_t) and the elastic interface normal stiffness (K_n) can be derived using the virtual interface factor (n_{VIF}) (Plaxis Reference Manual, 2025). The default setting for the interface factor is 0.1. The mesh element size is measured to be 326.55 mm. Therefore, the interface stiffnesses can be determined:

$$K_t = \frac{G_i}{n_{VIF} * l_{el}} = \frac{2083}{0.1 * 326.55} = 63.8\ N/mm^2$$

$$K_n = \frac{E_i}{n_{VIF} * l_{el}} = \frac{22.9 * 10^3}{0.1 * 326.55} = 702\ N/mm^2$$

Virtual thickness

"Each interface has assigned to it a 'virtual thickness' which is an imaginary dimension used to define the material properties of the interface. The higher the virtual thickness is, the more elastic deformations are generated. In general, interface elements are supposed to generate very little elastic deformations and therefore the virtual thickness should be small. On the other hand, if the virtual thickness is too small, numerical illconditioning may occur. The virtual thickness is calculated as the Virtual thickness factor times the global element size" - (Plaxis Reference Manual, 2025)

Lastly, a tension cut-off criterion is specified at 0 N/mm^2.

<u>Connection Floor-Soil and Wall-Soil</u>

The connection between the floor and wall is defined through an interface, which is set to be derived from the adjacent soil. For the Hardening Soil model G_{soil} is related to E_{50} as slipping (shearing) is considered the most important behaviour for interfaces (Plaxis Reference Manual, 2025):

$$G_{soil} = \frac{E}{2(1+\nu)} = \frac{3.7268}{2(1+0.3)} = 1.43\ N/mm^2$$

The shear and compression moduli are related by the expressions (Plaxis Reference Manual, 2025):

$$G_i = R_{inter}^2 G_{soil} \leq G_{soil}$$

$$E_{oed,i} = 2G_i \frac{1-\nu_i}{1-2\nu_i}$$

In these expressions ν_i is Poisson's ratio for the interface, which is equal to 0.45. R_{inter} is the interface stiffness, which in this case is set so *Rigid*, thus $R_{inter} = 1$. This option is used when the interface should not have a reduced strength with respect to the strength in the surrounding soil (Plaxis Reference Manual, 2025). This gives the following values:

$$G_i = 1^2 1.43 \leq 1.43$$

$$G_i = 1.43\ N/mm^2$$

$$E_{oed,i} = 2 * 1.43 \frac{1-0.45}{1-2*0.45} = 15.8\ N/mm^2$$

With those values the elastic interface shear stiffness (K_t) and the elastic interface normal stiffness (K_n) can be derived using the virtual interface factor (n_{VIF}) (Plaxis Reference Manual, 2025). The default setting for the interface factor is 0.1. The mesh element size is measured to be 326.55 mm. Therefore, the interface stiffnesses for the clay are determined:

$$K_t = \frac{G_i}{n_{VIF} * l_{el}} = \frac{1.43}{0.1 * 326.55} = 0.0439\ N/mm^2$$

$$K_n = \frac{E_i}{n_{VIF} * l_{el}} = \frac{15.8}{0.1 * 326.55} = 0.483\ N/mm^2$$

Additional parameters are the cohesion, friction angle and dilation factor. Those are based upon R_{inter}, which is set to 1, thereby not changing the parameters in Table 18. For completeness, if R_{inter} is lowered those should change according to (Plaxis Reference Manual, 2025):

$$c_i = R_{inter} * c_{soil}$$

$$\tan(\varphi_i) = R_{inter} \tan(\varphi_i) \leq \tan\ (\varphi_{soil})$$

$$\psi_i = 0\ for\ R_{inter} < 1, otherwise\ \psi_i = \psi_{soil}$$

Lastly, a tension cut-off criterion is specified at 0 N/mm^2.

4.2.2 Boundary conditions and loads

The boundary conditions for the Plaxis 2D are like those of DIANA in Figure 52. The supports at the bottom restrain translation in both the X- and Y-direction (horizontal and vertical). The supports at the left and right side of the model restrain movement in the X-direction (horizontal). This is the default setting of Plaxis 2D.

The loads present in Plaxis 2D are the same as in DIANA and have been illustrated in Table 21. The combinations have been listed in Table 22. Note that in Plaxis 2D it is not possible to have multiple line loads overlap, therefore they were superimposed and saved as different models.

4.2.3 Mesh and analysis

Plaxis automatically generates the mesh according to the structure defined in the earlier stages. When the default settings are used, for which no input is required, the mesh in Figure 59 is obtained. It can be observed that closer to the structural elements a finer mesh is created, which is wished for. The default settings of the mesh are therefore used.

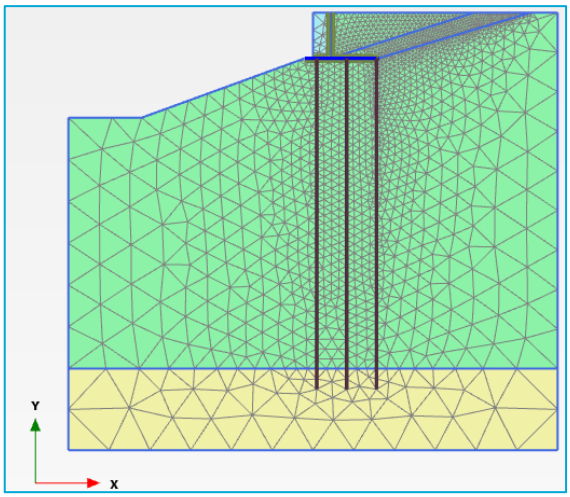

Figure 59 - Mesh traditional model Plaxis 2D

In Table 33 the stages phases of the analysis are shown. In the last stage the load combination TAK was added. For the other combinations, only the last phase changes, as another load is applied there. In the initial phase gravity loading is used, which can be used for non-horizontal layers. A difference with the model in DIANA is the implementation of the second stage, the Plastic 0-step. After applying gravity loading to simulate the initial conditions of a quay wall system, the plastic phase is used to capture the nonlinear behaviour of the soil and structure. During the gravity loading phase, the system's response is typically elastic. However, quay walls are subjected to complex soil-structure interactions that often involve yielding and plastic deformations. The plastic phase allows for the consideration of soil failure, yielding of materials, and the redistribution of forces, enabling the model to predict more realistic horizontal stresses, deformations, This stage is not used in DIANA, but this step was added as it was used in the TAK (Ingenieursbureau Gemeente Amsterdam, 2023) for modelling in Plaxis 2D.

Regarding the numerical control parameters, the default settings are used. For plastic calculations in Plaxis 2D, different error norms are used to evaluate convergence, including (Plaxis 2D Scientific Manual, 2025):

1. Global Force Error Norm (0.01)– This measures the imbalance of forces in the system. A Quasi-Newton method is used, which is described in Appendix C (Plaxis 2D Scientific Manual, 2025).
2. Global Moment Error Norm (0.001)– This measures the imbalance of moments.
3. Inaccurate Soil Plastic Point Tolerance (0.1) – This tracks the number of soil points that have significant changes in their plastic state.
4. Inaccurate Soil Elastic Point Tolerance (0.1) – Similar to the above, but for elastic points.
5. Integrated Interface/Discontinuity Local Error (0.1) – Measures error along interfaces and discontinuities.
6. Inaccurate Interface/Discontinuity Plastic Point Tolerance (0.1) – Checks errors in plasticity at interfaces.

These norms are evaluated together to determine convergence. A step is considered converged, when all these criteria are satisfied simultaneously. If any one of them fails, Plaxis will continue iterating up to the maximum allowed iterations, set to 60.

Table 33 - Phases traditional model Plaxis 2D

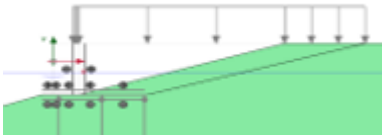	**Initial Phase (K0_procedure)** Clear displacements Calculation Gravity
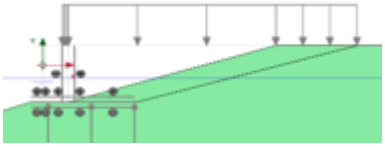	**Plastic 0-step** Clear displacements TRUE Calculation Staged
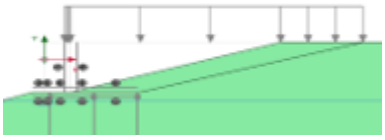	**Lower water table** Clear displacements TRUE Calculation Staged
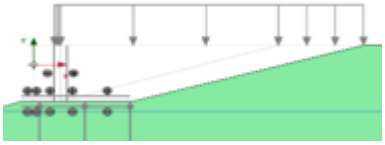	**Excavate** Clear displacements Calculation Staged
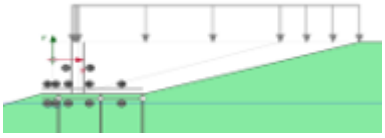	**Add piles** Clear displacements TRUE Calculation Staged
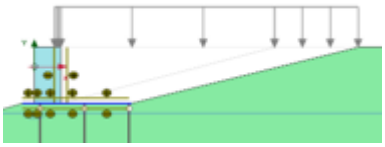	**Add wall** Clear displacements Calculation Staged
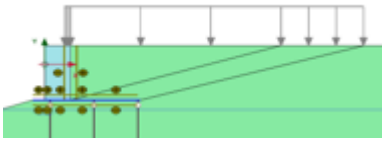	**Backfill soil** Clear displacements Calculation Staged
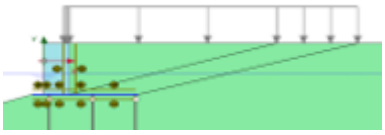	**Heighten water table** Clear displacements Calculation Staged
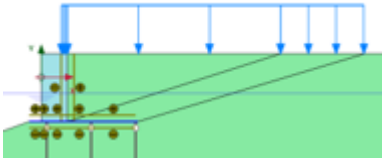	**Add loads** Clear displacements Calculation Staged

4.3 Sheet pile model DIANA

For the model in DIANA FEA a structural analysis was carried out in a plane strain model using plane strain elements (Figure 46). The model thickness was set to 1000mm. The default mesh type Hexa/Quad elements was chosen. This means that by default quadrilateral elements are used. To prevent distorted elements, triangular elements have also been used. In Figure 62 the mesh can be seen. Furthermore, the default mesh order is set be quadratic and the mid-side node location on shape. The units used in DIANA are listed in Table 12. Note that all these properties are like the traditional model.

4.3.1 Geometry and materials

The general overview of the geometry can be found in Figure 60. The geometry consists of a sand layer at the bottom, a clay layer on top of this, and a sheet pile wall. Note that this is the geometry of the quay wall at the end of the construction sequence. Again, a Geomechanical staged construction analysis is used. The top triangle will be filled after the sheet pile is constructed.

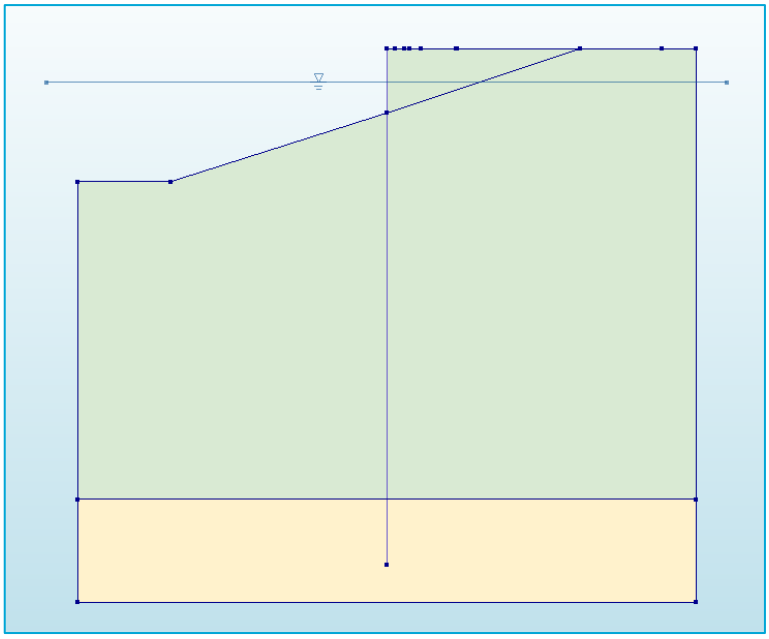

Figure 60 - Overview geometry sheet pile model DIANA

The water level is also shown as a horizontal blue line at the top of the model going through the soil. This water level is referred to as the *Normal water level* and is assumed to be at NAP-400mm. NAP coincides with the x-axis of the model, which is located 580 mm below the soil surface at the right side of the quay. The y-axis coincides with sheet pile. Note that during the construction another water level is used, which is referred to as *Excavation water level*. This water level is located at NAP-1400mm. This is like the traditional model.

<u>Soil</u>

The soil consists of multiple polygons. The Bottom consists of sand. The Top and Backfill consist of clay. The division of the soil into various polygons is necessary for the Geomechanical staged construction analysis to allow parts to be switched on and off. For both clay and sand a Hardening Soil with small strain has been adopted with similar properties as the traditonal model shown in Table 18. The soil polygon coordinates for this model are listed in Table 34.

Table 34 - Coordinates soil polygons in sheet pile model DIANA (values in millimetres)

Bottom		Top		Backfill	
X	Y	X	Y	X	Y
-9000	-15530	-9000	-12530	0	0
9000	-15530	9000	-12530	0	580
9000	-12530	9000	580	5610	580
-9000	-12530	5610	580	0	0
-9000	-15530	0	-1290		
		-6300	-3290		
		-9000	-3290		
		-9000	-12530		

<u>Sheet pile</u>

For the sheet pile the specific sheet pile wall wizard has been used in DIANA. The Sheet Pile Wall Wizard streamlines the modelling process of sheet pile walls by automatically incorporating interfaces between the sheet pile wall and the adjacent soil elements. This functionality significantly simplifies the modelling of geotechnical applications, as the explicit definition of these interfaces can be a time-consuming and complex task when performed manually (DIANA User Manual, 2025). The sheet pile is 15 m long and modelled as a line between the top and bottom coordinates, (0 580) and (0 -14420) respectively.

The cross-sectional properties are defined with library selection, for which the AU14 profile of ArcelorMittal was used and modelled as Linear Elastic. This results in the properties listed in Table 35. The connection between the Sheet Pile and Soil is defined through an interface, which is set to be derived from soil properties. The element size (l_{el}) is 50 mm and virtual interface factor (n_{VIF}) is 0.1. The shear modulus of the soil (G_{soil}) has been derived earlier in section 4.2. The multiplication factor (f) varies between 10 and 100 and is set to 100.

$$K_t = \frac{G_{soil}}{n_{VIF} * l_{el}} = \frac{1.43}{0.1 * 50} = 0.287\ N/mm^2$$

$$K_n = f * K_t = 100 * 0.0287 = 28.67\ N/mm^2$$

A similar procedure, using the properties from the sand in Table 18 resulted in the interface stiffnesses between the sheet pile and the sand below:

$$K_t = 2.92\ N/mm^2$$

$$K_n = 292\ N/mm^2$$

Table 35 - Sheet pile properties DIANA

Property	Value	Unit
Poisson's ratio	0	-
Distributed mass	1.04E-07	T/mm
EI	6.02E+10	Nmm
EA	2.78E+12	N/mm
Stiffness specification	Derived from soil properties	-
Virtual thickness factor	0.1	-
R factor	1	-

4.3.2 Boundary conditions and loads

The boundary conditions for this FE model are like that of the traditional model and visualised in Figure 61. The supports at the bottom restrain translations in both the X- and Y-direction (horizontal and vertical). The supports at the left and right side of the model restrain movement in the X-direction (horizontal).

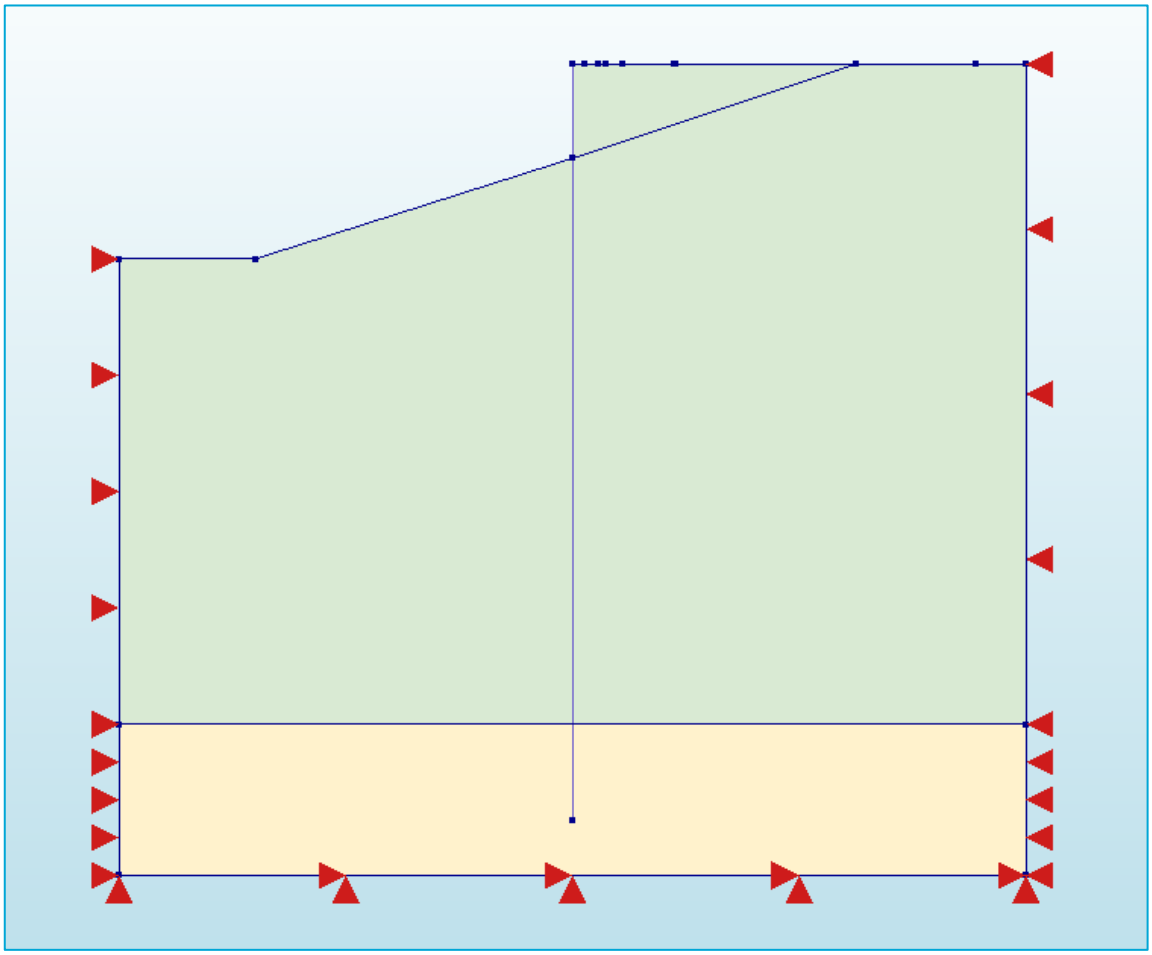

Figure 61 - Boundary conditions sheet pile model DIANA

The loads acting on the quay at the right side of the sheet pile wall are the same as in the traditional model for the quay wall and visualised in Table 21. The different load combinations are given in Table 22.

4.3.3 Mesh and analysis

The mesh that is used for the analysis is given in Figure 62. A triangular mesh size has been chosen to prevent distorted elements with a size of 200 mm for most elements. Along the sheet pile wall the mesh is refined to have a size of 50 mm.

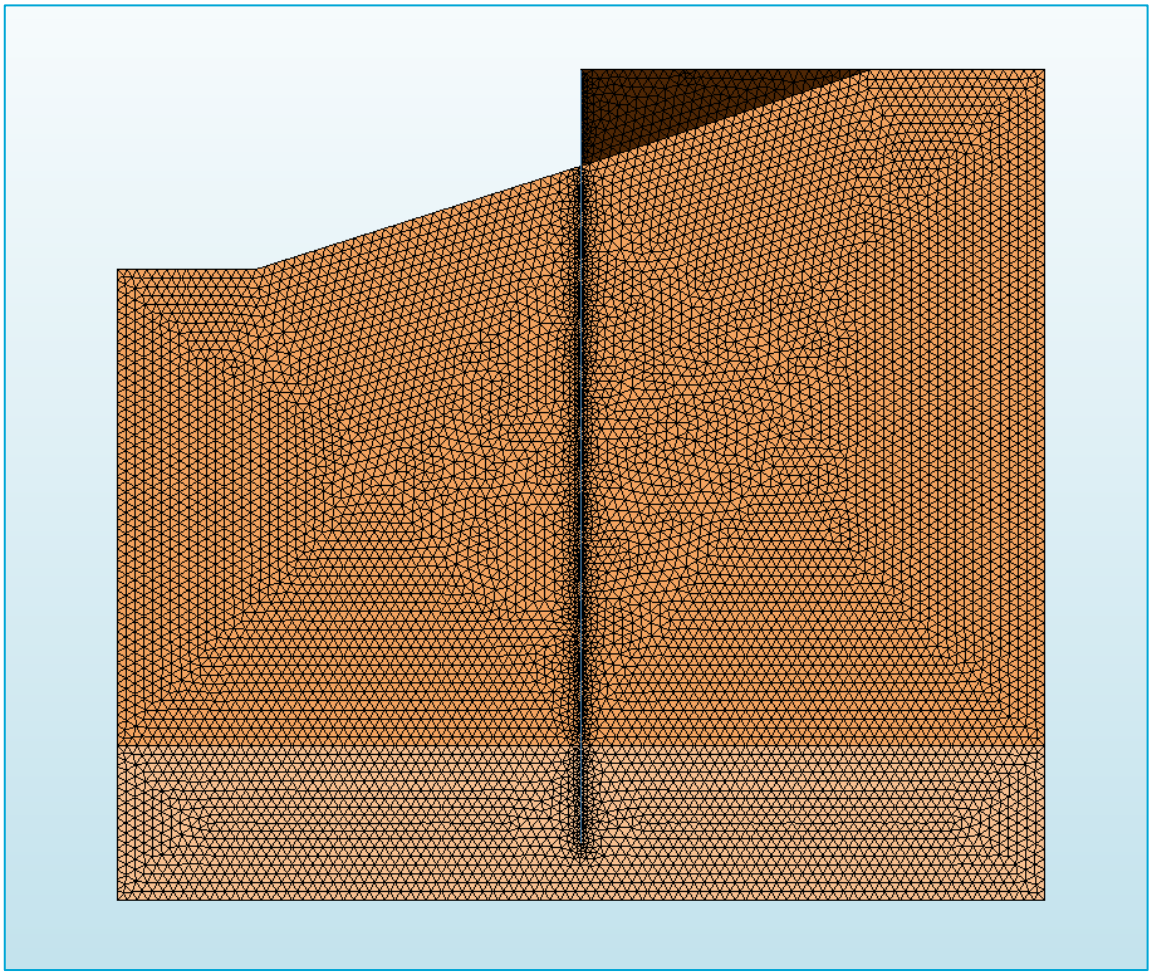

Figure 62 – Mesh sheet pile model DIANA

For the analysis a Geomechanical staged construction analysis is again selected. The construction sequence is illustrated in Table 36. In the latest stage the load combination TAK was added. For the other combinations, only the last phase changes, as another load is applied there.

The solution was set to Parellel Direct Sparse. This solver shows both a high performance and memory efficient usage for solving large sparse symmetric and unsymmetric linear systems of equations by shared multiprocessors (DIANA User Manual, 2025).

The iteration method selected for the phases when the phreatic level is varied is Newton regular with a maximum number of iterations of 100 and a convergence tolerance of 0.001. A Secant (Quasi-Newton) approach is used as iteration method for the remaining structural phases, where the maximum number of iterations is set to 200. The type of the method is set to BFGS, which is the Broyden-Fletcher-Goldfarb-Shanno Algorithm (Nayak, 2020). First tangent is set to previous iteration. The convergence norm is set to satisfy both a displacement and a force norm, with a convergence tolerance of 0.001. If convergence is not found, the analysis is set to continue.

Table 36 - Stages of the construction of the sheet pile model in DIANA

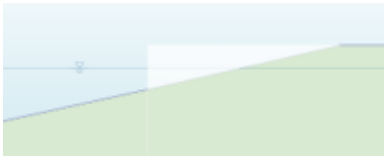	**Initial Phase (K0_procedure)** Clear displacements TRUE Init stresses TRUE
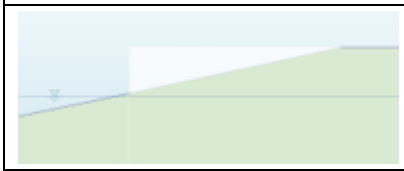	**Lower water table** Clear displacements TRUE Init stresses
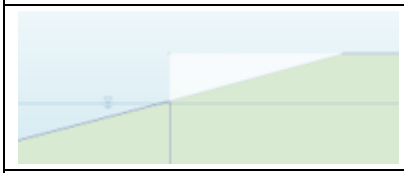	**Add wall** Clear displacements TRUE Init stresses
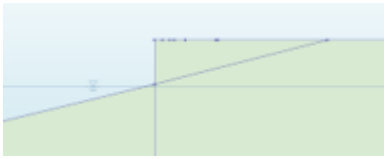	**Backfill soil** Clear displacements Init stresses
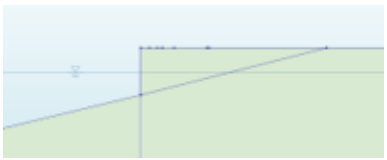	**Heighten water table** Clear displacements Init stresses
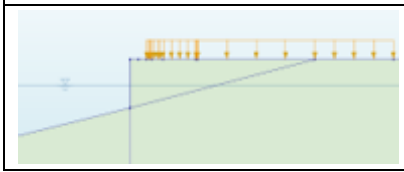	**Add loads** Clear displacements Init stresses

4.4 Sheet pile model Plaxis

A plane strain model is used to model the sheet pile geometry in Plaxis 2D. 15-Noded elements are selected. The model units are defined as in Table 24. This is like the traditional model.

4.4.1 Geometry and materials

The general overview of the geometry can be found in Figure 63 and mimics the structure modelled in DIANA. The geometry consists of a sand layer at the bottom, a clay layer on top of this and a sheet pile wall. Note that this is again the geometry of the sheet pile model at the end of the construction sequence. In Plaxis 2D the Staged construction analysis is used again.

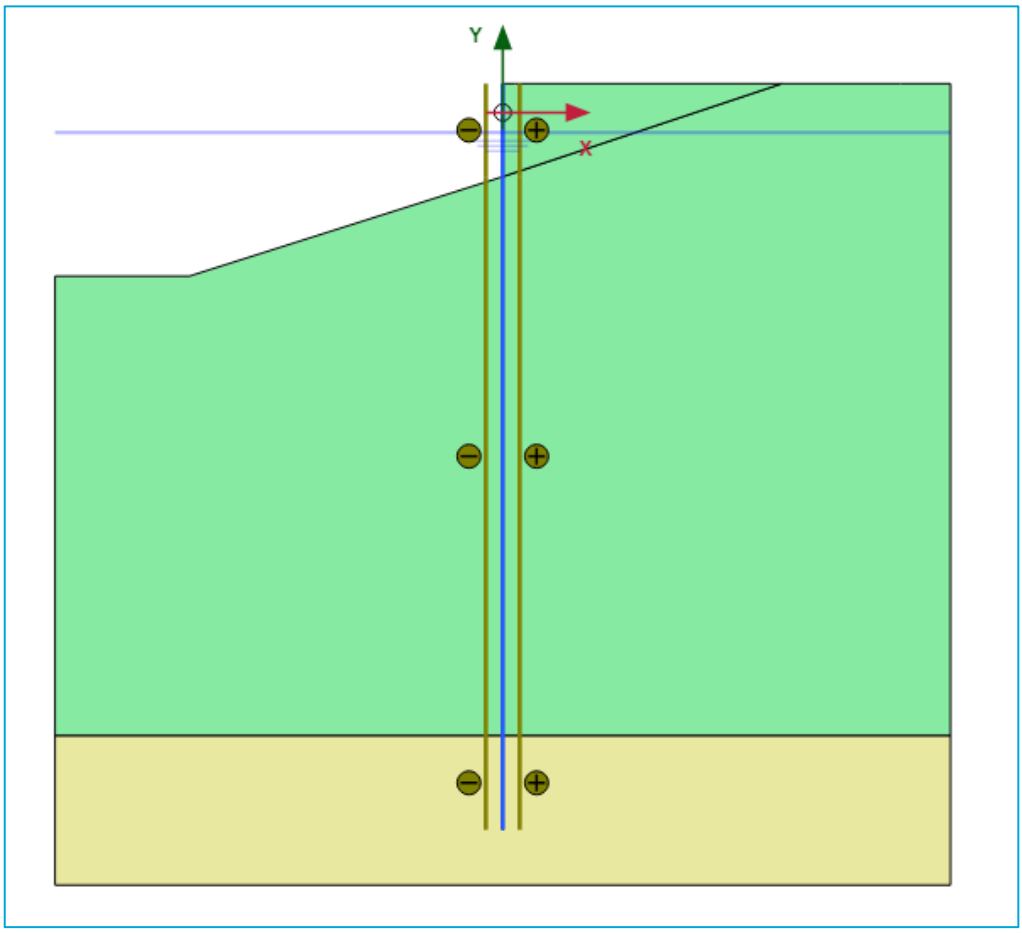

Figure 63 - Overview geometry sheet pile model Plaxis 2D

The geometry is modelled in the same way as in DIANA using the polygon coordinates from Table 34. The material properties of the soil for the traditional model have already been given in Table 18 and Table 31 and are also used in the sheet pile model. For the sheet pile a plate element was used, initially modelled as a line between the coordinates (0 580) and (0 -14420). The material properties that were imported from the ArcelorMittal library in DIANA are used after conversion of the units and displayed in Table 37.

Table 37 - Properties sheet pile plate Plaxis 2D

Property	Value	Unit
w	1.02E-03	N/mm/mm
Isotropic	TRUE	
EA	2.77E+06	N/mm
EI	6.02E+10	N/mm²/mm
Poisson's ratio	0	-

<u>Connection Sheet Pile-Soil</u>

The connection between the Sheet Pile and Soil is defined through an interface, which is set to be derived from the adjacent soil, a similar procedure as for the connections with the soil in the traditional model. A small difference is the mesh element size, which is measured to be 323.785 mm for this case. Therefore, the interface stiffnesses can be determined with the properties derived earlier for the traditional model as:

$$K_t = \frac{G_i}{n_{VIF} * l_{el}} = \frac{1.43}{0.1 * 323.785} = 0.0443\ N/mm^2$$

$$K_n = \frac{E_i}{n_{VIF} * l_{el}} = \frac{15.8}{0.1 * 323.785} = 0.487\ N/mm^2$$

For the interface stiffnesses between the sheet pile and the sand soil, the following stiffnesses are obtained using the properties from Table 18:

$$K_t = 0.450\ N/mm^2$$

$$K_n = 4.95\ N/mm^2$$

Additional parameters are the cohesion, friction angle and dilation factor. Those are based upon R_{inter}, which is set to 1, thereby not changing the parameters in Table 18. Lastly, a tension cut-off criterion is specified at 0 N/mm^2.

4.4.2 Boundary conditions and loads

The boundary conditions for the sheet pile model in Plaxis are the same as for DIANA and visualised in Figure 61. The supports at the bottom restrain translations in both the X- and Y-direction (horizontal and vertical). The supports at the left and right side of the model restrain movement in the X-direction (horizontal).

The loads acting on the quay at the right side of the sheet pile wall are the same as for the traditional model quay wall and visualised in Table 21. The different load combinations are given in Table 22.

4.4.3 Mesh and analysis

Plaxis automatically generates the mesh according to the structure defined in the earlier stages. When the default settings are used, for which no input is required, the mesh in Figure 64 is obtained. It can be observed that closer to the structural elements a finer mesh is created, which is wished for. The default settings of the mesh are therefore used.

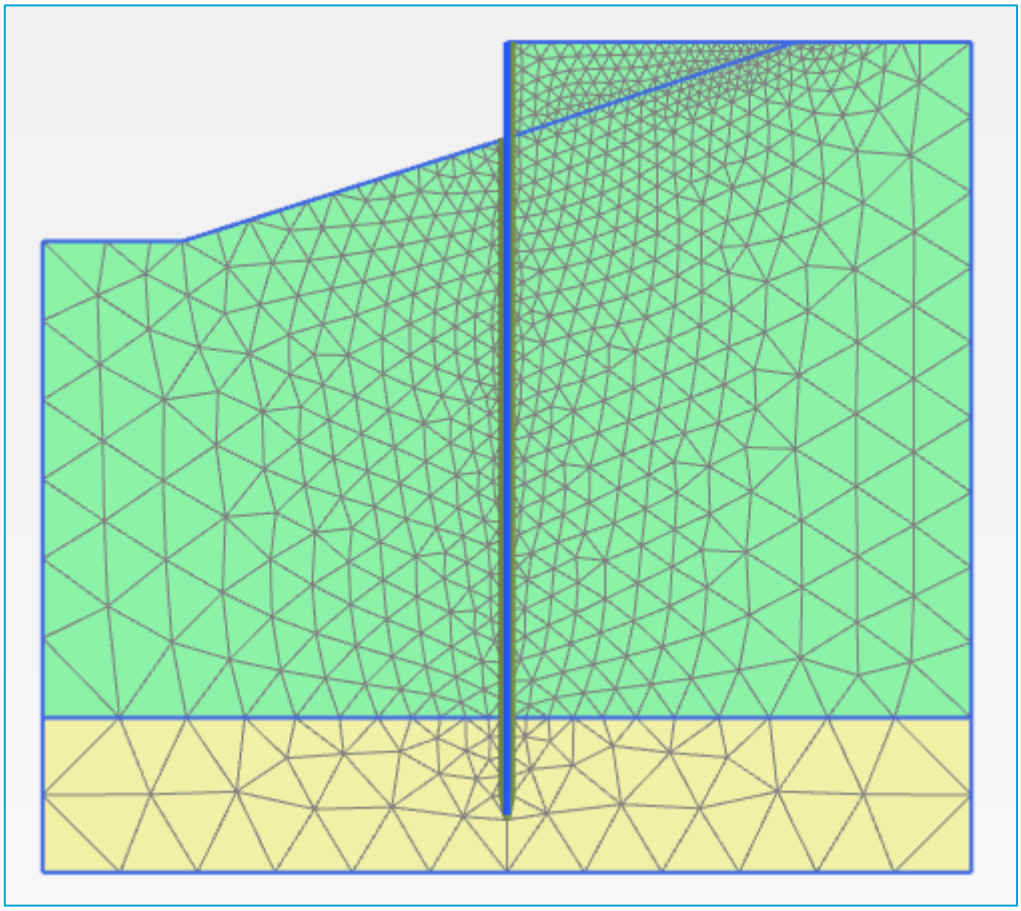

Figure 64 - Mesh sheet pile model Plaxis 2D

Staged construction is the analysis used in Plaxis 2D. The construction sequence is illustrated in Table 38. In the latest stage the load combination TAK is added. For the other combinations, only the last phase changes, as another load is applied there. In the initial phase gravity loading is used, which can be used for non-horizontal layers. In other stages, plastic is used as the calculation type. Regarding the numerical control parameters, the default settings are used. For plastic calculations in Plaxis 2D, different error norms are used to evaluate convergence, including (Plaxis 2D Scientific Manual, 2025):

1. Global Force Error Norm (0.01)– This measures the imbalance of forces in the system. A Quasi-Newton method is used, which is described in Appendix C (Plaxis 2D Scientific Manual, 2025).
2. Global Moment Error Norm (0.001)– This measures the imbalance of moments.
3. Inaccurate Soil Plastic Point Tolerance (0.1) – This tracks the number of soil points that have significant changes in their plastic state.
4. Inaccurate Soil Elastic Point Tolerance (0.1) – Similar to the above, but for elastic points.
5. Integrated Interface/Discontinuity Local Error (0.1) – Measures error along interfaces and discontinuities.
6. Inaccurate Interface/Discontinuity Plastic Point Tolerance (0.1) – Checks errors in plasticity at interfaces.

These norms are evaluated together to determine convergence. A step is considered converged, when all these criteria are satisfied simultaneously. If any one of them fails, Plaxis will continue iterating up to the maximum allowed iterations, set to 60.

Table 38 - Phases sheet pile model Plaxis 2D

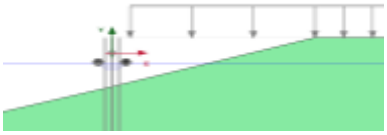	**Initial Phase (K0_procedure)**	
	Clear displacements	
	Calculation	Gravity
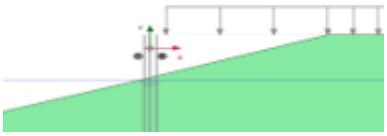	**Lower water table**	
	Clear displacements	TRUE
	Calculation	Staged
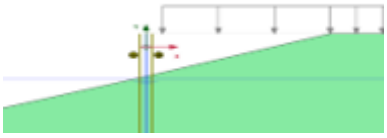	**Add wall**	
	Clear displacements	
	Calculation	Staged
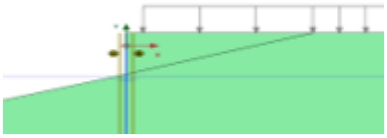	**Backfill soil**	
	Clear displacements	
	Calculation	Staged
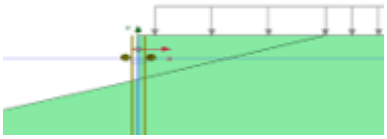	**Heighten water table**	
	Clear displacements	
	Calculation	Staged
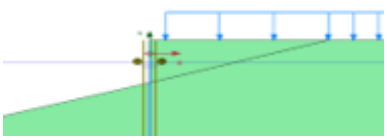	**Add loads**	
	Clear displacements	
	Calculation	Staged

5 Numerical Results

This chapter is divided into two sections, section 5.1 shows the results of the traditional model, whereas section 5.2 shows the results of the sheet pile model. Initially the serviceability, thus deformations are illustrated to show the global behaviour of the structure. Thereafter, the cross-section of both geometries is checked. Both geometries include unity checks that enables a cross-comparison between the two different geometries. The last subsection of the traditional and sheet pile geometries is on the verification of the results.

5.1 Traditional model

This section presents the comparative analysis of the structural behaviour of the traditional (as build) geometry using DIANA and Plaxis models for five different load cases. The differences between the two software tools are allocated to the implementation, especially that of Soil-Structure Interaction (SSI). The implications of this are discussed in more detail in Chapter 6. The comparison starts with the horizontal and total phase displacements during the last loading stage, which are shown and compared against each other for the different software. Thereafter, normal forces, shear forces, and bending moments in the piles, as well as the resulting unity checks because of these forces are shown.

5.1.1 Failure mechanism: excessive displacements

Serviceability criteria for displacements play a large role in Amsterdam due to ductile requirements of the pipelines for the water network. Therefore, the horizontal and total displacement are considered in this section. The limit for the horizontal displacement of the capstone is set to 50 mm (Ingenieursbureau Gemeente Amsterdam, 2023).

<u>Horizontal displacement</u>

The horizontal displacement during the loading phase (note that the previous phases displacements are reset) at the top of the wall on the waterside (visualised in Figure 65) is taken as output from both DIANA and Plaxis for the various load cases. The displacements are displayed in Table 39. For the reference TAK load case, an average (mean between the two software) horizontal displacement of 15.07 mm to the left is observed. As a result of the multifunctionalities the displacements increase to 38.99 mm on average. This effectively means that because of the multifunctionalities the displacement is increased by 23.92 mm, an increase of 159%. Note that the displacements in DIANA are approximately 37% less than in Plaxis.

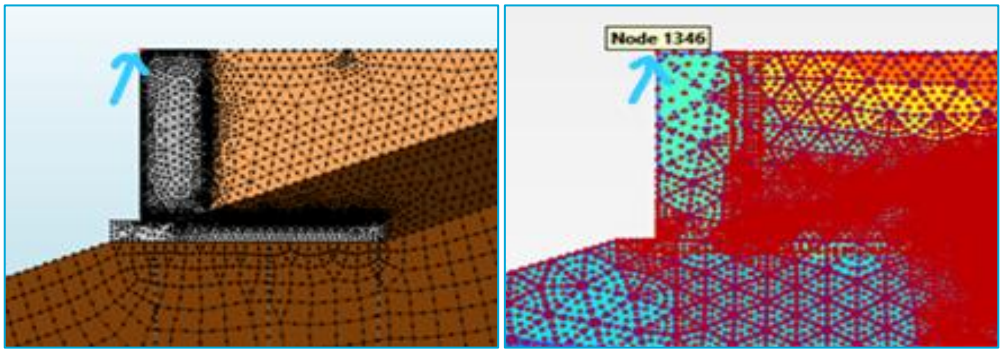

Figure 65 - Selected left top nodes indicated by blue arrow for capstone horizontal phase displacement during loading (left: DIANA, right: Plaxis)

Table 39 - Horizontal phase displacement during loading for both software, average is the mean of the software, and the difference illustrates the differences between the software

Pu_x [mm]				
	DIANA	Plaxis	Average	Difference
TAK	-12.18	-17.97	-15.07	32.2%
TAK+Tree	-23.23	-39.37	-31.30	41.0%
TAK+Energy	-15.26	-23.45	-19.36	34.9%
TAK+Panel	-12.37	-18.04	-15.20	31.4%
TAK+AllMF	-28.13	-49.85	-38.99	43.6%

The limit for the horizontal displacement of the capstone is set to 50 mm (Ingenieursbureau Gemeente Amsterdam, 2023). With the resulting displacements from Table 39, the resulting unity check can be determined by dividing the observed displacement by the maximum allowed displacement. This results in the unity checks in Table 40. It is observed that unity check increases from 0.30 for the TAK load case to 0.78 for when all functionalities are applied. This is an increase of 0.48 or 160%.

Table 40 - Unity check horizontal phase displacement during loading for both software, average is the mean of the software, and the difference illustrates the differences between the software

$UC_{def,hor}$ [-]				
	DIANA	Plaxis	Average	Difference
TAK	0.24	0.36	0.30	32.2%
TAK+Tree	0.46	0.79	0.63	41.0%
TAK+Energy	0.31	0.47	0.39	34.9%
TAK+Panel	0.25	0.36	0.30	31.4%
TAK+AllMF	0.56	1.00	0.78	43.6%

<u>Total displacement</u>

The global behaviour of the structure is observed in Table 41. The phase displacements during loading are qualitatively and quantitatively observed in Table 42 for the different load cases. The largest displacements are given in red, and it is observed that they are the largest at the location of the applied loading, which is expected. Additionally, in the TAK load case it is observed that the quay wall structure prevents large displacements from happening above the quay, whereas near the right

boundary, where the soil is not supported by the timber piles, larger displacements take place. The maximum displacements are given in Table 43. Note that the displacements observed for the TAK are 35.01 mm and for the multifunctionalities 96.90 mm, an increase of 61.89 mm, which is 177%.

It is interesting to observe that the results between the observed displacements in DIANA and Plaxis for the TAK and TAK+Panel load case are only 2%, where for the other load cases 17% or more is observed. From the visualisation of the TAK load case in Table 42, it can be observed that the largest displacement takes places between the quay and the boundary, and the vertical component is significantly larger than the horizontal component. At this specific location, the influence of the structure is limited compared to the surface above the quay, as it is not supported by the piles. It is thus important to note that the vertical displacement in DIANA and Plaxis have almost similar values regarding the vertical component, which indicates that the soil models are showing similar behaviour in the same manner for both software. Additionally, even in the quay the vertical displacement is similar, showing that the vertical SSI component is not that different for both software. However, regarding the horizontal component of the SSI, because of a different implementation, Plaxis will have greater displacements than DIANA. The interface stiffnesses between the piles and soil are much larger set in DIANA than in Plaxis as derived in section 4.2.1, and expanded upon in the Discussion in section 6.4.1. After resetting the stiffnesses to similar values as DIANA, this appeared not make the models more aligned. Therefore, the horizontal differences remain unexplained but are attributed to the limitations in Plaxis of the Embedded Beams ability to take transversal forces as explained in section 4.2.1.

Table 41 - Magnified total displacement traditional structure at the end of the construction sequence for the TAK load case. The plotted Figures serve as a qualitative indication of the movement of the structure. For a quantitative expression the reader is referred to the other Tables.

DIANA	Plaxis
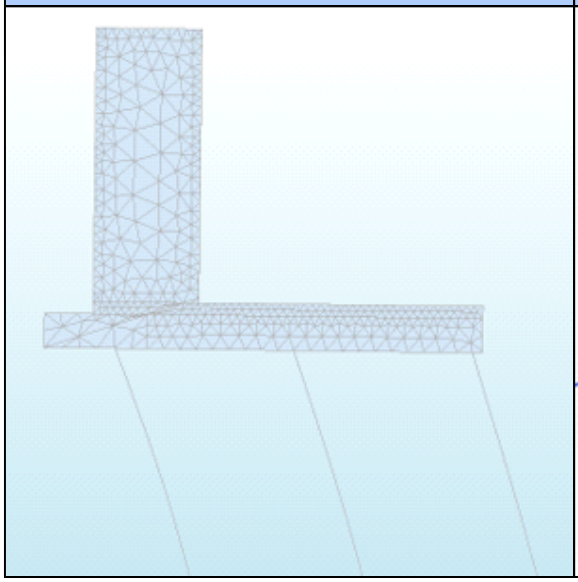	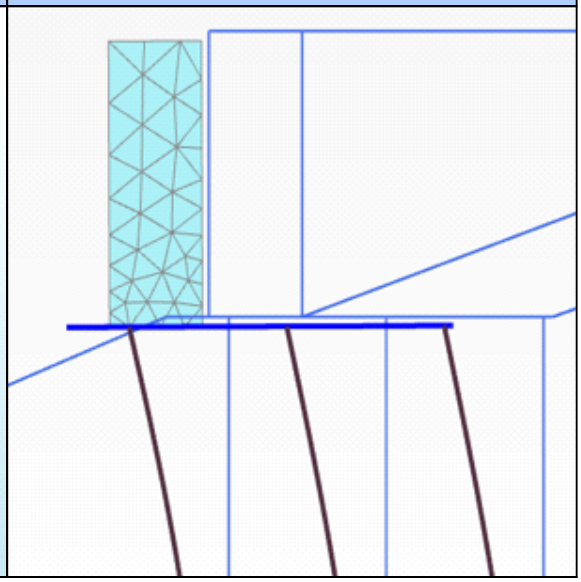

Table 42 - Phase displacements traditional model during Add loads stage/phase for different load cases for both software, DIANA is displayed on the left and Plaxis on the right. The contour scale is taken from DIANA but set to the same values in Plaxis

Phase displacements during Add loads stage/phase

TAK

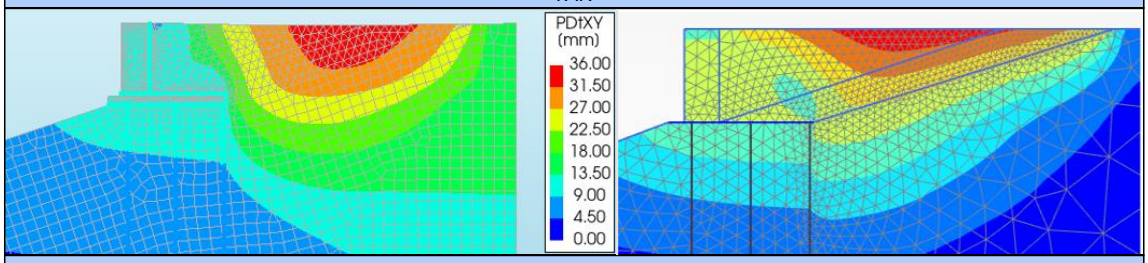

TAK+Tree

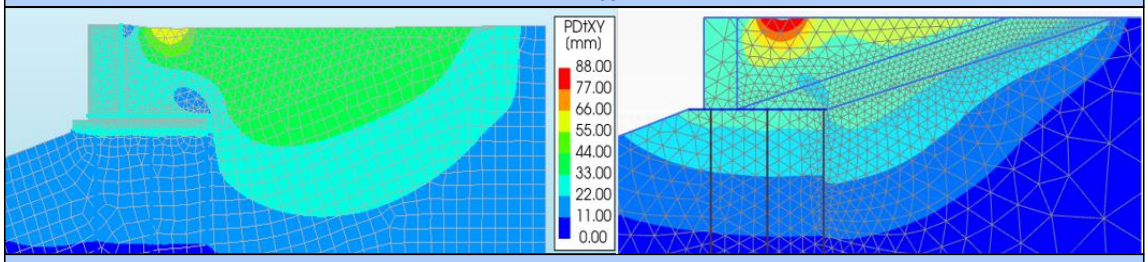

TAK+Energy

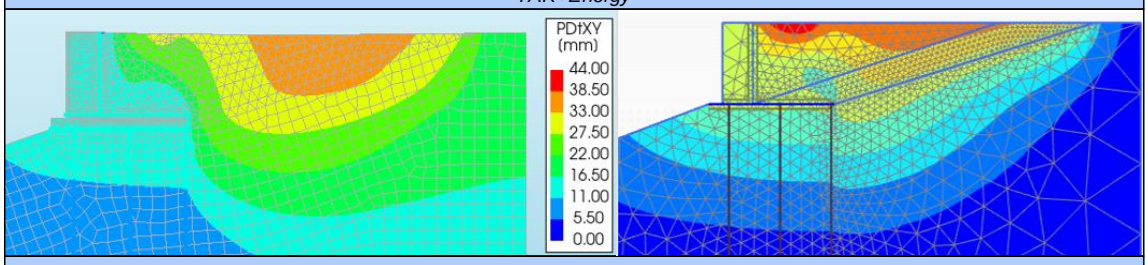

TAK+Panel

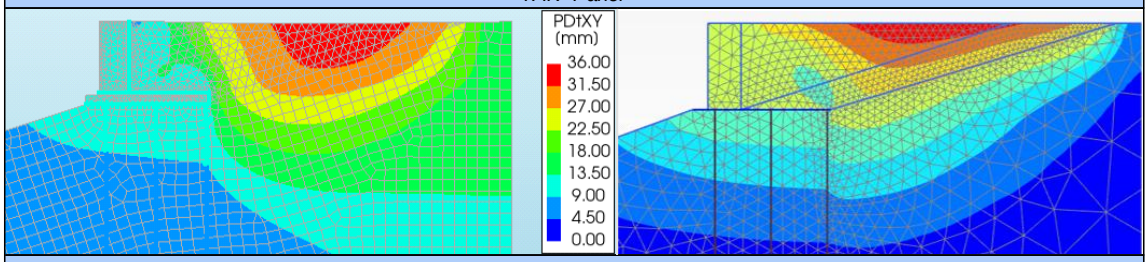

TAK+AllMF

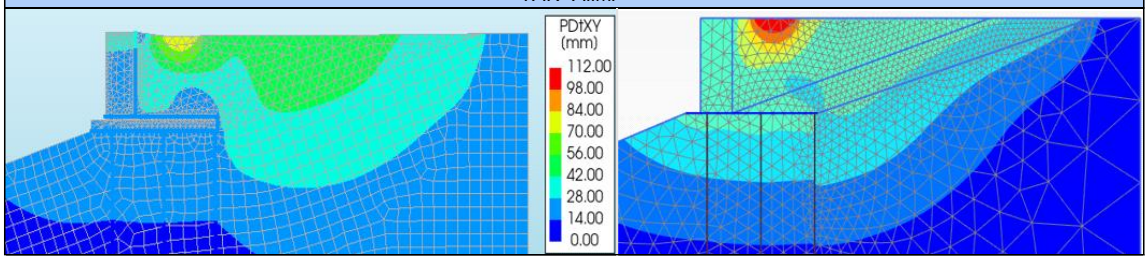

Table 43 - Maximum phase displacements during Add loads stage/phase for different load cases for both software, average is the mean of the software, and the difference illustrates the differences between the software

Pu [mm]				
	DIANA	Plaxis	Average	Difference
TAK	34.6	35.42	35.01	2.3%
TAK+Tree	63.41	89.66	76.54	29.3%
TAK+Energy	37.04	44.4	40.72	16.6%
TAK+Panel	34.72	35.41	35.07	1.9%
TAK+AllMF	80.89	112.9	96.90	28.4%

A unity check is also performed for the total displacement. Ductile pipes and cables have a limited displacement of 50nmm. Therefore, the displacement from Table 43 can be divided by this limit. The results are displayed in Table 44. The TAK load case gives a value of 0.70, whereas all multifunctionalities give a unity check of 1.94, or an increase of 1.24 (+177%). It should be noted that in the models no stiff sand layer is applied as a top layer, which will redistribute the surface load more evenly, thereby limiting differential settlement and total displacements. This will effectively reduce the unity check for displacement of this model.

Table 44 - Unity check phase displacements during Add loads stage/phase for different load cases for both software, average is the mean of the software, and the difference illustrates the differences between the software

$UC_{def,tot}$ [-]				
	DIANA	Plaxis	Average	Difference
TAK	0.69	0.71	0.70	2.3%
TAK+Tree	1.27	1.79	1.53	29.3%
TAK+Energy	0.74	0.89	0.81	16.6%
TAK+Panel	0.69	0.71	0.70	1.9%
TAK+AllMF	1.62	2.26	1.94	28.4%

5.1.2 Failure mechanism: timber piles

The cross-sectional forces and moment diagrams for Plaxis and DIANA are illustrated in Table 45 for the governing piles. The maximum forces and moments are extracted and displayed in Table 46, also the conversion is made to the resulting normal, shear and bending stresses as explained in the Literature Study in section 2.4.1. The comparison between DIANA and Plaxis highlights key differences in the implementation of the structure in the soil in both software.

Table 45 - Cross-sectional forces and moment diagrams for governing piles for different load cases in Add loads stage/phase

	DIANA	Plaxis
N	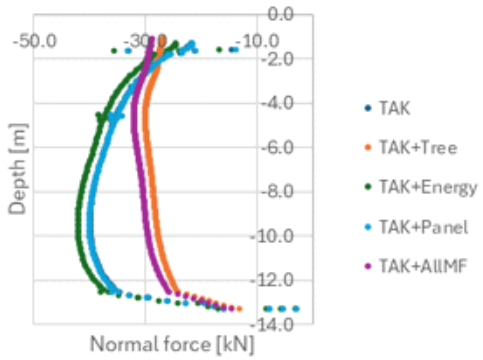	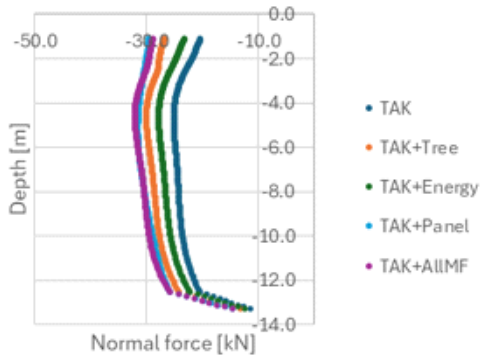
V	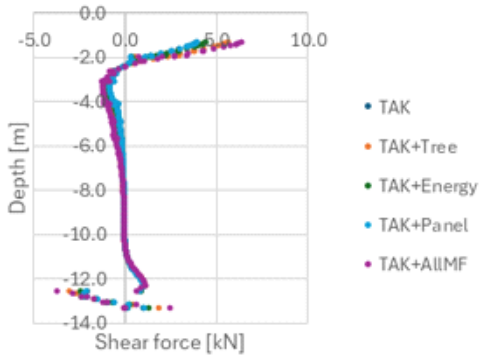	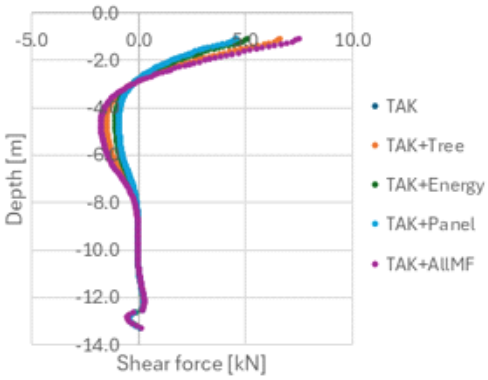
M	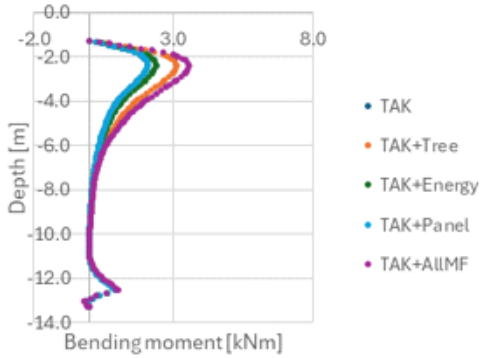	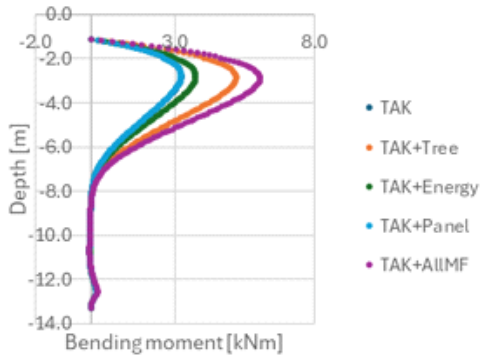

Normal force distributions in DIANA appear more concentrated, with sharper transitions along depth, whereas Plaxis results are more gradual, reflecting a stronger consideration of soil-pile interaction. This suggests that DIANA assumes a stiffer pile response, while Plaxis accounts for more deformation, which can be verified from the displacements in Table 42. Reflecting on the different load cases described in Table 21, it is observed in DIANA that a higher additional load causes a greater normal force, which is an expected result. The magnitude of loads of the additional functionalities loads in ascending order is panel, energy storage and tree, in which the additional loading of the panel is small compared to that of the energy storage and tree. In Plaxis the panel, however, also causes a significant increase in the normal force. In Plaxis the governing normal force

switched from the right pile to the left pile in this load case, which is not the case in DIANA, although the differences are small.

Shear force distributions in DIANA show distinct variations, particularly near the pile head, indicating a more rigid structural response. In contrast, Plaxis presents smoother shear force transitions, likely due to its geotechnical focus, where lateral soil resistance is more pronounced. These differences suggest that DIANA models pile forces more in line with structural engineering principles, while Plaxis incorporates a smoother interaction with the surrounding soil. An observation that strengthens this is that the bump in the shear force diagram at the boundary of the clay and sand layer is much larger in the DIANA model than in the Plaxis model. Between the different load cases not many differences occur. This is in line with our expectation as the difference in loading is in the vertical (y-direction) for the various load cases, whereas the shear force in the piles is horizontal (x-direction). The present shear force is the result of the active soil pressure on the quay wall, which is influenced by the vertical loading, causing an increase in vertical effective stresses.

Bending moments in DIANA are concentrated near the pile head, with a sharp decrease along depth, while in Plaxis, they are more evenly distributed. This indicates that Plaxis captures lateral soil effects more effectively, leading to higher bending moments at depth. Across different load cases, DIANA consistently shows a stiffer response, while Plaxis provides a more flexible representation of pile behaviour. The bump in the bending moment diagram at the boundary of the clay and sand layer is much larger in the DIANA model than in the Plaxis model. The transition from the softer clay to the stiffer sand creates a discontinuity in the support provided by the surrounding soil. This difference in stiffness can cause the pile to experience uneven settlement or lateral movement. The clay, being more compressible, may settle more easily, while the sand, which is stiffer, resists movement more strongly. This creates a localized shift in the pile's behaviour, leading to increased bending moments at the interface between the two soil layers. Lastly, the bending moments in the piles perform a strong correlation with the magnitude of the loading.

With the resisting strength of the timber determined in the Literature Study in section 2.4.1, the unity checks can be performed for compression, shear, bending and the combination of compression and bending. These checks have been briefly listed below. The results of the unity checks in DIANA, Plaxis, the averages and differences are stated in Table 47.

Compression: $UC_c = \frac{\sigma_{c,0,d}}{f_{c,0,d}} \leq 1.0$

Shear: $UC_s = \frac{\tau_d}{f_{v,d}} \leq 1.0$

Bending: $UC_m = \frac{\sigma_{m,z,d}}{f_{m,z,d}} \leq 1.0$

Compression and bending: $UC_{c,m} = \frac{\sigma_{c,0,d}}{f_{c,0,d}} + \frac{\sigma_{m,z,d}}{f_{m,z,d}} \leq 1.0$

From Table 47 it can be observed that the check for combined bending and compression is governing, in which the bending stresses have a much larger contribution compared to the normal forces. The average unity check for bending goes up from 0.33 for the TAK case to 0.60 for when all multifunctionalities are considered, which is an increase of 0.27 or 82%. DIANA gives approximately 33% lower results than Plaxis. Note that for all load cases the resistance of the structure is greater than the effect of the loads. In this unity check no reduction of the timber cross-section because of deterioration of the piles has been considered, which will be discussed later. Additionally, partial load factors have not been considered.

Table 46 - Governing cross-section forces and moments and resulting stresses for different load cases for both software, average is the mean of the software, and the difference illustrates the differences between the software

Plaxis								
	N_{max} [kN]	V_{max} [kN]	M_{max} [kNm]	$N_{M,max}$ [kN]	$\sigma_{c,0,d}$ [N/mm²]	τ_d [N/mm²]	$\sigma_{m,z,d}$ [N/mm²]	$\sigma_{c,0,d}$ [N/mm²]
TAK	-29.86	4.58	3.24	-28.87	0.951	0.194	4.123	0.919
TAK+Tree	-40.92	6.63	5.20	-39.86	1.302	0.281	6.626	1.269
TAK+Energy	-35.01	5.09	3.75	-34.04	1.114	0.216	4.779	1.083
TAK+Panel	-31.54	4.58	3.23	-30.62	1.004	0.194	4.117	0.975
TAK+AllMF	-47.98	7.51	6.06	-46.97	1.527	0.319	7.714	1.495
DIANA								
	N_{max} [kN]	V_{max} [kN]	M_{max} [kNm]	$N_{M,max}$ [kN]	$\sigma_{c,0,d}$ [N/mm²]	τ_d [N/mm²]	$\sigma_{m,z,d}$ [N/mm²]	$\sigma_{c,0,d}$ [N/mm²]
TAK	-39.89	3.91	2.07	-22.35	1.270	0.166	2.640	0.711
TAK+Tree	-44.20	5.61	3.12	-35.51	1.407	0.238	3.977	1.130
TAK+Energy	-42.10	4.42	2.38	-28.22	1.340	0.188	3.031	0.898
TAK+Panel	-40.02	3.93	2.08	-24.12	1.274	0.167	2.649	0.768
TAK+AllMF	-49.82	6.35	3.57	-42.91	1.586	0.269	4.540	1.366
AVERAGE								
	N_{max} [kN]	V_{max} [kN]	M_{max} [kNm]	$N_{M,max}$ [kN]	$\sigma_{c,0,d}$ [N/mm²]	τ_d [N/mm²]	$\sigma_{m,z,d}$ [N/mm²]	$\sigma_{c,0,d}$ [N/mm²]
TAK	-34.88	4.25	2.66	-25.61	1.11	0.18	3.38	0.82
TAK+Tree	-42.56	6.12	4.16	-37.69	1.35	0.26	5.30	1.20
TAK+Energy	-38.55	4.75	3.07	-31.13	1.23	0.20	3.91	0.99
TAK+Panel	-35.78	4.25	2.66	-27.37	1.14	0.18	3.38	0.87
TAK+AllMF	-48.90	6.93	4.81	-44.94	1.56	0.29	6.13	1.43
% DIFFERENCE								
	N_{max} [kN]	V_{max} [kN]	M_{max} [kNm]	$N_{M,max}$ [kN]	$\sigma_{c,0,d}$ [N/mm²]	τ_d [N/mm²]	$\sigma_{m,z,d}$ [N/mm²]	$\sigma_{c,0,d}$ [N/mm²]
TAK	-33.6%	14.5%	36.0%	22.6%	-33.6%	14.5%	36.0%	22.6%
TAK+Tree	-8.0%	15.4%	40.0%	10.9%	-8.0%	15.4%	40.0%	10.9%
TAK+Energy	-20.3%	13.2%	36.6%	17.1%	-20.3%	13.2%	36.6%	17.1%
TAK+Panel	-26.9%	14.2%	35.7%	21.2%	-26.9%	14.2%	35.7%	21.2%
TAK+AllMF	-3.8%	15.4%	41.1%	8.6%	-3.8%	15.4%	41.1%	8.6%

Table 47 - Unity checks failure of the timber piles for different load cases for both software, average is the mean of the software, and the difference illustrates the differences between the software

Plaxis					DIANA			
	UC_c	UC_s	UC_m	$U_{c,m}$	UC_c	UC_s	UC_m	$U_{c,m}$
TAK	0.08	0.09	0.32	0.40	0.11	0.08	0.20	0.27
TAK+Tree	0.12	0.13	0.51	0.62	0.12	0.11	0.31	0.41
TAK+Energy	0.10	0.10	0.37	0.47	0.12	0.09	0.23	0.31
TAK+Panel	0.09	0.09	0.32	0.40	0.11	0.08	0.21	0.27
TAK+AllMF	0.14	0.15	0.60	0.73	0.14	0.13	0.35	0.47
AVERAGE					**% DIFFERENCE**			
	UC_c	UC_s	UC_m	$U_{c,m}$	UC_c	UC_s	UC_m	$U_{c,m}$
TAK	0.10	0.08	0.26	0.33	-33.6%	14.5%	36.0%	33.2%
TAK+Tree	0.12	0.12	0.41	0.52	-8.0%	15.4%	40.0%	34.8%
TAK+Energy	0.11	0.09	0.30	0.39	-20.3%	13.2%	36.6%	32.6%
TAK+Panel	0.10	0.08	0.26	0.34	-26.9%	14.2%	35.7%	32.6%
TAK+AllMF	0.14	0.14	0.47	0.60	-3.8%	15.4%	41.1%	35.3%

5.1.3 Verification of the results

In this section, initially the convergence behaviour of the models is studied. Thereafter a mesh sensitivity is performed. This allows us to check the numerical procedure employed by the FE software. Thereafter, analytical checks of the obtained soil stresses are performed to gain insight into the soil models. Lastly, the masonry is studied, for which the assumption of linear elastic behaviour in Plaxis is verified with the results from DIANA.

<u>Convergence behaviour</u>

The convergence norm is set to satisfy both a displacement and a force norm, with a convergence tolerance of 0.01. The maximum number of iterations is 1000. If convergence is not found, the analysis is set to continue. In Table 48 it is observed that convergence is always reached as the number of iterations for most steps does not reach over 40 iterations for all load cases. Thereby the FE model converges in DIANA and the numerical procedure for the traditional model is verified.

Table 48 - Iterations to converge for different load cases DIANA traditional model

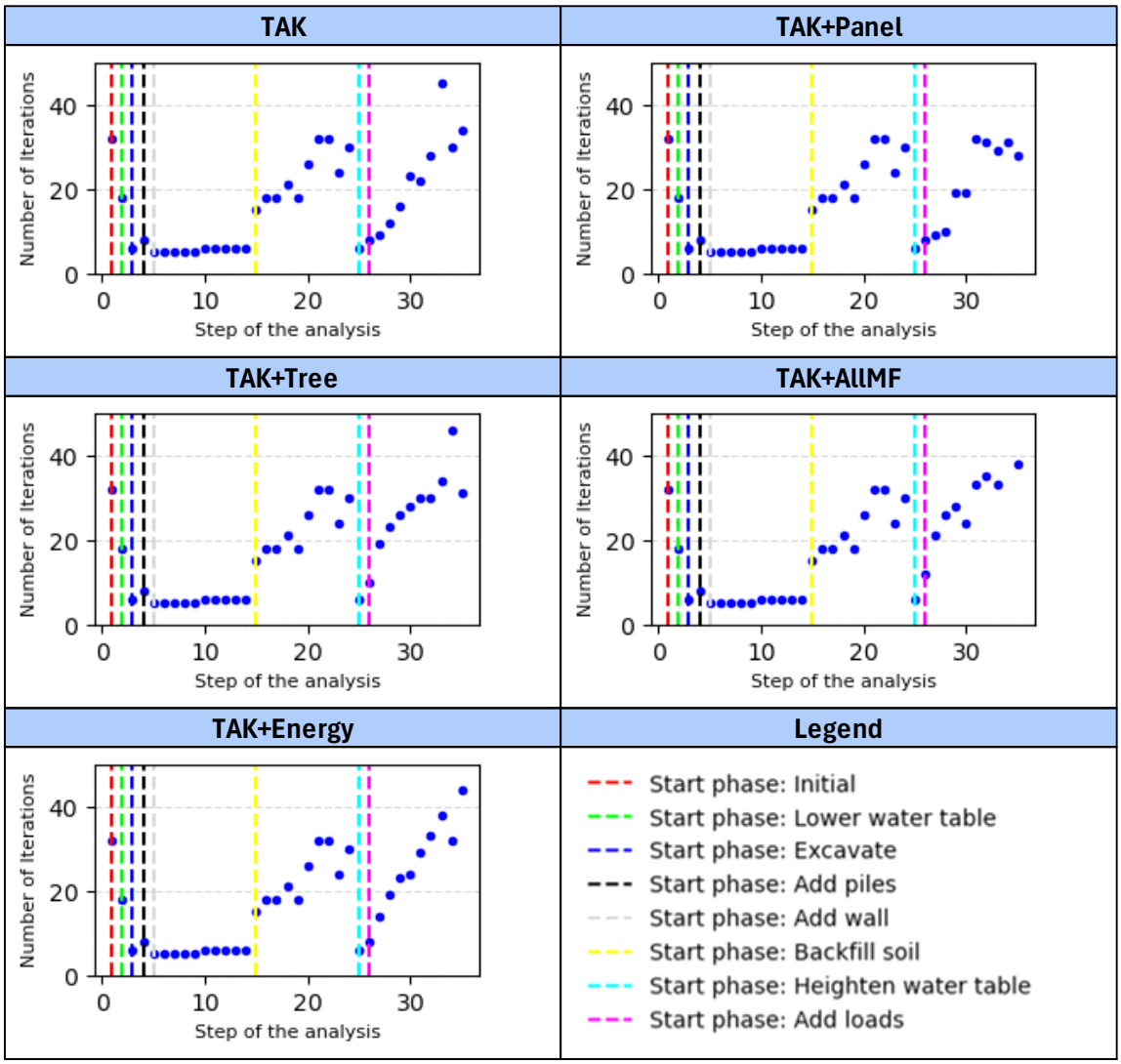

Plaxis is keeping track of convergence using the convergence log file in which the error for each iteration is stored. The tolerated error is defined by default and kept as 0.01 for both norms specified:

1. Global Force Error Norm
2. Integrated Local Soil Error

Plaxis will continue iterating up to the maximum allowed iterations, set to 60. Convergence is obtained and visualised in Figure 66. Note that this is the TAK load case and the same behaviour is observed for the other load cases.

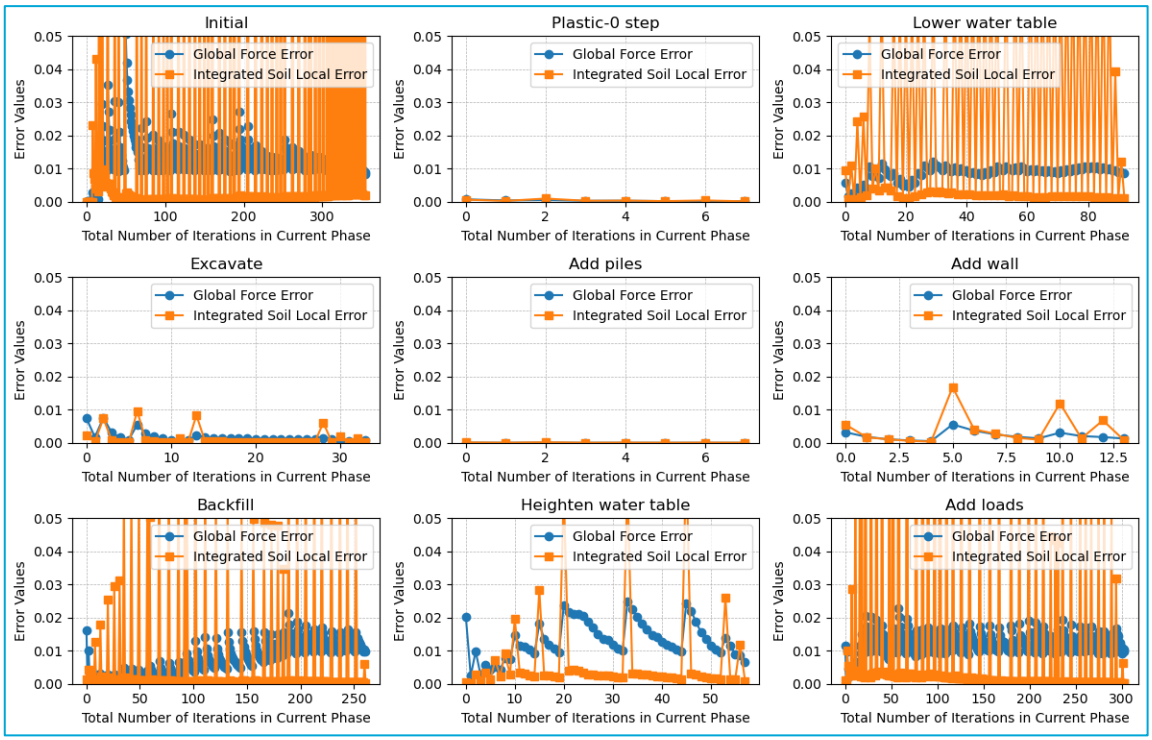

Figure 66 - Convergence plots of different phases traditional model in Plaxis in terms of Global Force Error and Integrated Soil Local Error for which both norms are specified as 0.01. In the last phase the TAK-load is applied.

<u>Mesh sensitivity</u>

In Finite Element software the mesh size has an important role. It always is a trade-off between accuracy and computational time. Therefore, initially the mesh generation will be explained. Thereafter, the mesh is refined, and the selected target variables are monitored. This allows verification of the mesh size.

In DIANA a manual selection for all the different shapes is to be made. For the initial analysis, the different elements have a mesh size according to Table 49. Also, the refined mesh size for the sensitivity analysis has been given. Thes refined mesh size is half the mesh size of the original elements, except for the Floor that already has a small mesh size of 50 mm. The mesh size is created so that along the structural element the mesh size is reduced. Both meshes are given in Figure 67.

Table 49 - DIANA element sizes of different elements for sensitivity study

Element	Mesher type	Size [mm]	
		Analysis	*Refined*
Soil_Bottom	Hexa/Quad	250	125
Soil_Top	Hexa/Quad	250	125
Soil_Backfill	Tetra/Triangle	200	100
Soil_Excavation	Tetra/Triangle	200	100
Soil_Timber	Tetra/Triangle	100	50
Wall	Tetra/Triangle	200	100
Kesp	Tetra/Triangle	100	50
Floor	Tetra/Triangle	50	50

In Plaxis 2D, the mesh generation is more automatic. The mesh is defined by the global meshing parameter l_e, which represents the target element dimension (Plaxis Reference Manual, 2025). It is calculated from the outer geometry dimensions (x_{min}, x_{max}, y_{min}, y_{max}) and the *Element distribution* selected by the user. The target element direction is calculated using:

$$l_e = r_e * 0.06 * \sqrt{(x_{max} - x_{min})^2 + (y_{max} - y_{min})^2}$$

The element distribution can be selected from Table 50. Initially as Element distribution Medium was chosen to perform the analysis as starting point, which is the default of the software. The dimensions (x_{min}, x_{max}, y_{min}, y_{max}) are set to (-9000, 9000, -15530, 1000) with unit in mm. It should be noted that Plaxis automatically reduces the mesh size around the structural elements.

Table 50 - Element distribution and relative element size (Plaxis Reference Manual, 2025)

Element distribution	r_e
Very coarse	2.00 (30 - 70 elements)
Coarse	1.33 (50 - 200 elements)
Medium	1.00 (90 - 350 elements)
Fine	0.67 (250 - 700 elements)
Very fine	0.50 (500 - 1250 elements)

The results of the mesh sensitivity analysis have been displayed in Table 51. The target variables have changed less than 2% for the considered mesh refinement. Therefore, the results are verified.

Table 51 - Mesh sensitivity DIANA traditional model

Variable	Element distribution		Difference
	Analysis	*Refined*	
Pu during loading [mm]	3.46E+01	3.48E+01	0.43%
Bending moments [Nmm]	2.07E+06	2.06E+06	0.48%
Shear force [N]	3.91E+03	3.89E+03	0.46%
Normal force [N]	-3.99E+04	-3.91E+04	1.98%

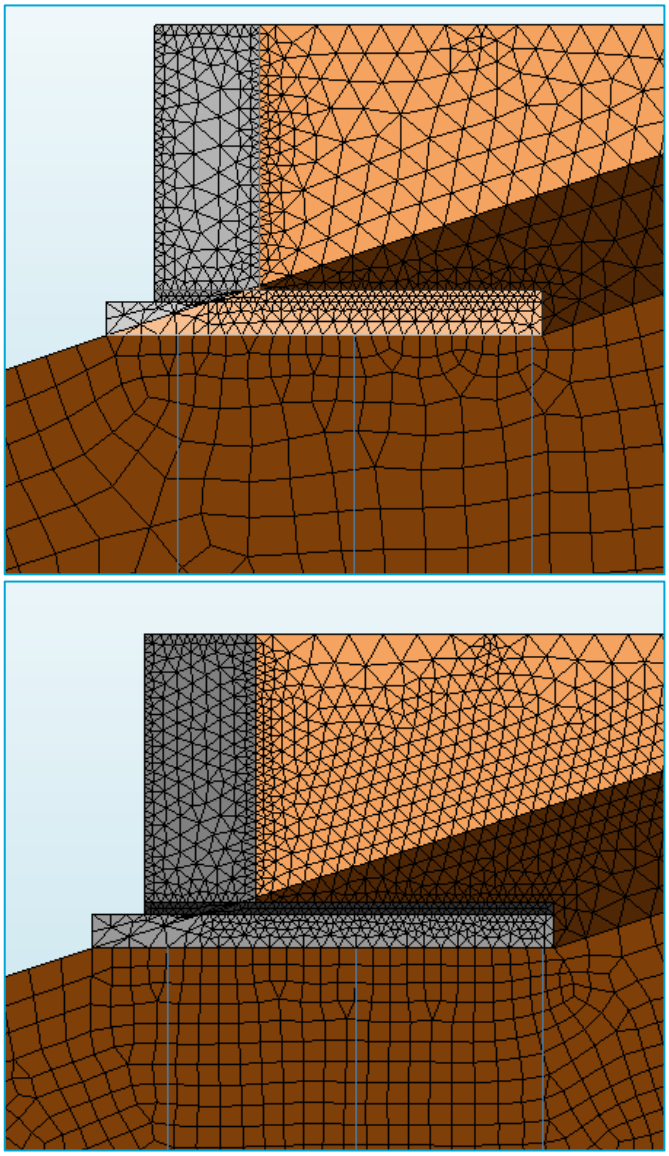

Figure 67 - Mesh DIANA for analysis (top) and refined for mesh sensitivity study (bottom)

The selected target variables for the Plaxis traditional model are given in Table 52. The maximum of each variable is displayed after the stage in which the loading is applied. After the initially selected *Medium* element distribution, the mesh is refined to *Fine* (both displayed in Figure 68). The respective element dimensions are 1449.4 mm and 966.7 mm). The differences are given in Table 52. Thereupon, the initial mesh size *Medium* is considered verified.

Table 52 - Mesh sensitivity Plaxis traditional model

Variable	Element distribution		Difference
	Medium	*Fine*	
Pu during loading [mm]	3.54E+01	3.54E+01	0.08%
Bending moments [Nmm]	3.24E+06	3.21E+06	0.83%
Shear force [N]	4.58E+03	4.47E+03	2.49%
Normal force [N]	-2.99E+04	-2.98E+04	0.33%

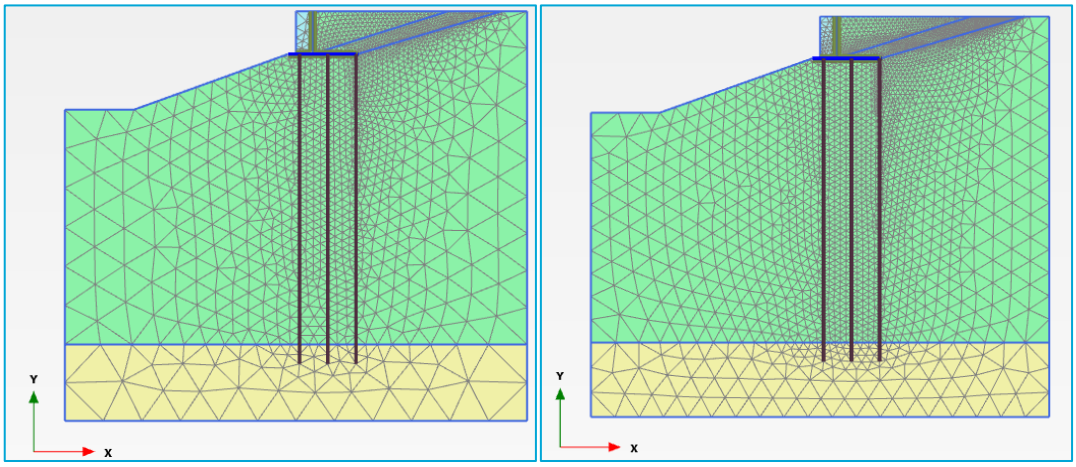

Figure 68 - Mesh Plaxis with Element distribution set to Medium (left) and Fine (right)

<u>Analytical check 1: Active pressure on wall and resulting shear in piles</u>

Using the surcharge load of the soil of 10 kN/m, and the volumetric weight of the clay soil $\gamma = 14.02$ kN/m^3, the total vertical stress can be calculated at various depths. Note that in this calculation, the top of the masonry wall located at 580 mm above NAP is taken as $h = 0$. This results in the pore water pressure starting from NAP-400 mm, thus at -0.98 m in this reference system. The effective vertical stresses (σ') can be calculated by subtracting the pore pressures (p) from the total stresses (σ) (Verruijt, 2001):

$$\sigma' = \sigma - p$$

The horizontal pressure can be calculated analytically use the coefficient for earth pressure at rest (K_a). This can be calculated from the following formula:

$$K_a = (1 - \frac{1 - \sin(\varphi)}{1 + \sin(\varphi)}$$

From a friction angle of 23.8°, the coefficient can be determined as $K_0 = 0.425$. The results have been visualized in Table 53.

Table 53 - Pressures on masonry wall resulting from analytical calculations

Earth and water pressures								
Layer	**Depth**				**Vertical total stress**	**Pore water pressure**	**Vertical effective stress**	**Horizontal pressure**
	h	γ	t_j	$\gamma_{sat} * t_j = \Delta\sigma_v$	σ_v	u	σ_v'	σ_h'
	[m]	[kN/m^3]	[m]	[kPa]	[kPa]	[kPa]	[kPa]	[kPa]
Active side								
	0.00	-	-	-	10.00	0.00	10.00	4.25
I	-0.98	14.02	0.98	13.74	23.74	0.00	23.74	10.09
II	-1.60	14.02	0.62	8.69	32.43	6.20	26.23	11.15

The graph in Figure 69 displays the result of the analytical estimation. To verify the model in Plaxis 2D, the horizontal total and effective stresses have been plotted. The place where the total and

effective stresses differentiate is clearly at -0.98 m, which is expected. Furthermore, the horizontal effective stresses are very close to earth pressure, therefore the results of the Plaxis model can be noted trustworthy. In DIANA the same observations can be made regarding the pore pressures. It does however take longer to active the full earth pressure in DIANA which is expected to be a result of the *Init stresses* not being activated, thereby causing a wrong initiation of the lateral earth pressure. This discussed in the Discussion.

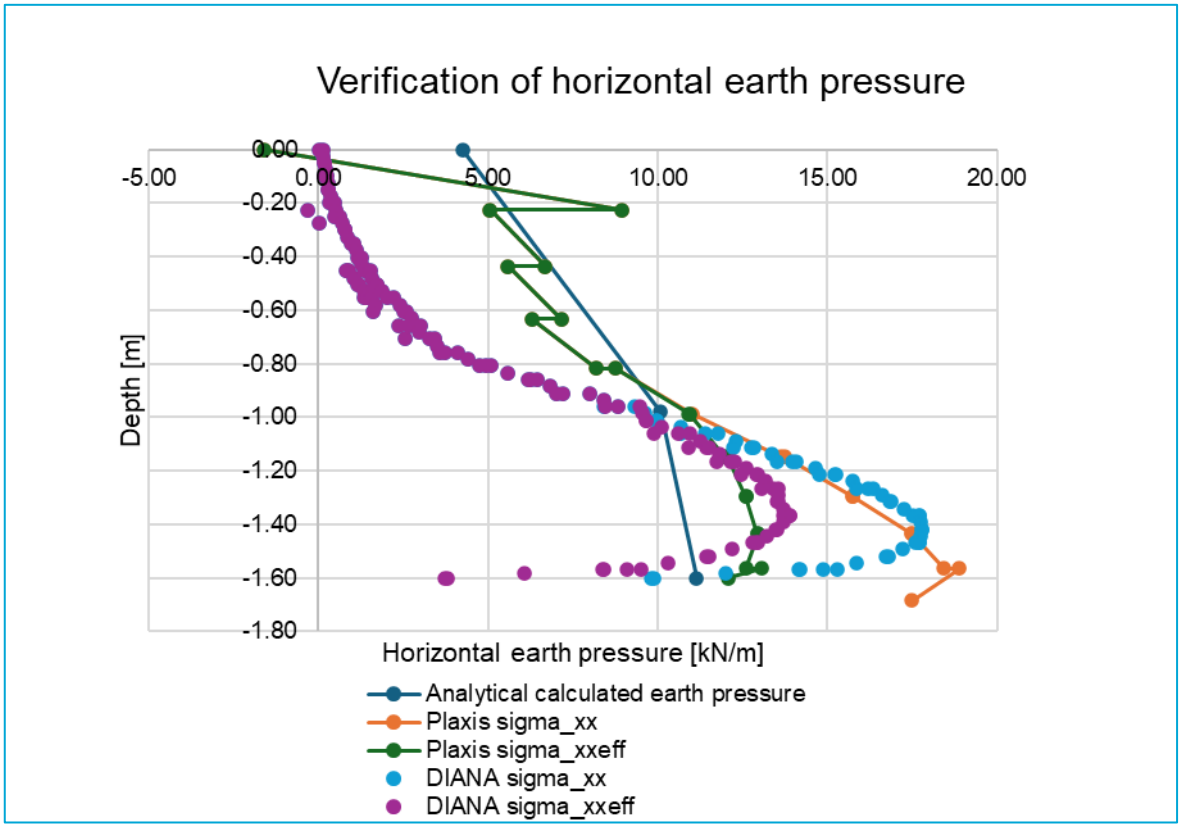

Figure 69 - Verification of horizontal earth pressure; a depth of 0 m indicates that this is the top of the masonry wall. Note that this is a different reference than in the FE models, where the top of the wall is located at +0.58m.

The area below the curves can be calculated using a method such as employed in Figure 70 to obtain the total force acting to the left on the masonry wall. This results in a total force of 17.28 kN/m for the analytical method in active earth pressure, 9.71 kN/m for DIANA (56.2% of the analytical solution) and 13.87 kN/m for Plaxis (80.3%) when looking at the effective horizontal stresses. When looking at the total horizontal stresses the following values are reached: 11.60 kN/m for DIANA (67.1% of the analytical solution) and 17.31 kN/m for Plaxis (100.2%). The results in DIANA are not in line with the expectation, especially at the top due to previously described stress initialisation issues. Regarding Plaxis, it is observed that the total stresses on the masonry wall coincides accurately with the expected active earth pressure. Upon reflection in the manual, it is not found how these stresses exactly are initialised. However, it is stated that for initialisation lateral stresses K_0^{nc} is used for the *K0 procedure* (which would analytically result in 19.1 kN/m), whereas the lateral stress state is not specified for the *Plastic* and *Gravity loading* analysis type. Upon reflection, it remains unclear, however results of Plaxis are expected to more reliable than those of Plaxis, as the result closely approximate the expected pressures.

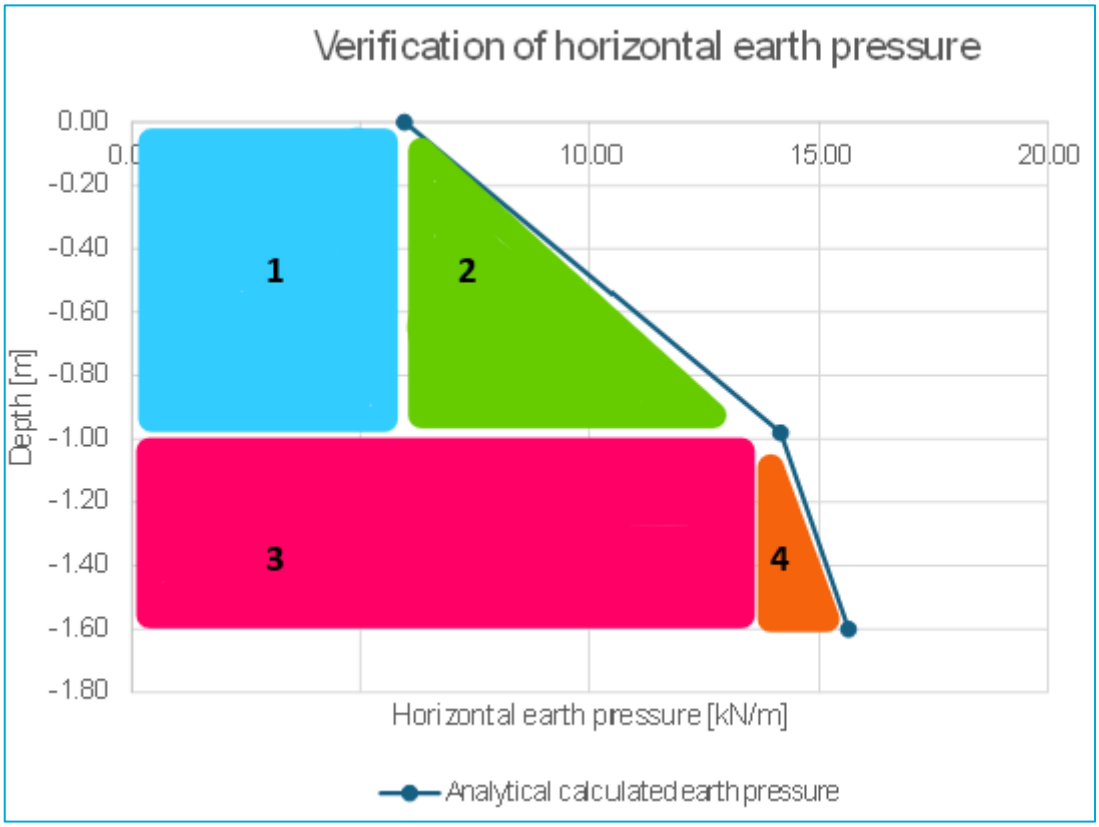

Figure 70 – Horizontal earth pressure analytical calculation total force by sum of 4 areas

The shear force in the piles is expected to take most of the active earth pressure generated by the soil and compared for DIANA and Plaxis. The shear forces of the 3 piles are summed and for DIANA 5.46 kN is obtained, which is 56.3% of the active earth pressure on the masonry wall. For Plaxis the total shear force in the piles is 10.41 kN, which is 75.0% of the active earth pressure on the wall.

<u>Analytical check 2: Earth pressures right side of the boundary</u>

The earth pressure on the right of the model can be calculated analytically use the coefficient for earth pressure at rest (K_0). This can be calculated from the following formula:

$$K_0 = 1 - \sin(\varphi)$$

For the clay and sand value this results in the values of 0.596 and 0.5 respectively. By using the effective vertical stresses and earth pressure coefficients, the earth pressure at the boundary can be calculated. By calculating the area between the y-axis, the total force can be calculated. For the analytical method, a total of 492 kN/m is obtained. By summing the right boundary forces of the FE model in DIANA a total of 553.9 kN//m is calculated. Thus, a difference of 12.6% is observed. In Plaxis the cross-section tool was made to calculate the stresses at the right side of the boundary. By integration of the area a total force of 376 kN/m is obtained, which is a difference of 23.5%.

It is verified that the jump in earth pressure at the boundary of the clay and sand layer is present in DIANA and Plaxis as can be viewed in Figure 71.

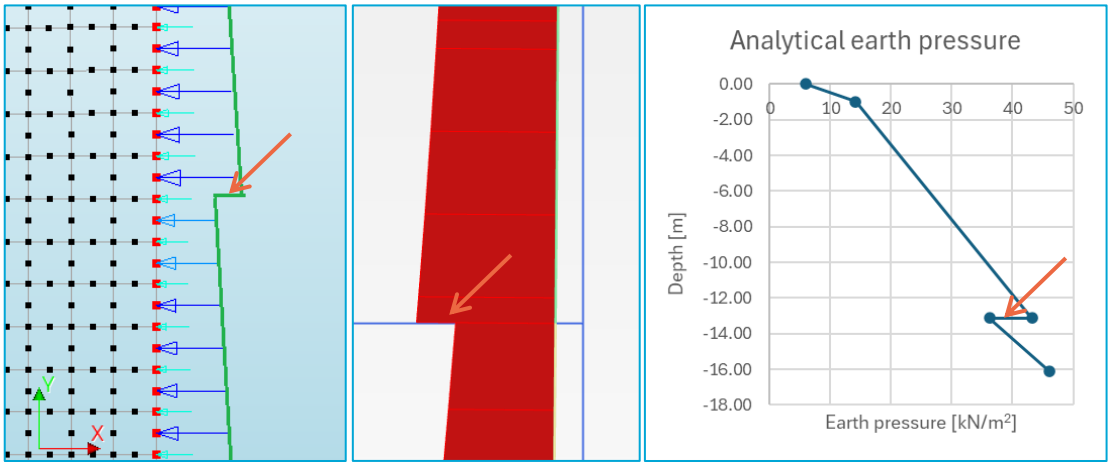

Figure 71 - Jump in earth pressure at boundary clay and sand layer in DIANA (left), in Plaxis (middle) and analytical solution (right). The jump is indicated by the orange arrows

<u>Check assumption linear elastic masonry</u>

In the DIANA model, a Total Strain Based Crack Model was used, whereas in Plaxis 2D a linear elastic model was chosen. It is verified in this section, that an elastic model is a valid choice in this case as the masonry remains within the ultimate strength defined in section 2.2.2.

- Compression: $f_c = 8.5\ N/mm^2$
- Tension: $f_t = 0.1\ N/mm^2$

In Plaxis the principal stress (σ_1) in Figure 72 are observed. It is observed that for the left bottom the compressive strength of the masonry is not reached as $0.1457 < 8.5\ N/mm^2$. Also, the tension limit is not reached as $0.01759 < 0.1\ N/mm^2$. It can be concluded that a linear elastic material may be used.

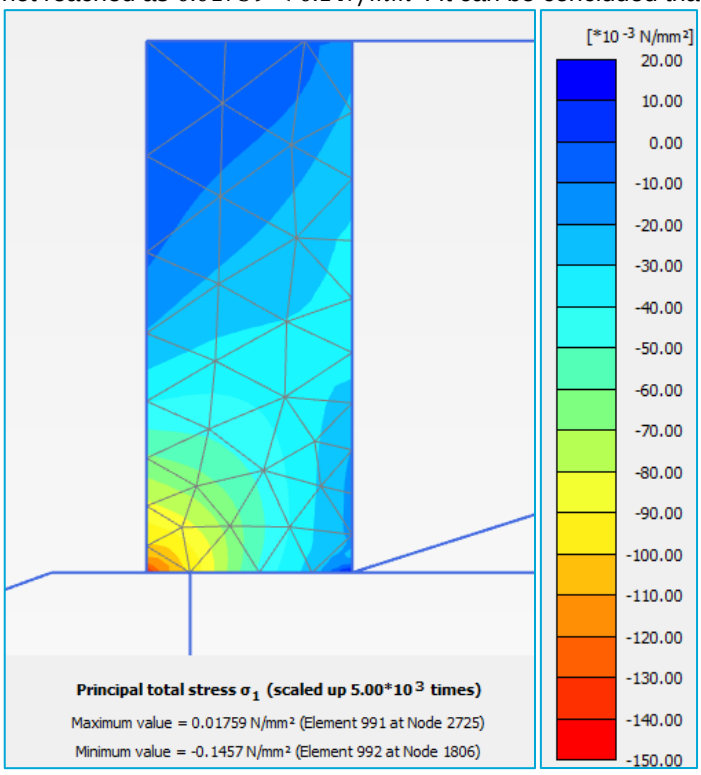

Figure 72 - Principal total stresses Plaxis masonry during phase Add loads in TAK load case

If the stress surpasses the strain at which these elastic limits are observed, cracking or nonlinearity may occur. Therefore, the strain levels are checked to see if the strain does not exceed the elastic limit. This means that the principal strain should not be larger than:

$$\varepsilon < \frac{\sigma}{E}$$

Note that masonry has the following Young's modulus: $E = 5000\ N/mm^2$. This means that for the strains the following limits are set to stay in the elastic region:

$$\varepsilon_t = \frac{f_t}{E} = \frac{0.1}{5000} = 2.0 * 10^{-5}$$
$$\varepsilon_c = \frac{f_c}{E} = \frac{8.5}{5000} = 1.7 * 10^{-3}$$

In DIANA, the principal stresses and strains (σ_1 and ε_1 in the final stage when the loads have been added) are extracted and illustrated in Table 54. By setting the contour limit scale to the strain limits for the elastic part, it is observed that the maximum strain for this elastic limit is not reached. It is also confirmed that the stresses are not close to the maximum failure stress, in either tension or compression.

Table 54 - Principal stresses in masonry DIANA

Principal stress σ_1	**Principal strain ε_1**
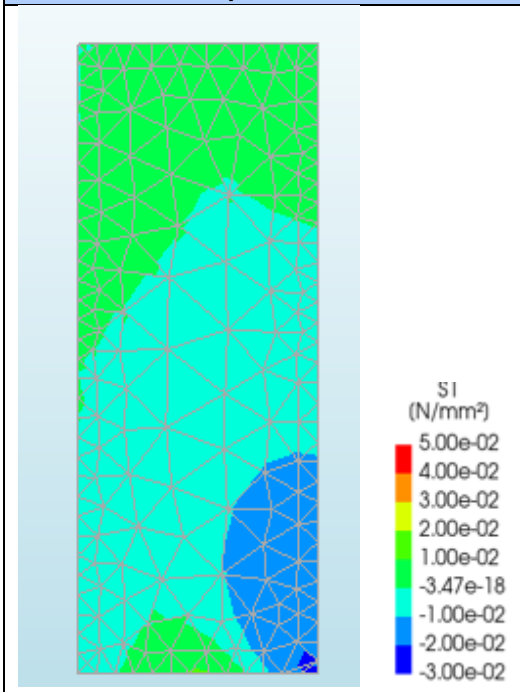	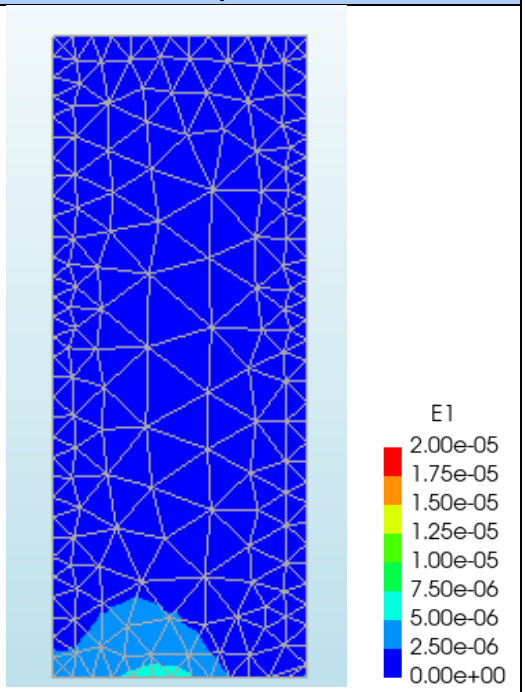

5.2 Sheet pile model

This section presents the comparative analysis of the structural behaviour of the sheet pile geometry using DIANA and Plaxis models for five different load cases. The differences between the two software tools are allocated to the soil-structure interaction. The focus of DIANA is on structural stiffness and that of Plaxis on the soil-structure interaction. The implications of this are discussed in more detail in the Discussion. Initially, the displacements are shown and checked. Furthermore, the comparison includes normal forces, shear forces, and bending moments in the piles, as well as the resulting unity checks because of these forces.

5.2.1 Failure mechanism: excessive displacements

Serviceability criteria for displacements, both horizontal and total are again considered in this section. The limit for the horizontal displacement is set to 50 mm like that of the traditional model (Ingenieursbureau Gemeente Amsterdam, 2023).

Horizontal displacement

The maximum horizontal displacement is taken as output from both DIANA and Plaxis for the various load cases. The displacements are displayed in Table 55. For the reference TAK load case, an average horizontal displacement of 13.59 mm to the left is observed. As a result of the multifunctionalities the displacements increase to 63.46 mm on average. This effectively means that because of the multifunctionalities the displacement is increased by 49.87 mm, an increase of 367%. This large increase can be expected by the increase of horizontal effective stresses, resulting from the high surcharge load near the quay, mainly resulting from the tree and energy storage. Note that the displacements in DIANA are greater than in Plaxis for most cases. It is observed that the differences between DIANA and Plaxis decrease from 48% for smaller loads to 3% for larger loads on the structure.

Table 55 - Horizontal phase displacement during Add loads stage/phase for both software, average is the mean of the software, and the difference illustrates the differences between the software

	Pu_x [mm]			
	DIANA	Plaxis	Average	Difference
TAK	-16.23	-10.95	-13.59	-48.2%
TAK+Tree	-46.43	-45.26	-45.85	-2.6%
TAK+Energy	-27.70	-22.38	-25.04	-23.8%
TAK+Panel	-16.46	-11.08	-13.77	-48.6%
TAK+AllMF	-62.23	-64.68	-63.46	3.8%

The limit for the horizontal displacement of the capstone is set to 5 0mm (Ingenieursbureau Gemeente Amsterdam, 2023). With the resulting displacements from Table 55, the resulting unity check can be determined by dividing the observed displacement by the maximum allowed displacement. This results in the unity checks in Table 56. It is observed that unity check increases from 0.27 for the TAK load case to 1.27 for when all functionalities are applied. This is an increase of 1.0 (+370%).

Table 56 - Unity check horizontal phase displacement during Add loads stage/phase for both software, average is the mean of the software, and the difference illustrates the differences between the software

$UC_{def,hor}$ [-]				
	DIANA	Plaxis	Average	Difference
TAK	0.32	0.22	0.27	-48.2%
TAK+Tree	0.93	0.91	0.92	-2.6%
TAK+Energy	0.55	0.45	0.50	-23.8%
TAK+Panel	0.33	0.22	0.28	-48.6%
TAK+AllMF	1.24	1.29	1.27	3.8%

<u>Total displacement</u>

The global behaviour of the structure is observed in Table 57. The phase displacements during loading are qualitatively and quantitatively observed in Table 60 for the different load cases. The largest displacements are given in red, and it is observed that they are again the largest at the location of the applied loading, which is expected. The maximum displacements are given in Table 58. Note that the displacements observed for the TAK are 36.34 mm and for the multifunctionalities 192.71 mm, an increase of 156.37 mm (430%).

It is interesting to observe that the results between the observed displacements in the software comparison of DIANA and Plaxis for the greatest loads, which are the load combinations TAK+Tree and TAK+AllMF, are smallest. Again, the Soil-Structure-interaction plays an important role. The vertical deformation plays a larger role when the total loading is larger and is not resisted by the sheet pile. The horizontal deformation is influenced by the sheet pile and only has a significant effect when the vertical load is smaller.

A unity check is also performed for the total displacement. Therefore, the displacement from Table 55. can be divided by the ductile limit of 50 mm. The results are displayed in Table 59. The TAK load case gives a value of 0.73, whereas all multifunctionalities give a unity check of 3.85, or an increase of 3.12 (+427%). It should again be noted that in the models no stiff sand layer is applied as a top layer, which will redistribute the surface load more evenly, thereby limiting differential settlement and total displacements. This will effectively reduce the unity check for displacement of this model.

Table 57 - Magnified total displacement sheet pile structure at the end of the construction sequence for the TAK load case. The plotted Figures serve as a qualitative indication of the movement of the structure. For a quantitative expression the reader is referred to the other Tables.

DIANA	Plaxis
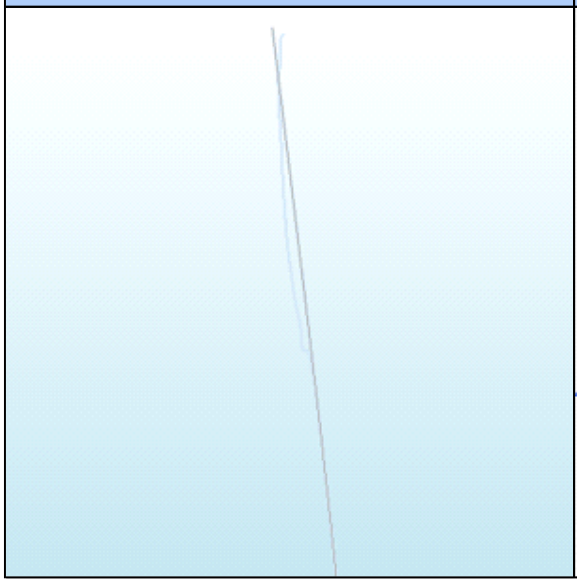	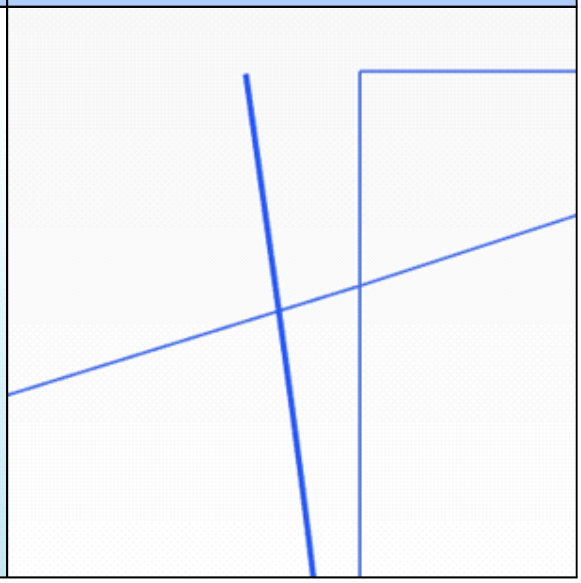

Table 58 - Maximum phase displacements during loading for different load cases for both software, average is the mean of the software, and the difference illustrates the differences between the software

Pu [mm]				
	DIANA	Plaxis	Average	Difference
TAK	41.24	31.43	36.34	-31.2%
TAK+Tree	139.7	137.2	138.45	-1.8%
TAK+Energy	69.54	62.17	65.86	-11.9%
TAK+Panel	41.63	31.02	36.33	-34.2%
TAK+AllMF	190.32	195.1	192.71	2.5%

Table 59 - Unity check phase displacements during Add loads stage/phase for different load cases for both software, average is the mean of the software, and the difference illustrates the differences between the software

$UC_{def,tot}$ [-]				
	DIANA	Plaxis	Average	Difference
TAK	0.82	0.63	0.73	-31.2%
TAK+Tree	2.79	2.74	2.77	-1.8%
TAK+Energy	1.39	1.24	1.32	-11.9%
TAK+Panel	0.83	0.62	0.73	-34.2%
TAK+AllMF	3.81	3.90	3.85	2.5%

Table 60 - Phase displacements sheet pile model during Add loads stage/phase for different load cases for both software, DIANA is displayed on the left and Plaxis on the right. The contour scale is taken from DIANA but set to the same values in Plaxis

Phase displacements during Add loads stage/phase

TAK

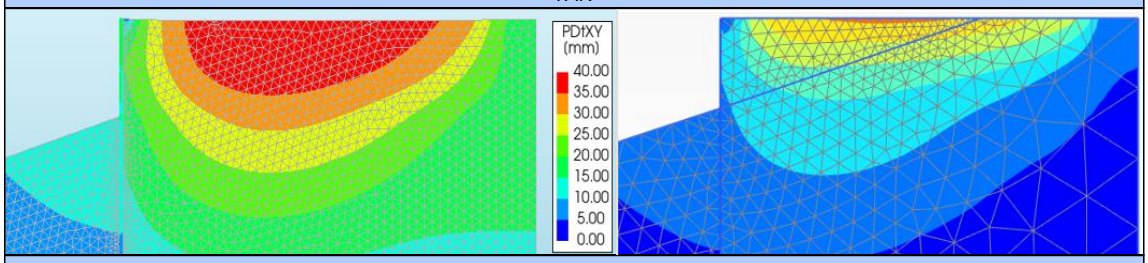

TAK+Tree

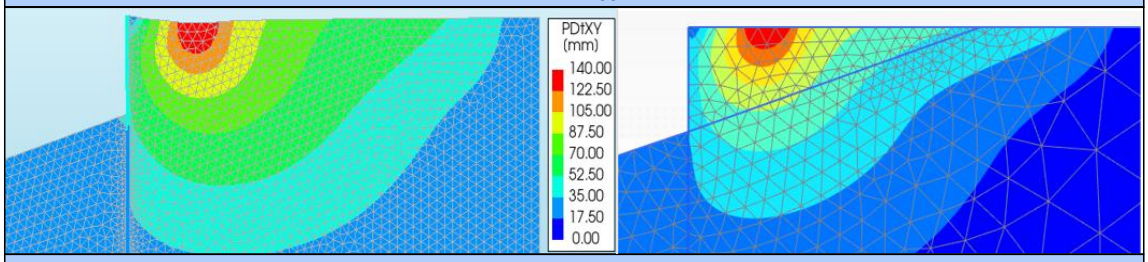

TAK+Energy

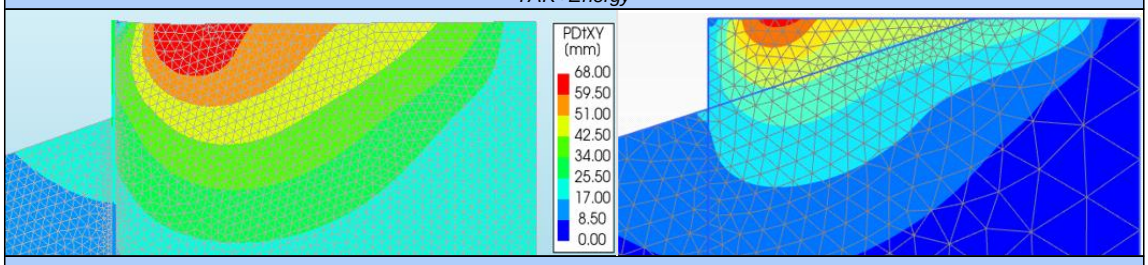

TAK+Panel

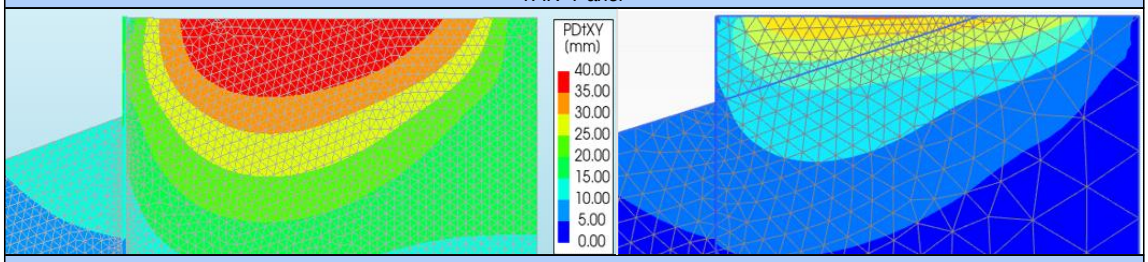

TAK+AllMF

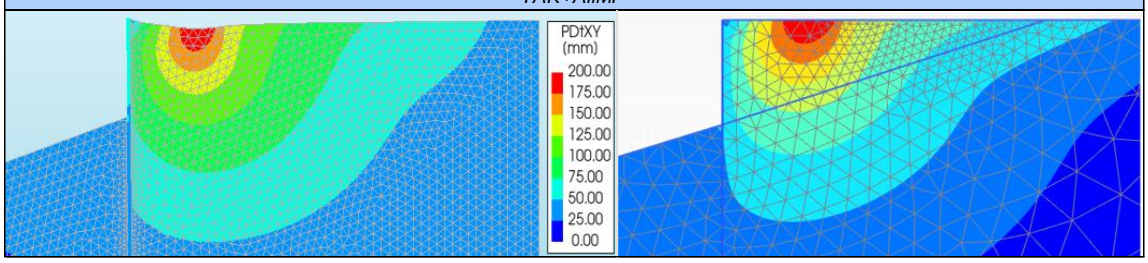

5.2.2 Failure mechanism: structural failure

The cross-sectional forces and moment diagrams for Plaxis and DIANA are illustrated in Table 61.

Normal force diagrams from DIANA and Plaxis exhibit similar trends. The TAK+AllMF case (purple) has the highest values, indicating that this loading condition generates more significant axial forces, which can be explained by the fact that indeed the loading in the normal force direction of the sheet pile is the largest. Furthermore, the normal force increases progressively until reaching the interface between the clay and sand layer at a depth of 12.53 m. Beyond this boundary, the sand layer primarily resists the axial force through frictional resistance.

Shear force diagrams show overall comparable shapes in DIANA and Plaxis, but notable differences exist in their detailed distributions. In DIANA, the shear force fluctuates more prominently along the depth, showing local variations that are less pronounced in Plaxis.

Bending moment distributions between DIANA and Plaxis follow a similar trend, but Plaxis consistently predicts higher values. The variations among load cases indicate that the additional loads (Tree, Energy, Panel, and AllMF) generally lead to increased bending moments, with TAK+AllMF (purple) always yielding the highest values in both software models. The greater differences between DIANA and Plaxis suggest that each software handles interaction effects differently.

Table 61 - Cross-sectional forces and moment diagrams sheet pile for different load cases in Add loads stage/phase

	DIANA	Plaxis
N	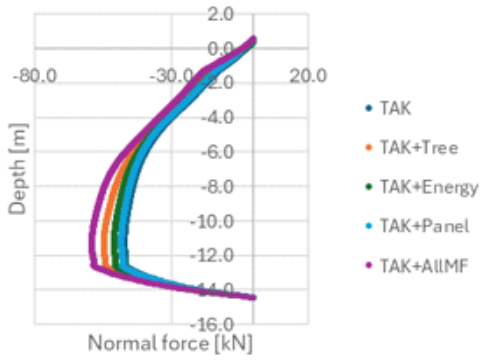	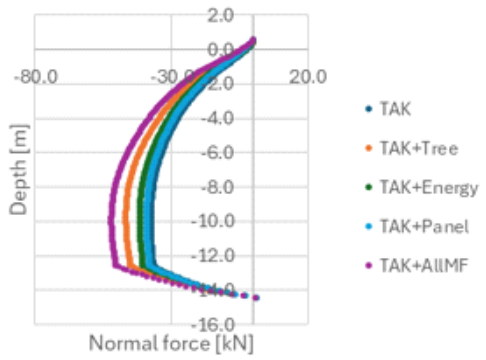
V	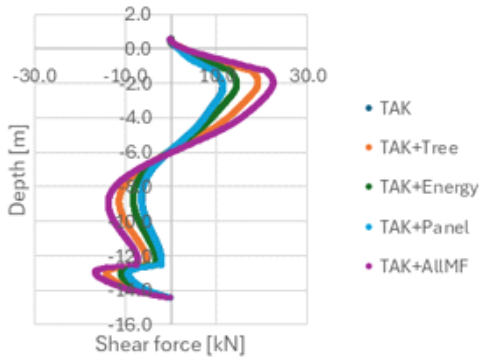	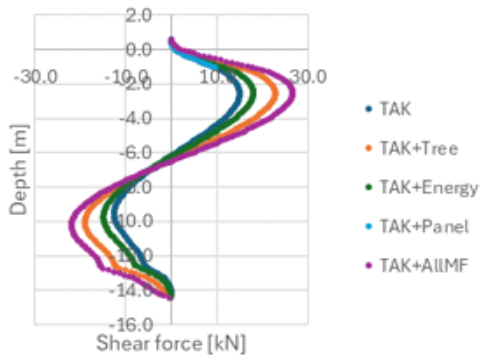
M	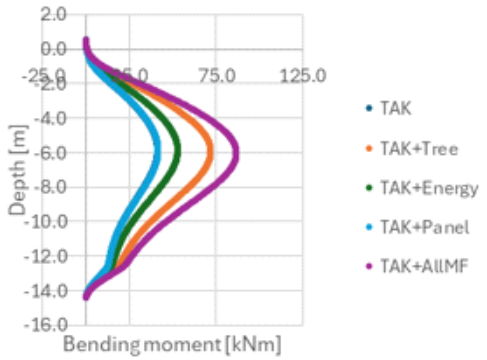	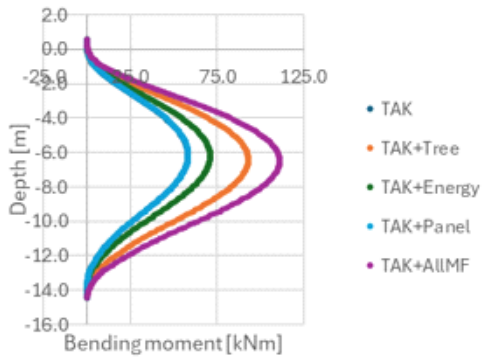

Table 62 - Governing cross-section forces and moments for different load cases for both software, average is the mean of the software, and the difference illustrates the differences between the software

Plaxis			
	N_{max} [kN/m]	V_{max} [kN/m]	M_{max} [kNm/m]
TAK	-37.49	14.95	58.18
TAK+Tree	-46.67	22.78	92.92
TAK+Energy	-41.62	17.96	70.91
TAK+Panel	-39.07	14.97	58.28
TAK+AllMF	-51.98	26.64	111.03
DIANA			
	N_{max} [kN/m]	V_{max} [kN/m]	M_{max} [kNm/m]
TAK	-46.97	11.34	41.10
TAK+Tree	-54.54	19.10	71.81
TAK+Energy	-50.77	14.42	52.77
TAK+Panel	-48.13	11.48	41.51
TAK+AllMF	-58.95	22.42	86.63
AVERAGE			
	N_{max} [kN/m]	V_{max} [kN/m]	M_{max} [kNm/m]
TAK	-42.23	13.14	49.64
TAK+Tree	-50.60	20.94	82.36
TAK+Energy	-46.20	16.19	61.84
TAK+Panel	-43.60	13.23	49.89
TAK+AllMF	-55.47	24.53	98.83
% DIFFERENCE			
	N_{max} [kN/m]	V_{max} [kN/m]	M_{max} [kNm/m]
TAK	-25.3%	24.2%	29.4%
TAK+Tree	-16.9%	16.2%	22.7%
TAK+Energy	-22.0%	19.7%	25.6%
TAK+Panel	-23.2%	23.3%	28.8%
TAK+AllMF	-13.4%	15.8%	22.0%

Using the cross-sectional forces and moments from Table 62 and the resistances of the sheet pile section determined with the method explained in the Literature Study in section 2.4.2, the unity checks can be performed for compression, shear and bending. These checks have been briefly listed below. The result of the unity checks in DIANA, Plaxis, the average and difference are stated in Table 63.

Normal force: $$UC_N = \frac{N_d}{N_{pl,Rd}} \leq 1.0$$

Shear force: $$UC_V = \frac{V_d}{V_{pl,Rd}} \leq 1.0$$

Bending moment: $$UC_M = \frac{M_d}{M_{c,Rd}} \leq 1.0$$

Table 63 - Unity checks structural failure of the sheet pile for different load cases for both software, average is the mean of the software, and the difference illustrates the differences between the software

Plaxis				DIANA		
	UC_N	UC_V	UC_M	UC_N	UC_V	UC_M
TAK	0.012	0.033	0.157	0.015	0.025	0.111
TAK+Tree	0.015	0.050	0.251	0.017	0.042	0.194
TAK+Energy	0.013	0.039	0.191	0.016	0.032	0.142
TAK+Panel	0.012	0.033	0.157	0.015	0.025	0.112
TAK+AllMF	0.016	0.058	0.299	0.019	0.049	0.234
AVERAGE				**% DIFFERENCE**		
	UC_N	UC_V	UC_M	UC_N	UC_V	UC_M
TAK	0.013	0.029	0.134	-25.3%	24.2%	29.4%
TAK+Tree	0.016	0.046	0.222	-16.9%	16.2%	22.7%
TAK+Energy	0.015	0.035	0.167	-22.0%	19.7%	25.6%
TAK+Panel	0.014	0.029	0.135	-23.2%	23.3%	28.8%
TAK+AllMF	0.017	0.054	0.266	-13.4%	15.8%	22.0%

From Table 63 it can be observed that the check for bending is governing. The average unity check for bending goes up from 0.134 for the TAK case to 0.266 for when all multifunctionalities are considered, which is an increase of 0.132 (+98.5%). DIANA gives approximately 25% lower results than Plaxis. Note that for all load cases the resistance of the structure is greater than the effect of the loads. In this unity check no reduction of the sheet pile cross-section because of deterioration due to corrosion has been considered, which will be discussed later. Additionally, partial load factors have not been considered.

5.2.3 Verification of the results

In this section, initially the convergence behaviour of the models is studied. Thereafter a mesh sensitivity is performed. This allows us to check the numerical procedure employed by the FE software.

<u>Convergence behaviour</u>

The convergence norm for DIANA is set to satisfy both a displacement and a force norm, with a convergence tolerance of 0.01. The maximum number of iterations is 100. If convergence is not found, the analysis is set to continue. In Table 64Table 48 it is observed that convergence is reached, except for the case where all the multifunctionalities are added, there in one of the load steps difficulties with convergence are found.

Table 64 - Iterations to converge for different load cases DIANA sheet pile model with a maximum of 100 iterations and force and energy norm of 0.01

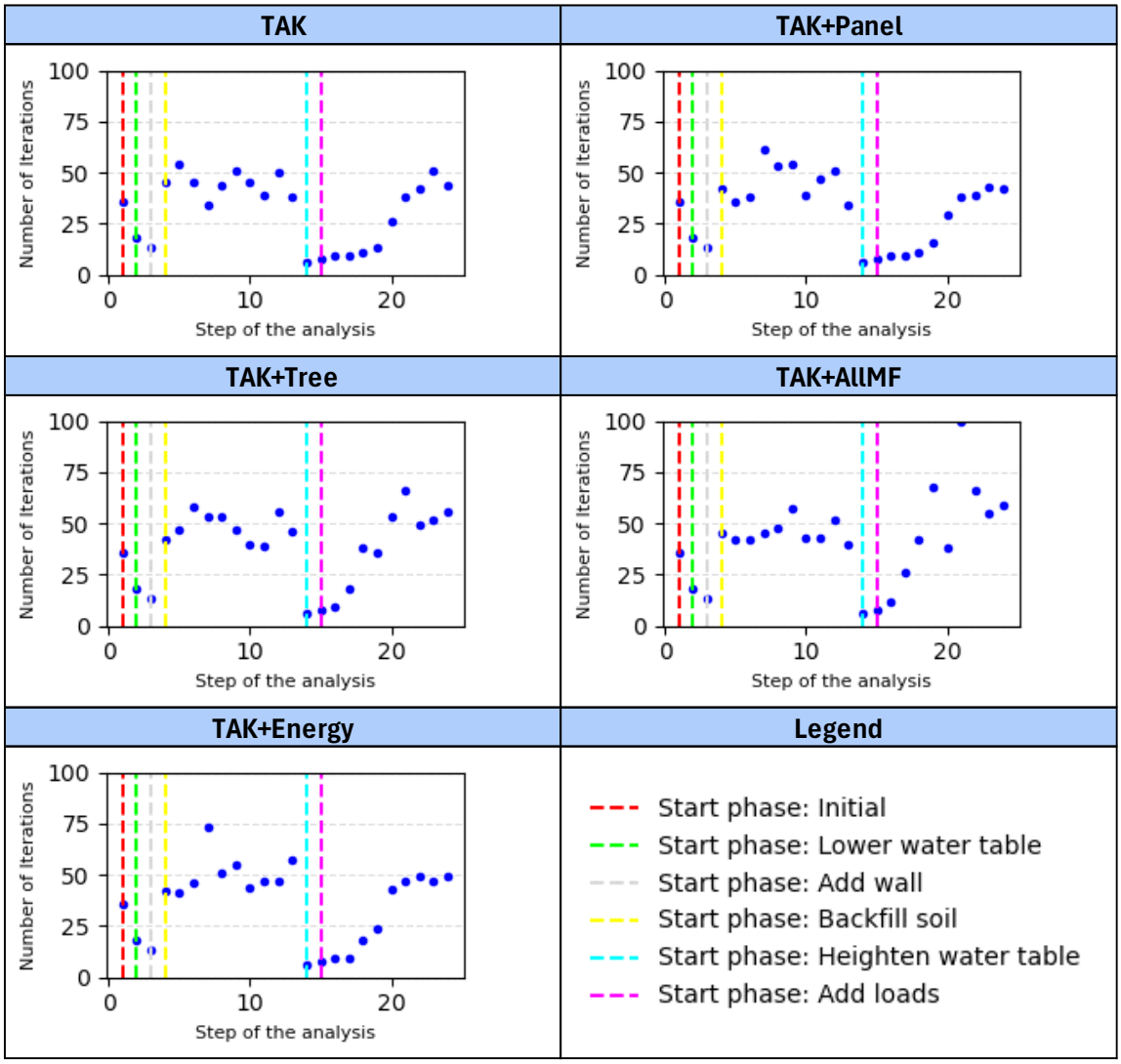

Thereafter, it was tried to reduce the error to 0.001 and allow for a maximum of 200 iterations, to see if the results would improve. The convergence behaviour is plotted in Table 65. It is observed that convergence is not found for this stricter norm. However, upon reflection of the displacement norm in Figure 73 and force norm in Figure 74 it is found that the solution is still improving and thereby getting more accurate than for the 0.01 norm. Therefore, although convergence is not reached with the strict norm, the results from this model are used.

Table 65 - Iterations to converge for different load cases DIANA sheet pile model with a maximum of 200 iterations and force and energy norm of 0.001

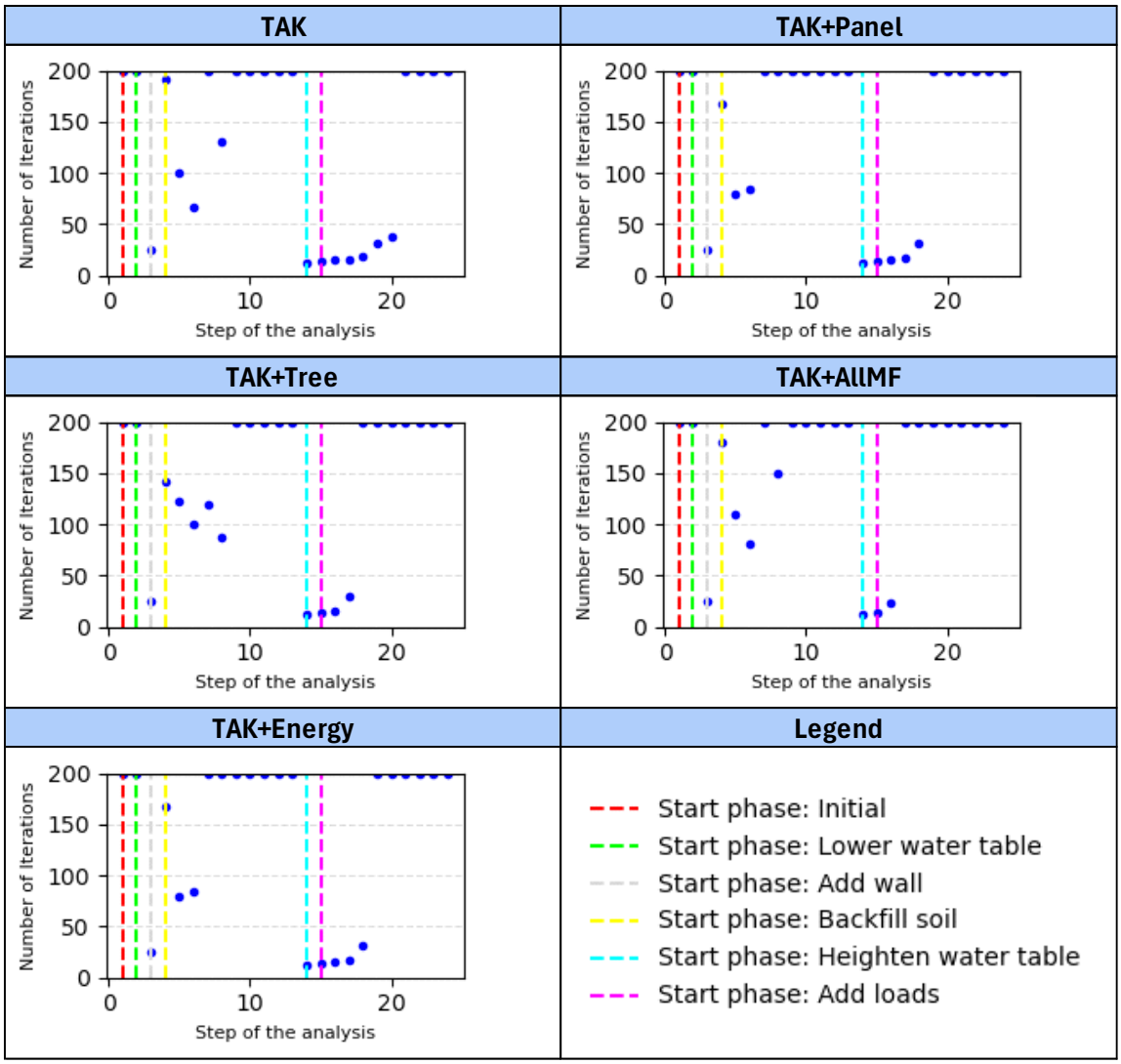

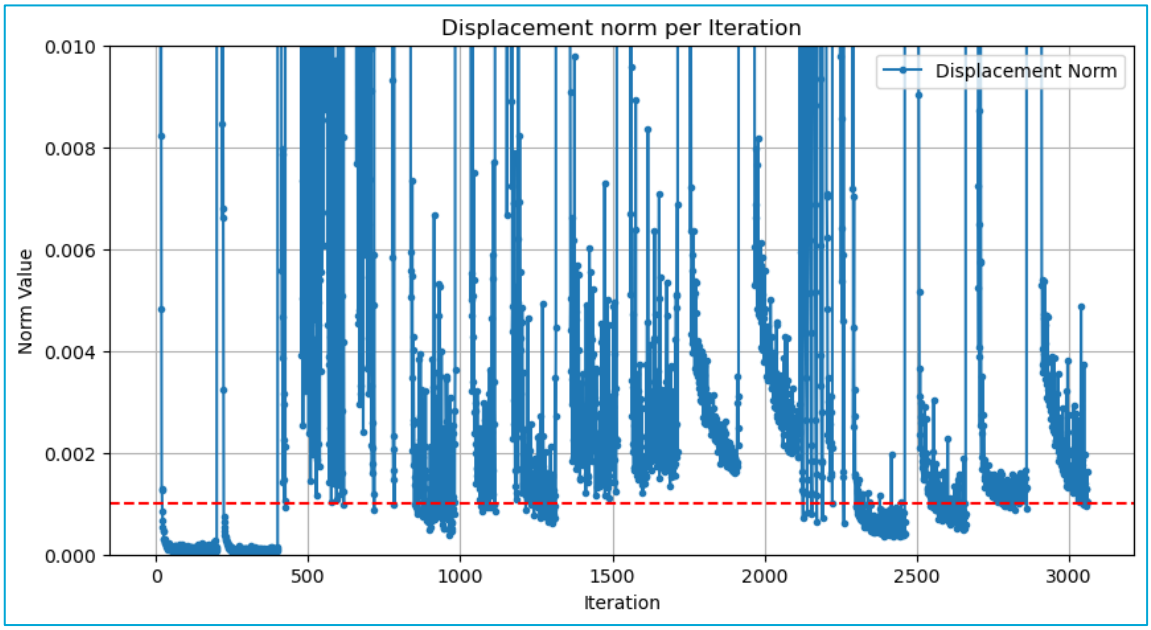

Figure 73 - Displacement norm for sheet pile model. The old norm is 0.01, which is the top of this plot. The new norm of 0.001 is showed by the dashed red line. Convergence is not reached, although with the refined norm a smaller error is obtained

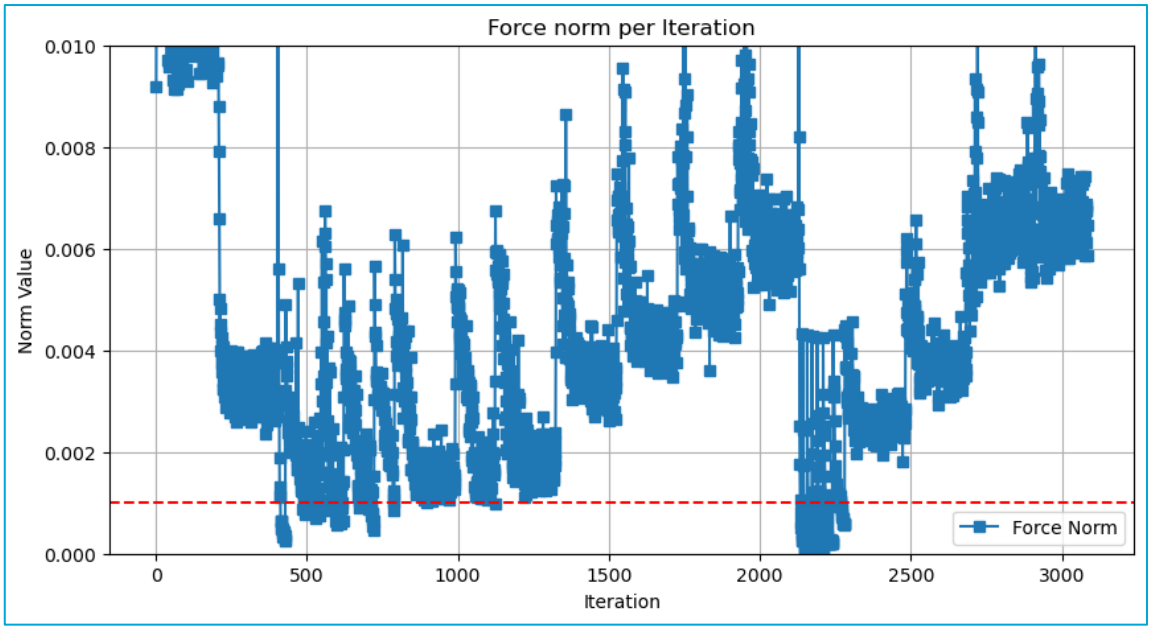

Figure 74 - Force norm for sheet pile model. The old norm is 0.01, which is the top of this plot. The new norm of 0.001 is showed by the dashed red line. Convergence is not reached, although with the refined norm a smaller error is obtained

Plaxis is keeping track of convergence using the convergence log file in which the error for each iteration is stored. The tolerated error is defined by default and kept as 0.01 for both norms specified:

1. Global Force Error Norm
2. Integrated Local Soil Error

Plaxis will continue iterating up to the maximum allowed iterations, set to 60. Convergence is obtained and visualised in Figure 75.

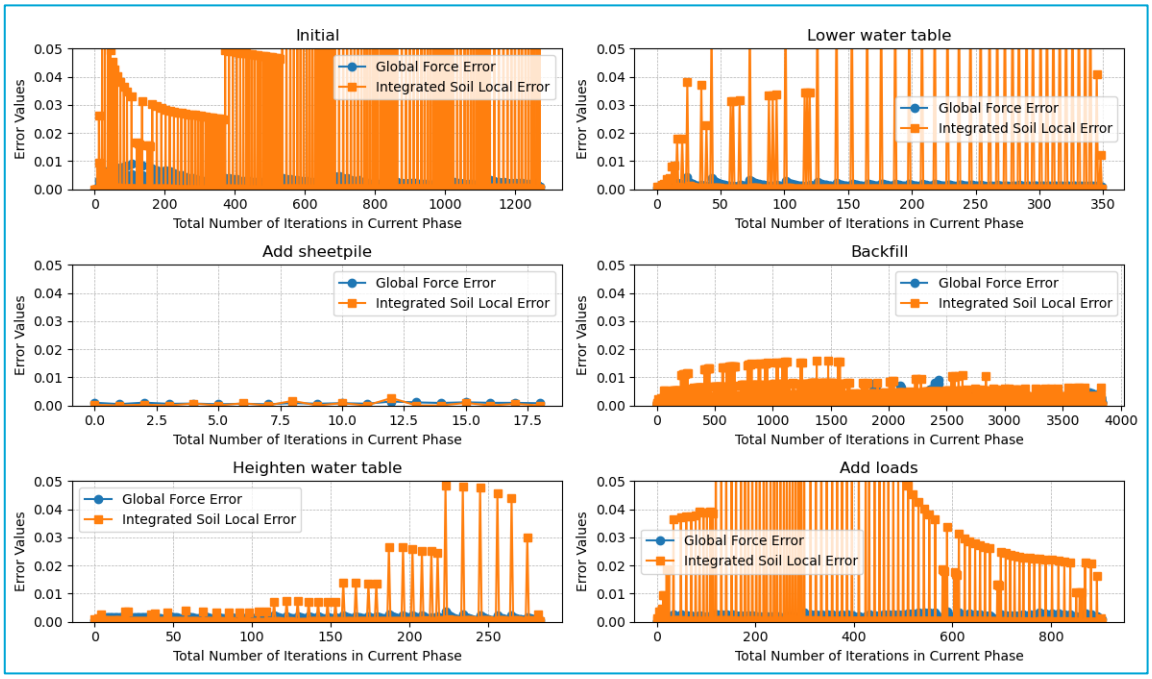

Figure 75 - Convergence plots of different phases sheet pile model in Plaxis in terms of Global Force Error and Integrated Soil Local Error for which both norms are specified as 0.01

<u>Mesh sensitivity</u>

The mesh sensitivity for the sheet pile model is like that of the traditional model. In DIANA, the mesh size is reduced from 200 mm to 100 mm for the different elements as displayed in Table 66. Note that an additional constraint is added that along the line of the sheet pile, an element size of 50 mm is required. The meshes are visualized in Figure 76.

Table 66 - DIANA element sizes of different elements for sensitivity study

Element	Mesher type	Size [mm]	
		Analysis	*Refined*
Soil_Bottom	Tetra/Triangle	200	100
Soil_Top	Tetra/Triangle	200	100
Soil_Backfill	Tetra/Triangle	200	100

The results of the mesh sensitivity analysis have been displayed in Table 67Table 51. The target variables have changed less than 2% for the considered mesh refinement. Therefore, the results are verified.

Table 67 - Mesh sensitivity DIANA sheet pile model

Variable	Element distribution		Difference
	Analysis	*Refined*	
Pu during loading [mm]	4.12E+01	4.07E+01	1.24%
Bending moments [Nmm]	4.11E+07	4.14E+07	0.73%
Shear force [N]	1.13E+04	1.15E+04	1.41%
Normal force [N]	-4.70E+04	-4.65E+04	0.94%

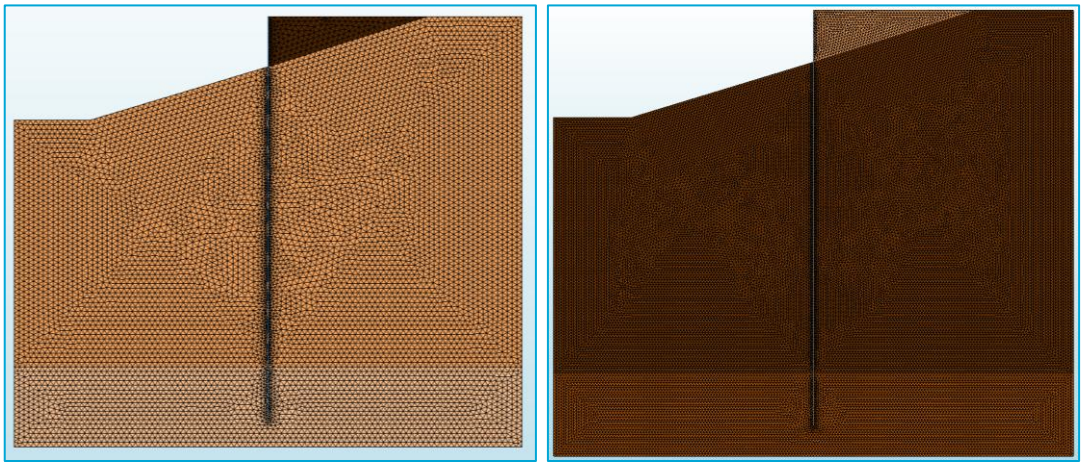

Figure 76 - Mesh DIANA for analysis (left) and refined for mesh sensitivity study (right)

The selected target variables for the Plaxis sheet pile model are given in Table 68. The maximum of each variable is displayed after the stage in which the loading is applied. After the initially selected *Medium* element distribution, the mesh was refined to *Fine* (both displayed in Figure 77). The respective element dimensions are 1449.4 mm and 966.7 mm). The differences are given in Table 68. Thereupon, the initial mesh size Medium is considered verified.

Table 68 - Mesh sensitivity Plaxis sheet pile model

Variable	Element distribution		Difference
	Medium	*Fine*	
Pu during loading [mm]	3.14E+01	3.15E+01	0.25%
Bending moments [Nmm]	5.82E+07	5.82E+07	0.07%
Shear force [N]	1.50E+04	1.50E+04	0.20%
Normal force [N]	-3.75E+04	-3.77E+04	0.53%

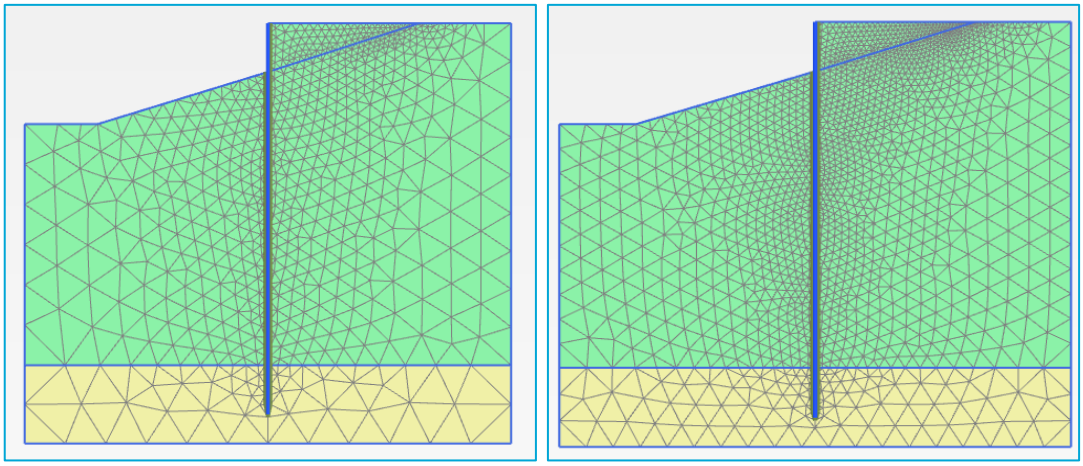

Figure 77 - Mesh with Element distribution set to Medium (left) and Fine (right)

<u>Upper bound analysis</u>

In the Literature Study an initial design for the sheet pile was developed based on the equilibrium of horizontal forces and the summation of moments around the pile's bottom to determine the required embedment depth (*D*). Additionally, the location where the passive zone transitions to an active state,

measured from the bottom (*z*), was calculated. This analysis facilitated the construction of the shear force diagram and the identification of the maximum bending moment, which occurs at the point of zero shear. The initial design yielded a maximum bending moment of 91.94 kNm at a depth of 2.56 m from the bottom of the sheet pile. The calculations can be found in Appendix A.

Subsequently, the embedment depth was increased to incorporate a Factor of Safety (*FoS*), leading to a more uniform distribution of pressures along the pile depth. Consequently, the maximum bending moment is expected to decrease. This hypothesis can be validated by comparing it with the bending moment resulting from the TAK-load, which is calculated to be 49.64 kNm, significantly lower than the previously determined maximum moment. This confirms that the initially computed upper bound remains valid.

6 Discussion

6.1 Interpretation of key findings

The displacements in Plaxis are significantly larger than in DIANA. The maximum total displacements are observed away from the quay. This cannot be considered accurate, as it is a lot higher than what is expected due to the absence of the stiff pavement layer and sand fill layer, therefore no redistribution of forces can take place. Additionally, no compaction is considered, which is often performed to strengthen the soil, this is explained below. Therefore, the maximum vertical displacements obtained are not further considered and only the horizontal component is considered. The horizontal displacement limit is set due to the ductile pipes of the water distribution network. The horizontal displacement of the top left node of the quay wall is selected for DIANA and Plaxis, which is confirmed to have the maximum horizontal displacement and divided by the allowance of 50 mm to obtain the unity check, which is displayed in Table 69 for the various load cases. The excessive vertical deformation is also visualized in Figure 78.

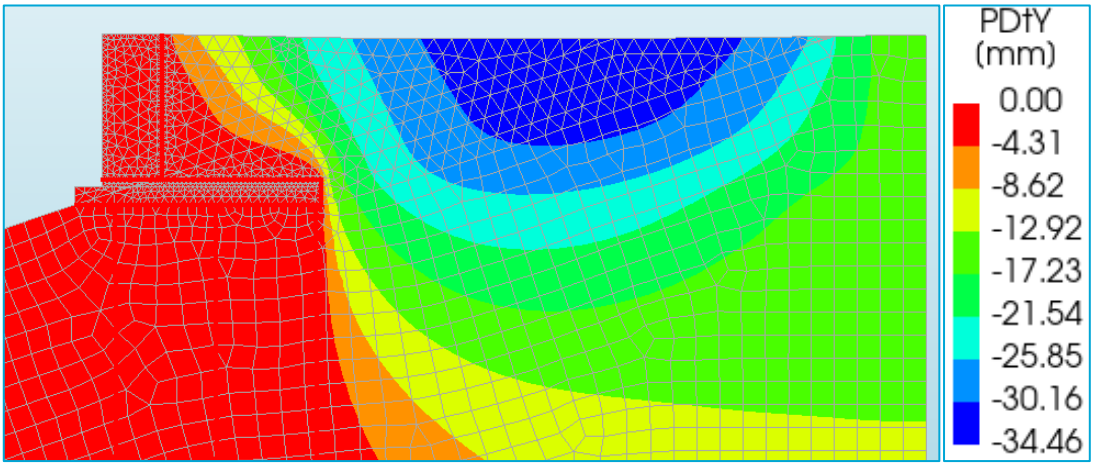

Figure 78 – Vertical phase displacements during Add loads stage for TAK load case in DIANA

Compaction

Compaction is necessary to improve soil performance under loading by reducing compressibility, increasing shear strength, and enhancing stiffness, all of which contribute to lower settlement. By densifying the soil and reducing air voids, compaction minimizes further volume reduction when loads are applied, thereby decreasing compressibility. The closer packing of soil particles also increases shear strength, making the soil more resistant to deformation and shear failure. Additionally, greater stiffness means the soil can better distribute loads without excessive deformation. These combined effects result in lower settlement, ensuring stability and durability in construction and geotechnical applications.

The outputs of the FE models cross-sectional forces are in line with the expectations of the input. For the traditional model, the masonry quay wall on a timber floor and supported by the kesp with 3 timber foundation piles, DIANA and Plaxis show similar cross-sectional forces diagram shapes.

Differences are observed at the sand and clay boundary, especially for DIANA, which was much less smooth. Additionally large differences are observed in the displacement contours. This gives insight demonstrates the different implementation of SSI in both software. Concerning numerical values, the models from Plaxis resulted to greater normal forces, shear forces and bending moments for all load cases. In terms of unity checks of the timber piles this results in average value of both software of approximately 0.33 for combined compression and bending, of which the greatest part can be allocated to bending for the base (TAK) load case. When additional loads are added, the unity checks increase significantly. This is in line with the expectation as the normal forces in the piles will increase, and, more importantly, the surcharge loading will increase effective stress levels in the soil causing more lateral pressures, which will develop a larger bending moment. The resulting increase in the unity check is displayed in Table 69.

Table 69 - Results traditional model unity checks of combined compression and bending ($UC_{c,m}$) and horizontal deformation ($UC_{def,hor}$); the five load cases represent the base load TAK combined with the multifunctionalities: Tree, Energy and/or Panel. AllMF means that All Multi-Functionalities are applied to the structure.

	$UC_{c,m}$	$UC_{def,hor}$
TAK	0.33	0.30
TAK+Tree	0.52	0.63
TAK+Energy	0.39	0.39
TAK+Panel	0.34	0.30
TAK+AllMF	0.60	0.78

In the output of the sheet pile geometry, an AU 14 section from ArcelorMittal with steel grade S240GP with a length of 15m, in Plaxis and DIANA, the cross-sectional forces and respective shapes look similar. The numerical values of Plaxis are again approximately 27% larger than that of DIANA with regards to the governing bending moments in the cross-section. The differences between the two software are smaller than 33% for the traditional model, which is explained by the fact that the simplicity of the structure simplifies the SSI interaction slightly. The maximum bending moment for the base (TAK) load case is 58.18 kNm in Plaxis and 41.10 kNm in DIANA, averaging 49.64 kNm. All values are lower than the upper limit of 91.91 kNm determined using Maple in the Literature Review. The average unity check for the base case is 0.13 in bending and this value is increased up to 0.27 for the case with all the multifunctionalities, displayed in Table 70. In this table, also the horizontal displacements are displayed and those turn out to be governing for the sheet pile wall, which is not the case for the traditional model. Especially when additional loading is applied, the displacements become large. Whereas the check for bending roughly doubles, the horizontal displacement becomes almost five times larger when adding functionalities compared to the base case.

Table 70 – Results sheet pile model unity checks of bending (UC_M) and horizontal deformation ($UC_{def,hor}$); the five load cases represent the base load TAK combined with the multifunctionalities: Tree, Energy and/or Panel. AllMF means that All Multi-Functionalities are applied to the structure.

	UC_M	$UC_{def,hor}$
TAK	0.13	0.27
TAK+Tree	0.22	0.92
TAK+Energy	0.17	0.50
TAK+Panel	0.13	0.28
TAK+AllMF	0.27	1.27

The original structural behaviour is significantly influenced by the added functionalities. While both quay wall types see increased loads, the timber-masonry structure is more vulnerable to stress concentrations in the timber piles, whereas the sheet pile wall is more affected by excessive horizontal displacements. This indicates the need for careful consideration of displacement limits, particularly in the design of the steel sheet pile wall.

However, the adaptability of these structures differs. The steel sheet pile wall was analysed using a relatively small sheet pile section, which can be easily modified by selecting a section with a higher strength (greater section modulus, higher steel grade). In contrast, the timber-masonry structure has more limited reinforcement options—the number of timber piles can only be increased from 3 to a maximum of 5, the diameter can be slightly enlarged, and the masonry thickness can be increased.

6.2 Comparison with reality

The location of the Marnixkade is modelled in this thesis and can be observed in real life. It is interesting to see how the quay wall has been supported with steel sheet piles to temporarily strengthen the quay wall in Figure 79. Additionally, local settlements of the surface are found. The deformation found in Figure 78 is thus also found, although in a more localised form, due to a partially failing foundation as mentioned in the Besluit Toekomstbestendige Maatregelen SIG0201 (Gemeente Amsterdam, 2023), which has been translated below.

This document also informs that the local deformations are currently not acceptable and the connection between the piles and kesp are deteriorated. The effects of deterioration on the timber piles is briefly expanded upon in 6.4.5, which explains why the municipality is so distressed about current quay walls that are failing, although the unity checks in Table 69 of 0.33 for the bending moment capacity and 0.30 for the horizontal deformation are small. Note that the total deformation of 34.60 mm was neglected due to absence of the stiff soil layers. These still turn out to be governing in the design.

Figure 79 - Photos of the steel support structure of the Marnixkade and local settlements (van Vliet, 2025)

Decision on Future-Proof Measures SIG0201

The substructure is difficult to inspect: to stabilize the quay wall, a wooden sheet pile wall with rubble filling was placed under water. The sheet piles are in poor condition and barely function as a stability structure, with the tongue-and-groove connections of the wooden sheet piles being open. A diving inspection revealed that 100% of the walls in sections B and D are split. Bulging and misalignment have also been observed in the masonry wall.

Based on the observed damage in the nearby section A, it is expected that both the substructure and superstructure are in poor condition.

The condition of the ground surface is poor: the pavement shows open joints and subsidence.

From this, it can be concluded that too many components of both sections are critical, making demolition and reconstruction necessary.

This text has been translated from Dutch (Gemeente Amsterdam, 2023)

6.3 Comparison with literature

In his doctoral thesis Hemel (Hemel, 2023) described experiments that were conducted at the Overamstel. Multiple experiments on different sections have been performed. A comparison is between the results on section A.I. in Figure 80 and the modelled TAK load case in this thesis. However, major differences do exist, which are briefly listed.

- The soil is not modelled using multiple layers as actually present at the Overamstel in the models employed in this thesis, a top stiff sand layer is not present. This is expected to result in larger lateral deformations in my model than in the compared experiment. Hemel also states when multiple sections are compared in his experiments: “A thicker layer of sand fill provides greater bearing capacity for the top load, leading to shallow lateral soil deformations, shallow pile clamping depths, and an overall stiffer system with small lateral deflections” (Hemel, 2023).
- The geometry has significant differences. The largest is the presence of a fourth pile in the experiments, whereas in the case study of the Marnixkade only 3 are modelled. This will result in better division of loads over the piles and less deflection. Other differences are a higher quay wall up to NAP+0.7m in the experiment compared to NAP+0.58m in my model and a water level of NAP-0.47m in the experiment compared to NAP-0.4m in the model in this thesis. This greater retaining height is expected to increase the loads and thus lateral deflections on the quay in the experiment.
- The loading is different. “The full container and the LEGIO blocks, as shown in Figure 80, have a combined weight of 115.66 tonnes, which corresponds to a maximum pressure of 56.5kN/m^2. This weight is composed of 11.15 tonnes from the container, 48.6 tonnes from the water basin, and 55.91 tonnes from the LEGIO blocks and gravel” (Hemel, 2023). The load steps are visualised in Figure 81. In the model in this thesis the TAK load is applied in 10 steps resulting in a final load of 10 kN/m from 0.5m from the waterfront up to 8m from the waterfront. This is thus very different than the 29 steps up to 56.5 kN/m^2 over 3.2 m

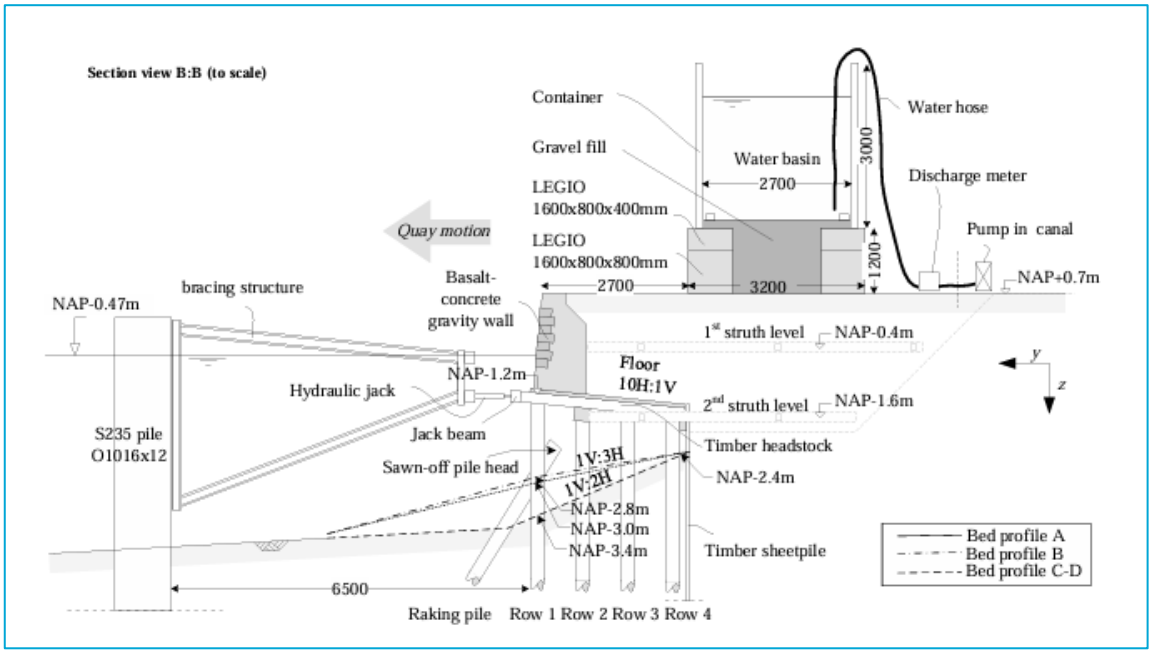

Figure 80 - Section view B:B of quay wall experiment for segment A.I.. The load is applied 2.7m behind the waterfront. (Hemel, 2023)

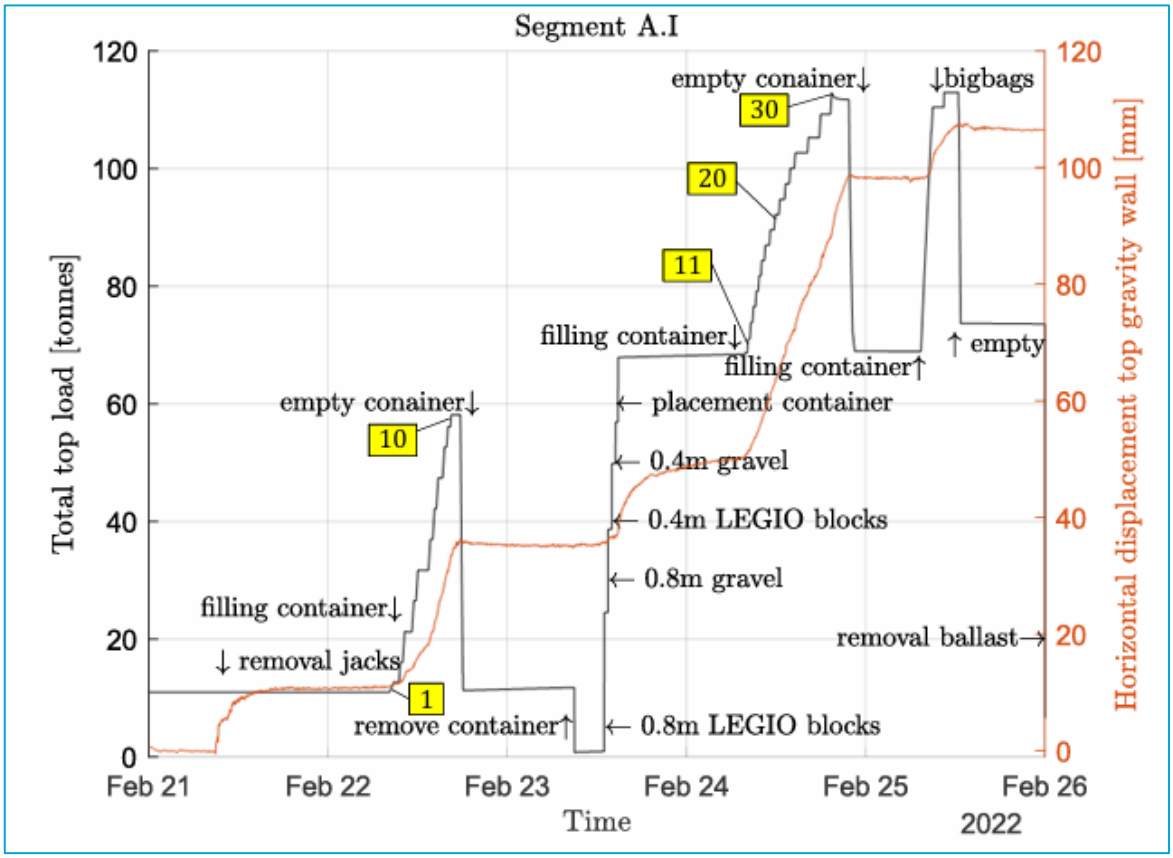

Figure 81 - Timeseries of quay wall experiment A.I. The left axis presents the load applied on the quay and the right axis presents the corresponding quay displacement (in orange). Descriptions of important handlings are provided in the figure. (Hemel, 2023)

The global behaviour in this thesis under the TAK load is found in Table 71, which indicates an average displacement for both software of 15.07 mm to the left. Since the global load in tonnes is indicated in the graph with a maximum of 115.666, which corresponds to 56.5 kN/m, 10 kN/m corresponds to 20.47 tonnes. Reflecting on Figure 81, 20.47 tonnes corresponds to a displacement of roughly 15 mm. This similar the average of both FE software models, 23.1% more than modelled in DIANA and 16.5% less than Plaxis. Considering the significant differences between both models, this a satisfying result, as the general behaviour can be considered similar.

Table 71 - Phase displacements of stage/phase Add loads of the traditional model in which the TAK loadcase is applied

	Pu_x [mm]		
	DIANA	Plaxis	Average
TAK	-12.18	-17.97	-15.07

6.4 Limitations and sources of uncertainty

6.4.1 Differences between software DIANA and Plaxis

The observed differences in the output of the models in DIANA and Plaxis are roughly 30%. The reader is referred to Table 46 for the traditional model and to Table 62 for the sheet pile model for the exact percentage differences for the different load cases. The results of the sheet pile model are slightly better aligned than the traditional model.

In section 4.2 a reflection is made on the implementation of the piles in Plaxis, in which three statements with highlighted sections are given from Plaxis (Plaxis Reference Manual, 2025). Whereas the first statement states that Embedded Beams are not able to accurately model laterally loaded piles (which is the case for the modelled timber quay wall piles), the second states that the Embedded Beams can deal with this application. Therefore, it is questionable whether Plaxis can accurately model the piles for this specific application. Additionally, the 3rd statement advises to calibrate the bearing capacity with test results, which cannot be performed for this thesis. This limitation is expected to have a large impact on the results. The writer of this thesis strongly believes that the differences in implementation of Soil-Structure Interaction (SSI) in the piles causes the difference of 30% between the software DIANA and Plaxis. Therefore, below a brief comparison is made in terms of interface stiffness parameters between the two software in terms of Floor-Wall, Floor-Soil and Wall-Soil, Piles and Sheet Pile.

Floor-Wall

In DIANA the normal (K_n) and shear (K_t) interface stiffness is determined using the following relations:

$$K_n = 1000 * \frac{E_{adj}}{l_{el}} = 1000 * \frac{5000}{50} = 1 * 10^5\ N/mm^3$$

$$K_t = \frac{K_n}{100} = \frac{1 * 10^5}{100} = 1000\ N/mm^3$$

In Plaxis the stiffnesses are derived in a different manner, which results in lower stiffnesses:

$$K_n = \frac{E_i}{n_{VIF} * l_{el}} = \frac{22.9 * 10^3}{0.1 * 326.55} = 702\ N/mm^2$$

$$K_t = \frac{G_i}{n_{VIF} * l_{el}} = \frac{2083}{0.1 * 326.55} = 63.8\ N/mm^2$$

Upon closer inspection, the influence of the mesh size should be disregarded, as Plaxis has a larger element size (l_{el}). This will reduce the differences between the two software stiffnesses by a factor $\frac{326.55}{50} = 6.5$. These large differences are observed, which are attributed to the fact that different stiffnesses are used, the Young's Modulus (E_{adj}) of the masonry in DIANA, where Plaxis defines a new stiffness (E_i), which is lower. Furthermore, DIANA uses a factor 1000 to account for the fact that deformations in the interface should be kept small, whereas Plaxis divides by a virtual interface (n_{VIF}) thickness factor of 0.1, which is equal to multiplication of a factor of 10 in DIANA. DIANA (DIANA User Manual, 2025) states that a value for this multiplication factor of between 100 and 1000 should be chosen but later calibrated, which is performed. This explains the large difference between the two software for the normal stiffness. The shear stiffness (K_t) is derived from the normal stiffness (K_n) in DIANA, whereas in Plaxis it is derived from the shear modulus (G_i).

It should be noted that the stiffnesses K_n and K_t can be specified manually in Plaxis, if the interface is set to *Direct* rather than *Derived*. This might improve the differences between the software, although it is not investigated.

Floor-Soil and Wall-Soil

In DIANA the interface stiffness is determined using the following relations:

$$K_n = 1000 * \frac{E_{adj}}{l_{el}} = 1000 * \frac{11.8}{50} = 236\ N/mm^3$$

$$K_t = \frac{K_n}{100} = \frac{236}{100} = 2.36\ N/mm^3$$

In Plaxis the interface stiffnesses are determined according to:

$$K_t = \frac{G_i}{n_{VIF} * l_{el}} = \frac{1.43}{0.1 * 326.55} = 0.0439\ N/mm^2$$

$$K_n = \frac{E_i}{n_{VIF} * l_{el}} = \frac{15.8}{0.1 * 326.55} = 0.483\ N/mm^2$$

The same observations as with the Floor-Wall interface are made.

Piles

In DIANA for the pile shaft to soil interface is set manually for the normal stiffness (R_n) to 75 N/mm^3. The shear stiffness (G) is approximated by taking the normal stiffness (E) and dividing this by a factor 2.5 as can be derived by filling in the average Poisson's ratio ($\nu = 0.25$) for clay and sand.

$$G = \frac{E}{2(1+\nu)}$$

This results in 30 N/mm^3 for the shear stiffness (R_s). Following Plaxis documentation the normal stiffness and shear stiffness from the pile shaft to soil interface are extensively derived in section 4.2.1. The results are indicated in Table 72. It is observed that the manually set stiffness is DIANA appears to be too large. Upon setting the stiffness equal to that calculated in Plaxis, no convergence is found in the Backfill soil stage. However, since the analysis is set to continue, the bending moments at the end of the Add loads stage can still be observed. These appeared not to have changed.

Table 72 - Derived stiffnesses pile shaft to soil interface Plaxis

Symbol	Description	Unit	Clay	Sand
R_S	Stiffness lateral direction	[N/mm^3]	0.0029	0.0264
R_N	Stiffness axial direction	[N/mm^3]	0.0029	0.0264

For the pile tip 6.0*10^3 N/mm is used as normal stiffness, whereas 2.4*10^4 is used as shear stiffness. In the Plaxis manual (Plaxis Reference Manual, 2025) the stiffness of the base K_F is derived in N/mm^3, which can be multiplied by the area of the base to obtain the following value:

$$K_{n,Plaxis} = K_F * A = 2.28 * 3.14 * 10^4 = 7.17 * 10^4\ N/mm$$

For the shear stiffness of the base, no information was found in the documentation of Plaxis.

Sheet Pile

In DIANA the following procedure is used to derive the interface stiffnesses between the soil and sheet pile, as specified for the setting *Derived from soil properties* (DIANA User Manual, 2025). For a clay this resulted in:

$$K_{t,clay} = \frac{G_{soil}}{n_{VIF} * l_{el}} = \frac{1.43}{0.1 * 50} = 0.287\ N/mm^2$$

$$K_{n,clay} = f * K_t = 100 * 0.0287 = 28.67\ N/mm^2$$

A similar procedure, using the properties from the sand in Table 18 resulted in the interface stiffnesses between the sheet pile and the sand below:

$$K_{t,sand} = 2.92\ N/mm^2$$

$$K_{n,sand} = 292\ N/mm^2$$

The multiplication factor (*f*) varies between 10 and 100 and is set to 100 for the demonstration of the calculation, its actual value is not specified by the user and unknown. It is interesting to observe that in this case DIANA chooses to derive the normal stiffness (K_n) from the shear stiffness (K_t), whereas with the Floor-Wall and Floor-Soil and Wall-Soil interfaces, the shear stiffness (K_t) is found from the normal stiffness (K_n).

In Plaxis the interface stiffnesses can be determined with the properties derived earlier:

$$K_{t,clay} = \frac{G_i}{n_{VIF} * l_{el}} = \frac{1.43}{0.1 * 323.785} = 0.0443\ N/mm^2$$

$$K_{n,clay} = \frac{E_i}{n_{VIF} * l_{el}} = \frac{15.8}{0.1 * 323.785} = 0.487\ N/mm^2$$

For the interface stiffnesses between the sheet pile and the sand soil, the following stiffnesses are obtained:

$$K_{t,sand} = 0.450\ N/mm^2$$

$$K_{n,sand} = 4.95\ N/mm^2$$

The difference in the interface shear stiffness (K_t) can be attributed to the mesh size (l_{el}). The normal stiffness (K_n) is calculated differently for both software. Whereas DIANA calculates K_n based upon K_t and a multiplication factor, Plaxis uses the Young's Modulus (E_i).

It should be noted that the stiffnesses K_n and K_t can be specified manually in Plaxis, if the interface is set to *Direct* rather than *Derived*. This might improve the differences between the software, although it is not investigated.

Other influences

Furthermore, some additional modifications are made that have an influence on the results for the traditional model. Those are the setting regarding initialisation in DIANA and the density setting in Plaxis. The modifications are explained in detail below. The results of the modifications of the models are quantified in Table 73. Note that the renewed model for DIANA does not converge, which makes the results questionable. Upon reflection on the effect of updating both models, the effect in terms of software difference in the bending moment is negligible, whereas in terms of other structural forces a reduction is found. Since the bending moment is the governing failure mechanism, the comparison between the models does not change. Although the differences between the software does not change, both models bending moments increase by 10%, thereby increasing the unity check of both models. Another setting that is changed is the failure ratio (R_f [-]) in DIANA. However, a sensitivity analysis showed minor differences between the two models. This is also explained below.

Table 73 – Result in terms of structural forces of modification models on software differences. The initial difference is the difference between the models described in the implementation and results chapters of this thesis. The renewed models are those that are explained below. The effect of the modification is the differences observed between the differences of both models

Variable	Initial difference models	Renewed difference models	Effect of modification
Bending moments [Nmm]	36%	36%	0%
Shear force [N]	15%	8%	-48%
Normal force [N]	-34%	-23%	-33%

Initialise stresses

The specification *Init stresses* can be switched on in DIANA. It represents the pre-existing stress state in the model before any load is applied, accounting for factors like soil weight and lateral pressures. During stress initialization, DIANA adapts the initial stress in new elements according to the lateral pressure ratio K_0, when this setting is switched on.

If initial stresses are not applied, the newly activated soil elements would start with zero stress, leading to an unrealistic stress redistribution and potentially incorrect deformation behaviour. If initial stresses are applied: The newly placed soil will have the correct initial stress distribution, considering its own weight and lateral earth pressure, leading to a more realistic simulation of the construction process. In summary, selecting *Init stresses* ensures that the newly placed backfill soil elements do not start in an artificially unstressed state but instead have the appropriate pre-existing stress field that would naturally develop due to soil weight and lateral pressures.

Initially for the analysis in this thesis, this setting is switched off. However, later for further analysis during the Backfill soil stage, this setting is switched on, as the soil stresses are better initiated when the soil is added. Unfortunately, convergence with this setting on is not reached and very large displacements for the nodes next to the quay are found, as indicated in Figure 82. Furthermore, a large local displacement on the right side of the kesp is found, which disappeared in later stages.

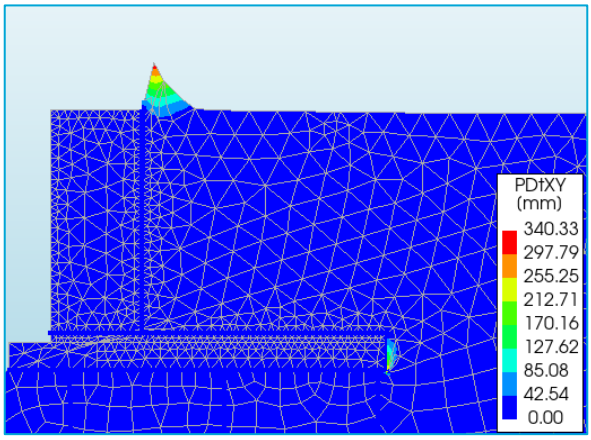

Figure 82 - Unrealistic phase displacement during the stage Backfill soil when "Init stresses" is switched on. This analysis does not converge

The results of this change are demonstrated in Table 74. Note that both the bending moments and shear forces in the Backfill soil stage are significantly increased, which is an expected result from higher initialised lateral stresses. This result is also observed in the Add loads case, although the effect is a bit reduced by the fact that a high TAK-load of 10 kN/m is applied, thereby reducing the effect of the soil contribution to the moments and forces. Note that in Plaxis it is not possible to specify this.

Table 74 - Resulting changes from switching on 'Init stresses' in Backfill soil stage in DIANA; both the Backfill soil stage and Add loads stage are monitored. In the Add loads stage the TAK load is applied. The differences for both stages without the setting switched (which is referred to as base case) are shown

Variable	Backfill soil	Difference with base case	Add loads	Difference with base case
Pu during loading [mm]	3.40E+02	943%	3.42E+01	-1.2%
Bending moments [Nmm]	1.28E+06	29%	2.28E+06	10.1%
Shear force [N]	2.99E+03	37%	4.91E+03	25.5%
Normal force [N]	-3.98E+04	-1%	-3.98E+04	-0.2%

Since convergence is not found, the results are not trustworthy. Additionally, it is tried to split the Backfill polygon for the soil into two different parts by a line at $y = 0$. Initially, the bottom part is activated, and immediately thereafter the top part, effectively splitting up the stage "Backfill soil" into two stages. Both stages are manually set to 10 steps. Additionally, duplicate polygons of the *Soil_Excavation* blocks are created. This makes it possible to have different polygons before excavation and for the backfill of the soil. However, this does not solve the issue of the top peak of the soil having a local unrealistic displacement. This is visualised in Figure 83. Again the analysis does not converge.

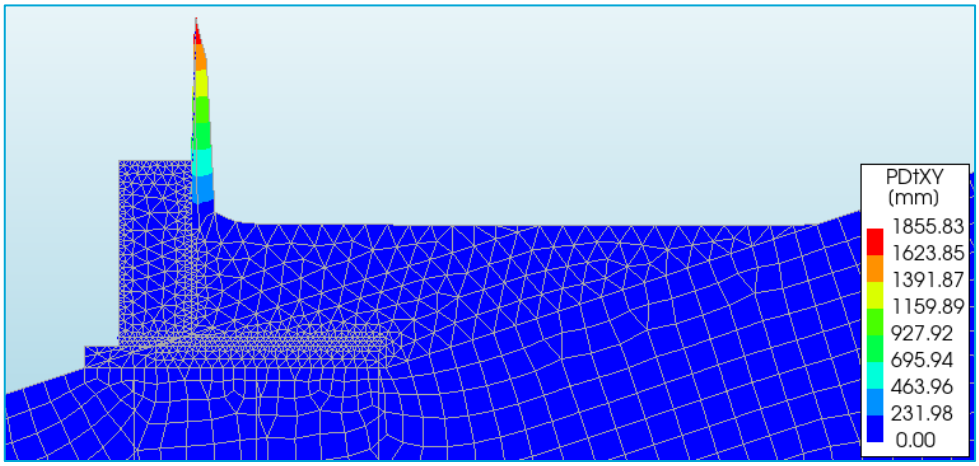

Figure 83 - Unrealistic phase displacement during the first (out of two) Backfill soil stage when "Init stresses" is switched on. This analysis does not converge

Density specification

In Plaxis the dry and saturated density are specified, whereas in DIANA the dry density and porosity are specified. In Plaxis, initially the dry and saturated density are set similar, as is recommended (Ingenieursbureau Gemeente Amsterdam, 2023) due to capillary rise. However, DIANA calculates the saturated density based upon the dry density and porosity, thereby increasing the saturated density for the clay and sand to 17.33 kN/m^2 (instead of 14.02 kN/m^2 in Plaxis) and 20.033 (instead of 16.6 kN/m^3 in Plaxis).

Upon modelling of a box of soil of 10 m wide and with the same soil layering as the right side of the quay in Figure 47, the vertical total and effective stresses in Plaxis turn out to be lower significantly lower than in Diana. This is expected as the saturated density is lower in Plaxis than in DIANA. After respecifying the saturated density in Plaxis to the values indicated for DIANA above, the results are similar. After adjustment of these settings in the traditional model, the results in Table 48 are found. The increase in vertical stresses in soil is expected to increase the strain in the soil and thereby the downward (negative) displacements, as well as vertical forces exerted on the piles. Additionally, the increases vertical pressure is expected to increase lateral stresses, resulting in higher shear forces and bending moments in the piles. Both behaviours are observed.

Table 75 - Resulting changes from adjusting saturated density in Plaxis; both the Backfill soil stage and Add loads stage are monitored. In the Add loads stage the TAK load is applied. The differences for both stages with the initial lower saturated density (which is referred to as base case) are shown

Variable	Backfill soil	Difference with base case	Add loads	Difference with base case
Pu during loading [mm]	4.39E+01	-14%	4.24E+01	20%
Bending moments [Nmm]	1.48E+06	5%	3.57E+06	10%
Shear force [N]	2.64E+03	6%	5.31E+03	16%
Normal force [N]	-2.97E+04	0%	-3.25E+04	9%

Failure ratio (R_f)

The failure ratio (R_f [-]) is set to 0.8 for clay and 0.7 for sand in DIANA, whereas in Plaxis for both soil layers the default setting of 0.9 is used. This initial setting in DIANA is wrong, but is set based upon

specification of R_{inter}, which can be estimated using: $R_{inter} = \frac{\tan(\delta)}{\sin(\varphi)}$. After changing both failure ratios to 0.9 in DIANA, the results do not change significantly, therefore, the initial analysis is kept.

6.4.2 Hinged connection pile-kesp

In a plane strain model in DIANA, it is not possible to restrain the rotation, as this is not a degree of freedom of the plane strain model (DIANA User Manual, 2025). Therefore, a hinged connection was set in Plaxis 2D to replicate the model in DIANA. This has severe implications for the bending moments in the piles as visualised in Figure 84 as well as the displacement in horizontal direction, both of which are quantified with to the TAK load case in Table 76. This is a very unconservative approach as the bending moment is reduced from 7.53 kNm to 3.97 kNm for a rigid respectively a hinged connection in Plaxis. With respect to the hinged connection in DIANA the increase when moving to rigid connection in Plaxis in the bending moment is a factor of 3.64..

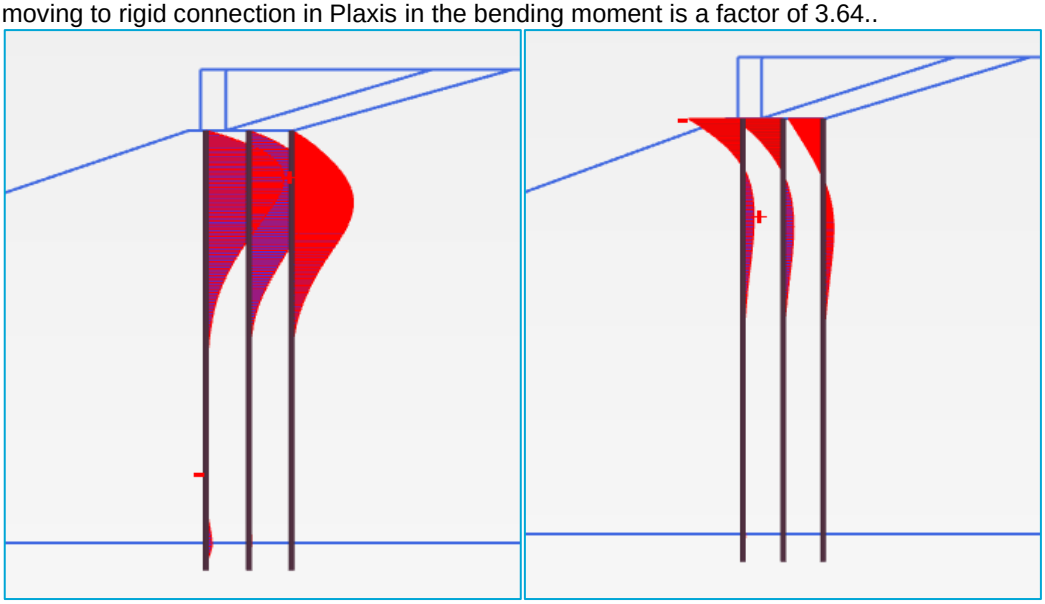

Figure 84 - Bending moments in Plaxis 2D for different pile-kesp connections: hinged (left) and rigid (right)

Table 76 - Bending moments and displacements in DIANA (hinged) Plaxis (hinged and rigid) for different pile-kesp connections during the stage/phase Add loads for the TA load case

Bending moments and displacements under TAK-loading			
	DIANA	*Plaxis*	
	Hinged	Hinged	Rigid
M_{min} *[kNm]*	-0.008	-0.04	-7.53
M_{max} *[kNm]*	2.07	3.97	1.51
u_x *[mm]*	-23.04	-35.86	-22.69
Pu_x *[mm]*	-13.08	-26.13	-15.55

The TAK3.2 (Ingenieursbureau Gemeente Amsterdam, 2023) states the following about the connection between the piles and kesp: *"in the quay walls, the piles and kesp are connected using a mortise-and-tenon joints, with steel or wooden dowels. TU Delft research indicates that joint stiffness varies, with limited elastic moment capacity. A theory for calculating this exists but isn't yet applicable*

in TAK calculations. Future TAK4.0 developments will refine this model for realistic pile-kesp connections." Currently, the following settings are used in the TAK in Plaxis 2D: a plastic moment capacity of 3 kNm/pile and a spring with a rotational stiffness of 400 kNm/m/rad (Ingenieursbureau Gemeente Amsterdam, 2023). This effectively means that the connection is in between hinged and rigid.

TU Delft research (Hemel, 2023) was performed to investigate the pile-headstock connection. In appendix H3 of his dissertation a pile-headstock interface model was derived with the following equation:

$$M_{rot} = M_e(\varphi, N_p) + M_{pin}(\varphi, V_p)$$

The first component (M_e) is related to the eccentricity of the stresses on top of the pile head and the second component (M_{pin}) is caused by the pinhole. A schematisation of the forces is illustrated in Figure 85 on the left. Also, in Figure 85 on the right, an actual connection is shown, indicating heavy deterioration.

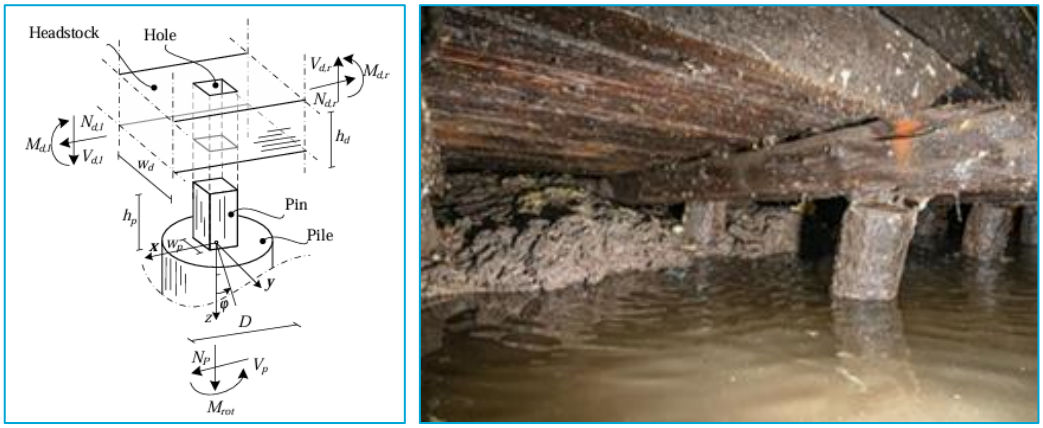

Figure 85 – Left: "Schematic representation of the pile-headstock connection with the internal forces indicated" (Hemel, 2023); right: "photograph of pile-headstock connections below a historic quay wall in Amsterdam" (Maarschalkerweerd, 2022)

In order to be able to capture the bending moments occurring in the structure, it is recommended to model the structure in 3D in a 1 meter configuration, similar to a cross-comparison that was performed prior to a masonry study (Longo, Sharma, & Messali, 2024). This allows selection of other elements rather than plane strain elements in DIANA. In Plaxis the implementation of a rigid connection is already possible in a plane strain model.

6.4.3 Soil layer simplifications

In the FE models of this thesis, the soil is simplified to consist out of the two top layers illustrated in Figure 30. Those layers are sand and clay. The sand layer corresponds to the first sand layer, which is also present in the modelling of the soil according to the TAK (Ingenieursbureau Gemeente Amsterdam, 2023). The clay layer consists of multiple layers in the TAK, those are the Geulopvulling, Holland veen, Oude zeeklei, Wad deposit, Hydrofobiaklei and Basisveen, illustrated in Figure 32. The properties of these layers (listed in Table 11) have been averaged to obtain the properties for the single modelled clay layer. Especially, the mudflat deposit might have significant influence as it is relatively stiff compared to the other layers. This stiffening effect is smeared out over all the soil layers.

Another simplification made in this thesis, is the fact that both the Ophooglaag and Verhardingslaag are not present in the models. These would significantly stiffen the top part of the soil in the FE

models and thereby significantly reduce the vertical deformation. It is expected that due to Poisson's effect also the horizontal deformation will reduce if this layer is modelled.

Lastly, erosion of the soil is not considered. The downwards slope of 1V:3H is employed. This follows the TAK recommendation of the initial stages of modelling in Plaxis (Ingenieursbureau Gemeente Amsterdam, 2023). It is recommended to model in the last step the actual soil profile including erosion. However, since no data is obtained, the initial soil profile is kept. The presence of soil, that might be eroded, is unconservative and should be noted.

6.4.4 Consolidation not considered

Consolidation is the process by which soil gradually expels water under sustained loading, leading to a decrease in volume and an increase in effective stress. It is crucial for modelling quay walls because it helps predict long-term settlements and pore pressure dissipation overt time.

In Plaxis the clay and soil properties are modelled as *Drained*. This means the stiffness and strength are defined in terms of effective values and no excess pore pressures are generated (Plaxis Reference Manual, 2025). This means the time-dependent behaviour is ignored, potentially underestimating both short-term deformations and long-term settlements, thereby misrepresenting the structural response of the quay wall. This is the result of the initial stiff soil response because of high effective stresses. A deformation control parameter is *Ignore under. Behaviour (A,B)*, which is not selected for the stages. However, this is not relevant as the soils in the model are modelled as *Drained*. One exception is the initial stage in which the calculation type is set to *Gravity Loading* for which undrained behaviour is always ignored. This is required as the initial stresses should be determined based on hydrostatic conditions. The following citation of Plaxis indicates that for the calculations after the initial phases, in which the calculation type is set to plastic, a reasonable accurate prediction is made for long term settlements:

Consolidation of drained material in plastic calculation

"Plastic calculation may be used for the limiting case of fully undrained behaviour using the Undrained (A), Undrained (B) or Undrained (C) option in the material data sets. On the other hand, performing a fully drained analysis can assess the settlements on the long term. This will give a reasonably accurate prediction of the final situation, although the precise loading history is not followed and the process of consolidation is not dealt with explicitly" (Plaxis Reference Manual, 2025).

In DIANA *Drainage* can be switched on the soil models, however it is not. Therefore, both the clay and sand are modelled as drained. This means that consolidation is not considered for both software.

6.4.5 Deterioration materials not considered

Deterioration of both the timber and steel has not been considered in analysis. It should be noted that if the structural degradation is considered, this will increase the unity checks. The effect degradation is expanded upon for the timber piles and steel sheet pile.

<u>Timber piles</u>

In Chapter 2 it is mentioned that the soft shell on average is 21 mm and up to a maximum of 45 mm (Hemel, 2023). This soft shell causes the effective cross-section to reduce, which lowers the section modulus and area of the sound (undecayed) cross-section as demonstrated in Figure 86. It is advised to include the diameter of the soft shell in geotechnical software, but to only use the sound cross-section in the verification of the bending moment (Hemel, 2023).

In the models employed in this thesis a diameter of 200 mm is used without any tapering. 200 mm is the minimum diameter found by inspections (NEBEST B.V., 2016), whereas an average and maxium of 235 mm and 260 mm respectively, are found. Assuming the minimum is a conservative assumption, whereas not including any tapering is unconservative. However, since the location of the observed maximum bending moment is relatively close to the pile head, this is acceptable, especially since the minimum diameter is already used.

It is important to observe that the effect of reduction of the diameter by of soft shell of 10%, results in decrease in area of 19% and a decrease in section modulus of 27.1%. Thus this has large consequences on both the compression and bending strenght of the cross section. Note that different notations occur, which are described below.

- *SS* [mm]: thickness of the soft shell
- A_{sound} [mm^2]: cross-sectional area of the sound (undecayed) cross section
- $A_{decayed}$ [mm^2]: cross-sectional area of the decayed cross section

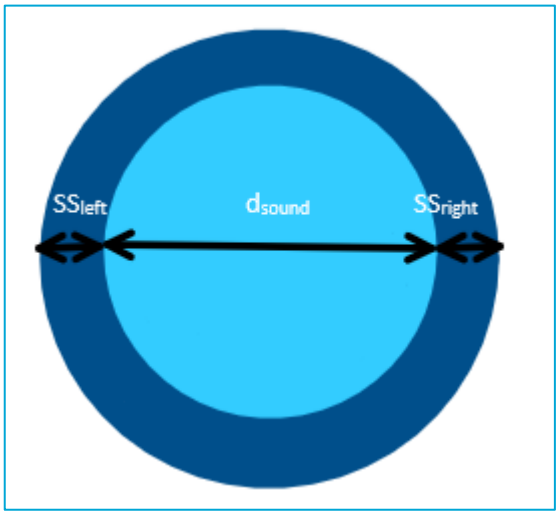

Figure 86 – Visualisation decayed cross-section of pile; the Soft Shell (SS) is demonstrated as well as the diameter of the effective undecayed cross-section (d_{sound})

The effect of choosing material properties from experiments rather than that of structural timber C24 according to the Eurocode (EN 338, 2016) for the sound cross-section are demonstrated. Remember from the Literature Review that according to the Eurocode (EN 1995-1-1, 2011) for structural timber the design stress for compression parallel to the grain ($f_{c,0,d}$) and design stress for bending ($f_{m,d}$) are derived using:

$$f_{c,0,d} = k_{mod} * \frac{f_{c,0,k}}{\gamma_M} = 0.7 * \frac{21}{1.3} = 11.31\ N/mm^2$$

$$f_{m,d} = k_{mod} * k_h * \frac{f_{m,k}}{\gamma_M} = 0.7 * 1.0 * \frac{24}{1.3} = 12.92\ N/mm^2$$

The characteristic compression ($f_{c,0,k}$) and bending stress ($f_{m,k}$) above are obtained for C24 structural timber from the Eurocode (EN 338, 2016).

Experiments have been conducted to obtain the compressive and bending strength of decayed timber pile (Pagella, Ravenshorst, Grad, & Van der Kuilen, 2022) (Hemel, 2023). Those have derived the following strength for compression and bending:

$$f_{c,0,mean,exp} = 15\ N/mm^2 \text{ with } \sigma_{dev} = 2.4\ N/mm^2$$
$$f_{m,mean,exp} = 23.2\ N/mm^2 \text{ with } \sigma_{dev} = 6.96\ N/mm^2$$

Using statistics, the characteristic values for the lower 5% boundary is derived. Using the methods described in the Eurocode (EN 1995-1-1, 2011), the following design values are obtained from the experiments:

$$f_{c,0,d} = k_{mod} * \frac{f_{c,0,k}}{\gamma_M} = 0.7 * \frac{11.04}{1.3} = 5.95\ N/mm^2$$
$$f_{m,d} = k_{mod} * k_h * \frac{f_{m,k}}{\gamma_M} = 0.7 * 1.0 * \frac{11.79}{1.3} = 6.35\ N/mm^2$$

The effects of an increases soft shell on the unity checks are visualised for compression in Figure 87. The effects on bending are visualised in Figure 88. Lastly, the combined effects of compression and bending are visualised in Figure 89. For a cross-section with a 200 mm diameter, the results are plotted of the corresponding unity check for a soft shell of 0 mm (0% decay of area) up to 50 mm (75% decay of area). It is clearly visible that the increase in unity check for bending outweighs the increase in unity check for compression, which verifies that indeed $f_{m,z} \sim d_{sound}^3$ and $f_{c,0,d} \sim d_{sound}^2$. The effects of the soft shells are not only visualised in plots but also quantified in Table 77.

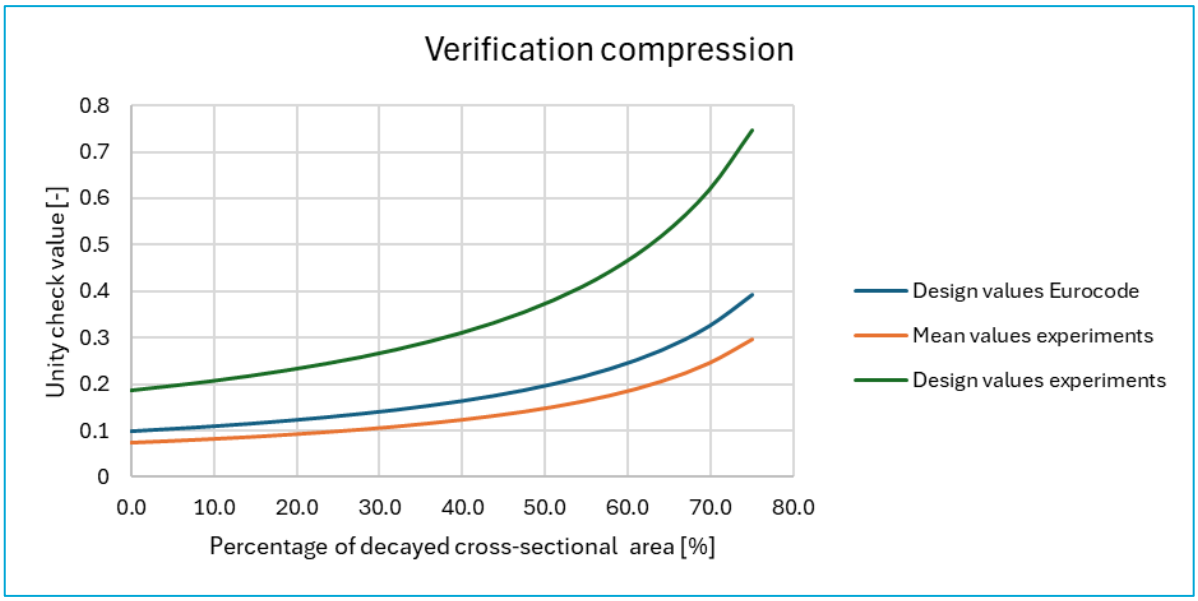

Figure 87 - Effects of deterioration of the timber pile on the unity check for compression

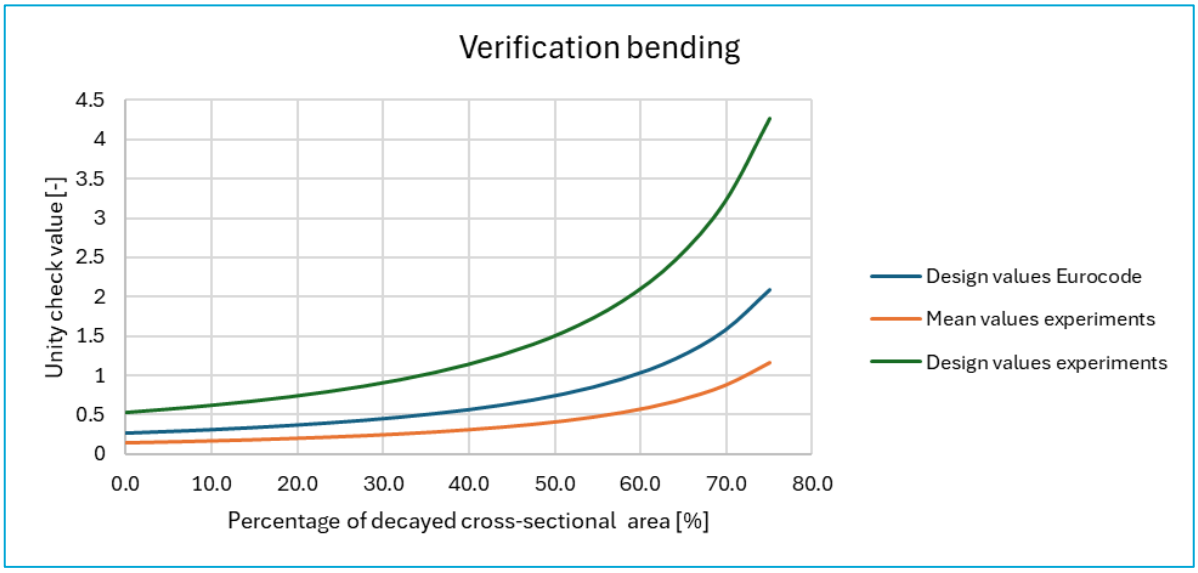

Figure 88 - Effects of deterioration of the timber pile on the unity check for bending

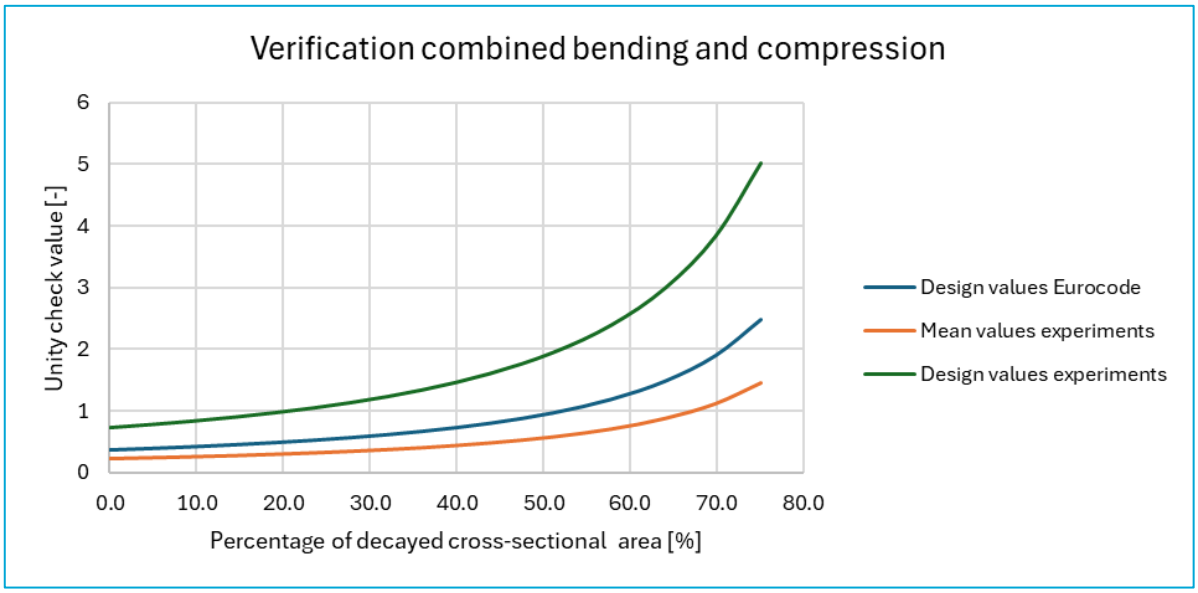

Figure 89 - Effects of deterioration of the timber pile on the unity check for bending and compression

Table 77 - Effects of soft shell (SS) on unity checks. Note that a soft shell of 0 mm corresponds to a perfectly modelled timber pile, as modelled in this thesis. Additionally, 21 mm corresponds to the average soft shell and 25 mm to the maximum soft shell observed in experiments (Hemel, 2023).

SS [mm]	0	21	45
d_{total} [mm]	200	200	200
A_{total} [mm^2]	3.14E+04	3.14E+04	3.14E+04
d_{sound} [mm]	200	179	155
A_{sound} [mm^2]	3.14E+04	1.96E+04	9.50E+03
Effective area [%]	100.00	62.41	30.25
Decay area [%]	0.00	37.59	69.75
C24 Structural Timber using sound-cross-section			
UC_c [-]	0.10	0.16	0.32
UC_m [-]	0.26	0.53	1.58
$UC_{c,m}$ [-]	0.36	0.69	1.90
Experimental mean values using sound cross-section			
UC_c [-]	0.07	0.12	0.24
UC_m [-]	0.15	0.30	0.88
$UC_{c,m}$ [-]	0.22	0.41	1.12
Experimental design values using sound cross-section			
UC_c [-]	0.19	0.30	0.62
UC_m [-]	0.53	1.08	3.21
$UC_{c,m}$ [-]	0.72	1.38	3.83

Sheet pile

The durability requirements of the Eurocode (EN 1993-5, 2008) have not been considered in this thesis. In this Eurocode it is stated that if the required design working life is longer than the duration of the protective effect of a coating, the loss of thickness occurring during the remaining design working life should be considered in serviceability limit state and ultimate limit state verifications. The loss of thickness for location of the case study can be taken from Table 78.

Table 78 - Recommended value for the loss of thickness [mm] due to corrosion for piles and sheet piles in soils, with or without groundwater. Note the following:
1) Corrosion rates in compacted fills are lower than those in non-compacted ones. In compacted fills the figures in the table should be divided by two.
2) The values given for 5 and 25 years are based on measurements, whereas the other values are extrapolated. (EN 1993-5, 2008)

Design Working Life (years)	Undisturbed Natural Soils (mm)	Polluted Natural Soils & Industrial Sites (mm)	Aggressive Natural Soils (mm)	Non-Compacted & Non-Aggressive Fills (mm)	Non-Compacted & Aggressive Fills (mm)
5	0	0.15	0.2	0.18	0.5
25	0.3	0.75	1	0.7	2
50	0.6	1.5	1.75	1.2	3.25
75	0.9	2.25	2.5	1.7	4.5
100	1.2	3	3.25	2.2	5.75

If a cross-section is to be reduced, this will have significant consequences on the properties of the sheet pile, as the design working life for quay walls is 100 years and preferably longer. This would mean a reduction of thickness of at least 3 mm according to Table 78. For an AU-14 profile shown in Figure 90, which has a thickness of 10.0 mm (ArcelorMittal, 2022), this is significant, especially if corrosion takes place on both sides. This means that the thickness of the sheet pile will reduce to 40% of its original value, to 4.0 mm. The section modulus will reduce even more, as part of the eccentricity is also lost with reduced thickness. However, coatings can be applied, which can protect the sheet pile against corrosion.

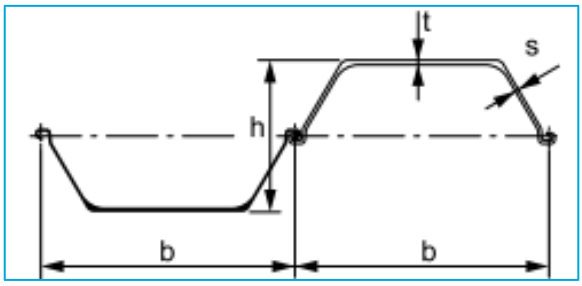

Figure 90 - AU section profile (ArcelorMittal, 2022)

6.4.6 Safety factors not considered

In the analysis of both the traditional model and the sheet pile model, partial safety factors have not been applied to the loads. This means that all loads have been considered at their characteristic values without factoring in safety margins. According to the Dutch National Annex to the Eurocode, for structures classified as Consequence Class 1 (CC1), the prescribed partial safety factors are 1.08 for permanent loads and 1.35 for variable loads (Schipper, et al., 2025).

Despite this simplification, the comparison between the two models remains valid as the primary objective of the analysis is to assess relative performance rather than absolute design compliance. If partial safety factors had been incorporated, the Unity Checks (UC) would be higher, primarily due to the variable load being increased by 35% because of the safety factor application. However, this increase in variable load would not lead to a proportional 35% increase in the UC values, as a significant portion of the bending moments in the structure are influenced by the soil that is being retained. Since the same assumptions are applied consistently to both models, the comparative conclusions drawn from this analysis remain unaffected.

6.4.7 Combining multifunctional loads with TAK-load

When incorporating multifunctionalities, the loads from the TAK are not removed. In the case of a tree, the load from the tree and the TAK are superimposed at the same location. However, this may not accurately represent actual loading conditions, as the presence of the tree would likely prevent other loads from being applied at the same position.

6.4.8 Energy load

Several assumptions have been made in this study, including the consideration of a 10-meter-wide residential unit designed for four occupants and the energy demands associated with charging an electric vehicle. Additionally, it is assumed that energy consumption will increase by a factor of 1.5 over a 100-year period. Furthermore, the energy infrastructure is modelled as being distributed uniformly along the entire quay wall, rather than being concentrated at specific locations. However, these assumptions are subject to debate. Energy demand may vary based on household size, technological advancements, and evolving energy efficiency measures. Similarly, localizing energy infrastructure at specific points rather than distributing it evenly could alter the load distribution and may, in some cases, improve energy efficiency by reducing transmission losses. Further research is needed to refine these assumptions and explore alternative scenarios that better reflect real-world conditions.

6.4.9 Tree load

The current assumptions result in a relatively large tree load, as they do not account for the significant volume of high-quality soil required for proper tree growth. Additionally, while a tree is typically considered an added load, it is possible that its root system could contribute to the structural stability of the quay wall rather than merely increasing the applied load. The root network may help distribute the load more evenly over a larger area, rather than concentrating it within a 1-meter section as initially assumed. Furthermore, the wind load acting on the tree has not been considered in the analysis. This horizontal force could have substantial implications for the quay wall’s structural behaviour, particularly by influencing bending moments. A more refined analysis incorporating these factors would provide a more accurate assessment of the tree's impact on quay wall performance.

6.4.10 Limited consideration of failure mechanisms

“Among the listed failure mechanisms, the lateral failure of the pile foundation is regarded as the most critical” (Hemel, 2023). Many failure mechanisms of the traditional quay wall model have therefore not been considered in this thesis and are only listed in the appendices. Only the failure of the piles, the cross-section of the sheet pile, and the displacements of the quay wall are considered.

To provide an accurate comparison, for the sheet pile model, the structural forces and bending moments are checked for the classification and the displacements are considered. Verification of this assumption was not performed due to time constraints.

6.4.11 Plane strain limitations

In numerical modelling of quay walls, the plane strain assumption is commonly employed to simplify the analysis by considering deformation only in the two-dimensional plane, while neglecting variations and displacements in the out-of-plane (third) direction. This assumption is valid when the geometry, loading, and boundary conditions are uniform along the length of the structure, and it effectively constrains out-of-plane deformations. As a result, it can lead to more stable and computationally efficient models. However, by artificially restricting the third dimension, the model may also impose unrealistic constraints on load redistribution mechanisms that naturally occur in three-dimensional space. It limits the ability of the soil-structure system to redistribute stress and strain laterally beyond the assumed 1-meter model width.

This simplification becomes particularly problematic when modelling discrete or widely spaced loads, such as tree loads or localized surcharges, which are distributed across a much broader area than the narrow model domain. In a full three-dimensional scenario, these loads would be shared across a wider section of the quay wall and surrounding soil, allowing for more efficient dissipation of stresses and potentially lower localized deformations. However, within a plane strain model, the inability to simulate this load spreading may lead to an overestimation of in-plane displacements and internal forces, especially in the vicinity of applied point loads. Thus, while useful for generalized analysis, the plane strain approach may yield conservative or non-representative results when applied to scenarios involving discontinuous loading conditions.

7 Final remarks and recommendations

7.1 Research problem and objectives

This study aimed to analyse how a timber-masonry quay wall and a steel sheet pile quay wall at the Marnixkade in Amsterdam respond to loads from added functionalities compared to their original behaviour, using Finite Element Analysis (FEA). The research was conducted by modelling these structural configurations in DIANA and Plaxis. Initially, the following preliminary questions are answered in the Literature Review:

What quay wall typologies do currently exist for inner-city quay walls?
The most occurring geometry is masonry quay wall on a timber floor, supported by a beam (sometimes named kesp), which is founded on timber piles. This type-1 quay wall is referred to as the traditional geometry in this thesis and modelled. Additionally, type-2 quay walls exist, which have an L-wall structure on piles. Other innovative quay walls are those from the Innovation partnership quay walls (IPK). In the Literature Review the traditional quay wall is expanded upon, whereas for the other geometries the reader is referred to Appendix B. Regarding sheet piles, different sections exist. In the Literature Review, AZ Sections, U-Type Sections (or AU), Combined Walls and Steel Tubes are reviewed. In this thesis the AU-14 section is used as derived in Appendix A.

What material models and corresponding properties provide an accurate basis for a structural Finite Element model (FE model) of the quay walls?
For the soil, a *Hardening Soil model with small-strain stiffness* (HSss) should be used with a clay layer and a sand base at the bottom with parameters from the TAK (Ingenieursbureau Gemeente Amsterdam, 2023). For the masonry both an *Isotropic Linear Elastic* and a *Total Strain Crack Model* (TSCM) may be used, with properties according to the Dutch guidelines (NPR 9998, 2020) for pre-1945 masonry. For the timber C24 Structural Timber (EN 338, 2016) should be used in an *Isotropic Linear Elastic* model. For the sheet pile geometry, for the steel an *Isotropic Linear Elastic* model is used with steel grade S240 and strength properties according to section AU-14 (ArcelorMittal, 2025).

What are the loads that currently need to be considered when designing a quay wall?
According to the TAK (Ingenieursbureau Gemeente Amsterdam, 2023), currently a top load of 10 kN/m needs to be used when designing quay walls within the ring S100.

What are the failure mechanisms of quay walls?
Multiple failure mechanisms exist. The considered failure mechanisms in this thesis are mentioned in the Literature Review. Both horizontal and total displacements checks are performed. Regarding the cross-sectional forces, failure of the timber foundation piles is considered, as well as the cross-sectional resistance of the sheet pile section. For all other failure mechanisms, the reader is referred to Appendix C.

The following sub-questions are answered:
What are the structural responses of the traditional timber-masonry quay wall configuration at the Marnixkade under standard loading conditions and when additional functionalities and their corresponding loads are added to the quay wall in a FE model?

What are the structural responses of the sheet pile wall configuration at the Marnixkade under standard loading conditions and when additional functionalities and their corresponding loads are added to the quay wall in a FE model?

The final research question is:
How do a structural configuration of timber-masonry and a steel sheet pile quay wall at the Marnixkade in Amsterdam respond to loads caused by added functionalities when compared to the original behaviour of the structure in a Finite Element Analysis (FEA)?

7.2 Key findings

In this section first the sub-questions are answered. After this, the main research question is answered. Additionally, a comparison of the FE software DIANA and Plaxis is made.

7.2.1 Sub-questions

What are the structural responses of the traditional timber-masonry quay wall configuration at the Marnixkade under standard loading conditions and when additional functionalities and their corresponding loads are added to the quay wall in a FE model?
The structural response of the quay wall shows that the traditional timber-masonry quay wall configuration can resist both standard loading conditions and loading by additional functionalities considering the unity checks in horizontal displacement and structural forces in the piles. The general behaviour is that the structure moves to the water side, thereby causing significant bending moments at the top of the timber piles. Under traditional loading conditions, Plaxis shows much larger total displacements than DIANA. The unity check for the total displacement of the base case of 0.70 increases to 1.94 when all multifunctionalities are applied. This is due to the excessive vertical deformation on the right side of the quay, which is overestimated due to the absence of a stiff pavement and sand fill layer. Therefore, these unity checks are disregarded. The unity check for the horizontal deformation is increased from 0.30 for the base case to 0.78 by the multifunctionalities. Additionally, the traditional FE model results for the masonry quay wall with three timber piles show similar cross-sectional force distributions in DIANA and Plaxis. Plaxis predicts higher normal forces, shear forces, and bending moments compared to DIANA, with an average unity check of 0.33 for combined compression and bending under the base (TAK) load case. When additional multifunctional loads are applied, the unity checks increase to 0.60, reflecting higher normal forces and lateral pressures leading to larger bending moments.

What are the structural responses of the sheet pile wall configuration at the Marnixkade under traditional loading conditions and when additional functionalities and their corresponding loads are added to the quay wall in a FE model?
The structural response of the sheet pile wall configuration shows that the structure can handle the current base case load in terms of unity checks for the horizontal displacement and structural forces in the sheet pile cross-section. The top of the structure moves to the water side and a bending moment in the sheet pile arises. When the multifunctionalities are applied, the horizontal deformation becomes too excessive, where the structural forces remain well within the limits. The cross-sectional forces in both Plaxis and DIANA are similar, though Plaxis predicts bending moments approximately 27% larger than DIANA. The maximum bending moment for the base (TAK) load case is 58.18 kNm in Plaxis and 41.10 kNm in DIANA, both of which are below the upper limit of 91.91 kNm. The average unity check for the base case is 0.13 in bending, which increases to 0.27 with the addition of

all multifunctionalities. Notably, the horizontal displacements become the governing factor for the sheet pile wall, with displacements increasing almost five times compared to the base case (0.27 and 1.27 respectively) when additional loads are applied, while the bending moment check roughly doubles. Note that again the total deformation, which is mostly relate to the vertical deformation, with a unity check value of 0.73 for the base case and 3.85 for the multifunctionalities, is again disregarded due to the absence of the stiff pavement an sand fill layer.

7.2.2 Main research question

How do a structural configuration of timber-masonry and a steel sheet pile quay wall at the Marnixkade in Amsterdam respond to loads caused by added functionalities when compared to the original behaviour of the structure in a Finite Element Analysis (FEA)?

The addition of functionalities significantly influences the structural behaviour of both quay wall types for the case study at the Marnixkade. The timber-masonry structure is more susceptible to stress concentrations in the timber piles, while the steel sheet pile wall experiences greater challenges from excessive horizontal displacements. It is important to mention that deterioration is not considered in this thesis, which explains why low unity check values of approximately 0.3 are found for the base case. For both structural configurations when the additional functionalities are applied, the total displacement exceed the limits, which is a result of the large vertical deformation. However, these vertical deformations are disregarded, as the absence of the stiff pavement and sand fill layer causes these values to be overestimated by the FE models.

Furthermore, large deformations are the result of the initial design choice and selection of the sheet pile profile based on the maximum bending moment. Deflections are initially not considered in the analytical method. Additionally, the fact that no anchors may be used due to the foundations of nearby buildings is not helpful for the displacements. These findings highlight the importance of considering horizontal displacements limits, especially in the design of the sheet pile walls. These can be considered using an iterative approach with the FE software. Additionally, in the industry D-Sheet Piling (Deltares, 2025) is often used to verify sheet piles.

7.2.3 Software comparison: DIANA and Plaxis

Various FE software exist. The writer of this thesis initially started with modelling both geometries in DIANA as this software is educated at Delft University of Technology in the course *Computational Modelling of Structures*. However, in a later stage, the usage of Plaxis 2D was recommended by the Ingenieursbureau of Amsterdam and was therefore also performed. The comparison provided insight in verification of both models' results, as no experimental data of the Marnixkade was available. Upon usage of both software and their respective manuals, reflection is given on both. The comparison is started with the text that both software use to promote themselves on their websites.

DIANA

"DIANA's reliable solution empowers engineers in creating lasting projects.

Equipped with powerful solvers for linear and nonlinear models, its robust functionalities include extensive materials, element libraries, and analysis procedures based on the most advanced finite element analysis techniques. The software comes with complete material models and elements for civil and geotechnical applications; full 2D and 3D modelling capabilities with tools for CAD/BIM interoperability; and user-friendly interface and optimized workflow for analysis, design, and reporting." - (DIANA FEA, 2025)

Plaxis 2D

"Solve Geotechnical Challenges Faster.

Perform advanced 2D finite element analysis of soil and rock deformation and stability. Consider ground-structure interaction, groundwater flow, heat flow, or seismic activity.

PLAXIS 2D is the most trusted tool among geotechnical engineers globally for the analysis of excavations, embankments, ground improvement measures, foundations, tunnels, and other critical structures." - (Bentley, 2025)

DIANA is a highly versatile finite element software offering extensive material and element libraries, making it suitable for both civil and geotechnical applications. Its robust solvers can handle both linear and nonlinear analyses, providing a comprehensive approach to structural modelling. With full 3D modelling capabilities, DIANA is especially useful for projects requiring CAD/BIM interoperability and for capturing complex geometries. One notable advantage of DIANA is the greater degree of manual input it offers, allowing users more flexibility to tailor models and analyses to specific needs. However, this flexibility comes with the drawback of increased complexity, which can make the software more challenging to use effectively. Furthermore, while DIANA's manuals provide concise descriptions of material models and elements, they often refer users to scientific papers for more detailed explanations, potentially requiring additional research to fully understand the software's capabilities.

Plaxis 2D, on the other hand, excels in geotechnical engineering and offers precise tools for analysing soil and rock deformation, stability, and ground-structure interaction. This specialization makes it particularly effective for scenarios involving groundwater flow, heat flow, or seismic activity, which are relevant for Amsterdam's saturated soils. Its 2D focus streamlines geotechnical modelling tasks, making it a trusted choice for engineers globally. Plaxis 2D simplifies the user experience by auto defining many properties, resulting in a tool that is easier to use but less flexible compared to DIANA. Additionally, the Plaxis manual offers extensive information on material models and simple elements, which facilitates a quicker understanding of the software's features without requiring external sources. That said, it is worth noting that Plaxis software also offers a 3D version, Plaxis 3D, which extends the tool's capabilities and enables detailed three-dimensional analysis for more complex geotechnical scenarios. While Plaxis 2D is highly efficient for geotechnical problems, it may need complementary tools or assumptions to fully address broader structural engineering concerns.

When deciding which software to use for specific applications, DIANA proves to be a better choice for modelling traditional quay wall structures, as it is capable of accurately assessing structural forces in laterally loaded piles, an area where Plaxis tends to be less effective. Additionally, DIANA allows for more intricate modelling of structural components, whereas Plaxis lacks detailed structural elements. On the other hand, Plaxis excels in its representation of soil behaviour due to its specialized geotechnical capabilities and the comprehensive information provided on its material models. A hybrid approach leverages the strengths of both software packages: Plaxis can be used to calculate soil deformations and assess soil-related failure modes, while DIANA can analyse the structural forces and failure modes of the quay wall itself. This integration can be achieved by first modelling the soil deformation in Plaxis, then applying the calculated forces as springs in DIANA to simulate the pile system. Notably, the Ingenieursbureau of Amsterdam has adopted a similar hybrid approach by combining Plaxis with SCIA Engineer, and this methodology is equally recommended for DIANA and Plaxis to optimize the analysis of both structural and geotechnical components.

Plaxis is particularly effective for assessing sheet pile walls on a global level, as its geotechnical focus allows for an accurate representation of soil-structure interaction and overall deformation behaviour. This makes it highly suitable for evaluating general stability, soil pressures, and large-scale responses of sheet piles. However, when a more refined analysis of localized loads and potential failure mechanisms is required, DIANA is the preferred tool. Its ability to incorporate structurally detailed properties and geometries allows for a more precise evaluation of the effects of concentrated forces, localized stresses, and complex structural interactions. This makes DIANA especially valuable for understanding the intricate behaviour of sheet piles under specific load conditions or in scenarios where higher structural detail is essential for accurate results.

7.3 Implications

This research into the structural responses of quay walls under varying functionalities offers valuable insights for the Municipality of Amsterdam, particularly in terms of ensuring the safety and adaptability of the waterfront infrastructure. The study provides a detailed comparison of timber-masonry and steel sheet pile quay walls, revealing how each configuration responds to additional loads. This is crucial for the city as it plans for future development and potential changes in waterfront usage, such as increased traffic, recreational activities, or climate adaptation measures.

By understanding how different quay wall types behave under loading conditions and the impact of additional functionalities, the municipality can make informed decisions regarding the design, maintenance, and upgrading of quay walls. The findings also underscore the importance of considering displacement limits, especially for steel sheet pile walls, which are more sensitive to horizontal displacements. Although different geometries are mentioned in the Literature Review, only the traditional geometry present at the Marnixkade, and the designed sheet pile geometry are investigated in this thesis.

It is found that the both the timber-masonry structure and sheet pile section can withstand the loads (TAK load case) acting currently on the structure, where the steel sheet pile has more margin in the design. Regarding the horizontal deformations, when all multifunctionalities are applied, the timber-masonry structure can stay within the 50 mm limit, whereas the steel sheet pile is exceeding this. Additionally, it should be noted that the total deformation of both structural configurations does not exceed the 50 mm limit for the base case, but it does exceed this limit when all multifunctionalities are applied for both configurations. However, due do the absence of the stiff pavement and sand layer, these values are overestimated and therefore disregarded.

However, the effect of deterioration on the structure is significant, it is briefly discussed in section 6.4.5. This effect of the reduction of the strength and stiffness of the timber and corrosion of the steel sheet pile is so large, that without including it in the modelling from experiments, a high level of uncertainty is introduced in the results. For the case study performed, implications are that the timber-masonry structure can resists both structural forces and displacements, whereas the steel AU-14 section is only able to pass the structural forces, although be it with more margin. Therefore, the timber-masonry structure is preferred for the conditions of no deterioration in this thesis.

If deterioration is to be included, thereby increasing both unity checks regarding the structural forces, the timber-masonry structure might fail earlier, as the deterioration of the timber sheet pile is expected

to be greater than corrosion of the sheet pile. However, this is not investigated. Regarding the deformation, the steel sheet pile is more prone to failure. In terms of adaptability, the steel sheet pile wall can be easily modified by selecting stronger sections (ArcelorMittal, 2025), such as those with higher section modulus or steel grade. In contrast, the timber-masonry structure has limited reinforcement options, such as increasing the number of piles (up to 5), slightly enlarging the pile diameter, or thickening the masonry. Therefore, if the multifunctional loads are large and deteriorations are modelled, an optimised design for the multifunctionalities for a steel sheet pile by choosing a larger section modulus might offer a better structural solution than that of the reinforced timber-masonry quay wall. However, this is not investigated and should be further studied.

7.4 Recommendations for future research

For future studies, it is recommended to make improvements to the models, which should be guided by experimental results and input from the municipality regarding multifunctional wishes. The following suggestions are used and explained in more detail below:

- *Increase soil layer complexity*: increase accuracy of models, with known data and possible experiments
- *Location of loading*: improve estimates by expectations and wishes of municipality for multifunctional loads, additionally sensitivity analysis could be performed
- *Deterioration of the structure*: include deterioration of strength and stiffness in models, guided by experiments
- *Environmental effects*: perform LCA analysis on different structural geometries to see the impact on the environment

7.4.1 Increase soil layer complexity

Increasing the complexity of the soil model by incorporating more detailed layers can significantly improve the accuracy of predictions, particularly for quay walls where Soil-Structure Interaction (SSI) is crucial. More layers provide a better representation of soil stiffness, strength, and permeability variations, leading to a more realistic response of the system. Simplifying multiple layers into one, as done in the study, may obscure key effects such as differential settlements and localized shear stresses, which are essential for assessing stability and deformations.

A refined model enhances the simulation of SSI by capturing transition zones between soil layers, which influence bending moments and lateral displacements. Without these details, the model may underestimate or overestimate structural responses, potentially affecting safety and design efficiency. More accurate modelling ensures better predictions of deformations and load distribution, leading to a more reliable quay wall design. Rather than a direct cross-comparison between DIANA and Plaxis, a hybrid approach could be considered, where the soil is first modelled in Plaxis, and then the structure in DIANA with springs representing the soil.

Although increasing model complexity comes with higher computational costs, this is not a major limitation with modern FEM software. Additionally, extensive geotechnical data is available for Amsterdam, making it feasible to incorporate more detailed stratifications without significant uncertainty. At the Ingenieursbureau of Amsterdam, a hybrid approach is often preferred, using Plaxis for soil modelling and SCIA Engineer with springs to represent soil-structure interaction. Following this method could improve reliability and lead to a more accurate model.

7.4.2 Location of loading

A valuable direction for future research is to investigate the effect of additional loads on the quay wall in a more refined manner. Currently, the base case (TAK) load is modelled as a 10 kN/m distributed load, applied from 0.5 m to 8 m behind the quay. Additional load cases, ranging from 7 to 27 kN/m, are also tested as distributed loads between the quay wall and 8 m behind it. These values are based on assumed loading conditions due to multifunctional use of the quay. However, the influence of load positioning and magnitude has not been thoroughly examined in terms of structural response and soil-structure interaction.

A more detailed sensitivity analysis, varying the location and intensity of these loads, could provide deeper insight into their specific effects on quay wall performance. Investigating how load placement influences bending moments, displacements, and soil stresses could enhance the understanding of structural behaviour under different loading scenarios. Furthermore, considering the potential nonlinear response of the system as loads increase would be important, as soil deformation and structural stiffness may not scale proportionally with applied loads. Incorporating these aspects into future studies could improve predictive accuracy and lead to more robust quay wall designs.

7.4.3 Deterioration of the structure

A relevant direction for future research is the investigation of structural deterioration in quay walls, particularly the effects of timber pile degradation and sheet pile corrosion. In the current study, the traditional model assumes intact structural elements, without accounting for the long-term reduction in cross-section due to environmental and material degradation. However, the deterioration of timber piles and the corrosion of steel elements can significantly impact both structural performance and safety over time.

For timber piles, it has been reported in the literature that the outer soft-shell layer does not contribute to the structural resistance, leading to an average reduction of 21 mm in the cross-section. For a 200 mm diameter pile, this corresponds to a reduction of over 10%, which can substantially affect the load-bearing capacity and stiffness of the foundation. Similarly, sheet pile corrosion can reduce the effective thickness of the steel, weakening its resistance to bending and shear forces. These degradations may lead to increased deflections and a reduction in unity check values, ultimately compromising the quay wall's stability.

Future studies could focus on quantifying the impact of different deterioration scenarios. Experiments into timber degradation or steel corrosion can give insight in the structural behaviour of time in non-ideal conditions. By incorporating degradation models from these experiments into more advanced 3D finite element simulations, the long-term behaviour of quay walls could be better predicted, allowing for more accurate assessments of service life and necessary maintenance interventions. 3D-modelling is especially useful, as it could investigate the results of a partially failing foundation, which has already been modelled in 2D (Voortman, 2021).

7.4.4 Environmental effects

With climate change driving the need for more sustainable infrastructure, the importance of incorporating sustainability into quay wall design is increasingly evident. This highlights the necessity for further research into the environmental impact of different design choices. Evaluating the sustainability of various quay wall configurations through comprehensive life cycle assessments (LCAs) could provide valuable insights into their long-term ecological and economic viability.

A structured approach to LCA could involve analysing different geometries while considering key factors such as material use, durability, and maintenance requirements. Timber is often regarded as a climate-friendly material due to its carbon sequestration properties, but this is only valid when sourced from FSC-certified forests that ensure responsible management. Conversely, steel is typically seen as a high-emission material, yet its environmental footprint can be significantly reduced if production shifts from traditional coke-fired blast furnaces to electric arc furnaces, particularly when powered by renewable energy. Additionally, while steel is stronger than timber, it should be evaluated whether this additional strength is necessary for the specific structural requirements of the quay wall, as overdesign could lead to unnecessary environmental impact. Assigning a shadow price to environmental effects would allow for a more quantifiable assessment of sustainability, integrating ecological impact into the decision-making process. Additionally, evaluating the added value of multifunctional loads, alongside material and construction costs, would enable a more holistic comparison of design alternatives.

Future research in this direction could support the development of quay walls that balance structural performance with environmental responsibility. By incorporating sustainability metrics into the design process, more resilient and resource-efficient infrastructure solutions can be achieved, aligning with the broader goals of climate adaptation and sustainable urban development.

7.5 Closing statement

This research provides a fundamental understanding of how timber-masonry and steel sheet pile quay walls respond to additional functionalities. The results serve as a basis for further development in quay wall design, ensuring both structural integrity and adaptability for future urban applications.

8 Bibliography

ArcelorMittal. (2022). *Piling Handbook 9th edition.*

ArcelorMittal. (2025, February 12). *ArcelorMittal Sheet Piling*. Retrieved from https://sheetpiling.arcelormittal.com/index.php/discover-steel-sheet-piles

Atkinson, & Sallfors. (1991).

Augustzoon, T. (2022).

Baginska, I. (2012). *The analysis of estimation the pile bearing capacity on the CPTU.*

Bentley. (2025, March 20). *Plaxis 2D*. Retrieved from https://www.bentley.com/software/plaxis-2d/

Benz, T. (2007). *The HS model with small-strain stiffness (HSsmall) (Benz, 2007).* Stuttgart: he HS model with small-strain stiffness (HSsmall) (Benz, 2007).

Besseling, J. (1958). A Theory of Elastic, Plastic, and Creep Deformations of an Initially Isotropic Material Showing Anisotropic Strain-Hardening, Creep Recovery, and Secondary Creep. *Journal of Applied Mechanics*, 529-336.

Cocoon Holland. (2025). *Anti corrosion methods & materials*. Retrieved from https://www.cocoon.eu/en/steel-corrosion-protection-methods/

Database, E. V. (2023, January). *ev-database.org*. Retrieved from https://ev-database.org/car/1404/Tesla-Model-S-Dual-Motor

Deltares. (2025). D-Sheet Piling.

DIANA FEA. (2025, March 20). *Homepage DIANA*. Retrieved from https://dianafea.com/

DIANA User Manual. (2025). *Theory Manual.* Retrieved from https://manuals.dianafea.com/d1010/?lang=en

Dienst Binnenwaterbeheer. (2024, 12 3). *Doorvaartprofielen binnenstad 2010.* Retrieved from https://www.amsterdam.nl/verkeer-vervoer/varen-amsterdam/varen-beroepsvaart/#h85e4aefa-de7b-4c27-94b9-f9f4ff670634

DINOloket. (2024). Retrieved from https://www.dinoloket.nl/ondergrondgegevens

DINOloket. (2024). *Subsurface models GeoTop v1.6*. Retrieved from DINOloket: https://www.dinoloket.nl/ondergrondmodellen/kaart

EarthBin. (2024). *Front-load semi-in-ground*. Retrieved from https://www.earthbin.com/front-load-semi-in-ground?utm_source=chatgpt.com

EN 1993-1-1. (2016). *Eurocode 3: Design of steel structures - Part 1-1: General rules and rules for buildings.* Retrieved from NEN connect.

EN 1993-5. (2008). *Eurocode 3: Design of steel structures - Part 5: Piling.* Retrieved from NEN connect: https://connect.nen.nl/Standard/Detail/64945?compId=10037&collectionId=0

EN 1995-1-1. (2011). *Eurocode 5: Design of timber structures - Part 1-1: General - Common rules and rules for buildings.* Retrieved from NEN connect.

EN 1997-1. (2005, 3 1). *Eurocode 7: Geotechnical design - Part 1: General rules.* Retrieved from NEN connect: https://connect.nen.nl/Standard/Detail/38056?compId=10037&collectionId=0

EN 338. (2016). *Structural timber - Strength classes.* Retrieved from NEN connect.

EN-1996-1-1. (2019). *Eurocode 6 - Design of masonry structures - Part 1-1: General rules for reinforced and unreinforced masonry structures.* Retrieved from NEN connect.

EnergieDirect. (2024, December). Monthly energy report.

Gemeente Amsterdam. (2023).

Gemeente Amsterdam: Bureau Monumenten & Archeologie. (2023).

Genes, M., & Kocak, S. (2004). Dynamic soil–structure interaction analysis of layered unbounded media via a coupled finite element/boundary element/scaled boundary finite element model. *International Journal for Numerical Methods in Engineering*, 798-823.

GeoEngineer. (2024). Retrieved from https://www.geoengineer.org/education/slope-stability/slope-stability-the-bishop-method-of-slices

Geotechnical design of structures - Part 1: General rules. (2017). *NEN 9997-1+C2:2017 nl.*

Ghally, A. (2025, March 5). *DESIGN OF CANTILEVER TYPE SHEET PILE PENETRATING SAND*. Retrieved from anchor.union.edu: https://anchor.union.edu/SP-cantilever-sand-SI.htm

Gibson Stainless & Specialty Inc. (2017, June). *Corrosion types and prevention*. Retrieved from https://www.gibsonstainless.com/types-of-corrosion.html

Giwangkara, G., Mohamed, A., Nor, H., Khalid, N., & Mudiyone, R. (2020). Analysis of Internal Friction Angle and Cohesion Value for Road Base Materials in a Specified Gradation. *Journal of Advanced Civil and Environmental Engineering.*

G-kracht. (2023). Retrieved from https://gkracht.nl/

Google Maps. (2024). Amsterdam.

(2001). *Grondonderzoek Noord/Zuidlijn; Parameterset definitief ontwerp en D4 en D5 kenmerk 01270L.* Amsterdam.

Haasnoot. (2020). Energy quay walls. *JournalE3S Web Conf.*

Hemel, M. (2023). *Amsterdam quays under pressure, Modelling and testing of historic canal walls.*

Ingenieursbureau Gemeente Amsterdam. (2023). *Toetsing Amsterdamse Kademuren 3.2.* Amsterdam: Gemeente Amsterdam.

Kade 2.020. (2022). *Kade 2.020*. Retrieved from https://kade2020.nl/

Kallitsas, P. (2016). *Fatigue loads identification on orhtotropic steel deccks.* Delft.

Kitch. (2015, January 30). *CE 540 Module 5.1 Sheet Pile cantilevered*. Retrieved from YouTube: https://www.youtube.com/watch?v=Gu7kKZM8szw

Kitch, W. (2015, January 30). CE 540 Module 5.1 Sheet Pile cantilevered. San Angelo, Texas, United States of America.

Korff, M., Hemel, M., & Peters, D. (2022). Collapse of the Grimburgwal, a hisotric quay in Amsterdam, Netherlands. *Forensic engineering*.

Kránitz, K. (2014). *Effect of natural aging on wood.* Zürich.

Kremer, L. (2024). *A data analysis of tree growth on the quays of the Amsterdam UNESCO-area.* Wageningen: Wageningen Environmental Research.

Labuz, J., & Zang, A. (2012). Mohr–Coulomb Failure Criterion. In *Rock Mechanics and Rock Engineering* (pp. 975–979).

Lankelma Geotechnisch Adviesbureau. (2018). *Sonderingsrapport Marnixkade.* Purmerend.

Lapper, C. (2024). *Garbage collection and recycling in the Netherlands*. Retrieved from https://www.expatica.com/nl/living/household/recycling-in-the-netherlands-133948/

Longo, M., Sharma, S., & Messali, F. (2024). *Structural Analyses and Material Characterisation of Masonry Urban Infrastructure.*

Maarschalkerweerd. (2022).

May, G., Davidson, A., & Monahov, B. (2018). Lead batteries for utility energy storage: A review. *Journal of Energy Storage*, 145-157.

Mouazen, A., & Neményi, M. (1999). Tillage Tool Design by the Finite Element Method: Part 1. Finite Element Modelling of Soil Plastic Behaviour. *Journal of Agricultural Engineering Research*, 37-51.

Mulder, K., Lubelli, B., & Dijkhuis, E. (2023). Factors favouring vegetation in quay masonry walls: A pilot field study. *Building and Environment*.

Nayak, S. (2020). Broyden-Fletcher-Goldfarb-Shanno Algorithm. In S. Nayak, *Fundamenteals of Optimization Techniques with Algorithms.*

NEBEST B.V. (2016). *Funderingsonderzoek.* Vianen.

Neijzing, L., & Altman, A. (2023). *Belastingnota voor nieuwe kademuren.* Amsterdam: Ingenieursbureau van Amsterdam.

NEN 8707. (2018). *Assessment of an existing structure in case of reconstruction and disapproval - Geotechnical structures.* Retrieved from NEN Connect.

NEN-EN 10248-1. (2023, March). *Hot-rolled steel sheet piles - Part 1: Technical.* Retrieved from https://connect.nen.nl/standard/openpdf/?artfile=3678640&RNR=3678640&token=aa06057c-321d-4836-9d7f-47c929a65738&type=pdf#pagemode=bookmarks

NPR 9096-1-1. (2023). *Masonry structures - Simple design rules, based on EN 1996-1-1.* Retrieved from NEN connect: https://connect.nen.nl/home/detail

NPR 9998. (2020). *Assessment of structural safety of buildings in case of erection, reconstruction and disapproval - Induced earthquakes - Basis of design, actions and resistances.* Retrieved from NEN connect: https://connect.nen.nl/home/detail

Pagella G, R. G. (2024, October). Innovative application of micro-drilling for the assessment of decay and remaining mechanical properties of historic wooden foundation piles in Amsterdam. *Developments in the Built Environment*.

Pagella, G., Ravenshorst, G., Grad, W., & Van der Kuilen, J. (2022). Characterization and assessment of the mechanical properties of. *4th International Conference on Timber Bridges.* Biel.

Plaxis 2D Scientific Manual. (2025, February 16). *PLAXIS 2D 2024.2 2D 4 Scientific Manual.* Retrieved from Bentley: https://bentleysystems.service-now.com/community?id=kb_article&sysparm_article=KB0107989

Plaxis Material Models Manual. (2025, February 24). Retrieved from https://bentleysystems.service-now.com/community?id=kb_article&sysparm_article=KB0107989

Plaxis Reference Manual. (2025, February 17). *PLAXIS_2D_2024.2_2D_2_Reference Manual.* Retrieved from https://bentleysystems.service-now.com/community?id=kb_article&sysparm_article=KB0107989

Robertson, P. (2010). Soil behaviour type from the CPT: an update. *2nd International Symposium on Cone Penetration Testing* (p. 8). Huntington Beach: CPT'10.

Royal BAM. (2022). *De Amsterdamse kademuren vernieuwen: innovatief, duurzaam, circulair en veilig*. Retrieved from https://www.baminfra.nl/projecten/de-amsterdamse-kademuren-vernieuwen-innovatief-duurzaam-circulair-en-veilig

Schanz, T., Vermeer, P., & Bonnier, P. (1999). The hardening soil model: Formulation and verification. In *Beyond 2000 in Computational Geomechanics.*

Schipper, R., Pasterkamp, S., Schuurman, M., Ravenshorst, G., Meinema, G., van Vliet, N., & van den Boogaard, M. (2025, February 17). *Structural Design Essentials.* Retrieved from Teachbooks: https://teachbooks.io/Structural_Design_Essentials/main/design_workflow/general_loads/loads_limit_states.html

Sharma, S., Longo, M., & Messali, F. (2024). Analysis procedures accounting for load redistribution mechanisms in masonry earth retaining structures under traffic loading. *Engineering Structures*.

SkyGeo. (2024). *SkyGeo*. Retrieved from https://skygeo.com/vulnerabiliy-of-historic-centre-amsterdam-quay-wall/

Spannenburg, T. (2020). *Timber creep of historic urban quay walls.*

Tsai, C., Huang, L., & Chen, C. (2023). Earthquake-induced persistent and instantaneous groundwater variations caused by volumetric strain of soil in Taiwan from 1999 to 2020. *Soil Dynamics and Earthquake Engineering.*

United States Steel. (1984, July). *Steel Sheet Piling Design Manual.*

Vakili, K., Barciaga, T., Lavasan, A., & Schanz, T. (2013). A PRACTICAL APPROACH TO CONSTITUTIVE MODELS FOR THE ANALYSIS OF GEOTECHNICAL PROBLEMS. *The Third International Symposium on Computational Geomechanics.* Krakow.

van Tussenbroek, G. (2012). *Historisch hout in Amsterdamse monumenten.* Amsterdam: Library of Amsterdam.

van Vliet, K. (2025, February 28). Photos of Marnixkade.

Verruijt, A. (2001). *Soil Mechanics.* Delft.

VJ Tech. (2023, July 14). *OCR: Understanding Over Consolidation Ratio in Geotechnical Design*. Retrieved from https://www.vjtech.co.uk/ocr-understanding-over-consolidation-ratio-in-geotechnical-design/#:~:text=There%20are%20various%20methods%20to,and%20the%20Rowe%20cell%20tests.

Voortman, R. (2021). *The historic quay walls of Amsterdam A study into the hidden structural capacity of masonry quay walls under the condition of a partly failing foundation.*

Zekkos, D., Bray, J., Kavazanjian, E., Matasovic, N., Rathje, E., Riemer, M., & Stokoe, K. (2006, October). Unit Weight of Municipal Solid Waste. *Journal of Geotechnical and Geoenvironmental Engineering*.

Appendix A: Maple worksheet sheet pile design

Limit Equilibrium Method

In this maple sheet the embedment depth and moments are determined using the Limited Equilibrium Method (LEM). This forms the basis for the sheet pile design as employed in the thesis. The method is explained on YouTube in a lecture intended for a graduate class in Geotechnical Engineering (Kitch, 2015).

The implementation of the method without surcharge loading is verified using an online tool: (Ghally, 2025). Note that this method is slightly different and uses an iterative approach, whereas in the implementation in Maple the systems of 2 equations with 2 unknowns is solved. After checking the implementation in the initial case without surcharge pressure, the surcharge load of the TAK (10 kN/m is applied as described in the thesis). Based on this a final sheet pile design is made. Additional visualisations are also worked out. Please note that the plots with the points that are described for the pressures are given at the bottom. This is done because it is preferred to have these images according to scale and therefore the system of 2 equations with 2 unknowns first needs to be solved in Maple.

Verification case without surcharge loading

```
restart:
L1:=0.4+0.58:
L2:=1.29-0.4:
g_dry:=14.02:
g_sat:=14.02:
phi:=23.8*(2*Pi)/360:
q:=0:
p:=10:
g_sub:= g_sat-p:
```

Step 1: Calculate earth pressure coefficients

Calculate Ka and Kp from angle of friction

```
Ka:=evalf((1-sin(phi))/(1+sin(phi)));
Kp:=evalf((1+sin(phi))/(1-sin(phi)));
```

$$Ka := 0.4249629174$$

$$Kp := 2.353146496$$

Step 2: Calculate the horizontal effective stresses

Multiply vertical effective stresses with earth pressure coefficients Ka and Kp for stresses at different depths.

```
p_A:=0:
p_Q:=g_dry*L1*Ka:
AQR:=(p_A+p_Q)/2*L1:
RQSB:=p_Q*(L2+Depth):
```

```
p_C:=g_dry*L1*Ka + g_sub*(L2+Depth)*Ka:
QCS:=(p_C-p_Q)/2*(Depth+L2):
p_Eacc:=g_sub*Depth*Kp-(g_dry*L1*Ka+g_sub*(L2+Depth)*Ka):
FaccCEacc:=(p_C+p_Eacc)/2*Depth:
p_J:=g_dry*L1*Kp + g_sub*(L2+Depth)*Kp - g_sub*Depth*Ka:
GJEacc:=z/2*(p_J+p_Eacc):
```

Step 3: Setup the equations

Equations should be set up in terms of unknowns Depth and z

Equation 1: horizontal equilibrium of forces

Equation 2: moment equilibrium around B

```
SUMF_hor:= -(AQR + RQSB + QCS) + FaccCEacc - GJEacc = 0:
r_AQR:= Depth + L2 + L1/3:
r_RQSB:= (Depth + L2)/2:
r_QCS:= (Depth + L2)/3:
r_FaccCEacc:= Depth/3:
r_GJEacc:= z/3:
SUMM_B:= -(r_AQR*AQR + r_RQSB*RQSB + r_QCS*QCS) + r_FaccCEacc*FaccCEacc -
r_GJEacc*GJEacc = 0:
```

Step 4: Solve the unknowns

Use the 2 equations to solve the unknowns: Depth and z

```
solution := solve([SUMF_hor, SUMM_B], [Depth, z]):
pos_sol:= solution[1]:
Depth:=rhs(op(1, pos_sol)); z:=rhs(op(2, pos_sol));
p_Facc:= g_dry*L1*Ka + g_sub*L2*Ka:
p_G:=p_Eacc - z * g_sub*(Kp-Ka):
d_0:=0:
d_L1:=L1:
d_L2:=L1+L2:
d_G:=L1+L2+Depth-z:
d_Depth:=L1+L2+Depth:
```

$$Depth := 4.879700810$$

$$z := 0.8738112691$$

Step 5: Find maximum moment

Use the obtained forces to obtain the point where the shear force is 0.

Derive the moment at the point where the shear force is 0, this is the maximum moment

```
L3:=p_Facc/(g_sub*(Kp-Ka)):
F1:=(p_A+p_Q)/2*L1:
F2:=p_Q*L2:
F3:=(p_Facc - p_Q)/2 * L2:
F4:=p_Facc/2*L3:
F:= F1 + F2 + F3 + F4:
a1:=L3 + L2 + L3/3:
a2:=L3 + L2/2:
a3:=L3 + L2/3:
```

```
a4:=L3*2/3:
SUMME:=F1*a1 + F2*a2 + F3*a3 + F4*a4-F*d=0:
sol:= solve({SUMME}, {d}):
d := rhs( op( 1, sol ) ):
eq_shear:= F - 1/2*(g_sub*(Kp-Ka))*x_shear^2 = 0:
values_shear := solve([eq_shear], [x_shear]):
# Extract the values
values_shear := [seq(rhs(entry[1]), entry in values_shear)]:
# Filter the positive value
positive_value := select(x -> x > 0, values_shear):
# Assign the positive value to x_shear
x_shear := positive_value[1];
                    x_shear := 1.776232720
M_max:= (d + x_shear)*F - (g_sub*(Kp-Ka)*x_shear)*x_shear/2*(x_shear/3);
                     M_max := 30.94803312
```

Step 6: Sheet pile design

Based on the ArcelorMittal section profile library, perform a check for an AU-14 profile.

Check the stress at the location of the maximum bending moment

Apply additional Factor of Safety (FoS) to sheet pile to obtain total length

```
W_el:=1410: #cm^3 AU14 section ArcelorMittal
sigma:=(M_max*1e6) / (W_el*1e3); #N/mm^2
                                        sigma := 21.94895966
L_sheetpile:=L1+L2+Depth*2;
L_Mmax:=L1+L2+L3+x_shear;
                                  L_sheetpile := 11.62940162
                                      L_Mmax := 4.595654718
```

Addition: Visualisation vertical stresses

Total vertical stresses in the soil are calculated at various depths on both sides of the quay wall.

Pore pressures are calculated.

Effective stresses are calculated as the total stress minus the pore pressure.

```
d_A:=0:
d_Q:=L1:
d_F:=L1+L2:
d_B:=L1+L2+Depth:
sigma_Ar:=0:
sigma_Qr:=g_dry*d_Q:
sigma_Fr:=sigma_Qr + g_sat*L2:
sigma_Br:=sigma_Fr + g_sat*Depth:
p_Ar:=0:
p_Qr:=0:
p_Fr:=L2*p:
p_Br:=(L2+Depth)*p:
sigma_Fl:=-0:
sigma_Bl:=-(sigma_Fl + g_sat*Depth):
p_Fl:=-0:
```

```
p_Bl:=-p*Depth:
sigma_r := [[sigma_Ar, d_A], [sigma_Qr, -d_Q], [sigma_Fr, -d_F], [sigma_Br,
-d_B]]:
p_r:=[[p_Qr, -d_Q], [p_Fr, -d_F], [p_Br, -d_B]]:
sigma_eff_r:= [[sigma_Ar-p_Ar, d_A], [sigma_Qr-p_Qr, -d_Q], [sigma_Fr-p_Fr,
-d_F], [sigma_Br-p_Br, -d_B]]:
sigma_l := [[sigma_Fl, -d_F], [sigma_Bl, -d_B]]:
p_l:= [[p_Fl, -d_F], [p_Bl, -d_B]]:
sigma_eff_l:= [[sigma_Fl-p_Fl, -d_F], [sigma_Bl-p_Bl, -d_B]]:
with(plots):
plot_sigma_r := pointplot(sigma_r, connect = true, color = red, linestyle =
solid, legend = "Total Stress (σ)"):
plot_p_r := pointplot(p_r, connect = true, color = blue, linestyle = solid,
legend = "Pore Pressure (p)"):
plot_sigma_eff_r := pointplot(sigma_eff_r, connect = true, color = green,
linestyle = solid, legend = "Effective Stress (σ')"):
plot_sigma_l := pointplot(sigma_l, connect = true, color = red, linestyle =
solid):  # No legend here
plot_p_l := pointplot(p_l, connect = true, color = blue, linestyle =
solid):  # No legend here
plot_sigma_eff_l := pointplot(sigma_eff_l, connect = true, color = green,
linestyle = solid):  # No legend here
# Combine the plots
display([plot_sigma_r, plot_p_r, plot_sigma_eff_r, plot_sigma_l, plot_p_l,
plot_sigma_eff_l],
    title = "Pressure distribution",
    labels = ["Pressure [kN/m]", "Depth [m]"]);
```

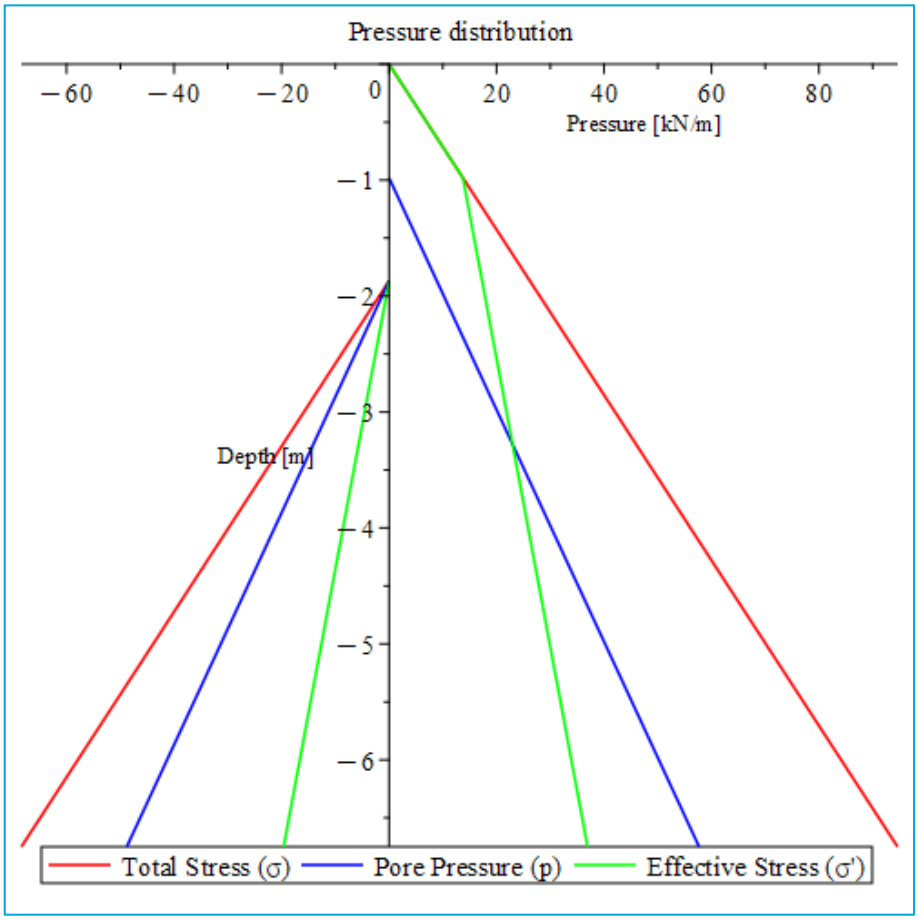

Figure 91 - Vertical total stresses, pore pressures and effective stresses in verification case

Addition: Visualisation horizontal pressures

The active and passive pressures are calculated from multiplication of Ka and Kp respectively with the effective stresses.

```
sigma_eff_r_act:= [[Ka*(sigma_Ar-p_Ar), d_A], [Ka*(sigma_Qr-p_Qr), -d_Q],
[Ka*(sigma_Fr-p_Fr), -d_F], [Ka*(sigma_Br-p_Br), -d_B]]:
sigma_eff_r_pas:= [[Kp*(sigma_Ar-p_Ar), d_A], [Kp*(sigma_Qr-p_Qr), -d_Q],
[Kp*(sigma_Fr-p_Fr), -d_F], [Kp*(sigma_Br-p_Br), -d_B]]:
sigma_eff_l_act:= [[Ka*(sigma_Fl-p_Fl), -d_F], [Ka*(sigma_Bl-p_Bl), -d_B]]:
sigma_eff_l_pas:= [[Kp*(sigma_Fl-p_Fl), -d_F], [Kp*(sigma_Bl-p_Bl), -d_B]]:
with(plots):
plot_sigma_eff_r := pointplot(sigma_eff_r, connect = true, color = green,
linestyle = solid, legend = "Effective Stress (σ')"):
plot_sigma_eff_r_act := pointplot(sigma_eff_r_act, connect = true, color =
darkblue, linestyle = solid, legend = "Active Pressure (σA)"):
plot_sigma_eff_r_pas := pointplot(sigma_eff_r_pas, connect = true, color =
purple, linestyle = solid, legend = "Passive Pressure(σP)"):
plot_sigma_eff_l := pointplot(sigma_eff_r, connect = true, color = green,
linestyle = solid):
plot_sigma_eff_l_act := pointplot(sigma_eff_l_act, connect = true, color =
darkblue, linestyle = solid):
```

```
plot_sigma_eff_l_pas := pointplot(sigma_eff_l_pas, connect = true, color =
purple, linestyle = solid):
plot_sigma_l := pointplot(sigma_l, connect = true, color = red, linestyle =
solid):  # No legend here
plot_p_l := pointplot(p_l, connect = true, color = blue, linestyle =
solid):  # No legend here
plot_sigma_eff_l := pointplot(sigma_eff_l, connect = true, color = green,
linestyle = solid):  # No legend here
# Combine the plots
display([plot_sigma_eff_r, plot_sigma_eff_r_act, plot_sigma_eff_r_pas,
plot_sigma_eff_l, plot_sigma_eff_l_act, plot_sigma_eff_l_pas],
    title = "Pressure distribution",
    labels = ["Pressure [kN/m]", "Depth [m]"]);
```

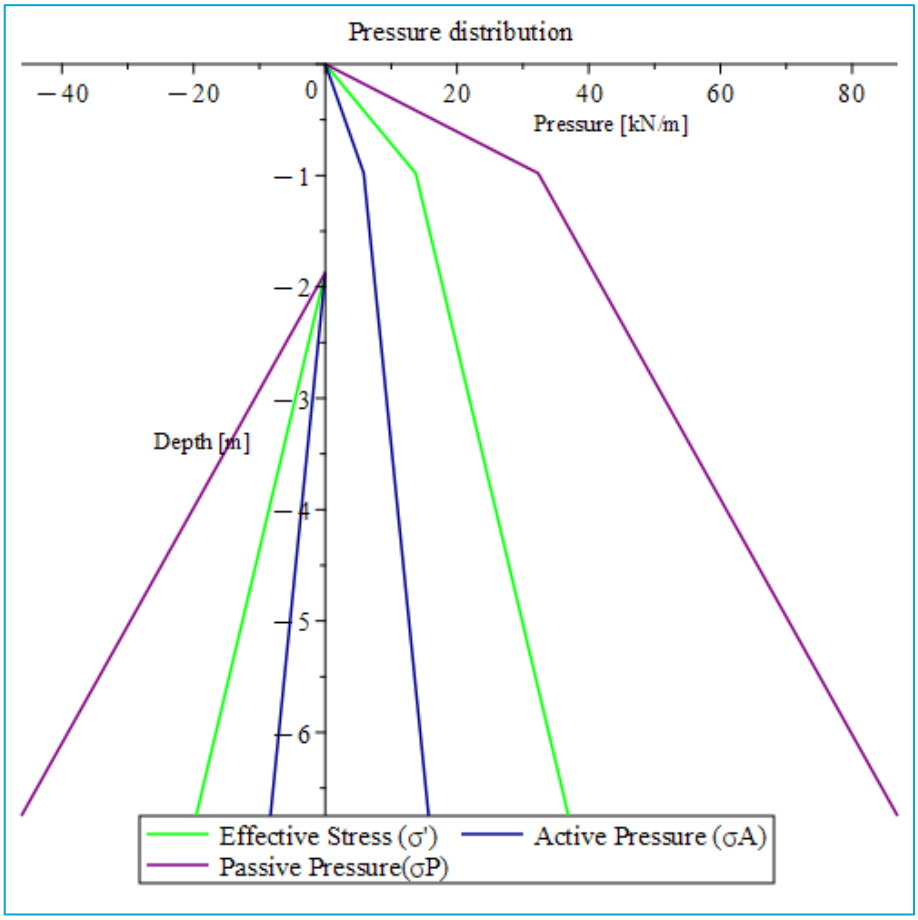

Figure 92 - Effective stresses, active soil pressure and passive soil pressure in verification case

Addition: Visualisation to obtain explanatory Figure

The following visualisation is used to explain the location of the points where the stresses are calculated after editing in the OneNote software.

```
# Define the set of points
points_AQFaccGJ := [[p_A, d_0], [p_Q, -d_L1], [p_Facc, -d_L2], [-p_G, -
d_G], [p_J, -d_Depth]]:
```

```
points_AQCBA := [[p_A, d_0], [p_Q, -d_L1], [p_C, -d_Depth], [0, -d_Depth],
[p_A, d_0]]:
points_FaccCEaccF := [[p_Facc, -d_L2], [p_C, -d_Depth], [-p_Eacc, -
d_Depth], [p_Facc, -d_L2]]:
points_GJEaccG := [[-p_G, -d_G], [p_J, -d_Depth], [-p_Eacc, -d_Depth], [-
p_G, -d_G]]:
# Plot the points with lines between them
plot_points_AQCBA := pointplot(points_AQCBA, symbol = box, symbolsize = 15,
color = blue):
plot_lines_AQCBA := plot([seq(points_AQCBA[i], i=1..nops(points_AQCBA))],
color = blue, linestyle = solid):
plot_points_FaccCEaccF := pointplot(points_FaccCEaccF, symbol = diamond,
symbolsize = 15, color = red):
plot_lines_FaccCEaccF := plot([seq(points_FaccCEaccF[i],
i=1..nops(points_FaccCEaccF))], color = red, linestyle = solid):
plot_points_GJEaccG := pointplot(points_GJEaccG, symbol = diamond,
symbolsize = 15, color = green):
plot_lines_GJEaccG := plot([seq(points_GJEaccG[i],
i=1..nops(points_GJEaccG))], color = green, linestyle = solid):
plot_points_AQFaccGJ := pointplot(points_AQFaccGJ, symbol = box, symbolsize
= 15, color = blue):
plot_lines_AQFaccGJ := plot([seq(points_AQFaccGJ[i],
i=1..nops(points_AQFaccGJ))], color = blue, linestyle = solid, legend =
"Resulting pressure sheet pile"):
# Define the horizontal line
horizontal_line1 := plot(-d_L2, x = Kp*(sigma_Bl-p_Bl)..0, color = grey,
linestyle = dash):
horizontal_line2 := plot(-d_G, x = Kp*(sigma_Bl-p_Bl)..Kp*(sigma_Br-p_Br),
color = grey, linestyle = dash):
# Combine the plots
display([horizontal_line1, horizontal_line2, plot_sigma_eff_r_act,
plot_sigma_eff_r_pas, plot_sigma_eff_l_act, plot_sigma_eff_l_pas,
plot_lines_AQFaccGJ, plot_points_AQCBA, plot_lines_AQCBA,
plot_points_FaccCEaccF, plot_lines_FaccCEaccF, plot_points_GJEaccG,
plot_lines_GJEaccG],
    title = "Pressure distribution",
    labels = ["Pressure [kN/m]", "Depth [m]"]);
```

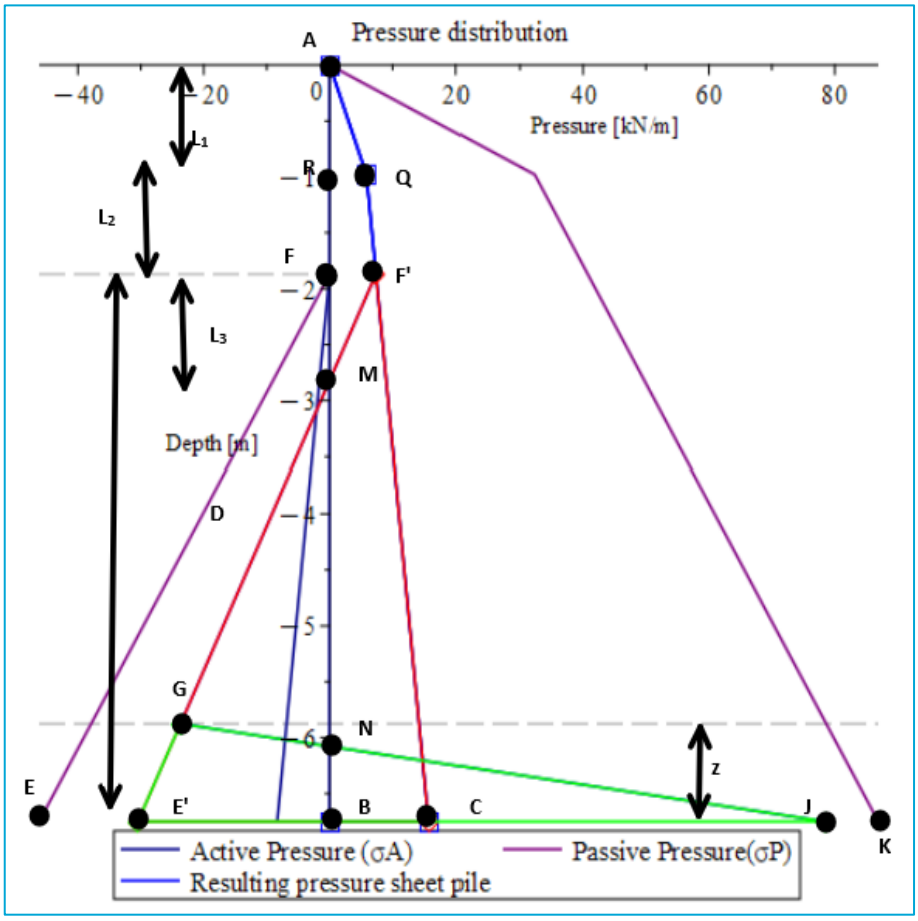

Figure 93 - Adopted notation system to calculate horizontal force and moment equilibrium to determine unknowns D and z for verification case. The red, blue and green polygon are shapes that are used to simplify the horizontal force equilibrium calculation.

Thesis case with surcharge loading

```
restart;
L1:=0.4+0.58:
L2:=1.29-0.4:
g_dry:=14.02:
g_sat:=14.02:
phi:=23.8*(2*Pi)/360:
Additional load (q=...; 10 is equal to TAK)
q:=10:
p:=10:
g_sub:= g_sat-p:
Step 1: Calculate earth pressure coefficients
Calculate Ka and Kp from angle of friction
Ka:=evalf((1-sin(phi))/(1+sin(phi)));
Kp:=evalf((1+sin(phi))/(1-sin(phi)));
```

$$Ka := 0.4249629174$$

$$Kp := 2.353146496$$

Step 2: Calculate the horizontal effective stresses

Multiply vertical effective stresses with earth pressure coefficients Ka and Kp for stresses at different depths.

```
p_A:=q*Ka:
p_Q:=p_A + g_dry*L1*Ka:
AQR_1:=p_A*L1:
AQR_2:=(p_Q-p_A)/2*L1:
RQSB:=p_Q*(L2+Depth):
p_A:
p_C:=p_A + g_dry*L1*Ka + g_sub*(L2+Depth)*Ka:
QCS:=(p_C-p_Q)/2*(Depth+L2):
p_Eacc:=g_sub*Depth*Kp -(p_A + g_dry*L1*Ka+g_sub*(L2+Depth)*Ka):
FaccCEacc:=(p_C+p_Eacc)/2*Depth:
p_J:=q*Kp + g_dry*L1*Kp + g_sub*(L2+Depth)*Kp - g_sub*Depth*Ka:
GJEacc:=z/2*(p_J+p_Eacc):
```

Step 3: Setup the equations

Equations should be set up in terms of unknowns Depth and z

Equation 1: horizontal equilibrium of forces

Equation 2: moment equilibrium around B

```
SUMF_hor:= -(AQR_1 + AQR_2 + RQSB + QCS) + FaccCEacc - GJEacc = 0:
r_AQR_1:= Depth + L2 + L1/2:
r_AQR_2:= Depth + L2 + L1/3:
r_RQSB:= (Depth + L2)/2:
r_QCS:= (Depth + L2)/3:
r_FaccCEacc:= Depth/3:
r_GJEacc:= z/3:
SUMM_B:= -(r_AQR_1*AQR_1 + r_AQR_2*AQR_2 + r_RQSB*RQSB + r_QCS*QCS) +
r_FaccCEacc*FaccCEacc - r_GJEacc*GJEacc = 0:
```

```
Step 4: Solve the unknowns
Use the 2 equations to solve the unknowns: Depth and z
solution := solve([SUMF_hor, SUMM_B], [Depth, z]):
pos_sol:= solution[1]:
Depth:=rhs(op(1, pos_sol)); z:=rhs(op(2, pos_sol));
p_Facc:= q*Ka + g_dry*L1*Ka + g_sub*L2*Ka:
p_G:=p_Eacc - z * g_sub*(Kp-Ka):
d_0:=0:
d_L1:=L1:
d_L2:=L1+L2:
d_G:=L1+L2+Depth-z:
d_Depth:=L1+L2+Depth:
```

$$Depth := 7.100697344$$

$$z := 1.183366052$$

Step 5: Find maximum moment

Use the obtained forces to obtain the point where the shear force is 0.

Derive the moment at the point where the shear force is 0, this is the maximum moment.

```
L3:=p_Facc/(g_sub*(Kp-Ka)):
F1_1:=p_A*L1:
F1_2:=(p_Q - p_A)/2*L1:
F2:=p_Q*L2:
F3:=(p_Facc - p_Q)/2 * L2:
F4:=p_Facc/2*L3:
F:= F1_1 + F1_2 + F2 + F3 + F4:
a1_1:=L3 + L2 + L3/2:
a1_2:=L3 + L2 + L3/3:
a2:=L3 + L2/2:
a3:=L3 + L2/3:
a4:=L3*2/3:
SUMME:=F1_1*a1_1 + F1_2*a1_2 + F2*a2 + F3*a3 + F4*a4-F*d=0:
sol:= solve({SUMME}, {d}):
d := rhs( op( 1, sol ) ):
eq_shear:= F - 1/2*(g_sub*(Kp-Ka))*x_shear^2 = 0:
values_shear := solve([eq_shear], [x_shear]):
# Extract the values
values_shear := [seq(rhs(entry[1]), entry in values_shear)]:
# Filter the positive value
positive_value := select(x -> x > 0, values_shear):
# Assign the positive value to x_shear'
x_shear := positive_value[1];
```

$$x_shear := 2.558722264$$

```
M_max:= (d + x_shear)*F - (g_sub*(Kp-Ka)*x_shear)*x_shear/2*(x_shear/3);
```

$$M_max := 91.94173469$$

Step 6: Sheet pile design

Based on the ArcelorMittal section profile library, perform a check for an AU-14 profile.

Check the stress at the location of the maximum bending moment.
Apply additional Factor of Safety (FoS) to sheetpile to obtain total length.

```
W_el:=1410: #cm^3 AU14 section ArcelorMittal
sigma:=(M_max*1e6) / (W_el*1e3); #N/mm^2
```

$$sigma := 65.20690404$$

```
L_sheetpile:=L1+L2+Depth*2;
L_Mmax:=L1+L2+L3+x_shear;
```

$$L_sheetpile := 16.07139469$$

$$L_Mmax := 5.926391689$$

Addition: Visualisation vertical stresses

Total vertical stresses in the soil are calculated at various depths on both sides of the quay wall.
Pore pressures are calculated.
Effective stresses are calculated as the total stress minus the pore pressure.

```
d_A:=0:
d_Q:=L1:
d_F:=L1+L2:
d_B:=L1+L2+Depth:
sigma_Ar:=q:
sigma_Qr:=sigma_Ar + g_dry*d_Q:
sigma_Fr:=sigma_Qr + g_sat*L2:
sigma_Br:=sigma_Fr + g_sat*Depth:
p_Ar:=0:
p_Qr:=0:
p_Fr:=L2*p:
p_Br:=(L2+Depth)*p:
sigma_Fl:=-0:
sigma_Bl:=-(sigma_Fl + g_sat*Depth):
p_Fl:=-0:
p_Bl:=-p*Depth:
sigma_r := [[sigma_Ar, d_A], [sigma_Qr, -d_Q], [sigma_Fr, -d_F], [sigma_Br,
-d_B]]:
p_r:=[[p_Qr, -d_Q], [p_Fr, -d_F], [p_Br, -d_B]]:
sigma_eff_r:= [[sigma_Ar-p_Ar, d_A], [sigma_Qr-p_Qr, -d_Q], [sigma_Fr-p_Fr,
-d_F], [sigma_Br-p_Br, -d_B]]:
sigma_l := [[sigma_Fl, -d_F], [sigma_Bl, -d_B]]:
p_l:= [[p_Fl, -d_F], [p_Bl, -d_B]]:
sigma_eff_l:= [[sigma_Fl-p_Fl, -d_F], [sigma_Bl-p_Bl, -d_B]]:
with(plots):
plot_sigma_r := pointplot(sigma_r, connect = true, color = red, linestyle =
solid, legend = "Total Stress (σ)"):
plot_p_r := pointplot(p_r, connect = true, color = blue, linestyle = solid,
legend = "Pore Pressure (p)"):
plot_sigma_eff_r := pointplot(sigma_eff_r, connect = true, color = green,
linestyle = solid, legend = "Effective Stress (σ')"):
plot_sigma_l := pointplot(sigma_l, connect = true, color = red, linestyle =
solid):  # No legend here
```

```
plot_p_l := pointplot(p_l, connect = true, color = blue, linestyle =
solid):  # No legend here
plot_sigma_eff_l := pointplot(sigma_eff_l, connect = true, color = green,
linestyle = solid):  # No legend here
# Combine the plots
display([plot_sigma_r, plot_p_r, plot_sigma_eff_r, plot_sigma_l, plot_p_l,
plot_sigma_eff_l],
    title = "Pressure distribution",
    labels = ["Pressure [kN/m]", "Depth [m]"]);
```

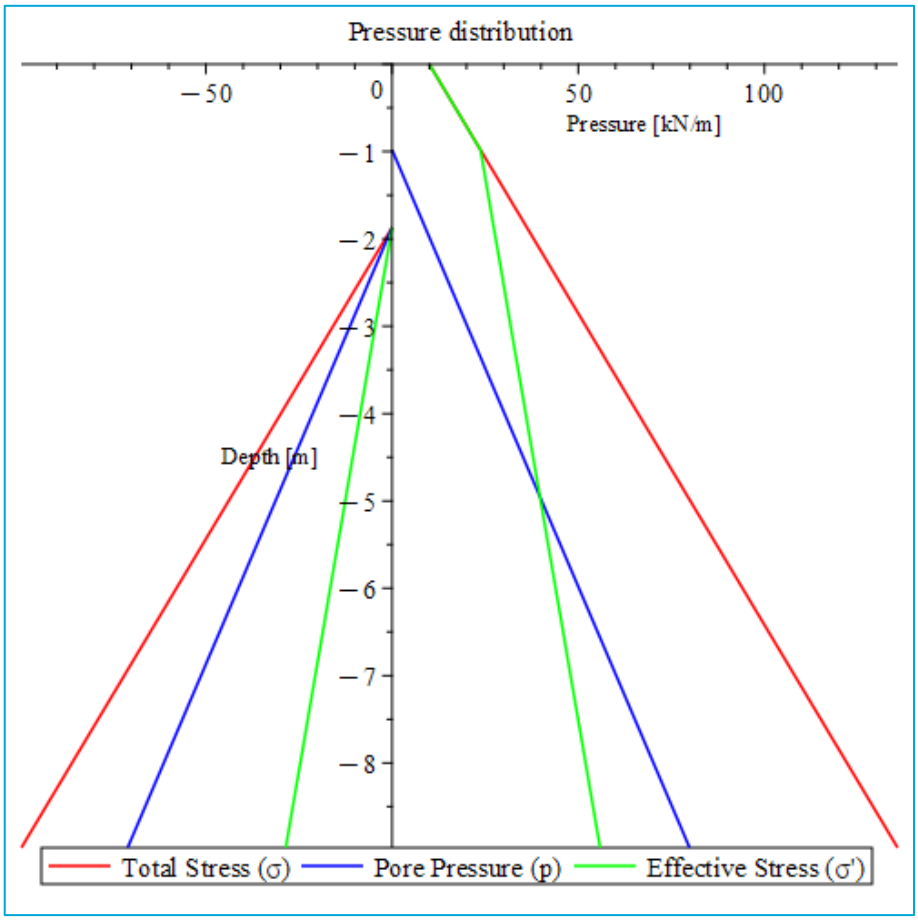

Figure 94 - Vertical total stresses, pore pressures and effective stresses in thesis case

Addition: Visualisation horizontal pressures

The active and passive pressures are calculated from multiplication of Ka and Kp respectively with the effective stresses.

```
sigma_eff_r_act:= [[Ka*(sigma_Ar-p_Ar), d_A], [Ka*(sigma_Qr-p_Qr), -d_Q],
[Ka*(sigma_Fr-p_Fr), -d_F], [Ka*(sigma_Br-p_Br), -d_B]]:
sigma_eff_r_pas:= [[Kp*(sigma_Ar-p_Ar), d_A], [Kp*(sigma_Qr-p_Qr), -d_Q],
[Kp*(sigma_Fr-p_Fr), -d_F], [Kp*(sigma_Br-p_Br), -d_B]]:
sigma_eff_l_act:= [[Ka*(sigma_Fl-p_Fl), -d_F], [Ka*(sigma_Bl-p_Bl), -d_B]]:
sigma_eff_l_pas:= [[Kp*(sigma_Fl-p_Fl), -d_F], [Kp*(sigma_Bl-p_Bl), -d_B]]:
with(plots):
```

```
plot_sigma_eff_r := pointplot(sigma_eff_r, connect = true, color = green,
linestyle = solid, legend = "Effective Stress (σ')"):
plot_sigma_eff_r_act := pointplot(sigma_eff_r_act, connect = true, color =
darkblue, linestyle = solid, legend = "Active Pressure (σA)"):
plot_sigma_eff_r_pas := pointplot(sigma_eff_r_pas, connect = true, color =
purple, linestyle = solid, legend = "Passive Pressure(σP)"):
plot_sigma_eff_l := pointplot(sigma_eff_r, connect = true, color = green,
linestyle = solid):
plot_sigma_eff_l_act := pointplot(sigma_eff_l_act, connect = true, color =
darkblue, linestyle = solid):
plot_sigma_eff_l_pas := pointplot(sigma_eff_l_pas, connect = true, color =
purple, linestyle = solid):
plot_sigma_l := pointplot(sigma_l, connect = true, color = red, linestyle =
solid):  # No legend here
plot_p_l := pointplot(p_l, connect = true, color = blue, linestyle =
solid):  # No legend here
plot_sigma_eff_l := pointplot(sigma_eff_l, connect = true, color = green,
linestyle = solid):  # No legend here
# Combine the plots
display([plot_sigma_eff_r, plot_sigma_eff_r_act, plot_sigma_eff_r_pas,
plot_sigma_eff_l, plot_sigma_eff_l_act, plot_sigma_eff_l_pas],
    title = "Pressure distribution",
    labels = ["Pressure [kN/m]", "Depth [m]"]);
```

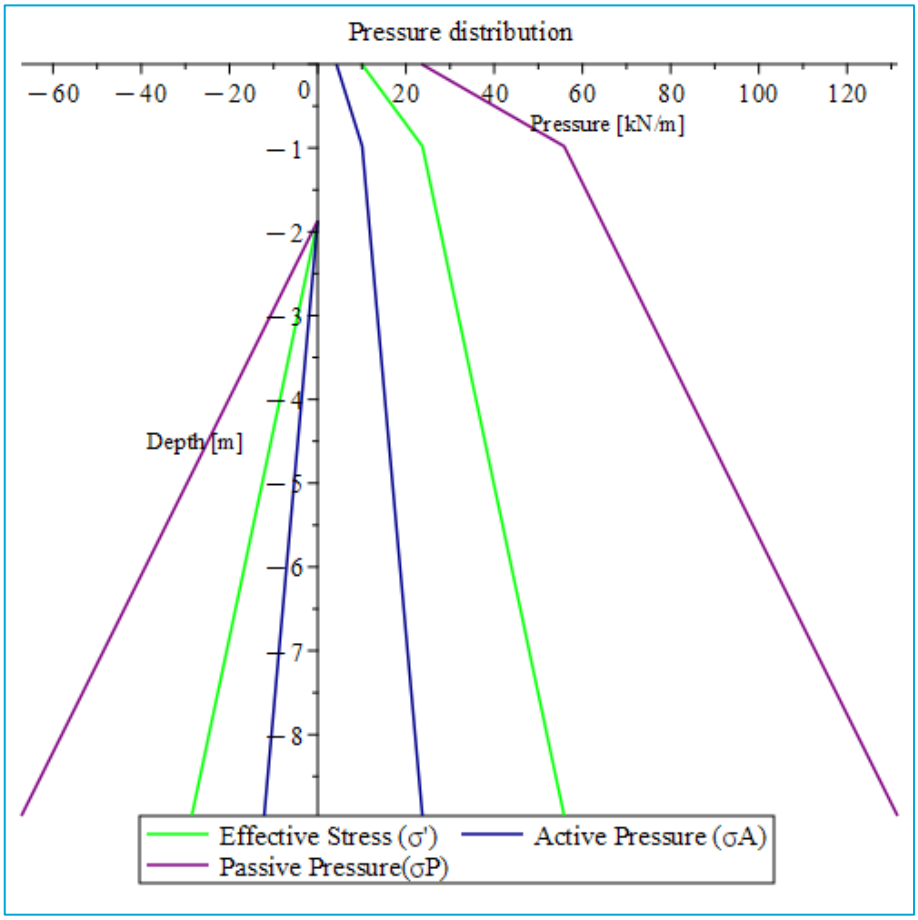

Figure 95 - Effective stresses, active soil pressure and passive soil pressure in thesis case

Addition: Visualisation to obtain explanatory Figure

The following visualisation is used to explain the location of the points where the stresses are calculated after editing in the OneNote software.

```
# Define the set of points
points_AQFaccGJ := [[p_A, d_0], [p_Q, -d_L1], [p_Facc, -d_L2], [-p_G, -
d_G], [p_J, -d_Depth]]:
points_AQCBA := [[p_A, d_0], [p_Q, -d_L1], [p_C, -d_Depth], [0, -d_Depth],
[p_A, d_0]]:
points_FaccCEaccF := [[p_Facc, -d_L2], [p_C, -d_Depth], [-p_Eacc, -
d_Depth], [p_Facc, -d_L2]]:
points_GJEaccG := [[-p_G, -d_G], [p_J, -d_Depth], [-p_Eacc, -d_Depth], [-
p_G, -d_G]]:
# Plot the points with lines between them
plot_points_AQCBA := pointplot(points_AQCBA, symbol = box, symbolsize = 15,
color = blue):
plot_lines_AQCBA := plot([seq(points_AQCBA[i], i=1..nops(points_AQCBA))],
color = blue, linestyle = solid):
plot_points_FaccCEaccF := pointplot(points_FaccCEaccF, symbol = diamond,
symbolsize = 15, color = red):
plot_lines_FaccCEaccF := plot([seq(points_FaccCEaccF[i],
i=1..nops(points_FaccCEaccF))], color = red, linestyle = solid):
```

```
plot_points_GJEaccG := pointplot(points_GJEaccG, symbol = diamond,
symbolsize = 15, color = green):
plot_lines_GJEaccG := plot([seq(points_GJEaccG[i],
i=1..nops(points_GJEaccG))], color = green, linestyle = solid):
plot_points_AQFaccGJ := pointplot(points_AQFaccGJ, symbol = box, symbolsize
= 15, color = blue):
plot_lines_AQFaccGJ := plot([seq(points_AQFaccGJ[i],
i=1..nops(points_AQFaccGJ))], color = blue, linestyle = solid, legend =
"Resulting pressure sheet pile"):
# Define the horizontal line
horizontal_line1 := plot(-d_L2, x = Kp*(sigma_Bl-p_Bl)..0, color = grey,
linestyle = dash):
horizontal_line2 := plot(-d_G, x = Kp*(sigma_Bl-p_Bl)..Kp*(sigma_Br-p_Br),
color = grey, linestyle = dash):
# Combine the plots
display([horizontal_line1, horizontal_line2, plot_sigma_eff_r_act,
plot_sigma_eff_r_pas, plot_sigma_eff_l_act, plot_sigma_eff_l_pas,
plot_lines_AQFaccGJ, plot_points_AQCBA, plot_lines_AQCBA,
plot_points_FaccCEaccF, plot_lines_FaccCEaccF, plot_points_GJEaccG,
plot_lines_GJEaccG],
    title = "Pressure distribution",
    labels = ["Pressure [kN/m]", "Depth [m]"]);
```

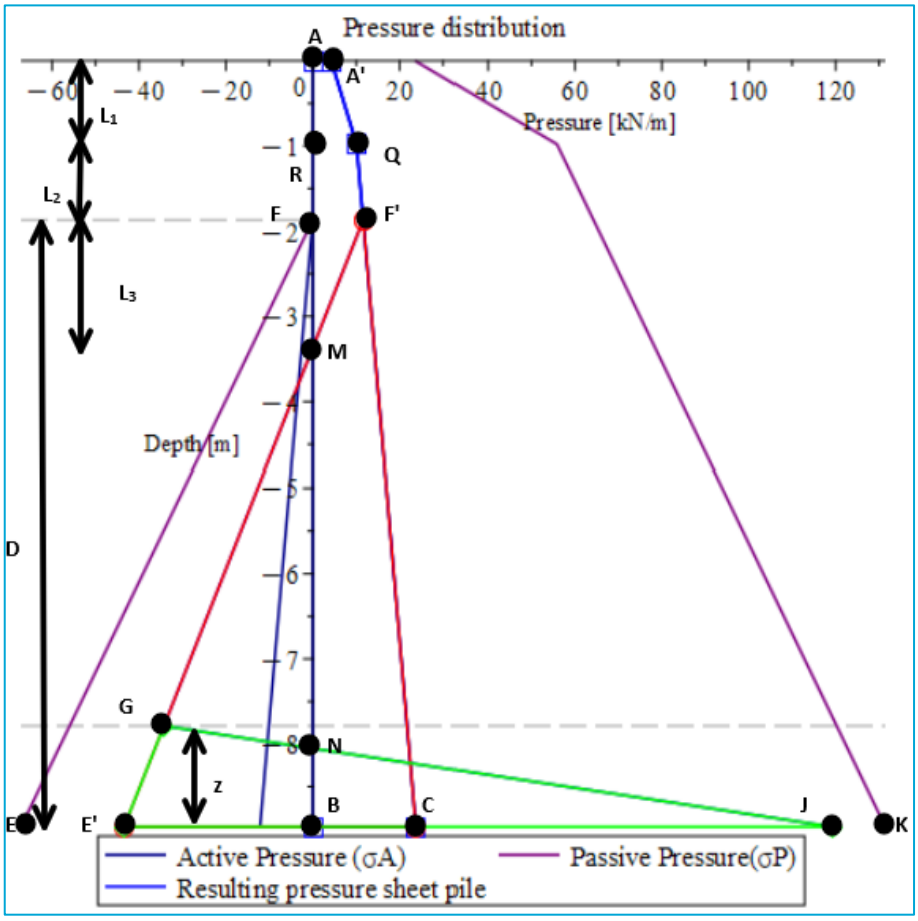

Figure 96 - Adopted notation system to calculate horizontal force and moment equilibrium to determine unknowns D and z for thesis case. The red, blue and green polygon are shapes that are used to simplify the horizontal force equilibrium calculation.

Appendix B: Geometries other quay wall construction types

Type 2

Concrete L-wall structures used for quay walls typically have a distinct L-shaped geometry consisting of a vertical wall and a horizontal base. These are called type 2 quay walls and can be seen in Figure 2. The vertical section of the L resists the lateral pressure from soil and water, while the base slab anchors the structure, providing stability by countering the forces acting on the wall. Common geometric parameters for these walls include:

- Vertical height: Typically, between 3 and 8 meters depending on the required retaining height.
- Base slab width: Usually between 1.5 and 3 meters, designed to prevent sliding and overturning.
- Thickness: The wall thickness can vary, typically ranging from 0.3 to 1 meter, depending on the load requirements and materials used (e.g., reinforced concrete).

In the past often timber foundation piles were used to support the quay wall. Currently, more and more concrete and steel foundations are used for this type of quay wall. They also contain a capstone and a masonry wall.

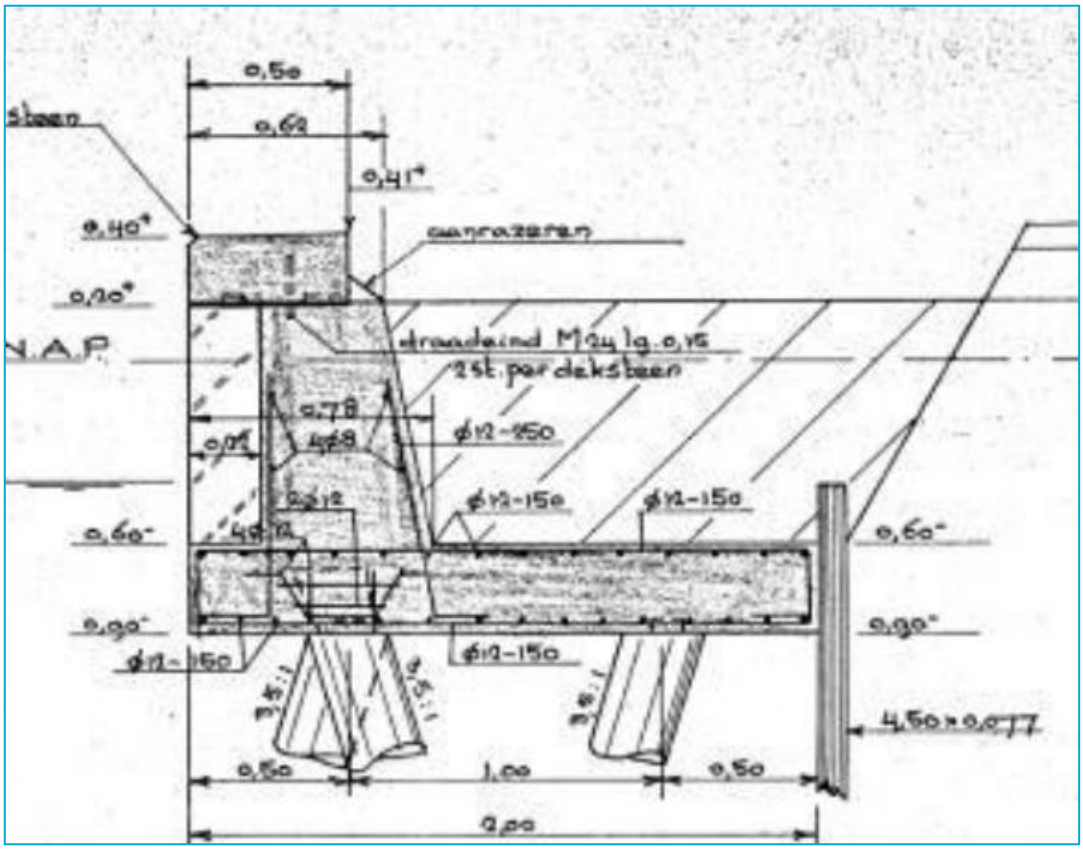

Figure 97 - Cross section type 2 quay walls (Gemeente Amsterdam, 2023)

IPK: G-force

Combi-wall systems, often used in urban quay walls, consist of a combination of large-diameter steel tubular piles (king piles) and intermediate sheet piles to create a retaining structure. These walls are frequently employed in waterfront infrastructure such as quay walls, piers, and ports due to their high load-bearing capacity, adaptability to deep excavations, and resistance to water and soil pressure. The strength of combi-walls is large relative to other geometries.

- King Piles (Tubular or H-Piles): These are the primary structural members in a combi-wall, typically made from large-diameter steel tubular piles or H-section piles. King piles are driven deep into the ground to provide significant vertical and lateral load capacity.
- Sheet Piles: These are lighter, interlocking steel sections placed between the king piles. Their primary role is to retain soil and prevent water ingress. The sheet piles fill the space between the king piles, forming a continuous retaining wall.

The IPK method for quay walls exists out of a combination exists of Giken, Van Gelder and Gebroeders de Koning. Unique is the application of the GRB-system (Giken Reaction Based) from Giken (G-kracht, 2023). The system (see Figure 98 – GRB-system) consists of three components: the gyropress (drilling rig), the clampcrane (lifting crane), and the pilerunner (small truck). These three systems are moved over the installed tube pile wall. The system was originally designed for harbours and railways in Asia but is modified to fit in the small urban environment of Amsterdam, thereby severely reducing its size. This allows roads and waterways to remain available for normal use.

Figure 98 – GRB-system (G-kracht, 2023)

G-kracht directly drills through the existing quay walls with a hollow steel tube pile with a special ring-bit. The tube piles (Figure 99 - G-force steel tube piles) are placed 750mm apart and have a 500m diameter. At the inland side, additional tube piles with a diameter of 273mm are places. By use of a filter construction, the groundwater level behind the quay wall is kept intact, which is of vital importance for the wooden pile foundations of the nearby monumental buildings. After the piles are

installed, prefabricated concrete cladding elements with prefabricated masonry is installed to keep the looks of the quay walls similar as required for this UNESCO World Heritage site.

Figure 99 - G-force steel tube piles (G-kracht, 2023)

<u>IPK: Kade 2.020</u>

This is a combination existing out of Combinatie Midden Delfland Civiele Werken, Oosterhof Holman Beton- en Waterbouw, Bouwadviesbureau Strackee and Sweco Nederland (Kade 2.020, 2022). The EZ-flow method is to be pronounced as 'easy-flow', which reflects on the way it is installed. This is since it is built according to the One-Piece-Flow principle, for which one prefab Z-element is designed, which can be viewed in Figure 100.

On the contrary to conventional methods, quay walls are replaced not all at once, but by only 5 meters at a time, moving from piece to piece. In this way all the work can be executed from one working pontoon. No construction pits must be made and there is no drilling. Trees, where possible, remain standing.

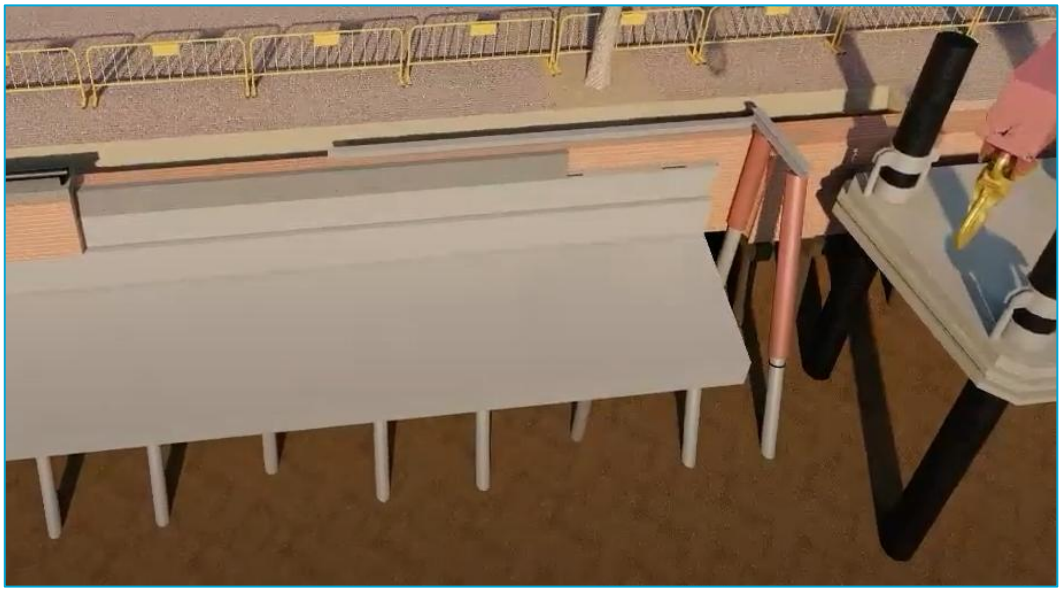

Figure 100 - Prefab Z-element (Kade 2.020, 2022)

IPK: Koningsgracht

The Koningsgracht is a combination of Royal BAM and Royal HaskoningDHV that replace quay walls using the SAVE method (Royal BAM, 2022). SAVE stands for 'Samen Amsterdamse kademuren VErnieuwen', which means ‘Replacing Quay Walls Together’ in Dutch. The SAVE Method approach involves renewing the quay wall incrementally. The work area moves along the quay wall on pontoons, like a ‘train’. As it advances, houseboats are temporarily relocated, and a newly completed quay ready for use is left. The floor of the new quay wall is constructed in segments within a trench box, which serves as a reusable mold for creating the structural floor. This trench box can be seen in Figure 102.

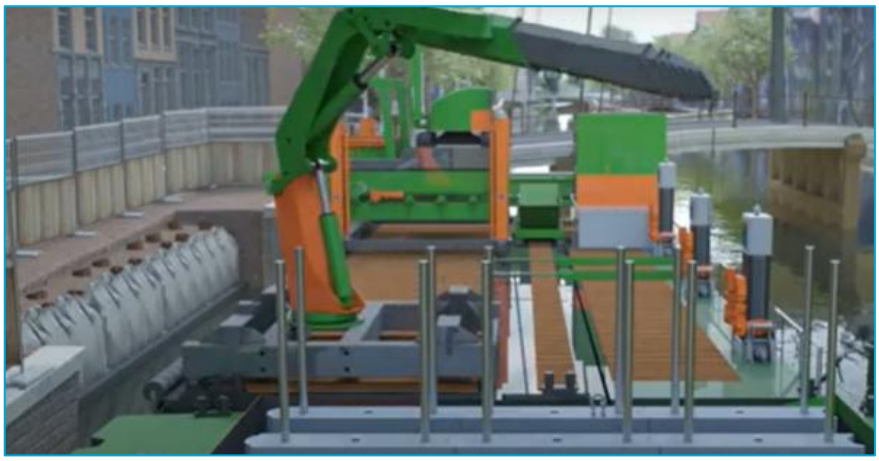

Figure 101 - Pontoons Koningsgracht (Royal BAM, 2022)

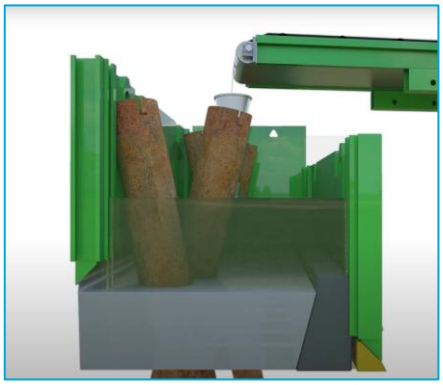

Figure 102 - Concrete casting in trench box Koningsgracht (Royal BAM, 2022)

Appendix C: Failure mechanisms not considered in thesis

Geotechnical bearing capacity

The geotechnical bearing capacity of the piles can be calculated. This gives the resistance (R_d) of the structure. Also, the effects on the structure (E_d) can be estimated.

The bearing resistance of the piles is the sum of the shaft resistance and bottom resistance of the piles as displayed in Figure 103 - Calculating of bearing capacity of a single pile by $R_{s,k}$ (shaft resistance) and $R_{b,k}$ (base resistance) respectively. The shaft and bottom resistance depend on the type of soil. Since the piles often go through multiple soil layers, different shaft frictions of the different soil layers should be multiplied with their respective areas and summed to obtain the bearing resistance of the pile (Baginska, 2012).

$$R_{ck} = R_{b,k} + R_{s,k} = A_b * q_{b,k} + \sum_{i=1}^{n} A_{s,i} * q_{s,k,i}$$

Often software is used to perform this step, especially with multiple layers, as the calculation can become cumbersome. However, this can also be verified analytically.

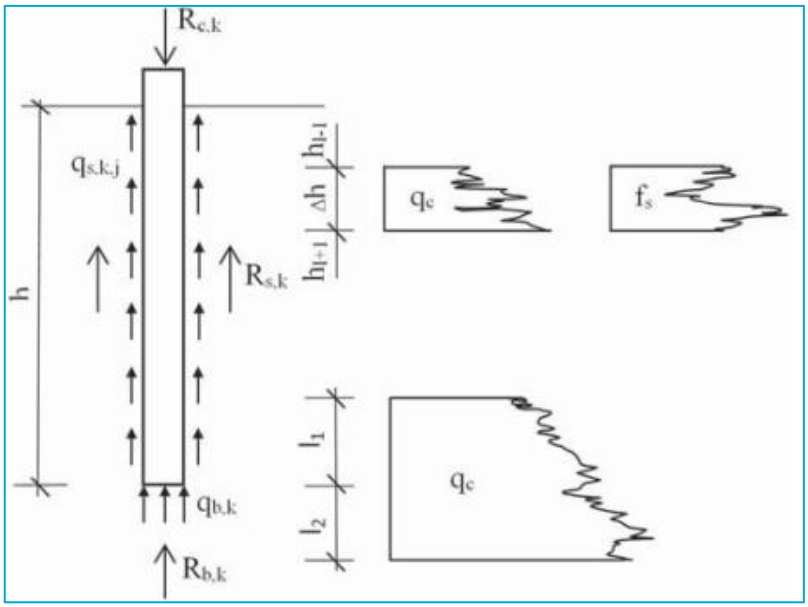

Figure 103 - Calculating of bearing capacity of a single pile (Baginska, 2012)

In E_d, the following elements must be accounted for: the weight of the foundation, the weight of all backfill materials, and all soil pressures, both favourable and unfavourable. Additionally, any water pressures not directly resulting from the foundation itself must be included as part of the load considerations.

After both E_d and R_d are determined, the unity check can be performed (Geotechnical design of structures - Part 1: General rules, 2017):

$$UC = \frac{E_d}{R_d} \leq 1.0$$

If the geotechnical resistance is not enough, the structure will fail as depicted in Figure 104. Often software is used to obtain the bearing capacity of the piles.

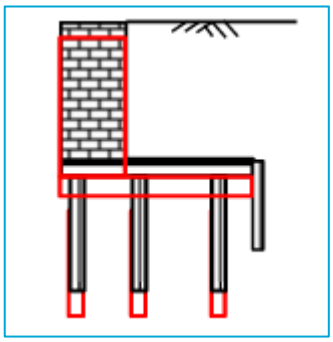

Figure 104 – Exceeding geotechnical bearing capacity (Ingenieursbureau Gemeente Amsterdam, 2023)

Sliding of the wall

The horizontal sliding of the masonry wall is caused by the resulting horizontal force pushing the wall into the canal, visualised in Figure 105. The resulting horizontal force F_h is the active earth pressure of the soil behind the quay wall minus the water pressure. The resisting force is caused by friction and can be calculated by summing the vertical force F_v of the masonry wall and the soil and multiplying that with the friction coefficient of the masonry μ, which is 0.7. This results in the following check (Ingenieursbureau Gemeente Amsterdam, 2023):

$$F_h \leq F_v * \mu$$

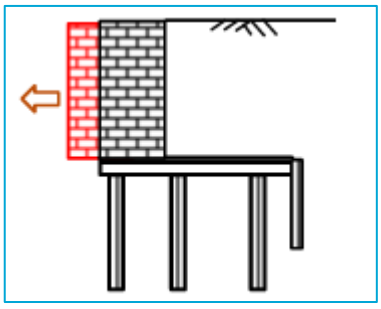

Figure 105 - Sliding of the wall (Ingenieursbureau Gemeente Amsterdam, 2023)

Tilting of the masonry wall

The masonry wall can also tilt outwards, which is shown in Figure 106 - Tilting of the masonry wall. This failure mechanism is mechanically illustrated in Figure 107. The tilting point (kantelpunt in Dutch) is the point at the left bottom. Forces considered for equilibrium are the gravity of the masonry wall (F_1) downwards, the active soil pressure acting to the left (F_2), bollard forces to the left (F_3), the water pressures at both sides which cancel each other (F_4 and F_5) and the friction of the wall (F_6).

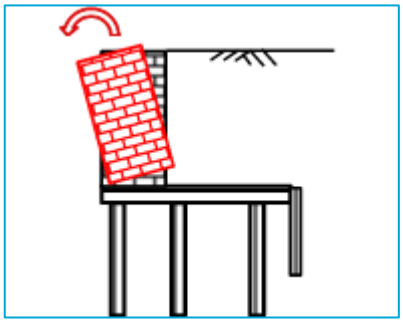

Figure 106 - Tilting of the masonry wall (Ingenieursbureau Gemeente Amsterdam, 2023)

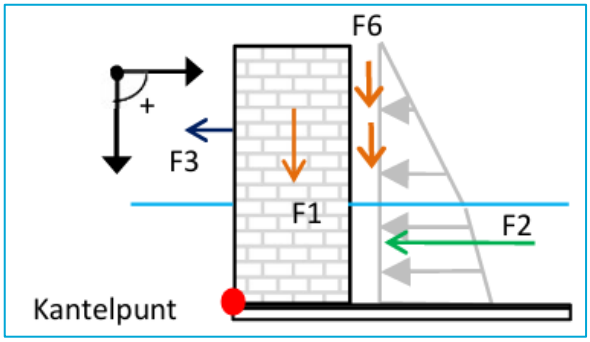

Figure 107 - Mechanics scheme of tilting (Ingenieursbureau Gemeente Amsterdam, 2023)

<u>Failure of the structural wall</u>

Currently, little information is known about the material properties and strength of the masonry and research is ongoing (Ingenieursbureau Gemeente Amsterdam, 2023) in the failure mechanism in Figure 108. Therefore, this mechanism is often not considered.

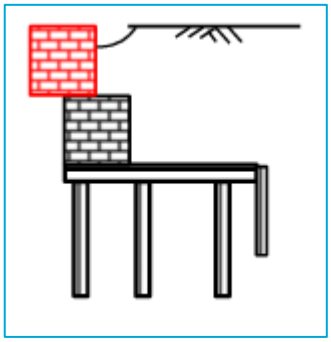

Figure 108 - Failure of the structural wall (Ingenieursbureau Gemeente Amsterdam, 2023)

<u>Failure of the general stability</u>

The general stability failure mechanism is given in Figure 109. This failure mechanism is checked in the finite element software Plaxis 2D with φ_c reduction.

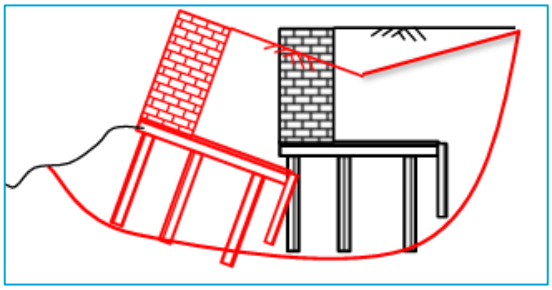

Figure 109 - Failure of the general stability (Ingenieursbureau Gemeente Amsterdam, 2023)

A method to do this without software is to use the Bishop's method of slices (GeoEngineer, 2024). In this method slices are created as shown in Figure 110 - Slice of Bishop's method, where the shear interslice forces are neglected. In this method 3 equilibrium equations are used:

1. Moment equilibrium of the surface of failure with respect to the centre of rotation
2. Horizontal force equilibrium for the surface of failure
3. Vertical force equilibrium for each slice.

It should be checked if the resisting moment is greater than the overturning moment by a Factor of Safety (*FoS*). This means that the sum of the shear forces (*T*) of the slices multiplied with their lever arm should be greater than the sum of the downward forces caused by the gravity.

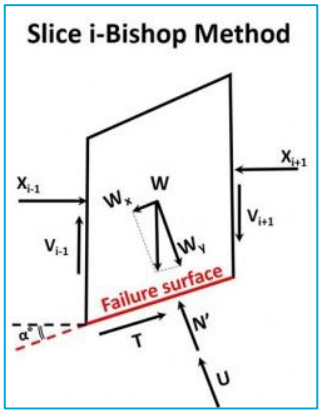

Figure 110 - Slice of Bishop's method (GeoEngineer, 2024)

By using the Mohr-Coulomb failure criterion, the shear force T of a slice can be expressed in the following way:

$$\tau = c + \sigma_n * \tan(\varphi)$$

$$T = \frac{c * L + N' * \tan(\varphi)}{FoS}$$

Where:

- *L*: arc length of the slice's base which is approximated to a line segment
- *c*: cohesion
- φ: friction angle of the soil
- σ_n: normal effective stress

Note that the vertical equilibrium is used. This results in the following equation:

$$(N' + U) * \cos(\alpha) + \frac{1}{FoS} * [(c * L + N * \tan(\varphi) * \sin(\alpha)] - W = 0$$

The moment equilibrium around the centre of rotation in Figure 111 – Bishop's method of slices can be obtained and by rewriting it in terms of *FoS* an implicit formulation can be derived, which can be solved iteratively.

$$FoS = \sum \{ \frac{[c * B + (W - \frac{U}{\sec(\alpha)}) * tan(\varphi)] * sec(\alpha)}{1 + \frac{\tan(\alpha)\tan(\varphi)}{FoS}} \} * \frac{1}{\sum W * \sin(\alpha)}$$

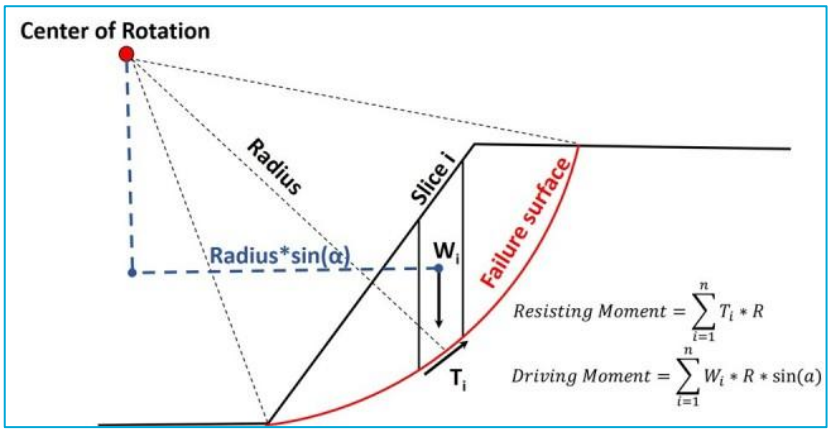

Figure 111 – Bishop's method of slices (GeoEngineer, 2024)

Structural failure of the beams

When checking the structural failure of the beams (also known as kesps), the reduced cross-section due to decay should be taken. The beam should be checked according to (EN 1995-1-1, 2011) for both the shear force and the bending moment. This failure mechanism is shown in Figure 112 - Structural failure of the beams.

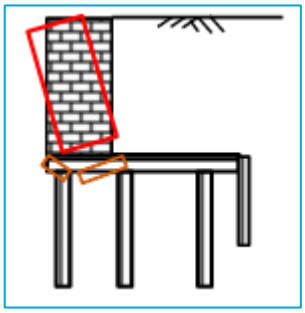

Figure 112 - Structural failure of the beams (Ingenieursbureau Gemeente Amsterdam, 2023)

The normal force acts in the perpendicular to the beams, which is perpendicular to the grain, therefore the compressive stresses should be checked according to the following formula:

$$\sigma_{c,0,d} \leq f_{c,90,d}$$

For these combinations $f_{c,0,d}$ can be determined using:

$$f_{c,0,d} = k_{mod} * \frac{f_{c,90,k}}{\gamma_M}$$

Where γ_M = 1.0 for special load combinations and 1.3 for sawn timber sections. For quasi-permanent loads $k_{mod} = 0.6$ and for a variable load $k_{mod} = 0.7$.

The compressive stress can be calculated by dividing the normal force acting on the beam by the area of the beam.

$$A_{beam} = b_{beam} * h_{beam}$$
$$\sigma_{c,90,d} = \frac{N_d}{A_{beam}}$$

The following combinations should also be checked for bending and axial forces (Ingenieursbureau Gemeente Amsterdam, 2023):

- Shear:

$$f_{v,d} = k_{mod} * \frac{f_{v,k}}{\gamma_M}$$
$$\tau_d = \frac{3 * V_{z,s,d}}{2 * A_b}$$
$$\frac{\tau_d}{f_{v,d}} \leq 1.0$$

- Bending combined (EN 1995-1-1, 2011):

$$\frac{\sigma_{m,y,d}}{f_{m,y,d}} + k_m \frac{\sigma_{m,z,d}}{f_{m,z,c}} \leq 1.0$$
$$k_m \frac{\sigma_{m,y,d}}{f_{m,y,d}} + \frac{\sigma_{m,z,d}}{f_{m,z,c}} \leq 1.0$$

- Bending and tension combined (EN 1995-1-1, 2011):

$$\frac{\sigma_{t,0,d}}{f_{t,0,d}} + \frac{\sigma_{m,y,d}}{f_{m,y,d}} + k_m \frac{\sigma_{m,z,d}}{f_{m,z,d}} \leq 1.0$$
$$\frac{\sigma_{t,0,d}}{f_{t,0,d}} + k_m \frac{\sigma_{m,y,d}}{f_{m,y,d}} + \frac{\sigma_{m,z,d}}{f_{m,z,d}} \leq 1.0$$

- Bending and tension (EN 1995-1-1, 2011):

$$\frac{\sigma_{c,0,d}}{f_{c,0,d}} + \frac{\sigma_{m,y,d}}{f_{m,y,d}} + k_m \frac{\sigma_{m,z,d}}{f_{m,z,d}} \leq 1.0$$

$$\frac{\sigma_{c,0,d}}{f_{c,0,d}} + k_m \frac{\sigma_{m,y,d}}{f_{m,y,d}} + \frac{\sigma_{m,z,d}}{f_{m,z,d}} \leq 1.0$$

In case of timber construction products for a circular cross-section k_m = 1.0 may be used.

$$f_{m,y,d} = k_{mod} * k_{h,y} * \frac{f_{m,y,k}}{\gamma_M}$$

$$f_{m,z,d} = k_{mod} * k_{h,z} * \frac{f_{m,z,k}}{\gamma_M}$$

The bending stresses can be obtained by using the section modulus in the following formula:

$$W_y = \frac{1}{6} h_{beam} * b_{beam}^2$$

$$W_z = \frac{1}{6} b_{beam} * h_{beam}^2$$

$$\sigma_{m,y,d} = \frac{M_y}{W_y}$$

$$\sigma_{m,z,d} = \frac{M_z}{W_z}$$

Structural failure of the floor

This failure mechanism is generally not considered as little information is known about the floor, as it is embedded in the soil and not easily inspected. This claim is defended by stating that failing of the floor is not a direct failure mechanism and warns in case of a defect of the entire structure (Ingenieursbureau Gemeente Amsterdam, 2023). It is visualised in Figure 113. Therefore, this failure mechanism will not be further discussed in this thesis.

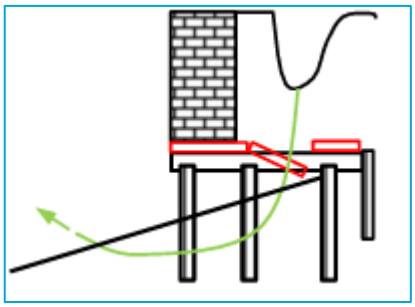

Figure 113 - Structural failure of the floor (Ingenieursbureau Gemeente Amsterdam, 2023)

Absence or failure of the underwater screen

Like the floor, often little information is known about the underwater screen. It is also generally not considered a direct failure mechanism and therefore also neglected (Ingenieursbureau Gemeente Amsterdam, 2023). It is visualised in Figure 114.

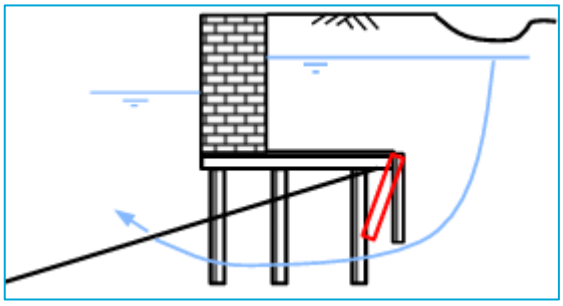

Figure 114 - Absence or failure of the underwater screen (internal erosion, underflow, piping) (Ingenieursbureau Gemeente Amsterdam, 2023)

Appendix D: Comparison of phase displacements traditional model from DIANA and Plaxis

The following Tables show a comparison of the phase displacements for the traditional model. The contour scales are set to similar specified bound as indicated. The results of DIANA are given on the left and those of Plaxis on the right. This serves as a sanity check for the models. In general, the global behaviour is general for both software, but Plaxis has larger displacements for most phases.

Phase: Lower water table

Table 79 - Phase displacements in phase Lower water table (left: DIANA; right: Plaxis); contour scale is similar for both software and taken from DIANA

Phase: Lower water table	
Phase displacements x	
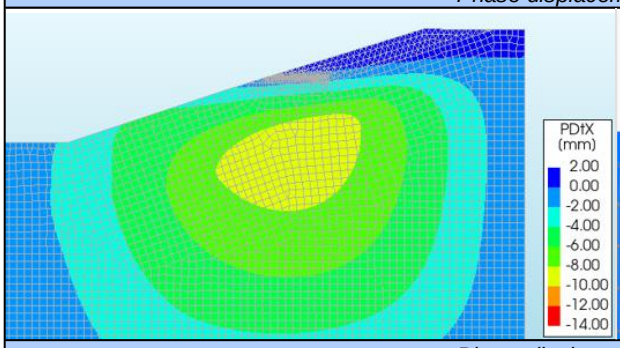	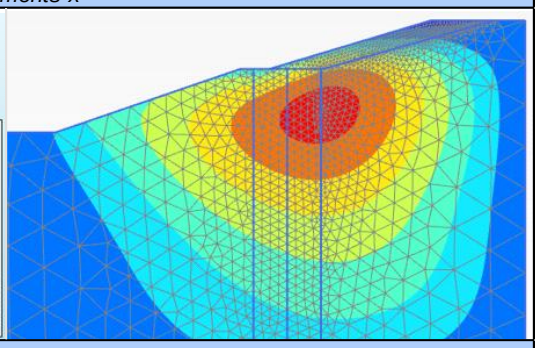
Phase displacements y	
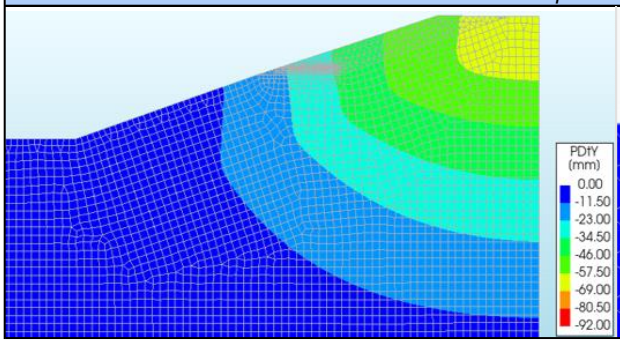	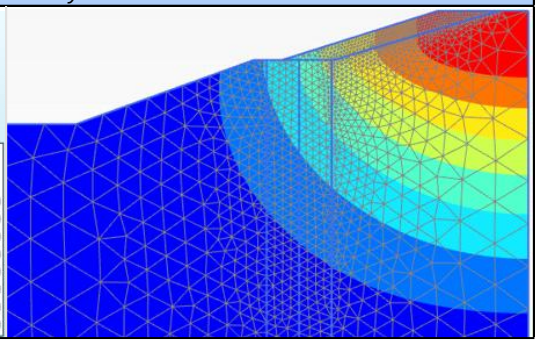

Phase: Excavate

Table 80 - Phase displacements in phase Excavate (left: DIANA; right: Plaxis); contour scale is similar for both software and taken from DIANA

Phase: Excavate

Phase displacements x

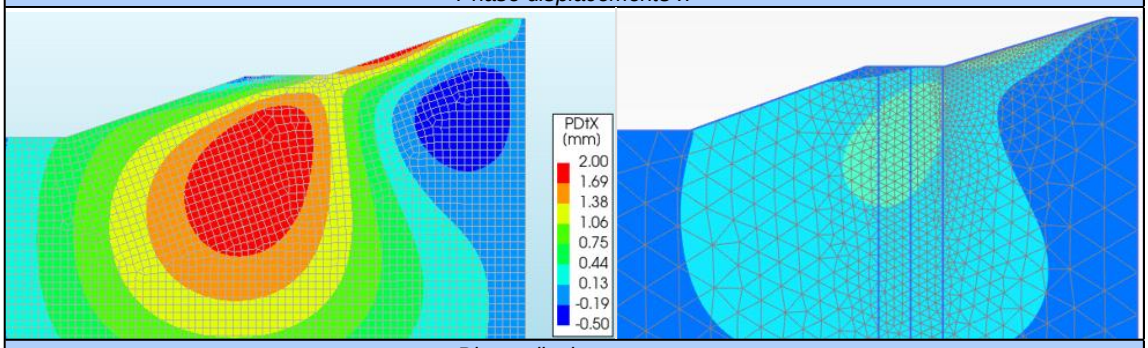

Phase displacements y

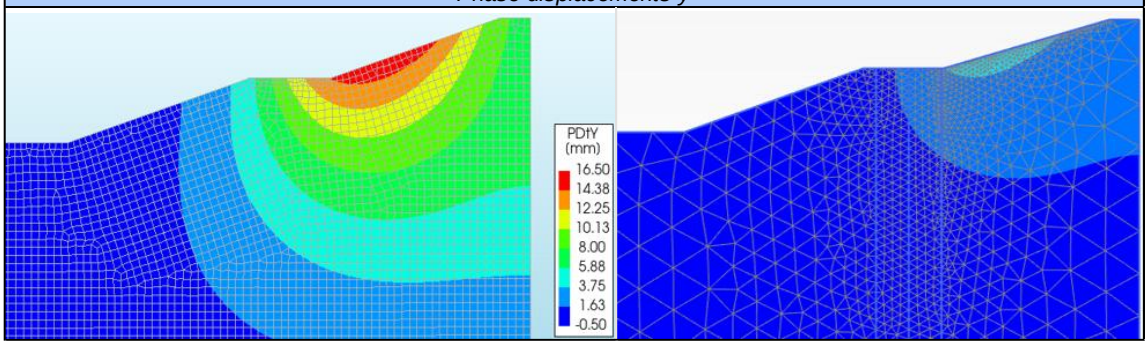

Phase: Add piles

Table 81 - Phase displacements in phase Add piles (left: DIANA; right: Plaxis); contour scale is similar for both software and taken from DIANA

Phase: Add piles

Phase displacements x

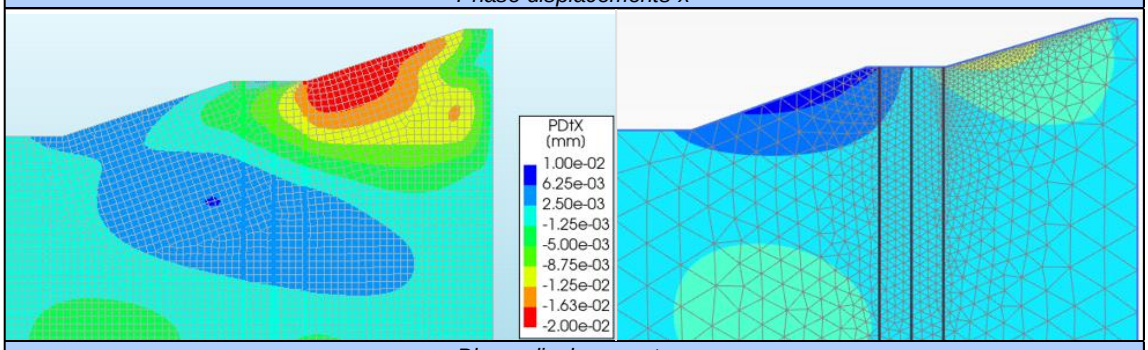

Phase displacements y

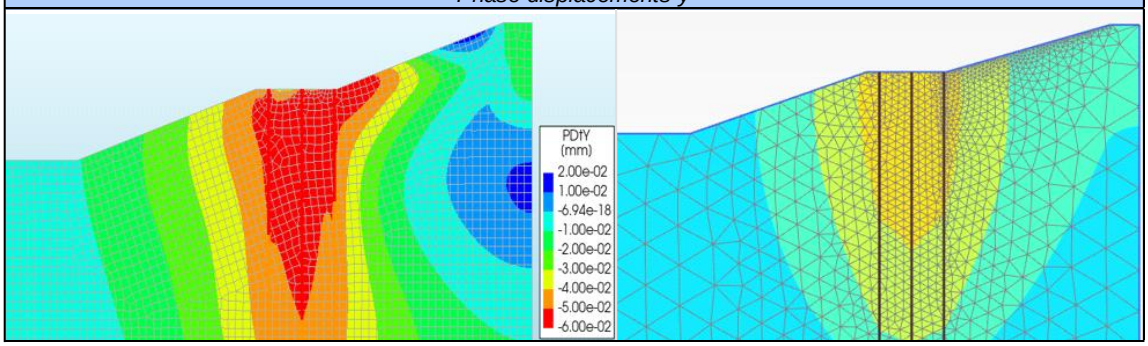

Phase: Add wall

Table 82 - Phase displacements in phase Add wall (left: DIANA; right: Plaxis); contour scale is similar for both software and taken from DIANA

Phase: Add wall
Phase displacements x
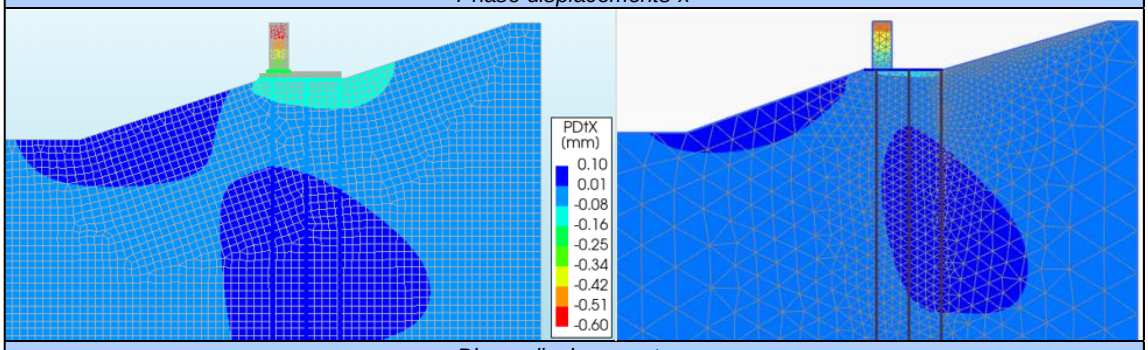
Phase displacements y
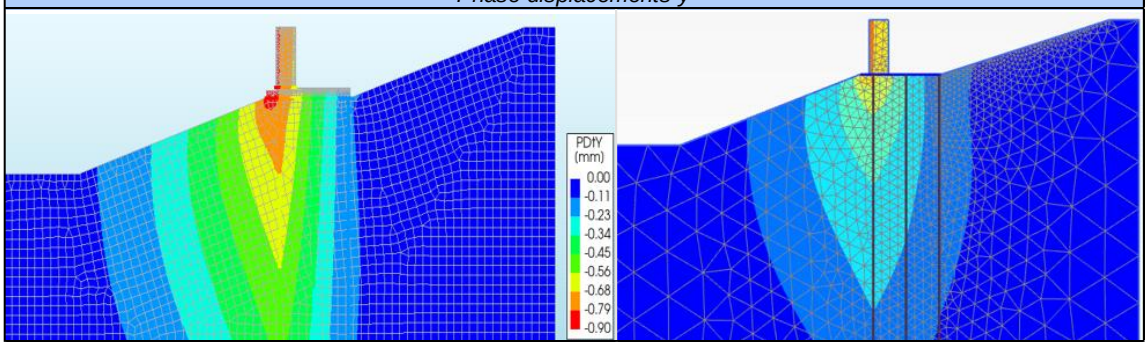

Phase: Backfill soil

Table 83 - Phase displacements in phase Backfill soil (left: DIANA; right: Plaxis); contour scale is similar for both software and taken from DIANA

Phase: Backfill soil
Phase displacements x
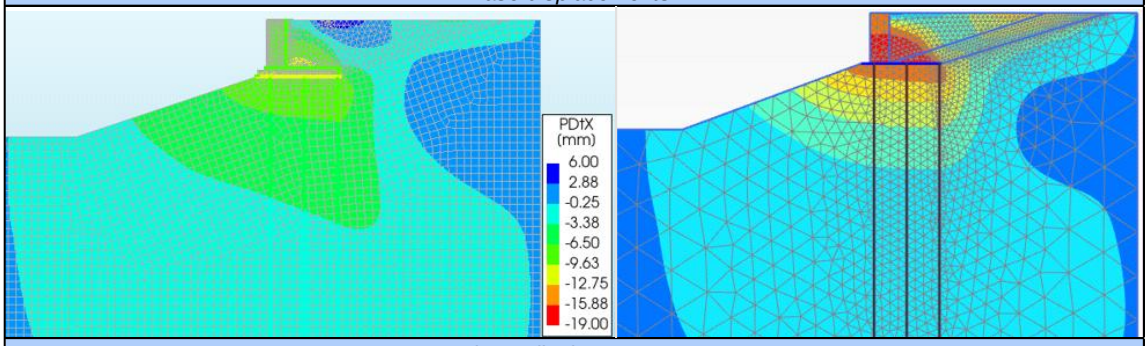
Phase displacements y
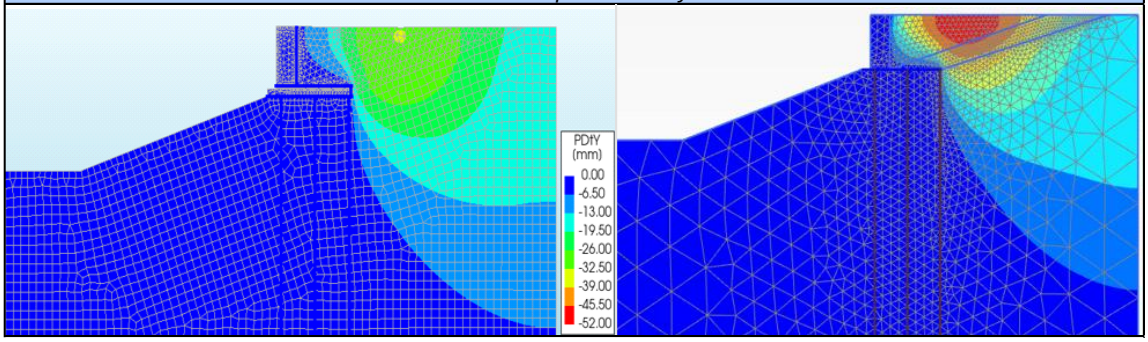

Phase: Heighten water table

Table 84 - Phase displacements in phase Heighten water table (left: DIANA; right: Plaxis); contour scale is similar for both software and taken from DIANA

Phase: Heighten water table
Phase displacements x
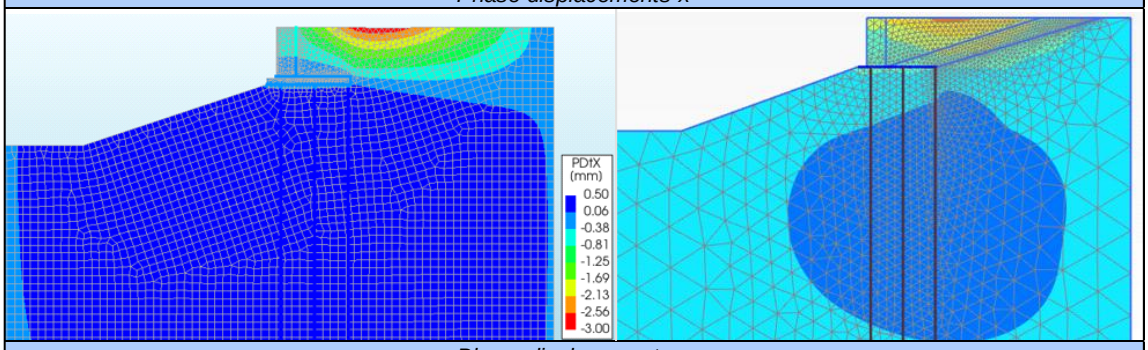
Phase displacements y
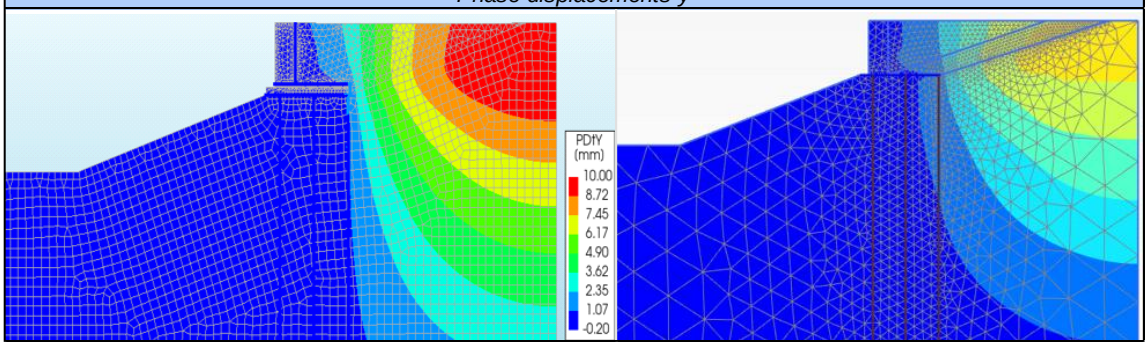

Phase: Add loads

Table 85 - Phase displacements in phase Add loads (left: DIANA; right: Plaxis); contour scale is similar for both software and taken from DIANA

Phase: Add loads
Phase displacements x
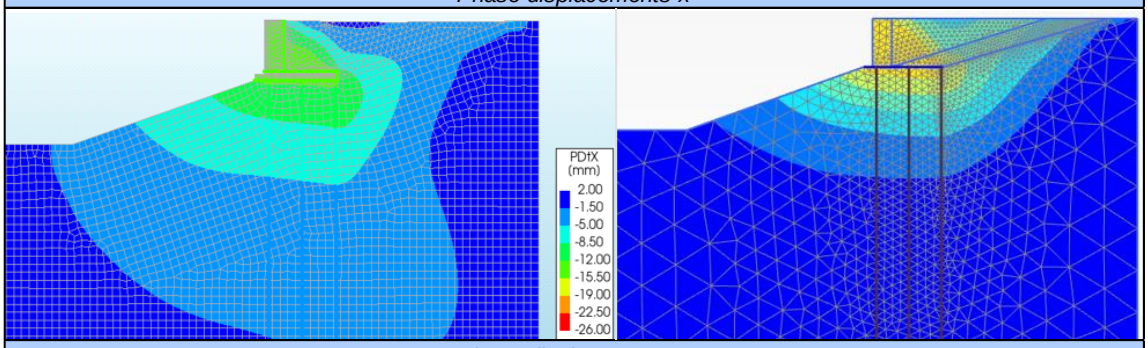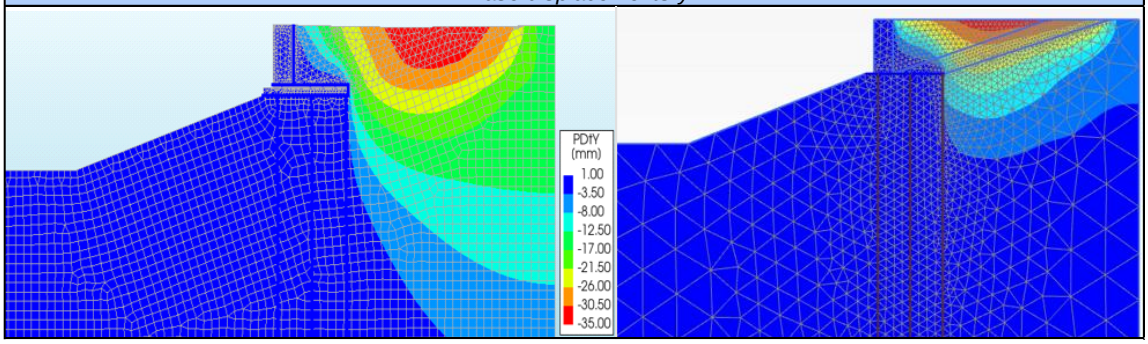
Phase displacements y